WARWICK
THE UNIVERSITY OF WARWICK

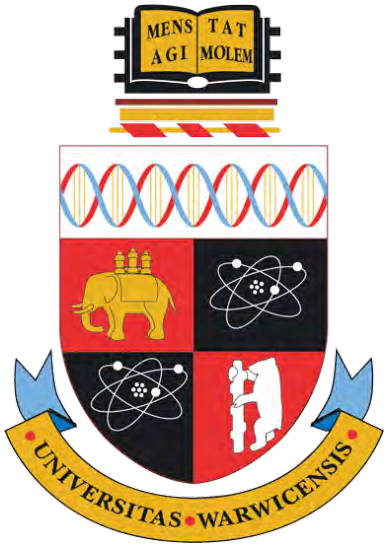

Iron Oxide Nanoparticles for Biological Research and Biomedicine

by

Charlotte Fletcher

A thesis submitted in fulfilment of the requirements for the degree of

Doctor of Philosophy

Molecular Analytical Science Centre for Doctoral Training, University of Warwick

August 2021

Contents

List of Tables

List of Figures

Acknowledgments

I would like to thank my supervisor Professor Matt Gibson for his never-ending support throughout my time in his group and for "adopting" me at a time when I felt I could not finish this work. I would like to thank Dr. Gemma-Louise Davies for her support throughout the first half of this work. The patience and help from both these individuals towards a "biologist doing chemistry" has been astonishing. I would also like to thank the Gibson group for welcoming me so warmly. I also want to acknowledge all the PhD students of MAS CDT 2015 but especially my friends and supporters Georgina Charlton, James Town, Matthew Turner and George Henry Lee without whom life would have been much more boring.

On a more personal note, Jo Dimmock and Russell Sime have been a constant source of fun, laughter and when needed sympathy. Friday nights have been a much-needed break at times.

I wish to express my love and gratitude to my children, Lauren, Eloise, Iian and Ethan. I have at times been unavailable and not once have I heard you moan or complain. Thank you! Iian I finally wrote my book!

To my husband Paul Fletcher, I have no words, back in 2011 you pushed me to return to university for my undergraduate degree and then were the reason I applied and began my journey through masters and PhD. You have never failed to support me, to encourage me or say the right words. Without your love and support I would not be here now. You have sacrificed so much and never complained. You are my world and for that I thank you.

Finally, to my dad, Roger Allford, who left us in 2011, your loss inspired me back into education. I miss you every day but when things get hard the pride and love I know you would have felt never leaves me.

Declarations

All the work presented in this thesis is entirely my own work, except where it is acknowledged. I confirm that this thesis has not been submitted for a degree at another university.

Preparation of Poly (N-(2hydroxypropyl) methacrylamide) (PHPMA) and characterisation was performed by Panagiotis Georgiou of the University of Warwick.

Cell preparation of the cell line MC148 for *in vivo* work was carried out by Emmanuele Roscioli of the University of Warwick.

Scanning Electron Microscopy Images taken in conjunction with Houari Amari and Steve York of the University of Warwick.

X-Ray Diffraction performed in conjunction with Dr David Walker of the University of Warwick.

All VSM analysis was carried out in conjunction with Martin Lees of the University of Warwick Physics department.

Image of the prosthetic eye for Chapter 3 obtained with permission from Paul Fletcher, owner of the prosthetic eye.

Abstract

Nanoscience is becoming of great importance to biological research and for use in biomedicine. This is due to nanoparticles' unique properties, which often differ to the bulk material due to their nanoscale size. Nanoparticles have extremely tuneable properties including size, shape, surface functionalisation and charge. A thorough understanding is needed of their structure, properties and behaviour if they are to be used in any biological environment. Here, **Chapter 2** discusses the design for superparamagnetic multifunctional silica coated iron oxide nanoparticles and their synthesis. It then looks at characterisation to understand the chemical nature of the nanoparticles synthesised. Surface functionalisation of nanoparticles is established with addition of amine groups and fluorescent dye, to allow for the work in **Chapter 3** and **Chapter 4**. **Chapter 3** looks at the addition of polymers to the synthesised nanoparticles resulting from the work in **Chapter 2** and evaluates their effect on nanoparticle size therefore aggregation by DLS measurements. This is monitored over time and in different buffers/solvents to evaluate longer term behaviour and storage conditions. Finally, **Chapter 4** begins to study the effect on incorporating the nanoparticles into cells and their behaviour once there. This includes a comparison of two methods of introducing nanoparticles to cells – microinjection and endocytosis with the advantages and disadvantages discussed. It also looks at imaging and the fluorescence exhibited during light microscopy and the effect of photobleaching due to excitation due to lasers. **Chapter 4** also discuses why highly designed and synthesised nanoparticles are needed for biological research when commercial beads are available. Lastly, some early protocol design for attachment of nanoparticles to DNA are discussed and the ability to manipulate the superparamagnetic nanoparticles tethered to DNA is tested. The work demonstrates that the nanoparticles through precise design, synthesis and characterisation have attractive properties for use biological research and also for potential use as an MRI contrast agent and for drug delivery.

Acronyms

AC Alternating Current.

APTES (3-aminopropyl) Triethoxysilane.

AuNPs Gold Nanoparticles.

c@s Core at Shell.

CTAB Cetrimonium bromide.

CTF Corrected Total Fluorescence.

DLS Dynamic Light Scattering.

DMSO Dimethyl Sulfoxide.

DVI Digital Microscope.

EtOH Ethanol.

FDA Food and Drug Administration.

FTIR Fourier Transform Infrared Spectroscopy.

GRAS Generally Regarded as Safe.

GSH Glutathione.

InTDen Integrated Density.

IONPs Iron Oxide Nanoparticles.

LCST Lower Critical Solution Temperature.

MPS Mononuclear Phagocyte System.

MRI Magnetic Resonance Imaging.

MSNs Mesoporous Silica Nanoparticles.

MW Molecular Weight.

NIR Near Infra Red.

NMs Nanomaterials.

NOC Nocodazole.

OAm Oleylamine.

PBA Polyvinyl Alcohol.

PBS Phosphate Buffer Solution.

PDT Photo Dynamic Therapy.

PEG Polyethylene Glycol(PEG).

PHPMA Poly (N - (2-hydroxypropyl) methacrylamide).

PMA Poly(methyl acrylate).

QDs Quantum Dots.

ROS Reactive Oxygen Species.

SEM Scanning Electron Microscopy.

SiNPs Silica Nanoparticles.

siRNA Small Interfering RNA.

SPIONs Superparamagnetic Iron Oxide Nanoparticles.

SPR Surface Plasmonic Resonance.

SQUID Superconducting Quantum Interference Device.

STD Dev Standard Deviation.

TEM Transmission Electron Microscopy.

TEOS Triethyl Amine Tetraethyl Orthosilicate.

TGA Thermogravimetric Analysis.

TIRF Total Internal Reflection Fluorescence Microscopy.

UCST Upper Critical Solution Temperature.

VLSI Very Large Scale Integration.

VSM Vibrating Sample Magnetometer.

XRD (x-ray Diffraction.

Symbols

γ	The Gamma Symbol
μ	The Micro Symbol
α	The Alpha Symbol

Chapter 1

Introduction

1.1 The Nanoscale and Nanoscience

Substances with a size on the nanoscale are referred to as "nanomaterials". A nanometer (nm) is an International System of Units (Système international d'unités, SI) unit that represents 10^{-9} meter in length. Materials within a size range of approximately 1-100nm are officially considered as nanomaterials [1][2].

Nanoscience is the study and science of materials which fall within this size range. Nanoscience includes the study of nanoscale materials size and structure and their properties which are often dependent upon the materials being on the nanoscale [1]. A nanomaterial is any material which has any internal or external structures that are on the nanoscale dimension.

Nanomaterials (NMs) can be divided in further subcategories these include but are not limited to:

- Nanofibers are nanomaterials where there are 2 exterior nanoscale dimensions which are similar in nature and a third larger dimension,
- Nanoparticles(NPs) are materials which have three external nanoscale dimensions[2].
- Nanorods or nanoplates are similar to nanoparticles however these terms are used when the longest axes lengths and the shortest axes lengths of the nanoscale material are different [1][2].
- Quantum Dots (QDs) are materials that are on the nanoscale which often have a core-shell structure. They are semiconducting

materials with unique optical properties. These optical properties allow quantum dots to emit light of specific wavelengths [1][2].

Figure 1.1 illustrates just a few examples of how these structure can be used today. From the synthesis of nanoparticles as seen in Figure 1.1 (C) for use in biological environments to Figure 1.1 (A) which shows nanorods for photothermal cancer treatments

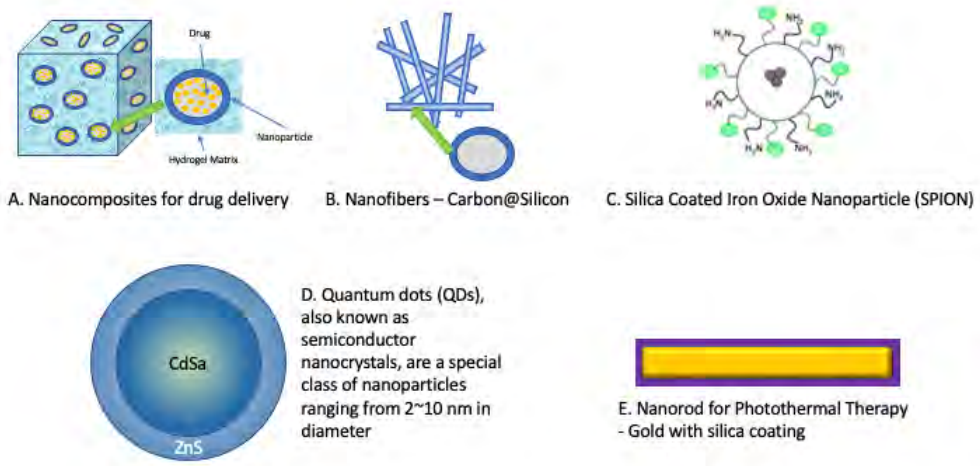

Figure 1.1: *Examples of sub categories of nanomaterials. A) Nanocomposite of a hydrogel with nanoparticles encased within for drug delivery, B) carbon silicon nanorods, C) Nanoparticles for use in a biological environment, D) Quantum Dots for use as semiconducting nano crystals and E) Nanorods for use in Photothermal cancer treatments.*

Nanoscience and the study of nanoparticles (NPs) and nanostructured materials are a popular and active area of scientific research. Research encapsulates many different areas, resulting in a variety of applications. Their popularity and prominence in research can be explained by their often unique and controllable characteristics [1][2][3]. These characteristics include melting point, conductivity, size, light absorption and catalytic activity. These tuneable characteristics can lead to enhanced performance in comparison to their bulk material equivalents [1][2][3].

1.1.1 Classification of Nanomaterials Based on their Origin

Nanomaterials (NMs) are also often classified according to their origin. This means whether they are synthetic (man-made) or natural.

As the name suggests, natural nanomaterials are those which occur in nature. These nanomaterials are the result of either biological species or through anthropogenic activities. These natural nanomaterials are present within the earths ecosystem such as the oceans, the soil, magma and both micro and higher organisms. These nanomaterials occur regardless of human activity. [4][5].

In contrast, synthetic nanoparticles are produced from human activities. This is not only in the lab through physical, biological, or chemical methods, but also as a by-product of activities such as engine exhausts or mechanical grinding. These nanoparticles are often associated with negative environmental impact however their potential as materials for good is also vast. [6]

1.1.2 Nanoscale Materials

It is common for nanomaterials and nanoparticles to be categorised in one of four major material-based categories. These are inorganic, organic, carbon based and composite based. These categories are outlined below [3][7].

The inorganic-based nanomaterials and nanoparticles category consists of nanoscale materials which are metals or metal oxides. Common inorganic metals associated with nanomaterials include gold (Au) and Silver (Ag), while commonly used metal oxides include Titanium oxide (TiO_2), iron oxide (Fe_3O_4) and zinc oxide (ZnO). Silicon and ceramic materials are also associated with this category in their role as semiconductors [3][8].

Nanomaterials which are made from organic matter are considered organic based nanomaterials. This subgroup uses non-covalent interactions for the self-assembly of structures such as micelles, liposomes and dendrimers [3].

The carbon based nanomaterials category are also organic however this subgroup contains nanopaticles made primarily of allotropes of carbon. These nanomaterials have easily influenced morphologies including spheres, tubes and ellipsoids. Fullerenes, carbon nanotubes and graphene are also included in this category. Unlike other organic nanomaterials covalent bonding means that carbon based nanomaterials are very strong [3].

Composite-based nanomaterials are nanomaterials which have any combination of nanomaterials from the previously described categories.

This could include a metal-inorganic structure, for example [3].

1.2 The History of Nanomaterials

Throughout history, nanomaterials have been used even with no understanding of the science behind them. For example, Egyptian blue, which is also known as calcium copper silicate or cuprorivaite, is a synthetic pigment used throughout the Roman empire and is also a nanomaterial. It is made using a sintered mixture of nanometer-sized quartz and glass. 4000 years ago in ancient Egypt, Lead(II) sulphide (PbS) nanoparticles of approximately 5nm diameter were being used for the purpose of dyeing hair. Examples of the synthesis of nanoparticles date back to the 14th and 15th centuries and red glass containing copper nanoparticles have been found as early as the bronze age (1200-100BC) [9]. These examples from history are only a few examples of the use of Nanomaterials in history with many more easily available.

Nanoparticles synthesised within a lab environment were first described in 1847 when Michael Faraday synthesised a colloidal gold nanoparticle solution [10]. This synthesis is credited with the beginning of nanomaterials as an area of scientific interest. This work describes how the synthesised gold colloids have different optical properties to their bulk equivalent.

The optical properties of gold nanoparticles (AuNPs) can be seen as early as the 4th century AD in the Lycurgus Cup, where in certain lights gold NPs are an olive green and when light is shone from the inside of the cup, they are seen as a ruby red. This property can also be seen with several of the displays in the British Museum, London, including several of the medieval church windows where it will shine a red and yellow due to the presence of nanoparticles, which are gold and silver. These NPs have fused with the glass itself [11-12].

In modern times, synthesised nanomaterials have greatly improved characteristics, and often these characteristics improve those seen in the bulk materials, such as the characteristic of superparamagnetism and increased surface area for functionalisation. Modern nanomaterials provide new scientifically and domestically useful properties such as antibacterial or antifreeze properties [13-14]. In recent times, deepening understanding of nanoparticle properties has been gained through research

and a greater understanding of chemistry on the nanoscale. This depth of knowledge has led to properties being utilised that in earlier centuries were not understood. For example the optical properties of AuNPs are now understood and can be manipulated by synthesis of size specific nanoparticles. Size, shape and surface functionality are amongst the characteristics which can now be controlled through a variety of synthesis methods. This allows for nanoparticles to be used in multiple situations from computer hardware to cancer treatments [13-14]. Nanoscience is an ever growing field of study and it is likely that the use of nanoparticles will continue to grow.

1.3 Inorganic Based Nanoparticles

Inorganic nanoparticles are nanoparticles made from inorganic materials. These include those made from metals such as gold (AuNPs), silver (Ag), titanium oxide (TiO_2) and iron oxide (SPIONs). Quantum dots and paramagnetic lanthanide nanoparticles are also inorganic nanoparticles. This type of nanoparticle tends to be biocompatible, stable, hydrophilic and non-toxic. These properties make them ideal for consideration for applications such as drug delivery, diagnostic techniques such as magnetic resonance imaging (MRI), tissue engineering, and bio labelling, to name a few [7][8].

1.3.1 Gold Nanoparticles

Gold nanoparticles (AuNPs) are extremely popular in academic and biomedical research, due to properties which include easy synthesis and manipulation of properties acquired, allowing for very good control over physical and chemical properties [15][16]. Gold nanoparticles have a high X-ray coefficient, unique optical properties which are tuneable, and show strong binding affinity to amines, disulphides and thiols [15-18].

AuNPs can be synthesised with many morphologies, including, but not limited to, nanorods, squares, spheres, stars and nanoshells (hollow structures)[73]

AuNPs have applications for use in drug delivery, catalytics, biological sensing and biolabeling to name a few [18-19]. They have low toxicity, a large surface-to-volume ratio and are biocompatible. These properties make the useful in the biotechnology research area [20].

Properties of AuNPs are summarised in Figure 1.2. Solvent, shape, charge, temperature and surface functionalisation all can affect the physical properties seen when synthesising AuNPs [20-21].

Optical properties are exceptionally evident with AuNPs. This is clearly seen when looking at the colour of AuNPs of different sizes. AuNPS show a range of colours from orange to red to purple as they increase in size from 1 to 100nm [20][22]. As size control during synthesis has become more precise, these optical properties have the potential to become important for therapeutic and diagnostic techniques [23].

Synthesis of AuNPs can be achieved using a variety of methods which can be classified as chemical, biological, and physical. For instance, chemical methods involve the use of a reduction agent in an aqueous medium. Reducing agents include sodium borohydride and citrate [21].

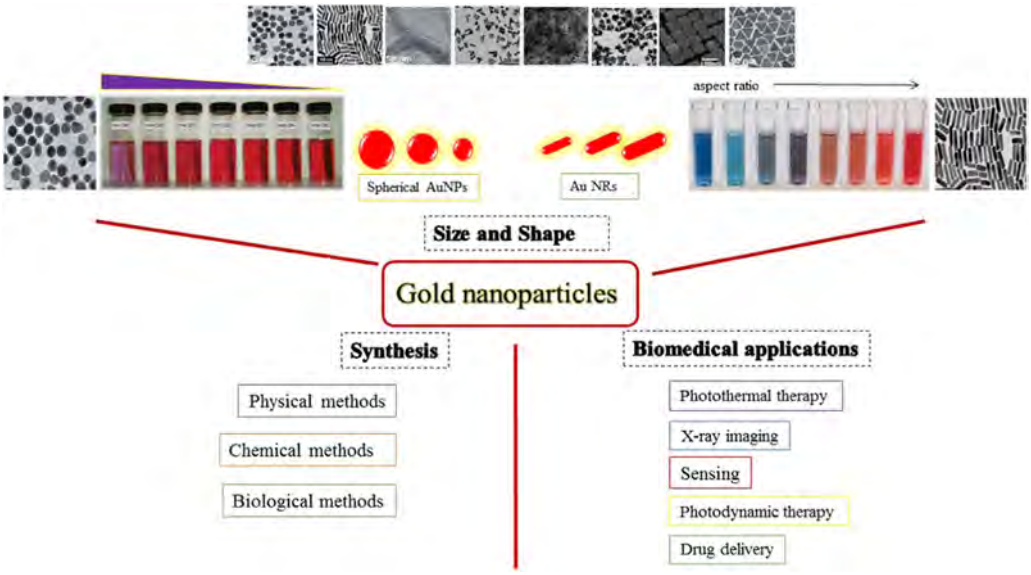

Figure 1.2: *Summary of properties seen for gold nanoparticles, including optical properties, synthesis methods and shape.[24]*

An example of how AuNPs are currently used in the biomedical field is for skin conditions and cancer treatment in the form of Photodynamic Therapy (PDT). AuNPs which show maximum absorption in the visible or near IR region can generate heat and receive light. The death of malignant tumours can result from this heat [19][23]. AuNPs used for PDT are spherical, solid and have a diameter of larger than 50nm. This therapy induces apoptosis and/or necrosis in cancer cells through the activity of free radicals [25][26].

1.3.2 Iron Oxide Nanoparticles (IONPs)

As previously described, inorganic based nanoparticles are nanomaterials and nanoparticles which consist of metals or metal oxides. Iron Oxide nanoparticles fall within this category of nanomaterials. In the past 20-30 years, iron oxide nanoparticles have received a considerable amount of interest. This is demonstrated by the increase in research papers published on the subject.

Iron oxide magnetic nanoparticles (IONPs) have a massive number of potential applications. Within the medical industry they have used, or are considering potential usage, for IONPs in imaging, hyperthermia treatments, drug delivery, atherosclerosis diagnosis, and cancer treatments.

1.4 Comparison of Iron Oxide (IONPs) and Gold (AuNPs) Nanoparticles

Iron oxide nanoparticles and gold nanoparticles both offer an attractive proposition for use within biological research. Here, within, this work iron oxide nanoparticles (IONPs) were chosen for development. This was mainly due to the ability of IONPs to exhibit superparamagnetic behaviour below a critical size and their suitability and previous use as MRI contrast agents. IONPs of both a maghemite (Fe_2O_3) and magnetite (Fe_3O_4) composition have previously demonstrate their ability to be used as potential diagnostic and therapeutic applications [27][28]. AuNPs also exhibit characteristics which make them suitable for use in biological research with unique optical properties such as surface-enhanced luminescence, surface plasmonic resonance (SPR), and surface plasmonic resonance. These characteristics can be tuned for suitability for use during synthesis.

Both AuNPs and IONPs are biocompatible in nature and are chemically stable in physiological conditions. Both can also be functionalised with ease allowing for bio conjugation and ligand targeting within a biological environment [29][30]

IONPs have use for magnetic hyperthermia therapy. This is due to the generation of heat under an alternating magnetic field [31][32][33]. AuNPs have recently been used for *in vivo* photothermal therapy. This therapy is possible when AuNPs, SPR wavelength is in the near-infrared

region (NIR), to avoid body tissues light scattering [34-38].

Whilst both IONPs and AuNPs are suitable for biological research, IONPs ability to exhibit magnetic properties including superparamagnetic behaviour provides for this work the potential for use of nanoparticles as MRI contrast agents and the ability to use magnetism as a way of manipulation location of nanoparticles within a biological behaviour. This characteristic means that for this work IONPs have been chosen for development and will be used throughout.

1.5 Current Uses of Iron Oxide Nanoparticles (IONPs)

Current uses of iron oxide nanoparticles both for research and biological research is extensive. Research into their use as MRI contrast agents, magnetic hyperthermia agents, and for drug delivery is common. This, alongside their potential applications for both diagnosis and treatment for diseases such as cancer, and the interest in their properties from emerging technologies such as gene therapy, make them of extreme interest to the biomedical field.

Outside of biomedicine, IONPs are used in other industries including the technology field as documented in their use in computing.

1.5.1 Iron Oxide Nanoparticles (IONPs) for Cancer Therapy and Diagnostics

The leading cause of death worldwide is still cancer [39]. This is despite the massive advances in diagnosis and treatment and continuing extensive research into the disease.[39][40] Cancer can be summarised as a condition where cells in a specific part of the human body begin to grow and reproduce uncontrollably.

Nanotechnology in general is emerging as an area of interest for both the diagnosis and treatment of cancer. Nanoparticles are seen to bring potential advantages to traditional cancer treatments in terms of better efficacy, less side effects, and protection against the development of drug resistance by patients [40-44].

Iron oxide nanoparticles (IONPs), especially magnetite - (Fe_3O_4) NPs and their magnetic properties, are of immense interest with potential

applications across diagnosis and therapy of many different cancers [39]. This includes their potential and current use as catalysts, MRI contrast agents, magnetic, hyperthermia treatment, and in drug delivery [45-50].

Photoresponsive therapies such as photodynamic and photothermal therapies have the potential to revolutionise cancer treatments (oncotherapy) [51]. This can be seen for example in the combining of Fe_3O_4 NPs with AuNPs. AuNPs are a classic photdynamic agent, but when combined with Fe_3O_4 NPs, the resulting nanocomposite brings the photodynamic effects to MRI, thus allowing for diagnosis and potential treatment combined [52][53]. These nanocomposites can be seen in Figure 1.3, acquired from [53].

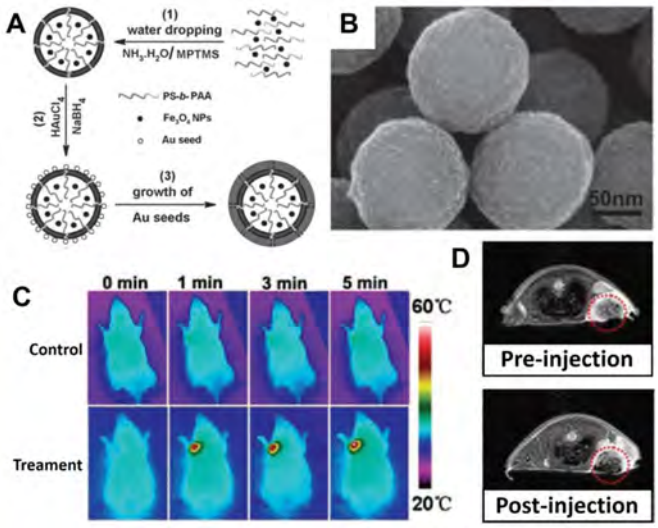

Figure 1.3: *(A) Schematic of Fe_3O_4/Au nanocomposite. (B) SEM images of Fe_3O_4/Au core-shell structure. (C) Thermal imaging effect of Fe_3O_4/Au nanocomposite under 808 nm irradiation. (D) The T2-weighted MRI effect of Fe_3O_4/Au nanocomposite in vivo. Image available from p. Zhao, S., Yu, X., Qian, Y., Chen, W. and Shen, J., 2020. Multifunctional magnetic iron oxide nanoparticles: an advanced platform for cancer theranostics. Theranostics, 10(14), pp.6278-6309 [53].*

Fe_3O_4 NPs offer many advantages for cancer treatment and diagnosis, such as fast clearance from the body combined with a long blood circulation time. They are also known as having excellent efficiency for imaging particular organs, especially the spleen and liver [54][55].

The coating of IONPs with inert materials is often desired for cancer treatments using nanoparticles. These coatings can include mesoporous silica, proteins, and biomoles such as nucleic acids [56][57]. This is often to create hydrophilic NPs, but also to allow for surface medication and improve potential issues with biocompatibility and circulation times [58][59]. The ability to alter the chemistry of the surface as well as attach ligands improves the potential of IONPs in drug delivery during a diagnostic technique such as an MRI, through targeting of cancer cells and then releasing of drugs [60][61].

Chemotherapy is probably the best known non-surgical treatment for cancers. It is, however, a treatment with often dramatic side effects that can result in patient distress [62]. These side effects are often due to the lack of specific targeting of tumours, with chemotherapy also damages healthy cells and tissues [63][64]. Freeman et al. in the 1960s successfully looked at the use of magnetic Fe_3O_4 NPs to guide anti-cancer drugs to the location of the tumour, with the aim of reducing the negative side effects of chemotherapy [65]. Recent interest in gene therapy for cancer treatment is also looking at the use of Fe_3O_4 NPs as nanocomposites with Small interfering RNA (siRNA) attached, although siRNA still shows severe side effect and is clinically limited for use

1.5.2 Iron Oxide Nanoparticles (IONPs) for Magnetic Hyperthermia Treatment

One notable property of Iron oxide nanoparticle (IONPs) is the ability for magnetic properties to be tuned. IONPs are used for the treatment of pathogenic microbes and diseased cells such as cancerous cells. This treatment is called therapeutic hyperthermia treatment. It works due to the excitation of IONPs with an alternating current (AC) magnetic field generating heat due to changes in electromagnetic energy in a localised area [66-75].

This heating is the result of three different mechanisms which can occur on the application of the alternating current [75][76].

- Hysteretic loss and relaxation of the IONPs [77].
- Induction of the magnetic AC inducing eddy current which results in heating [77].
- Interaction between surrounding environment and IONPs causing frictional heating [75].

Gilchrist et al. (1957) were the first to demonstrate IONPs for magnetic hyperthermia treatment in cancers, and in 2004 the first clinical magnetic hyperthermia treatment was developed at the Medical University of Berlin [78][79]. Magnetic hyperthermia treatment is currently used in Europe for the treatment of brain tumours, however it has still not achieved worldwide usage [80].

This lack of usage is attributed to the need for research and development of IONPs for this treatment which currently lack optimisation. The properties under consideration for optimisation for IONPs suitable for this treatment include size, structural properties, effects of magnetic dipole interactions and toxicity. There are also concerns over the instruments used to measure magnetic hyperthermia treatments in terms of their accuracy [66][69][71][81][82].

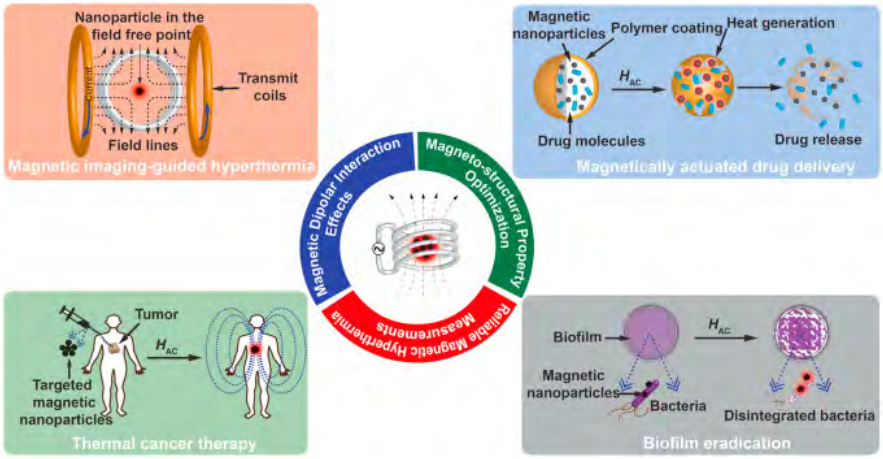

Figure 1.4: *Schematic illustration of parameters to be considered for the efficiency of magnetic hyperthermic treatment along with other biomedical applications. Image acquired from P. Abenojar, E., Wickramasinghe, S., Bas-Concepcion, J. and Samia, A., 2016. Structural effects on the magnetic hyperthermia properties of iron oxide nanoparticles. Progress in Natural Science: Materials International, 26(5), pp.440-448. [75].*

Size of IONPs used for magnetic hyperthermia treatment is of major consideration. The response to an applied AC field changes as size of

IONPs changes. Magnetic IONPs exhibit low saturation magnetization to due internal spin and surface canting effects as well as incomplete coordination of the metal ions.[83-85] Development of Fe_3O_4 (magnetite) has been widely explored, however the limits of Fe_3O_4 nanoparticles, due to the observed low saturation magnetization of bulk magnetite, has also led to other ferrites being researched as potential NPs for this treatment. One example is jacobsite ($MnFe_2O_4$) which shows a higher saturation magnetism than magnetite [86] [87]. One potential method of improving the potential of Fe_3O_4 for this treatment is by changing the shape of the nanoparticles; both nanorods and nanocubes made of Fe_3O_4 have been looked at and found to have a higher magnetic saturation more applicable to hyperthermia treatment as they result in more heat [86-88].

Magnetic hyperthermia treatment has great potential and the effect is now being extended to encompass other application which can utilise the release of heat. These include biofilm inactivation, the production of materials which display a response to heat, and drug delivery where drugs are release in response to heat [89-95].

1.5.3 Iron Oxide Nanoparticles (IONPs) as MRI Contrast Agents

Magnetic resonance imaging (MRI) is a non-invasive commonly used diagnostic tool. This is due to its excellent penetration depth whilst still providing a spatial resolution which is superior to other imaging techniques, and the fact that it does not involve the emission of ionizing radiation [96-101]. Although MRI has become common today there, is still room for improvement in the technique, especially when used at the early stages of disease development where the difference between healthy and diseased tissues can be difficult to determine [98].

Contrast agents can be used during MRI, and these significantly improve imaging. These work by shortening either the longitudinal (T_1) or the transverse (T_2) times of water protons [99][100].

The difference between T_1 and T_2 contrasts agents can be seen in Figure 1.5. T_1 images result in a brighter/positive contrast enhancement whereas T_2 agents cause a dark/negative enhancement [101].

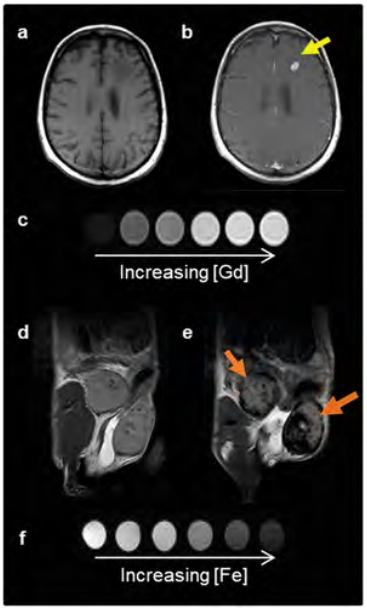

Figure 1.5: *Images show both T1 and T_2 a) Pre- and b) post- GBCA T_1-weighted MRI on a brain metastasis. c) T_1 contrast agents decrease the spin-lattice relaxation time, increasing signal with agent concentration. This produces brighter contrast images. d) Pre- and e) post- IONP-based contrast agent T_2-weighted MRI of mouse mammary gland tumors. f) T_2 contrast agents decrease the spin–spin relaxation time. This decreases signal with increased agent concentration, producing darker contrast images. a,b,d,e) (https://creativecommons.org/licenses/by/4.0/) [84]. Copyright 2017, The Author. Published by Frontiers. c) Reproduced with permission. Copyright 2018, Elsevier Ltd. f) Copyright 2016, Ivyspring International Publisher.*

The only T_1 medically used contrast agents are gadolinium (Gd3+) complexes (GBCAs) [100-105]. This is due to less issues with a phenomenon known as the Blooming effect. This is a long ranged magnetic field which distorts an images background and perturbs neighbouring tissues. This can result in misidentification of contrast agent location and of areas of calcification or bleeding [99][101]. Whilst this is an advantage, GBCAs can have serious side effects for patients including fatal nephrogenic systemic fibrosis.[9-13] and are also associated with issues for some patients clearing GBCAs from the body [106-107].

Iron oxide nanoparticles (IONPs) can be used as a T_2 contrast agent and several have received approval from the FDA, this has been widely studied [99][108][109]. IONPs also have potential as T_1 agents. IONPs are of interest as they have a short transverse relaxation time, have low toxicity and have surfaces which can be functionalised [99][108-110]. Being made of iron also means that IONPS can be metabolised into haemoglobin

providing an effective method of clearance from the body [111-116].

Whilst not widely used clinically, studies have shown IONPs to be of potential benefit. For example a study showed IONPs to be able to delineate healthy liver cells from hepatocellular carcinomas in mice [115][116]. They also have been shown to cause minimal toxicity in larger mammals such as dogs [117].

1.5.4 Iron Oxide Nanoparticles (IONPs) in Computing

The use of nanotechnology in general has had a material impact on the development of many electronic components, transportation, space/aeronautics and hundreds of other areas of everyday life.

In the field of Information Technology, large scale advances in data storage and the field of Very Large Scale Integration (VLSI) could not have been possible without the development and application of nanomaterials, making devices smaller, faster and able to store more data and access it quicker.

The increases in the speed and density of data storage, used in nearly every computational setting, has been driven in part by the development and novel use of nanoparticles and nanomaterials in general. The "bottom up" approach of nanoparticle synthesis is most used in data storage technologies. Allowing the parameters of these materials to be specified during the manufacture, has enabled engineers to push the limits of current data storage devices and to look toward the next generation of such devices/technology [118]. Aggregation of nanoparticles is a common problem in this method of synthesis. However, the use of organic chemicals and long chain hydrocarbons allow for a steric repulsion, reducing aggregation and increasing stability of the nanoparticles.

VLSI is the process of the design and manufacture of integrated circuits, more specifically microprocessors and other supporting components. It has been shown that Magnetotactic bacteria can be used to manipulate nanoparticles as part of the fabrication process in microprocessor and other VLSI applications [119].

Nanowires are also commonplace in VLSI also commonly using "top down" approach to synthesis. However, development and research into using a "bottom up" approach to synthesis, using vapour and solution phases to limit aggregation and provide an accurate and repeatable

manufacturing process is ongoing and seen as a necessity in the continued reduction size of the VLSI fabrication processes [120].

All of these applications of nanotechnology and nanomaterials are simply more advanced versions of techniques and processes dating back to the 1960's but they are the foundations of new advances in the field. Research and development in the fields of Carbon Nanotube computing, Quantum Computing, Nanoscale Computing Devices, Nanorobots and DNA Computing are ongoing and are moving closer to being industrialised [121][122].

1.6 Nanoparticle Nucleation and Growth

Nanoparticle nucleation is classically described through LaMer burst nucleation and growth by Ostwald ripening [123-125].

Iron ions when in solution usually form a hexahydrated ion which is dependent on both pH and oxidative state to undergo a hydroxylation reaction. At room temperature Fe(III) requires a pH of between 1 and 4.5 to undergo a hydroxylation reaction whereas Fe(II) requires a pH of 7-9.

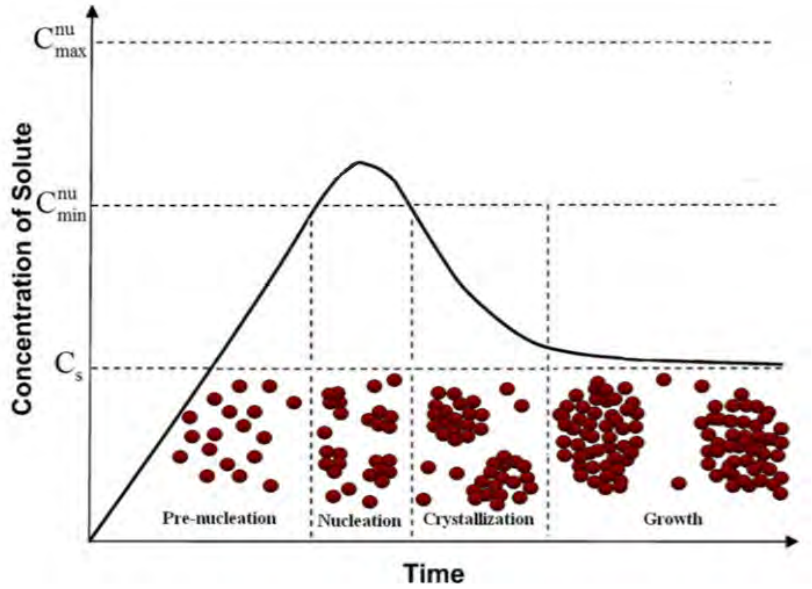

Figure 1.6: *LaMers theory explains nucleation of nanoparticles in terms of concentration of precursor solvent and its behaviour before and after it reaches a critical level.*

Figure 1.6 shows a generalised LaMer diagram as proposed by LaMer an Dinegar [123]. This graph illustrate how particles which are mon-

odispersed are formed in a homogeneous solution. It can be seen that there is a critical level for concentration of precursor , C_s, at which point nucleation occurs (C_{min}). Nucleation continues until C_{max} occurs. This is the point when precursor solute supply is outpaced by the consumption rate of nucleation and growth. This results in the graph curve declining. When the decline once more is at the critical level of C_s nucleation finishes. Growth will then continue below the critical level resulting in precursor solute still declining [126].

When these steps are distinct the nucleation process theoretically yields monodispersed particles.[127] This theory successfully describes the kinetic formation of nanoparticles and accounts for the diffusion of ion, particles etc. [125][128][129].

Classically growth is attributed to Ostwald ripening [130]. Growth occurs as a result of a change in solubility of NPs which is dependent on size. This dependency is described by the Gibbs-Thomson relationship as seen in the following equation:

$$C_r = C_b \exp\left(\frac{2\gamma v}{r k_B T}\right)$$

Given that small particles have high surface energy and solubility within a solution, small particles redissolve and this in turn allows larger particles to continue to grow [131][132]. This occurs via an intermediate mobile species [133].

Lee et al. described the opposite of Ostwald ripening, which is known as digestive ripening. Here, smaller particles grow at the expense of particles of a bigger size dissolving. This process is again controlled by the surface energy [134].

Alongside research aiming to further understand nucleation and growth of nanoparticles, current research is occurring to investigate how to control and when needed stop Ostwald ripening. This often involves controlling factors relating to synthesis methods [135][136].

1.7 Superparamagnetism

Magnetic iron oxide NPs have distinctive magnetic properties with size being the property with the most effect on magnetism [137-142].

Normally magnetite Fe_3O_4 NPs, have ferrimagnetic properties when

in in bulk and were found by Wu et al. (2015) to have high magnetization saturation, Ms of 92 emu/g at room temperature and a high Curie temperature, Tc of 577°C. This magnetism is, however determined, by size [137][143].

Magnetite (Fe_3O_4) NPs below approximately 20nm show superparamagnetism and are of interest due to the magnetic properties of superparamagnetism, low Curie temperature and no coercivity [142][144]. Superparamagnetic Fe_3O_4 NPS show high magnetic susceptibility and only one magnetic domain. This allows for a fast and strong magnetic response to a magnetic field [145][146].

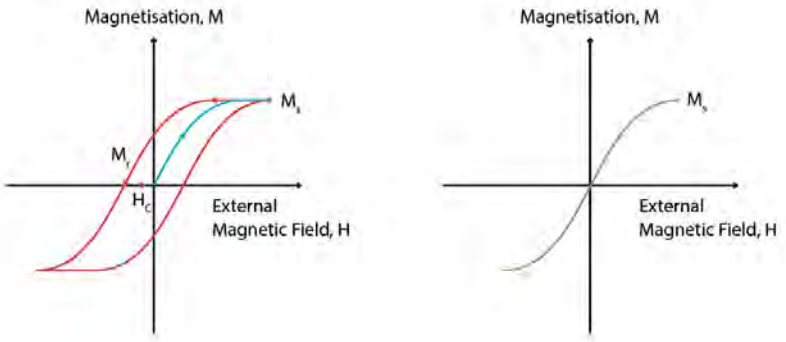

Figure 1.7: *Superparamagnetic Fe_3O_4 nanoparticles are different to ferrimagnetic particles. They do not exhibit coercivity or a hysteresis loop as ferrimagnetic particles do as seen here due to single-domain magnetism. This change occurs at approximately 20nm and below. This means they can only be magnetized in the presence of external magnetic field [147][148.]*

Ferrimagnetic materials have multi-domain magnetism as size of Fe_3O_4 NPs reduce in size this changes to a single domain. Coercivity increases as size decreases until a critical size is reached. At the peak of coercivity, all magnetic spins are in the same direction; this improves the magnetic properties and causes the magnetic NPs to become very difficult to demagnetise as a result of the high coercivity [147]. If nanoparticle size, however, is below this point, a reduction of coercivity is seen until, as size continues to reduce, a coercivity of zero is reached. It is when the coercivity reaches zero that the NPs are considered to be superparamagnetic. Superparamagnetism is exhibited below the critical size of 20nm [149-151]. Superparamagnetic NPs are only magnetic when magnetised by magnetic field [146]. They do however exhibit a stronger and faster

response to a magnetic field and therefore are of extreme interest to the biomedical field [147]. Superparamagnetic iron oxide nanoparticles are known as SPIONs [137].

1.8 Design of Multi functional Silica Coated Iron Oxide Nanoparticles for Biological Purposes.

Nanoparticle design involves considerations of many questions. These include what are the nanoparticles for? What material should be used? Is a coating needed? What size is required? [152]

These questions however are but a starting point. In the case of iron oxide nanoparticles as indeed with most other nanoparticles not discussed here, it is only the beginning of questions to be asked [152].

Firstly, when considering iron oxide nanoparticles, it is necessary to decide which iron oxide is required, most often this will be one of 3 oxides magnetite (FeFe), maghemite (γ-Fe_2O_3) or hematite (α-Fe_2O_3) [152][153]. Iron oxide below 20nm are superparamagnetic therefore design should consider if this is a requirement when determining size of nanoparticle [154][155]. The synthesis method should then be considered.

Use considerations especially if for use in biological environments should be considered at this point, do nanoparticles need to non cytotoxic, do they need to be coated in an inert material to achieve this? If yes how can this be achieved. If using the property of superparamagnetism do the cores need to be single or can multiple cores be coated in one nanoparticle? This is often determined by how important it is to understand the magnetic forces experience by an individual nanoparticle such as during a tethered particle assay or for the manipulation of location of cell components.

Shape of nanoparticles effect characteristics immensely due to change in crystal facets and there atomic arrangement [156]. Nanomaterials including iron oxide nanoparticles can be synthesised to be many shapes as seen in Figure 1.8. This image shows a variety of shapes including spherical, nanorods and nanosheets [157]. Shape of nanoparticles is important for nanoparticles to be used in a biological environment. Examples of how nanoparticle shape can effect behaviour are effective binding within a cell and tumour penetration [158]. For example research has shown

elongated rod-shaped particles provide greater binding ability *in vitro* than spherical shaped nanoparticles [158].

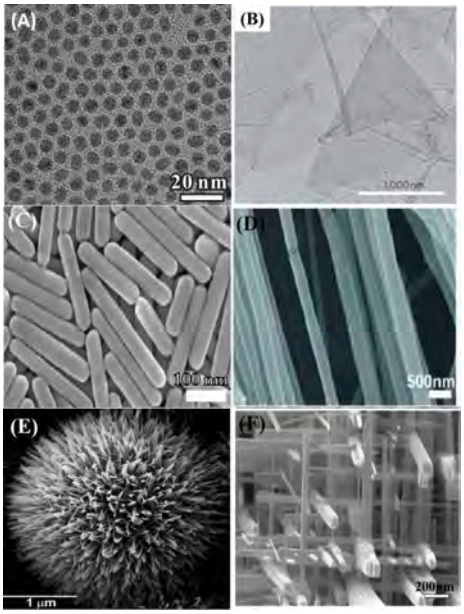

Figure 1.8: *Varying morphologies of iron oxide nanoparticles can effect the exhibited behaviour and properties of nanomaterials such as binding within a cell and tumour penetration: (A) nonporous Pd NPs (0D), copyright Zhang et al.; licensee Springer, 2012, (B) Graphene nanosheets (2D), copyright 2012, Springer Nature, (C) Ag nanorods (1D) [3], copyright 2011, American Chemical Society, (D) polyethylene oxide nanofibers (1D), copyright 2010 [157].*

Nanoparticles can be synthesised as desired by many different methods including sol-gel, solvothermal, co precipitation and pyrolysis amongst others. All of these methods have pros and cons, and all allow for manipulation of properties by changing often small variables such as temperature, pH and time [159].

Surface functionalisation is next to be considered do NPs need certain functional groups or ligands attached? Are the NPs going to be imaged and therefore need the addition of fluorophores? These questions are but a few, others include factors that effect how are nanoparticles to be incorporated in the biological environment they are intended for [159].

Finally, consideration must be given to are the nanoparticles once produced suitable for the environment intended for and their effect upon that environment. Are they cytotoxic? Do they aggregate? If aggregation is seen can the use of polymers reduce this?

Perhaps of less interest but often just as important are variables such

as time to synthesise, cost and reproducibility. Time must be given to the design process with careful thought and consideration to many variables that can be changed as well as the intended use [152].

1.8.1 Cytotoxicity

Superparamagnetic iron oxide nanoparticles (SPIONs), whilst of interest for the cell biology and biomedicine fields, do present potential concerns with regards to potential cytotoxic effects. These are due to IONP induced oxidative stress. This oxidative stress is the result of the release of Fe^{2+} ions due to an acidic environment into a cells cytoplasm or lysosomes [160][161]. The result of Fe^{2+} being released can be an inflammatory response of DNA damage as a consequence of the Fenton reaction, resulting in the generation of reactive oxygen species (ROS) [162].

Under normal body conditions, the body can control the internal concentration of iron. This, however, can be disrupted when IONPs are introduced. This is due to their ability to diffuse directly into the labile iron pool by means of the phagosome to lysosome route. This can lead to IONPs overloading important regulatory proteins and result in an increase in ROS generation in the mitochrodra [163][164]. The generation of ROS is normally low enough to be neutralised by antioxidant enzymes and glutathione (GSH) [163]. Oxidative stress is said to occur when the oxidise glutathione to GSH ratio is low and results in a response that causes injury or protective response in cells [163-168]. High ROS levels can lead to cell injury and apoptosis [168].

Research into the cytotoxicity of IONPS due to ROS is necessary with the monitoring and measurement of biological markers such as reduced GSH and antioxidant enzymes, including glutathione transferase, glutathione peroxidase and catalase, levels [169][170]. Studies have evaluated that the cytotoxicity is due to the release of Fe^{2+} ions, and have also shown that uncoated IONPs cause high levels of oxidative stress in rats [170][171]. It has also been shown that SPIONs, due to their smaller size, exhibit higher levels of cytotoxicity [172-174].

As well as size it has been shown that surface area, pH, shape, charge, and coating can all have an effect on cytotoxic behaviour [175-177]. For example, nanorods with a smaller surface area than spherical nanoparticles have been shown to exhibit more toxicity [175].

One potential method of reducing the cytotoxicity seen from IONPs

is the addition of a coating. This could be many different materials, however common and well researched coatings include, Dextran, poly(ethylene)glycol (PEG), silica, and Polyvinyl Alcohol (PVA) [160].

Dextran is FDA approved and demonstrates no signs of inflammation, or cytotoxicity at a concentration of 11.3 μg/mL [160]. PEG reduces cell or protein interactions with IONPs and allows other properties such as magnetism to be unaffected by coating [178]. Silica is cheap, biocompatible and is very tolerant to pH change [179][180]. It effectively reduces the release of Fe^{2+} ions and lowers the rate of excretion and metabolism making it a very good coating candidate [179-181]. Finally, PVA provides SPIONs with amino or carboxyl groups. Both of these functional groups can regulate the charge of the coating and allow for easy attachment of other entities such as proteins, antibodies, and peptides [182]. PVA has been shown to be non-toxic in mouse studies. When injected into a mouse knee no immune response was seen even with a concentration of 24 μg of Fe per knee [183].

Whilst the productive of ROS and the resulting cytotoxicity is a concern and one that must be evaluated and avoided when using SPIONs, it has been shown that this is possible. It can also be said that with adjustment, the benefits of SPIONs outweigh the potential risk [184].

1.9 Characterisation Techniques Of Nanoparticles

Nanoparticles' characterisation is necessary to the understanding and measurement of nanoparticle properties [185]. There are many techniques associated with nanoparticle characterisation. The use of these provides information regarding size, composition, charge, structure, shape amongst others. The techniques described below are the most common techniques which are considered essential for basic characterisation of nanoparticles.

1.9.1 Transmission Electron Microscopy (TEM) Scanning Electron Microscopy (SEM)

Transmission electron microscopy (TEM) involves the use of a high energy beam of electrons which is shone through a thin sample. The resulting interactions between atoms and electrons allow for imaging. This type

of microscopy works in a similar way to light microscopy using the same basic principles, however electrons have a smaller wavelength to light. This results in the resolution being orders of magnitudes higher than light microscopy. TEM provides high resolution images which can be used to observe and analyse features such as size and shape. Samples to be analysed using TEM must be thin as to allow the transmission of enough electrons whilst suffering minimum energy loss to form an image therefore for nanoparticles imaging sample preparation is important and should be always considered [185][186].

Like TEM, Scanning electron microscopy (SEM) uses a high energy focused beam of electrons. This generates signal this time at the surface of the sample. SEM can be used for analysis of properties including morphology, structure and chemical composition [187].

Both TEM and SEM can be used for characterisation of nanoparticles. The main difference is that TEM result in 2D images and SEM in 3D images. TEM images often require further interpretation.

TEM however is capable of a much higher resolution than SEM, with SEM often being limited to particles bigger than 50nm. This does not necessarily mean that TEM is the "better" technique for nanoparticle research. The choice is dependent on what properties are of most interest.

It should also be noted that sample preparation is often a more time consuming activity for TEM than SEM and the need for a sample to dry for TEM can cause aggregation of nanoparticles [188].

1.9.2 Dynamic Light Scattering

Dynamic Light Scattering (DLS) is the de facto imaging and analysis technique used for determining the size of nanoparticles while in suspension. This technique is also referred to as "photon correlation spectroscopy" [189]. DLS uses a light source, normally a laser, directed at a sample (for example, proteins, colloids, nanoparticles, etc.), creating Brownian motion which is picked up by a number of detectors. The signals from the detectors is then passed to a digital signal processor, this can be a stand alone or an embedded computer built into the DLS system, which runs a correlation algorithm to determine the different sizes of particles in the sample, as seen in Figure 1.9 [190].

While DLS has become the commonly accepted standard for imaging and sizing nanoparticles, it is not without its problems. DLS meas-

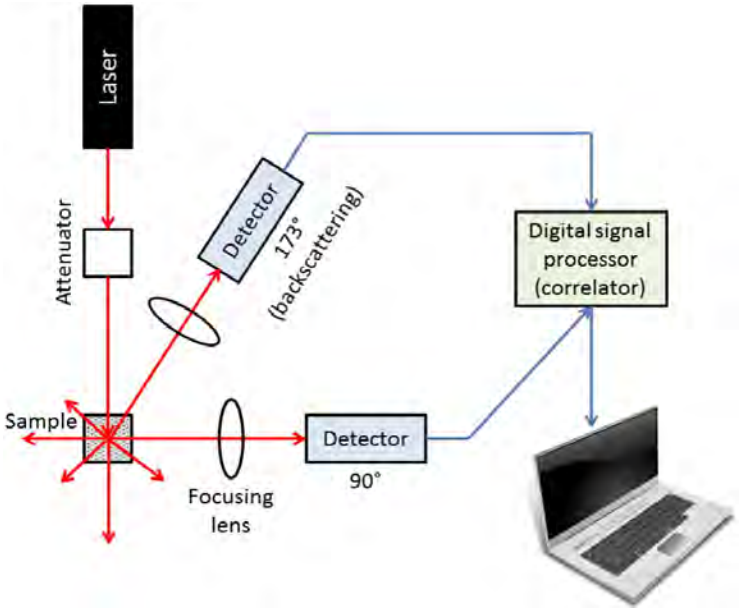

Figure 1.9: *Schematic of typical DLS instrument. Image courtesy of Sourav Bhattacharjee, DLS and zeta potential – What they are and what they are not?, Journal of Controlled Release, Volume 235, 2016, Pages 337-351,ISSN 0168-3659, https://doi.org/10.1016/j.jconrel.2016.06.017. (https://www.sciencedirect.com/science/article/pii/S0168365916303832)[190].*

urements can be affected by a number of factors. Preparation of the sample is a primary factor in determining the accuracy of measurements. Samples are normally prepared in solvents or diluents and need to be, as Bhattacharjee (2016) describes, "clear, homogeneous and without haze" [190]. However some of these solvents can scatter light in such a way that introduces large amounts of background noise, change the viscosity of the sample or it's temperature, which can also effect measurements [191]. Coloured and fluorescent samples should be avoided as this can influence or reduce the amount of light that is scattered, absorbed by the flurophores and will artificially reduce the measured size of the NPs in the sample.

DLS instruments will report a number of measurements; the two that are commonly used are Z-Average and Polydispersity Index (PDI). The Z-average provides a mean value for the size or particles in the sample, while the PDI measures the distribution of particles size [164] within a range of 0.0 and 1.0. In order to ensure a more accurate measurement of Z-average it is important to ensure that the concentration of the sample is within the accepted limits for the sample type, for example polymers should have a PDI of 0.2 or below, while NPs should have a PDI of between 0.4

and 0.6. A higher concentration of NPs can lead to aggregation making measurements difficult to obtain at all, or the extreme scattering of light causing measurements to be smaller than would be observed in a lower concentration of the same NPs [192][193].

There are only a few techniques which can determine the size of NPs within a solution. DLS measures the hydrodynamic size of particles. Hydrodynamic size can be defined as the diameter of a hard sphere that diffuses at the same speed as the particle or molecule being measured.

This is a measurement of size determined by how particles diffuse in a liquid. It is often larger than size determined by techniques such as TEM and SEM. DLS measures the speed of particles undergoing Brownian motion. This allows measurement of size due to larger particles causing slower Brownian motion than smaller particles [192].

The speed of Brownian motion is also influenced by other factors, including viscosity and temperature. DLS can also be used to measure surface charge via zeta potential and also provide a polydispersity index which is a measurement of the width of the overall distribution of the particles measured [192].

1.10 Conclusion

Nanoscience and nanotechnology have applications in many different areas of science, such as computing. Nanoparticles for biological research and biomedicine have great potential that are as yet not being fully exploited. Many factors need to be considered when designing and synthesising nanoparticles for any biological use. These include materials used, the use of coatings, whether magnetic properties are required, the ability to visualise whilst imaging and the surface chemistry of the nanoparticles. All these factors must be assessed according to need. Thorough characterisation of nanoparticles is needed to ensure their suitability for a desired task and for evaluation of safety when performing that task.

There are many different types of nanomaterials with a vast range of materials, size, shape and chemical and physical properties. Superparamagnetic multi functional silica coated nanoparticles are of great interest showing great potential for future use in biomedicine and biological research as they are suitable for use in a biological environment

and can be synthesised to perform many different tasks. This is due to their biocompatability and the ability to tune their size, shape, charge and surface chemistry. These uses include but are not limited to imaging as MRI contrast agents, cancer diagnosis and therapy,drug delivery, bioconjugation/targeting and gene therapy

1.11 Aims and Objectives of the PhD

To design and synthesis nanoparticles suitable for use within a biological environment. The nanoparticles should display characteristics which can be tuned for multiple uses and consider cost and ease of synthesis. This required the design and synthesis of silica coated superparamagnetic iron oxide nanoparticles. This was to involve synthesis of iron oxide NPs using a new novel oleylamine protocol, alongside other potential methodologies, and subsequently coating of these iron oxide cores with silica by multiple methodologies to decide which resulted in nanoparticles with a single core and an even coating of silica. This was followed by full characterisation of the resulting nanoparticles and investigation of their reproducibility and cost. The magnetic properties of the nanoparticles was to be measured and the effect of silica coating evaluated.

Once designed and synthesised the behaviour and ability to incorporate the nanoparticles within a biological environment was to be carried out. This included methods of incorporation of nanoparticles in cells and further development of surface functionalisation with polymers. We also looked at the storage and aggregation of nanoparticles over time. This provides new information regarding the storage of nanoparticles and the potential behaviour in biological environments which are mimic-ed by the buffer solutions. The specific aims were:

- To design nanoparticles suitable for use in a biological environment which could be functionalised for use in both medicine and research
- To create a simple, cheap and reproducible method of synthesis for fully functionalised silica coated superparamagnetic iron oxide nanoparticles. The nanoparticles should have the ability to add functional groups to the surface, be single cored, magnetic and able to be visualised through the use of fluorescent dyes
- Comparison of commercially available nanobeads for biological research with nanoparticles synthesised for this body of work
- To develop and perform synthesis protocols for iron oxide nanoparticles including a novel approach to synthesis using oleylamine
- To develop and perform synthesis protocols for silica coating of iron oxide nanoparticles which ensure even coating for which diameter

can be controlled

- To develop and perform surface functionalisation of silica coated iron oxide nanoparticles with both amine groups and fluorescent dye
- Incorporation of nanoparticles into cells by multiple routes including micro injection and endocytosis
- Use of surface functionalisation to add polymers to the surface of nanoparticles
- To carry out statistical analysis of the effect of adding multiple different polymers onto the nanoparticles surface in terms of size and aggregation by DLS
- To carry out statistical analysis of the effect of adding multiple different polymers onto the nanoparticles surface in terms of size and aggregation by DLS when stored in different buffers.
- To carry out characterisation of nanoparticles using multiple analytical techniques such as TEM, XRD, DLS, VSM and FTIR
- To determine the magnetic properties of the iron oxide nanoparticle with and without silica coating using an analytical technique.
- To bind nanoparticles to a DNA tether within a flow cell for *in vitro* to allow for future research using the magnetic properties of synthesised nanoparticles
- To visualise nanoparticles using standard light microscopy nanoparticles in cells and the effect of time on the ability to visualise the fluorescent dye functionalised nanoparticles.

1.12 References - Introduction

1. S. Bayda, M. Adeel, T. Tuccinardi, M. Cordani and F. Rizzolio, Molecules, 2019, 25, 112.
2.N. Xia, T. Hunt, B. Mayers, E. Alsberg, G. Whitesides, R. Westervelt and D. Ingber, Biomedical Microdevices, 2006, 8, 299-308.
3. J. Jeevanandam, A. Barhoum, Y. Chan, A. Dufresne and M. Danquah, Beilstein Journal of Nanotechnology, 2018, 9, 1050-1074.
4. M. Hochella, M. Spencer and K. Jones, Environmental Science: Nano, 2015, 2, 114-119.
5. V. Sharma, J. Filip, R. Zboril and R. Varma, Chemical Society Reviews, 2015, 44, 8410-8423.
6. S. Wagner, A. Gondikas, E. Neubauer, T. Hofmann and F. von der Kammer, Angewandte Chemie International Edition, 2014, n/a-n/a.
7. A. Pugazhendhi, T. Edison, I. Karuppusamy and B. Kathirvel, International Journal of Pharmaceutics, 2018, 539, 104-111.
8. J. Ma, A. L. Porter and T. M. Aminabhavi, Pharmaceutical Nanotechnology, 2016, 4, 293-307.
9. K. Parveen, V. Banse and L. Ledwani, AIP Conference Proceedings, 2016.
10. Z. Fan, M. Shelton, A. Singh, D. Senapati, S. Khan and P. Ray, ACS Nano, 2012, 6, 1065-1073.
11. K. MG, K. V and H. F, Journal of Nanomedicine amp; Nanotechnology, 2015, 06.
12. V. Torchilin, Pharmaceutical Research, 2006, 24, 1-16.
13. A. Wang, F. Gu, L. Zhang, J. Chan, A. Radovic-Moreno, M. Shaikh and O. Farokhzad, Expert Opinion on Biological Therapy, 2008, 8, 1063-1070.
14. M. Daniel and D. Astruc, Chemical Reviews, 2003, 104, 293-346.
15. Z. Zhang, J. Wang, X. Nie, T. Wen, Y. Ji, X. Wu, Y. Zhao and C. Chen, Journal of the American Chemical Society, 2014, 136, 7317-7326.
16. Y. Zhang, W. Chu, A. Foroushani, H. Wang, D. Li, J. Liu, C. Barrow, X. Wang and W. Yang, Materials, 2014, 7, 5169-5201.
17. Y. Zhou, C. Wang, Y. Zhu and Z. Chen, Chemistry of Materials, 1999, 11, 2310-2312.
18. Y. Zhang, J. Qian, D. Wang, Y. Wang and S. He, Angewandte Chemie, 2012, 125, 1186-1189.

19. E. Yeo, J. Cheah, D. Neo, W. Goh, P. Kanchanawong, K. Soo, P. Thong and J. Kah, Journal of Materials Chemistry B, 2017, 5, 254-268.
20. Y. Yeh, B. Creran and V. Rotello, Nanoscale, 2012, 4, 1871-1880.
21. Z. Yang, Z. Li, X. Lu, F. He, X. Zhu, Y. Ma, R. He, F. Gao, W. Ni and Y. Yi, Nano-Micro Letters, 2016, 9.
22. M. Yang, Y. Liu, W. Hou, X. Zhi, C. Zhang, X. Jiang, F. Pan, Y. Yang, J. Ni and D. Cui, Nanoscale, 2017, 9, 334-340.
23. E. Yan, M. Cao, Y. Wang, X. Hao, S. Pei, J. Gao, Y. Wang, Z. Zhang and D. Zhang, Materials Science and Engineering: C, 2016, 58, 1090-1097.
24. N. Elahi, M. Kamali and M. Baghersad, Talanta, 2018, 184, 537-556.
25. J. Narang, N. Malhotra, G. Singh and C. Pundir, Biosensors and Bioelectronics, 2015, 66, 332-337.
26. C. Murphy, L. Thompson, A. Alkilany, P. Sisco, S. Boulos, S. Sivapalan, J. Yang, D. Chernak and J. Huang, The Journal of Physical Chemistry Letters, 2010, 1, 2867-2875.
27. N. Lee, D. Yoo, D. Ling, M. Cho, T. Hyeon and J. Cheon, Chemical Reviews, 2015, 115, 10637-10689.
28. R. Revia and M. Zhang, Materials Today, 2016, 19, 157-168.
29. R. Stover, A. Murthy, S. Gourisankar, G. Nie, M. Martinez, T. Truskett, K. Sokolov and K. Johnston, SPIE Proceedings, 2014.
30. T. Zhou, B. Wu and D. Xing, J. Mater. Chem., 2012, 22, 470-477.
31. R. Ghosh, L. Pradhan, Y. Devi, S. Meena, R. Tewari, A. Kumar, S. Sharma, N. Gajbhiye, R. Vatsa, B. Pandey and R. Ningthoujam, Journal of Materials Chemistry, 2011, 21, 13388.
32. R. Araújo-Neto, E. Silva-Freitas, J. Carvalho, T. Pontes, K. Silva, I. Damasceno, E. Egito, A. Dantas, M. Morales and A. Carriço, Journal of Magnetism and Magnetic Materials, 2014, 364, 72-79.
33. E. Múzquiz-Ramos, V. Guerrero-Chávez, B. Macías-Martínez, C. López-Badillo and L. García-Cerda, Ceramics International, 2015, 41, 397-402.
34. A. Espinosa, M. Bugnet, G. Radtke, S. Neveu, G. Botton, C. Wilhelm and A. Abou-Hassan, Nanoscale, 2015, 7, 18872-18877.
35. Y. Gao, Y. Li, J. Chen, S. Zhu, X. Liu, L. Zhou, P. Shi, D. Niu, J. Gu and J. Shi, Biomaterials, 2015, 60, 31-41.
36. J. Choi, J. Yang, E. Jang, J. Suh, Y. Huh, K. Lee and S. Haam, Anti-Cancer Agents in Medicinal Chemistry, 2011, 11, 953-964.
37. J. Li, Y. Hu, J. Yang, P. Wei, W. Sun, M. Shen, G. Zhang and X.

Shi, Biomaterials, 2015, 38, 10-21.
38. Z. Fan, M. Shelton, A. Singh, D. Senapati, S. Khan and P. Ray, ACS Nano, 2012, 6, 1065-1073.
39. I. El-Sherbiny, N. Elbaz, M. Sedki, A. Elgammal and M. Yacoub, Nanomedicine, 2017, 12, 387-402.
40. S. Zhao, X. Yu, Y. Qian, W. Chen and J. Shen, Theranostics, 2020, 10, 6278-6309.
41. S. Yen, P. Padmanabhan and S. Selvan, Theranostics, 2013, 3, 986-1003.
42. J. Ni, Y. Li, W. Yue, B. Liu and K. Li, Theranostics, 2020, 10, 1923-1947.
43. L. Pradhan, B. Thakur, R. Srivastava, P. Ray and D. Bahadur, Theranostics, 2016, 6, 1557-1572.
44. H. Ke, J. Wang, S. Tong, Y. Jin, S. Wang, E. Qu, G. Bao and Z. Dai, Theranostics, 2014, 4, 12-23.
45. K. Gilroy, A. Ruditskiy, H. Peng, D. Qin and Y. Xia, Chemical Reviews, 2016, 116, 10414-10472.
46. N. Lee, D. Yoo, D. Ling, M. Cho, T. Hyeon and J. Cheon, Chemical Reviews, 2015, 115, 10637-10689.
47. M. Wu and Y. Yang, Advanced Materials, 2017, 29, 1606134.
48. P. Chandrasekharan, Z. Tay, D. Hensley, X. Zhou, B. Fung, C. Colson, Y. Lu, B. Fellows, Q. Huynh, C. Saayujya, E. Yu, R. Orendorff, B. Zheng, P. Goodwill, C. Rinaldi and S. Conolly, Theranostics, 2020, 10, 2965-2981.
49. C. Fan, Y. Cheng, C. Ting, Y. Ho, P. Hsu, H. Liu and C. Yeh, Theranostics, 2016, 6, 1542-1556.
50. H. Jin, Y. Qian, Y. Dai, S. Qiao, C. Huang, L. Lu, Q. Luo, J. Chen and Z. Zhang, Theranostics, 2016, 6, 2000-2014.
51. R. Ge, X. Li, M. Lin, D. Wang, S. Li, S. Liu, Q. Tang, Y. Liu, J. Jiang, L. Liu, H. Sun, H. Zhang and B. Yang, ACS Applied Materials amp; Interfaces, 2016, 8, 22942-22952.
52. Y. Hu, Y. Zhou, N. Zhao, F. Liu and F. Xu, Small, 2016, 12, 2459-2468.
53. S. Zhao, X. Yu, Y. Qian, W. Chen and J. Shen, Theranostics, 2020, 10, 6278-6309.
54. O. Veiseh, J. Gunn and M. Zhang, Advanced Drug Delivery Reviews, 2010, 62, 284-304.
55. L. Reddy, J. Arias, J. Nicolas and P. Couvreur, Chemical Reviews,

2012, 112, 5818-5878.
56. M. Rippe, M. Michelas, J. Putaux, M. Fratzl, G. Eslava, N. Dempsey, R. Auzély-Velty and A. Szarpak, Applied Surface Science, 2020, 510, 145354.
57. I. Almstätter, O. Mykhaylyk, M. Settles, J. Altomonte, M. Aichler, A. Walch, E. Rummeny, O. Ebert, C. Plank and R. Braren, Theranostics, 2015, 5, 667-685.
58. J. Zhao, Z. Zhang, Y. Xue, G. Wang, Y. Cheng, Y. Pan, S. Zhao and Y. Hou, Theranostics, 2018, 8, 6307-6321.
59. S. Zhao, X. Yu, Y. Qian, W. Chen and J. Shen, Theranostics, 2020, 10, 6278-6309.
60. K. Ulbrich, K. Holá, V. ?ubr, A. Bakandritsos, J. Tu?ek and R. Zbo?il, Chemical Reviews, 2016, 116, 5338-5431.
61. K. Ulbrich, K. Holá, V. ?ubr, A. Bakandritsos, J. Tu?ek and R. Zbo?il, Chemical Reviews, 2016, 116, 5338-5431.
62. B. Weir, M. Woo, G. Getz, S. Perner, L. Ding, R. Beroukhim, W. Lin, M. Province, A. Kraja, L. Johnson, K. Shah, M. Sato, R. Thomas, J. Barletta, I. Borecki, S. Broderick, A. Chang, D. Chiang, L. Chirieac, J. Cho, Y. Fujii, A. Gazdar, T. Giordano, H. Greulich, M. Hanna, B. Johnson, M. Kris, A. Lash, L. Lin, N. Lindeman, E. Mardis, J. McPherson, J. Minna, M. Morgan, M. Nadel, M. Orringer, J. Osborne, B. Ozenberger, A. Ramos, J. Robinson, J. Roth, V. Rusch, H. Sasaki, F. Shepherd, C. Sougnez, M. Spitz, M. Tsao, D. Twomey, R. Verhaak, G. Weinstock, D. Wheeler, W. Winckler, A. Yoshizawa, S. Yu, M. Zakowski, Q. Zhang, D. Beer, I. Wistuba, M. Watson, L. Garraway, M. Ladanyi, W. Travis, W. Pao, M. Rubin, S. Gabriel, R. Gibbs, H. Varmus, R. Wilson, E. Lander and M. Meyerson, Nature, 2007, 450, 893-898.
63. M. Stratton, P. Campbell and P. Futreal, Nature, 2009, 458, 719-724.
64. E. Green and M. Guyer, Nature, 2011, 470, 204-213.
65. L. Wu, A. Mendoza-Garcia, Q. Li and S. Sun, Chemical Reviews, 2016, 116, 10473-10512.
66. Y. Jun, J. Seo and J. Cheon, Accounts of Chemical Research, 2008, 41, 179-189.
67. M. Mahmoudi, S. Sant, B. Wang, S. Laurent and T. Sen, Advanced Drug Delivery Reviews, 2011, 63, 24-46.
68. A. Hervault and N. Thanh, Nanoscale, 2014, 6, 11553-11573.
69. S. Laurent, D. Forge, M. Port, A. Roch, C. Robic, L. Vander Elst

and R. Muller, Chemical Reviews, 2008, 108, 2064-2110.
70. K. Krishnan, IEEE Transactions on Magnetics, 2010, 46, 2523-2558.
71. A. Kolhatkar, A. Jamison, D. Litvinov, R. Willson and T. Lee, International Journal of Molecular Sciences, 2013, 14, 15977-16009.
72. E. Lim, T. Kim, S. Paik, S. Haam, Y. Huh and K. Lee, Chemical Reviews, 2014, 115, 327-394.
73. O. Veiseh, J. Gunn and M. Zhang, Advanced Drug Delivery Reviews, 2010, 62, 284-304.
74. E. Périgo, G. Hemery, O. Sandre, D. Ortega, E. Garaio, F. Plazaola and F. Teran, Applied Physics Reviews, 2015, 2, 041302.
75. E. Abenojar, S. Wickramasinghe, J. Bas-Concepcion and A. Samia, Progress in Natural Science: Materials International, 2016, 26, 440-448.
76. N. Lee, D. Yoo, D. Ling, M. Cho, T. Hyeon and J. Cheon, Chemical Reviews, 2015, 115, 10637-10689.
77. A. GIUSTINI, A. PETRYK, S. CASSIM, J. TATE, I. BAKER and P. HOOPES, Nano LIFE, 2010, 01, 17-32.
78. R. GILCHRIST, R. MEDAL, W. SHOREY, R. HANSELMAN, J. PARROTT and C. TAYLOR, Annals of Surgery, 1957, 146, 596-606.
79. U. Gneveckow, A. Jordan, R. Scholz, V. Brüß, N. Waldöfner, J. Ricke, A. Feussner, B. Hildebrandt, B. Rau and P. Wust, Medical Physics, 2004, 31, 1444-1451.
80. Magforce.de, 2022.
81. G. Liu, J. Gao, H. Ai and X. Chen, Small, 2012, 9, 1533-1545.
82. S. Kwon and T. Hyeon, Small, 2011, 7, 2685-2702.
83. M. Morales, C. Serna, F. Bødker and S. Mørup, Journal of Physics: Condensed Matter, 1997, 9, 5461-5467.
84. M. Morales, S. Veintemillas-Verdaguer, M. Montero, C. Serna, A. Roig, L. Casas, B. Martínez and F. Sandiumenge, Chemistry of Materials, 1999, 11, 3058-3064.
85. R. Chen, M. Christiansen and P. Anikeeva, ACS Nano, 2013, 7, 8990-9000.
86. C. Martinez-Boubeta, K. Simeonidis, A. Makridis, M. Angelakeris, O. Iglesias, P. Guardia, A. Cabot, L. Yedra, S. Estradé, F. Peiró, Z. Saghi, P. Midgley, I. Conde-Leborán, D. Serantes and D. Baldomir, Scientific Reports, 2013, 3.
87. R. Das, J. Alonso, Z. Nemati Porshokouh, V. Kalappattil, D. Torres, M. Phan, E. Garaio, J. García, J. Sanchez Llamazares and H. Srik-

anth, The Journal of Physical Chemistry C, 2016, 120, 10086-10093.
88. P. Hugounenq, M. Levy, D. Alloyeau, L. Lartigue, E. Dubois, V. Cabuil, C. Ricolleau, S. Roux, C. Wilhelm, F. Gazeau and R. Bazzi, The Journal of Physical Chemistry C, 2012, 116, 15702-15712.
89. F. Lu, A. Popa, S. Zhou, J. Zhu and A. Samia, Chemical Communications, 2013, 49, 11436.
90. M. Pernia Leal, A. Torti, A. Riedinger, R. La Fleur, D. Petti, R. Cingolani, R. Bertacco and T. Pellegrino, ACS Nano, 2012, 6, 10535-10545.
91. S. Kong, W. Zhang, J. Lee, K. Brammer, R. Lal, M. Karin and S. Jin, Nano Letters, 2010, 10, 5088-5092.
92. A. Riedinger, P. Guardia, A. Curcio, M. Garcia, R. Cingolani, L. Manna and T. Pellegrino, Nano Letters, 2013, 13, 2399-2406.
93. H. Park, H. Park, J. Kim, S. Lee, J. Kim, J. Yoon and T. Park, Journal of Microbiological Methods, 2011, 84, 41-45.
94. T. Nguyen, H. Duong, R. Selvanayagam, C. Boyer and N. Barraud, Scientific Reports, 2015, 5.
95. C. Yakacki, N. Satarkar, K. Gall, R. Likos and J. Hilt, Journal of Applied Polymer Science, 2009, 112, 3166-3176.
96. D. Kim, J. Kim, Y. Park, N. Lee and T. Hyeon, ACS Central Science, 2018, 4, 324-336.
97. J. Kim, N. Lee and T. Hyeon, Philosophical Transactions of the Royal Society A: Mathematical, Physical and Engineering Sciences, 2017, 375, 20170022.
98. J. Koikkalainen, H. Rhodius-Meester, A. Tolonen, F. Barkhof, B. Tijms, A. Lemstra, T. Tong, R. Guerrero, A. Schuh, C. Ledig, D. Rueckert, H. Soininen, A. Remes, G. Waldemar, S. Hasselbalch, P. Mecocci, W. van der Flier and J. Lötjönen, NeuroImage: Clinical, 2016, 11, 435-449.
99. Y. Peng, S. Tsang and P. Chou, Materials Today, 2016, 19, 336-348.
100. M. Legacz, K. Roepke, M. Giersig and U. Pison, Advances in Nanoparticles, 2014, 03, 41-53.
101. Y. Bao, J. Sherwood and Z. Sun, Journal of Materials Chemistry C, 2018, 6, 1280-1290.
102. M. Rogosnitzky and S. Branch, BioMetals, 2016, 29, 365-376.
103. H. Malikova and M. Holesta, The Journal of Vascular Access, 2017, 18, S1-S7.
104. D. Todd and J. Kay, Annual Review of Medicine, 2016, 67, 273-291.

105. K. Hasebroock and N. Serkova, Expert Opinion on Drug Metabolism amp; Toxicology, 2009, 5, 403-416.
106. J. Ramalho, R. Semelka, M. Ramalho, R. Nunes, M. AlObaidy and M. Castillo, American Journal of Neuroradiology, 2015, 37, 1192-1198.
107. C. Fang, N. Bhattarai, C. Sun and M. Zhang, Small, 2009, 5, 1637-1641.
108. N. Lee, D. Yoo, D. Ling, M. Cho, T. Hyeon and J. Cheon, Chemical Reviews, 2015, 115, 10637-10689.
109. R. Revia and M. Zhang, Materials Today, 2016, 19, 157-168.
110. Z. Stephen, F. Kievit and M. Zhang, Materials Today, 2011, 14, 330-338.
111. K. Briley-Saebo, A. Bjrnerud, D. Grant, H. Ahlstrom, T. Berg and G. Kindberg, Cell and Tissue Research, 2004, 316, 315-323.
112. L. Gu, R. Fang, M. Sailor and J. Park, ACS Nano, 2012, 6, 4947-4954.
113. D. Pouliquen, J. Le Jeune, R. Perdrisot, A. Ermias and P. Jallet, Magnetic Resonance Imaging, 1991, 9, 275-283.
114. R. Weissleder, D. Stark, B. Engelstad, B. Bacon, C. Compton, D. White, P. Jacobs and J. Lewis, American Journal of Roentgenology, 1989, 152, 167-173.
115. J. Lu, J. Sun, F. Li, J. Wang, J. Liu, D. Kim, C. Fan, T. Hyeon and D. Ling, Journal of the American Chemical Society, 2018, 140, 10071-10074.
116. F. Li, Z. Liang, J. Liu, J. Sun, X. Hu, M. Zhao, J. Liu, R. Bai, D. Kim, X. Sun, T. Hyeon and D. Ling, Nano Letters, 2019, 19, 4213-4220.
117. Y. Lu, Y. Xu, G. Zhang, D. Ling, M. Wang, Y. Zhou, Y. Wu, T. Wu, M. Hackett, B. Hyo Kim, H. Chang, J. Kim, X. Hu, L. Dong, N. Lee, F. Li, J. He, L. Zhang, H. Wen, B. Yang, S. Hong Choi, T. Hyeon and D. Zou, Nature Biomedical Engineering, 2017, 1, 637-643.
118. X. Teng and M. Aronson, Nist.gov, 2017.
119. I. Macwan, Z. Zhao, A. Aphale, S. Bhosale and P. Patra, Scholarworks.bridgeport.edu, 2022.
120. K. Gupta and T. Gopalakrishnan-Nair, Arxiv.org, 2008.
121. M. Shulaker, G. Hills, N. Patil, H. Wei, H. Chen, H. Wong and S. Mitra, ECS Meeting Abstracts, 2014, MA2014-01, 1188-1188.
122. S. Jadhav and S. Jadhav, 2018 International Conference on Circuits and Systems in Digital Enterprise Technology (ICCSDET), 2018.
123. V. LaMer and R. Dinegar, Journal of the American Chemical Society, 1950, 72, 4847-4854.

124. V. Mer, Industrial amp; Engineering Chemistry, 1952, 44, 1270-1277.
125. W. Ostwald, Zeitschrift für Physikalische Chemie, 1900, 34U, 495-503.
126. S. Arshadi, J. Moghaddam and M. Eskandarian, Korean Journal of Chemical Engineering, 2014, 31, 2020-2026.
127. D. Kim, J. Kim, Y. Park, N. Lee and T. Hyeon, ACS Central Science, 2018, 4, 324-336.
128. T. Sugimoto, Journal of Colloid and Interface Science, 2007, 309, 106-118.
129. T. Sugimoto, Colloids and Surfaces A: Physicochemical and Engineering Aspects, 2000, 164, 183-203.
130. J. KREUTER, International Journal of Pharmaceutics, 2007, 331, 1-10.
131. H. Reiss, The Journal of Chemical Physics, 1951, 19, 482-487.
132. I. Lifshitz and V. Slyozov, Journal of Physics and Chemistry of Solids, 1961, 19, 35-50.
133. T. Sugimoto, Journal of Colloid and Interface Science, 2007, 309, 106-118.
134. W. Lee, M. Kim, J. Choi, J. Park, S. Ko, S. Oh and J. Cheon, Journal of the American Chemical Society, 2005, 127, 16090-16097.
135. Q. Pankhurst, N. Thanh, S. Jones and J. Dobson, Journal of Physics D: Applied Physics, 2009, 42, 224001.
136. W. Yu, L. Qu, W. Guo and X. Peng, Chemistry of Materials, 2003, 15, 2854-2860.
137. S. Devi, A. Nivetha and I. Prabha, Journal of Superconductivity and Novel Magnetism, 2018, 32, 127-144.
138. K. Krishnan, A. Pakhomov, Y. Bao, P. Blomqvist, Y. Chun, M. Gonzales, K. Griffin, X. Ji and B. Roberts, Journal of Materials Science, 2006, 41, 793-815.
139. V. Singh, V. Banerjee and M. Sharma, Journal of Physics D: Applied Physics, 2009, 42, 245006.
140. M. Hansen, P. Jönsson, P. Nordblad and P. Svedlindh, Journal of Physics: Condensed Matter, 2002, 14, 4901-4914.
141. G. Guo, Y. Wang and Y. Chen, Journal of Magnetism and Magnetic Materials, 2004, 272-276, E1193-E1194.
142. P. Dutta, M. Seehra, S. Thota and J. Kumar, Journal of Physics: Condensed Matter, 2007, 20, 015218.

143. W. Wu, Z. Wu, T. Yu, C. Jiang and W. Kim, Science and Technology of Advanced Materials, 2015, 16, 023501.
144. S. Roy and T. Das, International Journal of Plant Biology Research, 2015.
145. K. Koo, A. Ismail, M. Othman, N. Bidin and M. A Rahman, Malaysian Journal of Fundamental and Applied Sciences, 2019, 15, 23-31.
146. W. Wu, Z. Wu, T. Yu, C. Jiang and W. Kim, Science and Technology of Advanced Materials, 2015, 16, 023501.
147. T. Scepka, PhD, Slovak University of Techonology, 2016.
148. S. Laurent, C. Henoumont, D. Stanicki, S. Boutry, E. Lipani, S. Belaid and L. Vander Elst, MRI Contrast Agents, Springer Singapore, 1st edn., 2017.
149. J. Baumgartner, L. Bertinetti, M. Widdrat, A. Hirt and D. Faivre, PLoS ONE, 2013, 8, e57070.
150. S. F. Hasany, I. Ahmed, R. J and A. Rehman, Nanoscience and Nanotechnology, 2013, 2, 148-158.
151. S. Sun, C. Wei, Z. Zhu, Y. Hou, S. Venkatraman and Z. Xu, Chinese Physics B, 2014, 23, 037503.
152. A. Ali, H. Zafar, M. Zia, I. ul Haq, A. Phull, J. Ali and A. Hussain, Nanotechnology, Science and Applications, 2016, Volume 9, 49-67.
153. A. Teja and P. Koh, Progress in Crystal Growth and Characterization of Materials, 2009, 55, 22-45.
154. D. Huber, Small, 2005, 1, 482-501.
155. M. De Cuyper and M. Joniau, European Biophysics Journal, 1988, 15, 311-319.
156. T. Naseem and M. Farrukh, Journal of Chemistry, 2015, 2015, 1-7.
157. J. Jeevanandam, A. Barhoum, Y. Chan, A. Dufresne and M. Danquah, Beilstein Journal of Nanotechnology, 2018, 9, 1050-1074.
158. A. Da Silva-Candal, T. Brown, V. Krishnan, I. Lopez-Loureiro, P. Ávila-Gómez, A. Pusuluri, A. Pérez-Díaz, C. Correa-Paz, P. Hervella, J. Castillo, S. Mitragotri and F. Campos, Journal of Controlled Release, 2019, 309, 94-105.
159. S. Sun, C. Wei, Z. Zhu, Y. Hou, S. Venkatraman and Z. Xu, Chinese Physics B, 2014, 23, 037503.
160. E. Vermeij, M. Koenders, M. Bennink, L. Crowe, L. Maurizi, J. Vallée, H. Hofmann, W. van den Berg, P. van Lent and F. van de Loo, PLOS ONE, 2015, 10, e0126687.

161. N. Nelson, J. Port and M. Pandey, Journal of Nanotheranostics, 2020, 1, 105-135.
162. K. Donaldson, A. Schinwald, F. Murphy, W. Cho, R. Duffin, L. Tran and C. Poland, Accounts of Chemical Research, 2012, 46, 723-732.
163. D. Galaris and K. Pantopoulos, Critical Reviews in Clinical Laboratory Sciences, 2008, 45, 1-23.
164. B. Halliwell and J. Gutteridge, Free Radical Biology and Medicine, 1991, 10, 449-450.
165. T. Kornberg, T. Stueckle, J. Antonini, Y. Rojanasakul, V. Castranova, Y. Yang and L. Wang, Nanomaterials, 2017, 7, 307.
166. A. Nel, Science, 2005, 308, 804-806.
167. A. Bell, Science, 2003, 299, 1688-1691.
168. G. Xiao, M. Wang, N. Li, J. Loo and A. Nel, Journal of Biological Chemistry, 2003, 278, 50781-50790.
169. H. Lum and K. Roebuck, American Journal of Physiology-Cell Physiology, 2001, 280, C719-C741.
170. P. Prabhakar, U. Reddy, S. Singh, A. Balasubramanyam, M. Rahman, S. Indu Kumari, S. Agawane, U. Murty, P. Grover and M. Mahboob, Journal of Applied Toxicology, 2011, 32, 436-445.
171. U. Reddy, P. Prabhakar and M. Mahboob, Saudi Journal of Biological Sciences, 2017, 24, 1172-1180.
172. M. Malvindi, V. De Matteis, A. Galeone, V. Brunetti, G. Anyfantis, A. Athanassiou, R. Cingolani and P. Pompa, PLoS ONE, 2014, 9, e85835.
173. A. Nel, T. Xia, L. Mädler and N. Li, Science, 2006, 311, 622-627.
174. N. Kobayashi, M. Naya, S. Endoh, J. Maru, K. Yamamoto and J. Nakanishi, Toxicology, 2009, 264, 110-118.
175. R. Duffin, L. Tran, D. Brown, V. Stone and K. Donaldson, Inhalation Toxicology, 2007, 19, 849-856.
176. J. Lee, J. Ju, B. Kim, P. Pak, E. Choi, H. Lee and N. Chung, Environmental Toxicology and Chemistry, 2014, 33, 2759-2766.
177. Z. Chen, J. Yin, Y. Zhou, Y. Zhang, L. Song, M. Song, S. Hu and N. Gu, ACS Nano, 2012, 6, 4001-4012.
178. M. Longmire, P. Choyke and H. Kobayashi, Nanomedicine, 2008, 3, 703-717.
179. R. Madru, P. Kjellman, F. Olsson, K. Wingårdh, C. Ingvar, F. Ståhlberg, J. Olsrud, J. Lätt, S. Fredriksson, L. Knutsson and S. Strand, Journal of Nuclear Medicine, 2012, 53, 459-463.

180. M. ALCALA and C. REAL, Solid State Ionics, 2006, 177, 955-960.
181. D. Ma, J. Guan, Fran?ois Normandin, S. Dénommée, G. Enright, T. Veres and B. Simard, Chemistry of Materials, 2006, 18, 1920-1927.
182. F. Tian, G. Chen, P. Yi, J. Zhang, A. Li, J. Zhang, L. Zheng, Z. Deng, Q. Shi, R. Peng and Q. Wang, Biomaterials, 2014, 35, 6412-6421.
183. A. Petri-Fink, B. Steitz, A. Finka, J. Salaklang and H. Hofmann, European Journal of Pharmaceutics and Biopharmaceutics, 2008, 68, 129-137.
184. E. Vermeij, M. Koenders, M. Bennink, L. Crowe, L. Maurizi, J. Vallée, H. Hofmann, W. van den Berg, P. van Lent and F. van de Loo, PLOS ONE, 2015, 10, e0126687.
185. P. Hirsch, A. Howie, R. Nicholson, D. Pashley, M. Whelan and L. Marton, Physics Today, 1966, 19, 93-95.
186. C. Carter and D. Williams, Microscopy and Microanalysis, 2019, 25, 2256-2257.
187. L. Reimer, Measurement Science and Technology, 2000, 11, 527-527.
188. Ivyroses.com, 2022.
189. J. Lim, S. Yeap, H. Che and S. Low, Nanoscale Research Letters, 2013, 8.
190. S. Bhattacharjee, Journal of Controlled Release, 2016, 235, 337-351.
191. E. Tomaszewska, K. Soliwoda, K. Kadziola, B. Tkacz-Szczesna, G. Celichowski, M. Cichomski, W. Szmaja and J. Grobelny, Journal of Nanomaterials, 2013, 2013, 1-10.
192. O. Salata, Journal of Nanobiotechnology, 2007, 5, 5.
193. J. Lim, S. Yeap, H. Che and S. Low, Nanoscale Research Letters, 2013, 8.

Chapter 2

Design, Synthesis and Characterisation of Multi-Functional Superparamagnetic Silica Coated Iron Oxide Nanoparticles.

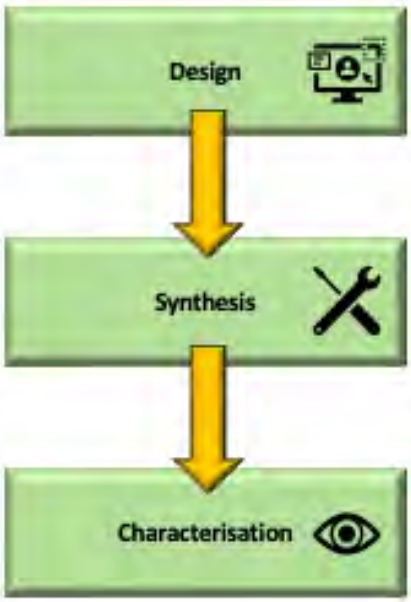

Figure 2.1: *Graphical representation of Chapter 3 - Nanoparticle design, synthesis and characterisation.*

2.1 Summary

The potential use of nanoparticles for research, drug delivery, cancer treatment and imaging is increasingly accepted and has become an area of substantial interest to the scientific community.

The design of nanoparticles for biology is dependent on the use case of the nanoparticles, and must consider the required chemical and structural properties. This includes chemical composition, size and surface functionalisation [1].

If nanoparticles are to be used for biological/biomedical applications, it is also essential to consider the impact a nanoparticle will have upon a biological environment, whether that be its toxicity or its capacity to undergo bio-conjugation as required [1].

The synthesis of nanoparticles has been widely researched, with many different methods and protocols available in the literature. However, issues still remain of reproducibility and ensuring the resulting nanoparticles meet the criteria of the desired nanoparticle design. It is therefore important to continue to develop and adapt synthesis methods to meet the requirements of nanoparticle use. It is also important to recognise that even small changes in variables such as temperature, pH or time given

for reaction to occur will have an effect on the outcome of a synthesis. This can be a problem when trying to reproduce a sample. However, it also allows for changes to be made to nanoparticles, as required, by using small variations in the protocol, giving nanoparticles potential great flexibility in application [2][3][4].

Surface functionalisation of nanoparticles is key to their potential within biology. The large surface area and the ability to add functional groups, dyes and other ligands to this surface is a fundamental component of nanoparticle design. When designing and synthesising nanoparticles it is always necessary to consider surface chemistry and its effect on nanoparticles behaviour. Issues such as aggregation of nanoparticles due to inter-molecular forces between nanoparticles can, for instance, be reduced by addition of polymers. The addition of fluorescent dyes can enable imaging of nanoparticles using light microscopy allowing for *in vitro* and *in vivo* cell research [5].

Thorough characterisation of nanoparticles is essential for understanding not only the nanoparticle structure but also for predicting behaviour within a biological environment. There are many analytical techniques which can be employed to characterise nanoparticles and their properties, such as size, charge, morphology and magnetic properties. These analytical techniques include SEM, TEM, DLS and XRD. Multiple analytical techniques are required, with no single technique providing all the required information [6][7].

In conclusion, a thorough understanding of the design requirements, synthesis methods and how small changes will effect the resulting nanoparticles along with thorough characterisation of nanoparticles is required for nanoparticles to be used for biological uses. This chapter will outline these concerns, looking at design principles, synthesis methods and characterisation of multifunctional silica coated superparamagnetic iron oxide nanoparticles.

2.2 Chapter 2: Aims and Objectives

2.3 Aims

Chapter 2 aims to design and synthesise silica coated single cored iron oxide NPs with physical and chemical properties which met the require-

ments of being biologically compatible, magnetic, able to be functionalised and imaged. Alongside the required physical and chemical properties listed above it was desired that the protocols designed should be simple, cheap with a high level of repeatability. Nanoparticles are designed and synthesised, with time given to developing a novel oleylamine protocol. Nanoparticles are characterised and imaged using TEM. Size is determined computationally using ImageJ. The specific aims were:

- To synthesise and characterise multifunctional silica-coated iron oxide nanoparticles.
- To validate the reproducibility of synthetic methods in respect to size, shape, magnetic response and functionalisation.

2.4 Introduction

2.4.1 Nanoparticles for biological Research, Imaging and Drug Delivery

The visualization of biological structures and processes is referred to as Bio-imaging. Bio-imaging requires imaging probes that can label specific targeted molecules or organs, providing enhanced visibility. This allows for the acquisition of images with increased structural and functional information at a subcellular or molecular level [8][9][10]. This increase in information obtained means the use of imaging probes is becoming essential for disease diagnosis and biology research.

Currently, the majority of the imaging probes approved for use in a clinical situation are organic molecules or metalorganic compounds [11][12][13]. These compounds are limited in use due to their intrinsic physical and physiological properties. These limitations are illustrated by traditional magnetic resonance imaging (MRI) contrast agents, which are made of Gd^{3+} chelates. Limitations of Gd^{3+} chelates are that they exhibit a weak contrast effect due to a low magnetic moment [14], or photobleaching suffered by fluorescent dyes in optical imaging. Gd^{3+} chelates also have a short life span, association with high toxicity and the negative effects of accumulation within a biological environment [14]. In general, these traditional probes, due to their small molecule size,

have a short circulation time *in vivo*. This causes a reduction in imaging enhancement and reduces targeting efficiency [15].

Inorganic nanoparticles are considered a potential alternative to the conventionally used molecular imaging probes, due to their nanoscale dimensions resulting in unique physical and chemical properties.[16] This means they have the potential to provide superior imaging performance, are potentially versatile in relation to targeted imaging, and have the potential for inorganic nanoparticles to be stimuli-responsive. Currently inorganic nanoparticles are not widely used in clinical settings, with very few approved for clinical use. Their use in biological research is limited by similar constraints. These concerns include toxicity of metal containing nanoparticles, low efficiency, magnetic susceptibility artefacts and lack of understanding of structure and composition.

Inorganic nanoparticle-based probes could, however, potentially be used many different imaging techniques including MRI, CT, and anti-Stokes shift-based optical imaging [8][9][10]. To date, there have been various nanoparticle probes developed for potential use in bio-imaging techniques. Examples include contrast agents for enhanced computed tomography (CT) using high-Z elements (e.g., gold, [17] bismuth, [18][19][20] and tantalum [21][22]), which demonstrate high X-ray attenuation and magnetic nanoparticles which have been used as strong T2 MRI contrast agents. These magnetic nanoparticles (superparamagnetic iron oxide nanoparticles) offer improved sensitivity over established Gd3+- MRI contrast agents [23][24][25].

Currently there are two clinically approved superparamagnetic iron oxide agents. These are ferumoxides (Endorem in Europer Feridex in the USA) and ferucarbotran (resovist). These have a particle size of 120-180nm and 60nm respectively. These agents are T2 relaxation agents and are approved only for use of MRI of the liver.

Recently, efforts have been made to overcome the problems associated with inorganic nanoparticle for imaging, drug delivery and research. Research is continuing into improving bio-compatibility alongside combining functionality to create attractive materials capable of targeted imaging, drug delivery, stimuli-responsiveness. In the case of biological research, the ability to alter surface chemistry to allow for modification dependent on purpose and the use of magnetism to manipulate cellular components is of interest. Further research is needed to produce inorganic nanoparticles

which match the requirements listed above as well as being easy and cheap to synthesise on a mass production scale.

2.4.2 Design of Nanoparticles for Biological Applications and Imaging

The advances over the past 4 decades of nanoscience into the design and synthesis of nanoparticles (NPs) for a broad range of applications means that it is now possible to design and synthesise nanoparticles for specific purposes. It is possible to use small changes in protocols such as variations in temperature, pH and time of reaction to alter the chemical and physical properties of the resulting NPs.

As with most designs, the initial step is to identify fundamental points of enquiry. For NPs in research, this is determining and then addressing the fundamental question of what is the end goal of any proposed research, and what is the purpose of the NPs within the proposed research. Once purpose has been determined, it is then necessary to consider the desired chemical and physical properties of the required NPs. This includes questions such as material to be used, shape and size of NPs, methods of synthesis, the requirements of the NPs in terms of functionalisation and whether things such as toxicity matter. These properties are determined by the purpose for which the NPs are to be used for. For example, NPs for use in nanoelectronics do not have the same requirements as those for biological purposes. Other considerations which also need to be evaluated include cost, safety and ability to be scaled up if desired.

The NPs considered here are for use in biological research. Figure 2.2 shows the chemical and physical properties that were considered during the design stage of the NPs.

The size of NPs has a direct effect on the behaviour of NPs. For example, iron oxide nanoparticles exhibit superparamagnetic behaviour within a critical size range of approximately 5-40nm. Superparamagnetism could provide, in principle, the potential to measure the force required to move cellular components.

Here, we aimed to synthesise NPs which meet a given set of requirements and provide multi-functional uses within a biological environment. This means that NPs needed to be non-cytotoxic, but also easily functionalised for bio-conjugation to different bio-molecules. It was also required that NPs should be superparamagnetic. The design requirements we

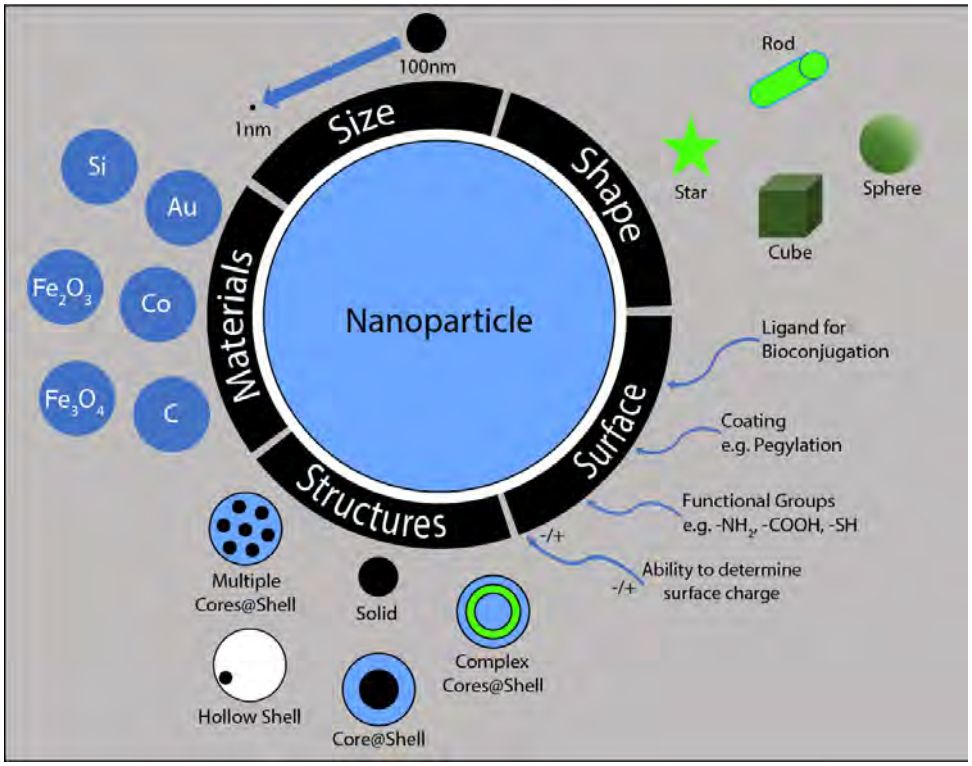

Figure 2.2: *Schematic representation of nanoparticle design considerations which were looked at for this work. They include shape,surface functionality, materials to be used and the structure of the nanoparticles for instance core@shell where a nanoparticle is coated in a different material.*

considered can be seen in Figure 2.5. These design requirements are in line with the aims of this work to create biocompatible nanoparticles as there is consideration given to their ability to be with a biological environment, the ability to be visualised, superparamagnetic and have surface functionality which can be adapted as required.

Iron oxide is a cheap and efficient material, prevalent both in nature and in use in industry. NPs made of iron oxide are becoming increasingly used as biological and medical tools due to their small size and unique magnetic properties. Fe_3O_4 (magnetite) NPs display a magnetic response to the application of a permanent external magnetic field (a property known as superparamagnetism). This property of superparamagnetism would allow for measurement of forces within a cellular environment if desired. Additionally, it provides the potential for eventual manipulation of NPs for drug delivery, or enabling their use as MRI contrast agents. In relation to the the potential to measure force in cells especially, it would be important to know the magnetic properties of individual NPs, and any

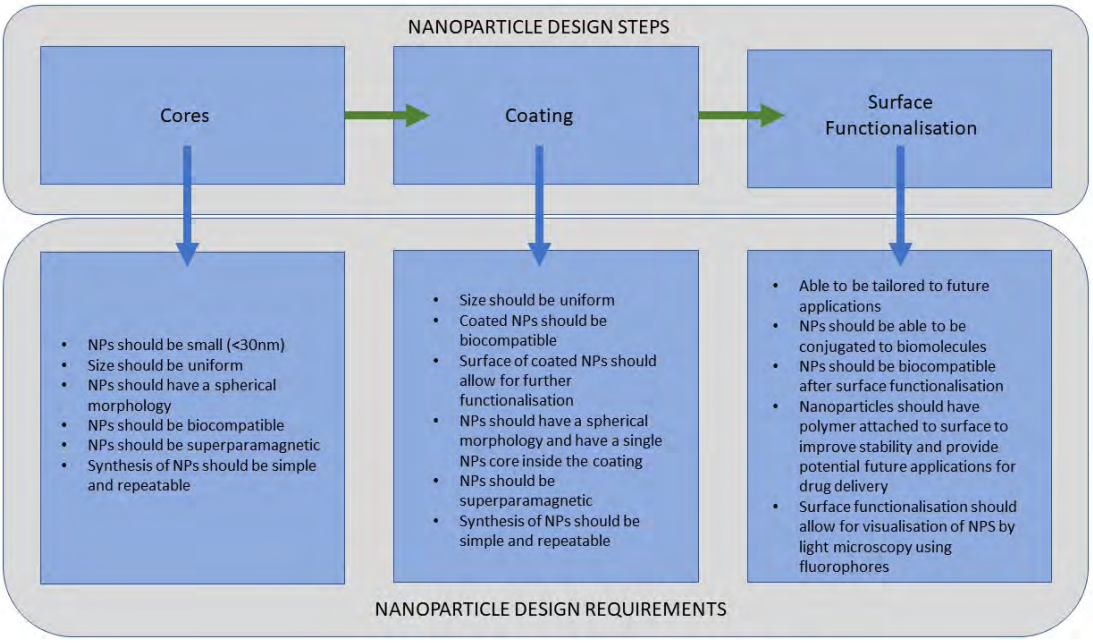

Figure 2.3: *Nanoparticle design summary for each part of the NPs design - core, coating and surface functionalisation. The requirements consider such concerns as size, shape, bio compatibility and the use of surface functionalisation to visualise NPs through microscopy and their future uses.*

coating decided upon should coat individual NPs.

The NPs designed and synthesised here are superparamagnetic iron oxide (SPIONS). SPIONS have been shown to have exciting potential for biomedical applications, due to them offering unique characteristics which are a direct result of the small size that can be obtained, and the ability to functionalise their surface. However, structure and cytotoxicity must be considered during the design and synthesis.

SPIONs exhibit size dependent magnetic properties and have an established role in biomedicine and cell biology [26][27]. They have been used as contrast agents for magnetic resonance imaging as well as for drug delivery, hypothermia treatment and as biosensors [28][29]. To be superparamagnetic the iron oxide NPs need to be below the critical size of 40nm.

An important feature of SPIONs is the property of superparamagetism which means there is a lack of remnant magnetization when no external magnetic field is applied. This allows for precise control over their magnetic action is possible.

Small ferromagnetic and ferrimagnetic nanoparticles such as those

discussed here display a characteristic called superparamagnetism. This characteristic can be seen in nanoparticles below the approximate critical size of 40nm. Superparamagnetic nanoparticles display a giant single magnetic domain which consists of all the magnetic moments of the atoms which form the nanoparticles. These characteristics are summarised in Figure 2.4

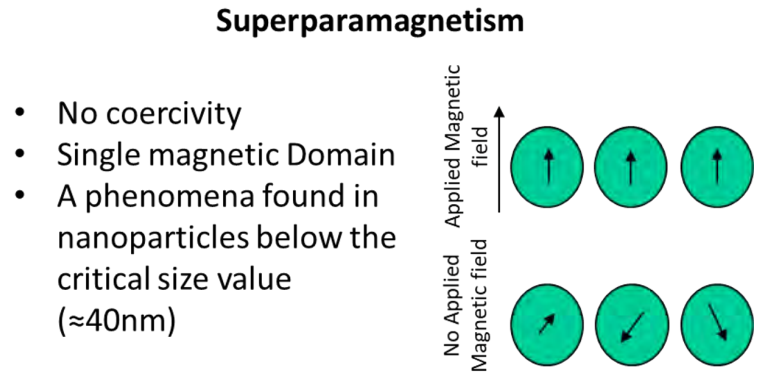

Figure 2.4: *Summary schematic drawing of superparamagnetic characteristics (created by author).*

Superparamagnetic iron oxide nanoparticles (SPIONs) when characterised using methods such as a vibrating sample magnetometer (VSM) analysis show no coercivity or hysteresis [8]. No coercivity means that the nanoparticles exhibit no resistance to changes in magnetisation, and when a magnetic field is removed no magnetism is retained. No hysteresis results in the absence of magnetic memory, both these characteristics are fundamental to superparamagnetic behaviour of small iron oxide nanoparticles.

When measured in electromagnetic units per gram the coating of iron oxide nanoparticles with silica is seen to decrease the magnetic saturation from approximately 10.70 $emug^{-1}$ to 7.22 $emug^{-1}$. This is due to the silica effectively shielding (blocking the effect of) the magnetic behaviour of the iron oxide cores. This shielding reduces the magnetic saturation of the nanoparticles once the silica coating is applied.

This adds to their potential as drug delivery systems and for their use in mechanochemical research .[8]

SPIONs are most commonly NPs formed by small crystals of iron oxide either magnetite Fe_3O_4 or maghemite γ-Fe_2O_3. SPIONs can be surface modified gaining colloidal stability in aqueous conditions. Coating

of SPIONs can be achieved using a variety of biocompatible agents such as hydrophilic polymers such as poly (ethylene glycol) (PEG), organic acids like citric acid, polysaccharides or inert silica. SPIONs are potentially easily synthesised, multifunctional, biocompatible and can undergo surface modification with various chemical agents.

Magnetite is chosen here in preference to maghemite. This is due to it containing $Fe_2{}^+$ and $Fe_3{}^+$ ions in a 1:2 ratio. The iron ion $Fe_2{}^+$ is known to trigger the Fenton reaction which results in reactive oxygen species (ROS) production in cells. The ratio of iron ions in magnetite therefore reduces this risk, making magnetite more suitable than maghemite for use in biological environments. Magnetite is also considered to have the strongest magnetic properties out of the transition metals. When the crystals have a diameter of less than the critical size, they become superparamagnetic, meaning that their magnetism is 0 when no external magnetic field is applied [3][7][30].

Iron oxide nanoparticles can be synthesised by multiple methods. Here both co-precipitation and solvothermal methods were developed. Co-precipitation methods of synthesis are commonly within literature, however whilst synthesis of iron oxide nanoparticles was possible it was found that IONPs synthesised using this method tended to, when coated with silica, form core@shell nanoparticles with multiple cores. The final method used for the synthesis of the iron oxide cores is an oleylamine only solvothermal methodology. The use of oleylamine for synthesis of iron oxide nanoparticles is available from literature. Oleylamine is suitable for use in synthesis of nanomaterials which have at least one magnetic element. Oleylamine is involved in solvothermal methods of synthesis due to its high boiling point of approximately 350°C [5][31]. Previously Oleylamine has been use as a reducing agent or surfactant or solvent for solvothermal synthesis of iron oxide nanoparticles. It has only been used as often one of the previous functions due for example the presence of a stronger reducing reagent within the methodology [5][31]. Here, however, oleylamine is used as reducing agent and surfactant and solvent. This results in a reproducible, cheap and easy synthesis method which does not require any specialised equipment. Development of the protocol also found that the temperature could be lowered from the expected 350°C to 200°C if time for the reaction to occur was increased. This has led to a novel synthesis method which results in uniform, spherical, stable and

superparamagnetic iron oxide nanoparticles in a safe reproducible manner. The nanoparticles when synthesised using this novel methodology are able to be coated with silica with ease and result in single cores silica coated nanoparticles. The size of the nanoparticles can be tuned by altering the ratio of Oleylamine to precursor ratio as previously seen in literature.

Having decided upon SPIONs (magnetite) as the cores for the NPs, it becomes necessary to discuss whether iron oxide NPs allow for the other requirements - non-toxic, able to be functionalised, etc.

For cell work, the NPs are required to be non-cytotoxic and able to undergo surface functionalisation as required for use. For example, surface functionalisation which would allow for imaging of NPs and for cell incorporation and binding to a targeted region [32]. It should be noted that iron ions catalyze both the Haber–Weiss and Fenton reactions. These reactions are responsible for the generation of ROS. This can induce cell-damage in the healthy cells[32][33].

A suitable non aggregated spherical coating such as that obtained from silica should encompass the synthesised magnetic Fe_3O_4 NPs. It has been shown that the reactivity of iron oxide particles increases as size decreases [34]. Uncoated Fe_3O_4 NPs undergo bio-degradation when used directly in a biological system [35]. Uncoated Fe_3O_4 is also associated with a lack of colloidal stability resulting in aggregation [35][36].

Colloidal stability of synthesised SPIONs is controlled by three principal forces: magnetic, hydrophobic–hydrophilic and van der Waals. It is common to see aggregation of SPIONS into clusters of the microscale range. This aggregation is often due to hydrophobic interactions between the sub nm size particles. These clusters can then undergo further aggregation as a result of magnetic dipole-dipole interactions with neighbouring cluster causing magnetisation. This is further increased if an external magnetic field is applied resulting in even more aggregation [37]

Attractive van der Waals in general cause particles on the nanoscale to form aggregates in suspension. This is to minimise interfacial energy or total surface energy.

These aggregations are detrimental to the efficacy of SPIONs, especially in drug delivery, as aggregation results in larger sizes and lower surface area. Aggregations are also unadvantageous in cell biology research if forces are to be measured or cellular components manipulated.

The stabilisation of SPIONS in suspension is therefore an important

issue to consider when designing and synthesising nanoparticles. Stabilisation can be achieved through surface modification either during synthesis or as a separate independent post-synthesis step. Materials suitable for increasing colloidal stability include silica, Polyethylene glycol (PEG), Polyvinyl pyrrolidine (PVP) and dextran [38]. A selection of these materials are summarised in Table 2.1 however there are many more.

Table 2.1: *Summary of some of the molecules/polymers which can be used for the stablisation of magnetic iron nanoparticles [38].*

Molecule/Polymer	**Beneficial Effect**
PEG	Biocompatibility is improved and blood circulation time increased
PVP	Stabilises the colloidal solution and increases the blood circulation time
Dextran	Stabilises the colloidal solution and increases the blood circulation time
Gelatin	Geling agent, biocompatible, natural polymer, hydrophilic
Polyacrylic acid	Improves biocompatibility, aids in bioadhesion, increases stability
PolyNIPAAM	Allows for cell separation and drug delivery
Oleic Acid	Stabilises magnetic nanoparticles
Oleylamine	Stabilises magnetic nanoparticles
Silica	Biocompatible, ability for futher surface functionalisation

Whilst the list of materials suitable for increasing colloidal stability is long, it is more common for stabilisation to be achieved using surfactants during synthesis. These surfactants include Oleylamine, oleic acid, alkane sulphonic/phosphonic acids and lauric acid [39]. These chemicals are amphiphilic and are effective at the interface between solvent and SPION. Therefore, surfactant mediated syntheses are associated with the use of organic solvents such as cyclohexane, toluene, and hexadecane amongst others, allowing the hydrophobic tail groups, i.e., the hydrocarbon chain, of the surfactant to be used to form a shell around the SPIONs. These SPIONs stabilised using surfactant and organic solvents are however not suitable for biological purposes. It is possible, for example, to invert the hydrophobic surface of SPIONs to a hydrophilic surface using alpha-cyclodextrin thus allowing the nanoparticles to disperse from the organic solution to an aqueous solution [40].

This inversion can also be achieved using an amphiphilic polymer shell. Polymers associated with this coating include polyvinylpyrrolidone (PVP), polyethylene glycol (PEG) and polyvinyl alcohol (PVA) [41][42].

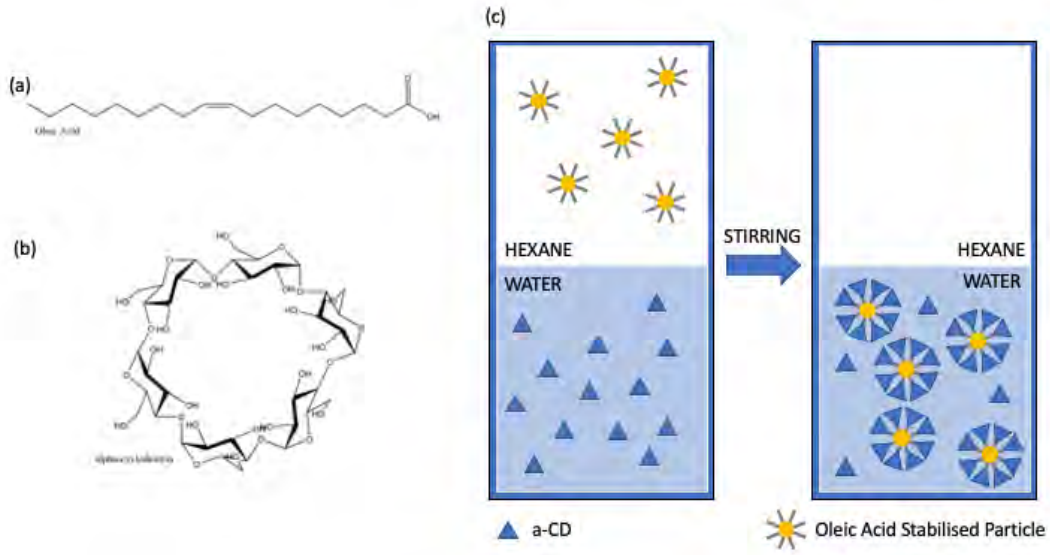

Figure 2.5: . *Image shows the chemical structures of (a) oleic acid and (b) R-CD molecules. Image (c) shows a schematic representation of the transfer of oleic acid stabilized nanoparticles from the organic into aqueous phase by surface modification using CD.*

Gelatin, starch, albumin dextran and ethyl cellulose are among many natural dispersants that have been used as natural dispersants of SPIONs in aqueous solution mainly for use in drug delivery.

The modification of SPIONS post synthesis to form core@shell NPs also increases stability. Silica, metals such as gold, and polymers have all be used to create core@shell NPs. As previously discussed, this shell not only increases colloidal stability but also protects against oxidation, therefore protecting the magnetic properties of the SPIONs. For biological purposes it is essential that the material which forms the shell is also biocompatible. Silica coating as used in this work is hydrophilic in nature and therefore silica coated core@shell iron oxide nanoparticles are well dispersed in aqueous suspension.

This along with the negative charge of silica coated SPIONs above the isoelectric point of silica (pH 2) allows their use in separation of biomolecules due to electrostatic interactions and the presence of silanol groups containing an hydroxyl group (Si-OH), which allows for further functionalisation through covalent bonding of organosilanes confirms silica as a good choice for increasing colloidal stability. The ability of silica to allow for further functionalisation also allows for further reduction of aggregation through increasing colloidal stability through the surface

addition of polymers such as PEG or PVA. However, it must be noted that any coating of magnetic SPIONs by non-magnetic materials such as silica or polymers will decrease the saturation magnetism of the SPIONs. This should be considered when trying to achieve colloidal stability [43][44][45].

Any chemical considered for stabilisation of SPIONS must be both biodegradable and biocompatible [46].

Here, Fe_3O_4 cores were coated in silica (SiO_2). Silica (SiO_2) is relatively inert to common degradation processes within a cell, but has silanol surfaces which lend themselves to chemical modification, allowing them to be functionalised with a wide variety of moieties, in turn allowing for tuning of their properties and behaviour. Their high surface area lends them to multiple modifications, enabling them to possess multiple groups providing unique optical and chemical properties [47]. One example of this ability for surface modification is the addition of amine groups via (3-aminopropyl) triethoxysilane (APTES). This results in a positive surface charge [47][48]. The silica coating around the Fe_3O_4 cores reduces cytotoxicity which is further reduced by the aforementioned amination process using APTES. This extra decrease in cytotoxicity is due to the addition of amine groups resulting in a more stable silica coating which is more compact and less porous [47]. Addition of fluorescent dyes such as fluorescein ($C_{20}H_{12}O_5$) enables visualisation of magnetic NPs in biological systems using light microscopy. It is important that NPs that are to be used for biological purposes have a pH of 7.0. This is due to intracellular pH being an average of 7.0 at 37 ^{o}C.

The design of NPs considered here requires a multi-step synthesis which can be adjusted dependent on the intended biological use of the NPs. Protocols for synthesis of core@shell (Fe_3O_4@SiO_2) NPs are plentiful and many different methods have been described. The decision of which synthesis method to use, and subsequent development of previously established protocols, is dependent on not only such things as required chemical and physical properties but also safety, facilities available, repeatability and cost. This work considered both co precipitation and solvothermal methods or iron oxide nanoparticle synthesis. Due to the previously stated requirement of single cored core@shell nanoparticles, co precipitation was eliminated as a suitable method. This was due to multiple cores being coated. Solvothermal methods were developed with the creation of a novel oleylamine protocol being the end result.

This protocol unlike those in the literature uses oleylamine as solvent, reducing agent and surfactant instead of as one of these three factors. This proved to be a highly reproducible and reliable protocol, resulting in nanoparticles which were small and uniform in size. superparamagnetic, and could have single cores coated.

2.5 Experimental Protocols

2.5.1 Materials

Triethyl amine tetraethyl orthosilicate (TEOS), iron (II) chloride tetrahydrate, iron (III) chloride hexahydrate, N-dimethylformamide (DMF), (3-aminopropyl) triethoxysilane (APTES), 70% technical grade Oleylamine, PEG-silane and Igepalco-530 were all purchased from Sigma Aldrich (Haverhill, UK). NHS fluorescein and NHS rhodamine were purchased from Thermo Scientific (Loughborough, UK). Absolute ethanol, acetone, methanol, polyvinylpyrrolidone (PVP) and aqueous hydrochloric acid (37v/v %) were supplied by VWR chemicals (Lutterworth, UK). All chemicals were used as provided. Note* All synthesised nanoparticles were stored in ethanol, once a fluorescent dye was added nanoparticles were stored in ethanol, wrapped in foil and stored in a dark cupboard to limit photo bleaching.

2.5.2 Preparation of Iron Oxide NPs (co-precipitation)

NaOH (5.04g) was dissolved in 250mL of millipore water and degassed for 30 minutes. A HCl solution was prepared using 12M HCl (0.82mL) with 25mL of distilled water and this was then degassed for 30 minutes. Once degassed, $FeCl_3 \cdot H_2O$ (6.53g,0.024 mol) and $FeCl_2 \cdot 4\,H_2O$ (2.49g,0.012 mol) were added to the degassed acid solution and magnetically stirred until fully dissolved. The NaOH solution was heated to 40°c and the iron solution added drop wise. The solution was stirred at 80°C for one hour.

The resulting NPs were precipitated using water and, following sonication for 10 minutes, centrifuged (10000 rpm, 15 minutes). This was repeated 3 times. Once washed nanoparticles were stored in 70% ethanol and resulted in a yield of approximately 3g. This synthesis results in black particles suspended in a clear solution.

2.5.3 Polyvinylpyrrolidone (PVP) Stabilisation of Fe_3O_4 Nanoparticles (co-precipitation)

0.13g of polyvinylpyrrolidone (PVP) was dissolved in 5 mL of H_2O and 14.70 mL of the previous Fe_3O_4 suspension added. This was magnetically stirred at room temperature for 1 day. The suspension was then separated by addition of aqueous acetone (H_2O/acetone, 1/10 v/v) and then centrifuged (13000rpm, 10 mins). The supernatant was decanted and the particles re-dispersed in ethanol (10mL). This washing was repeated 5 times. Nanoparticles once washed were stored in 70% ethanol with a yield of approximately 2.5g. This synthesis results in black particles suspended in a clear solution.

2.5.4 Preparation of Iron Oxide Nanoparticles (solvothermal)

Iron oxide cores were synthesised as described below, using a new method developed as a variation on previously published protocols using oleylamine. Here oleylamine acts as solvent, reducing agent and stabiliser. This synthesis results in black particles suspended in a clear solution and gives an approximate yield of 0.7g

$FeCl_2 \cdot 4\,H_2O$ (0.4g) were added to 50mL of oleylamine which was heated to 120°C for 30 mins under N_2 with magnetic stirring. The temperature was then increased to 200°C and stirred for 4 hours. After 4 hours the resulting nanoparticles were separated by washing with an acetone and hexane mix (1:1) followed by centrifugation (13000rpm for 15 mins), followed by a magnetic separation (15 mins). This was repeated at least 5 times. NPs were stored in an ethanol suspension for future use.

2.5.5 Silica Coating of Iron Oxide Nanoparticles

Silica coating of iron oxide cores, synthesised using a solvothermal methodology as previously described, was achieved by adding the surfactant Igepalco-520 (2mL) to 20 mL Cyclohexane and stirring at room temperature for 5 minutes. NH_4OH (33μL) and fetraethyl orthosilicate (TEOS) (5μL) were then added.

This was left for 72 hours with vigorous stirring at room temperature. After 72 hours excess methanol was added to precipitate thecore@shell

NPs. NPs were then washed with hexane and ethanol (1:1) and centrifuged (13000rpm, 15 mins)followed by magnetic separationat least 5 times.After washing nanoparticles were stored in 70% ethanol. Approximate yield of 4g. This synthesis results in dark brown particles suspended in a clear solution.

2.5.6 Addition of Amine groups to Silica Coated Nanoparticles

NH_2 groups to the silica surface of the NPs was achieved using 25μL of (3-Aminopropyl) triethoxysilane (APTES) (0.002 mol) added to 10mL of core@shell NPs (4mg/mL).

This was stirred vigorously overnight at room temperature. The NPs were then centrifuged (1000rpm,15 minutes) and then re-dispersed in ethanol using sonication (5 minutes). This was repeated 3 times. NPs were then separated using magnetic separation and re-suspended in ethanol twice. After washing nanoparticles were stored in 70% ethanol. This synthesis results in dark brown particles suspended in a clear solution.

2.5.7 Addition of Fluorescent dye - FITC-NHS-Rhodamine

Following the addition of amine groups to the NPs surface as previously described, 1.25mg of FITC-NHS-Rhodamine and 20μL of triethylamine was added to 2mL of the nanoparticle/ethanol suspension. The resulting suspension was stirred overnight in darkness at room temperature with magnetic stirring. Washing and centrifugation (13000 rpm, 20 Minutes) in ethanol was performed until supernatant was clear. Nanoparticles were then transferred to water after centrifugation and checked that a pH of 7 had been obtained. Nanoparticles were then stored in a dark location in ethanol.

2.5.8 Addition of Fluorescent dye - Fluorescein

The addition of fluorescien folled the same protocal as previously described for FTIC-NHS-Rhodamine. Following the addition of amine groups to the NPs surface as previously described, 1.25mg of Fluorescein and 20μL of triethylamine was added to 2mL of the nanoparticle/ethanol suspension. The resulting suspension was stirred overnight in darkness at

room temperature with magnetic stirring. Washing and centrifugation (13000 rpm, 20 Minutes) in ethanol was performed until supernatant was clear. Nanoparticles were then transferred to water after centrifugation and checked that a pH of 7 had been obtained. Nanoparticles were then stored in a dark location in 70% ethanol. This synthesis results in dark brown particles suspended in a clear solution.

2.5.9 Addition of PEG-Silane (5000)

40mg of the synthesised core@shell NPs were placed in a 2:1 ethanol to water solution (30mL). 0.0005mol% PEG-Silane was added and magnetically stirred at room temperature for 24 hours. The NPs were then washed with water and centrifuged (13200rpm, 15 mins) at least 3 times. NPs were retained in an ethanol suspension for future use. This synthesis results in dark brown particles suspended in a clear solution. Nanoparticles were store in 70%ethanol for future use.

2.6 Characterisation Techniques

2.6.1 Dynamic Light Scattering and Zeta Potential (DLS)

Using a Malvern Zetasizer Nano instrument, hydrodynamic diameters and zeta potentials were obtained for nanoparticle samples. Scattered light was measured at 173^{o} (back scattering) using a 4mW He-Ne 633n laser. 5 measurements for both size and zeta potential were taken each time and the average reported with attenuation and position automatically selected by the instrument. Samples for DLS were prepared at 1mg/mL concentrations using Ultrapure MilliQ water.

2.6.2 Infrared Spectroscopy (FTIR)

FTIR spectra (4000-400 cm^{-1}) were obtained from solid powder samples using a Bruker alpha FTIR spectrometer with a ZnSe crystal.

2.6.3 Transmission Electron Microscopy (TEM)

Transmission electron microscopy (TEM) imaging was achieved using a JOEL 2000FX TEM, 200KV, LaB_6 instrument which was operated with a

beam current of 115 mA. A Gatan Orius 11-megapixel cameras was used for image capture. Preparation of sample for TEM was performed using deposition and subsequent drying of nanoparticle samples. This used 10 μL nanoparticles suspended in water with a concentration of 1mg/mL. The nanoparticles were suspended on a TEM grid composed of a copper grid with a mesh size of 3 mm and a layer of plastic called a formvar and a thin film of carbon (300 mesh copper grid (Agar Scientific)). Post imaging analysis such as size determination was carried out in ImageJ version 3.2, with all averages calculated using a minimum of 150 nanoparticles from 10 different TEM images.

2.6.4 Scanning Electron Microscopy (SEM)

Scanning Electron microscopy was carried out using a Zeiss Supra 55-VP Field Emission SEM with EDAX Genesis EDX and EBSD instrument.

2.6.5 X-ray powder diffraction (XRD)

XRD is a non-destructive technique which is used here to identify crystalline phases of iron oxide. It can also be used for determination of orientation, atomic arrangement and measurement of thin film thickness amongst other things.

2.6.6 Superconducting Quantum Interference Device (SQUID) Magnetometry

SQUID was carried out using a 50 kOe (5 T) Quantum Design MPMS-5S SQUID magnetometer. This instrument allows for high sensitivity DC magnetisation measurements in the temperature range 1.8 to 400 K (800 K with oven) with a resolution of 5 x 10-8 emu. The instrument has Ultra-Low Field Capability ($\pm$0.05 G).

2.7 Design and Synthesis of Iron Oxide Nanoparticles

2.7.1 Iron Oxide Nanoparticles

Iron oxide nanoparticles are particles with diameters within the range 1 to 100 nanometers that consist of one of two main forms of iron oxide. These two main forms are magnetite (Fe_3O_4) and its oxidized form maghemite (-γ-Fe_2O_3).

Magnetite (Fe_3O_4) has an inverse spinel as seen in Figure 2.6 [81]. Within this structure oxygen forms a face-centred cubic crystal system. The inverse spinel structure for magnetite, involves all tetrahedral sites being occupied by $Fe_3{}^+$ and the octahedral sites are occupied by both $Fe_3{}^+$ and $Fe_2{}^+$. The structure of maghemite Fe_3O_4 is different from that of magnetite (Fe_2O_3) due to all or most of the iron found in magnetite being in the trivalent state ($Fe_3{}^+$) and by cation vacancies being present in the octahedral sites. Maghemite has a cubic unit cell in which each cell contains 32 Oxygen ions, 21 $\frac{1}{3}$ $Fe_3{}^+$ ions and 2 $\frac{2}{3}$ vacancies. In maghemite (γ-Fe_2O_3) the cations are found to be randomly distributed between the 8 tetrahedral and 16 octahedral sites.[48][49]

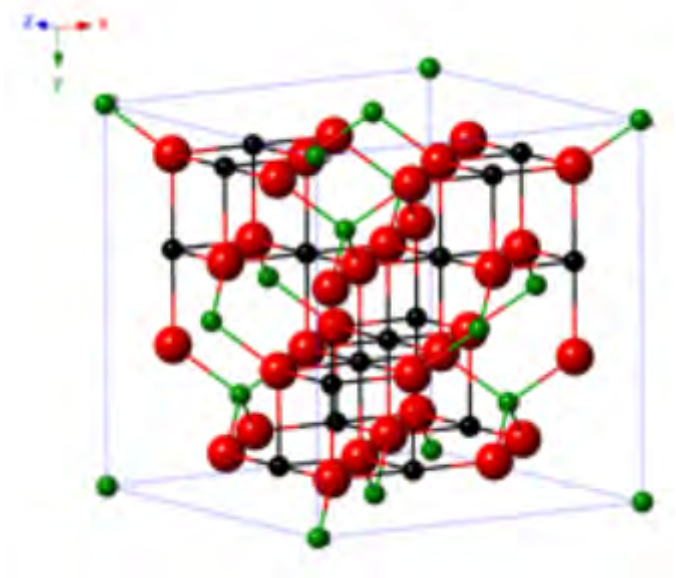

Figure 2.6: *Inverse Spinel structure of FE_3O_4, Green shows O^{2-} and red show $Fe_3{}^+$. Image obtained from literature [49].*

Iron oxide nanoparticles have seen extensive interest in research. This is due to their superparamagnetic properties (within a certain size range) and their potential applications across many fields. Whilst Iron Oxide is not the only material that exhibits magnetic properties, they are non toxic and no more easily oxidised as nanoparticles made of metals such as nickel or cobalt. Synthesis of iron oxide (Fe_3O_4) nanoparticles must be carried out in an oxygen-free environment. This is due to magnetite not being stable in oxygen, and the fact that it is prone to remain in the oxidised state.[50] Magnetite is converted to maghemite in the presence of oxygen as follows:

$$Fe_3O_4 + 2\,H^+ \longrightarrow \gamma Fe_2O_3 + {Fe_2}^+ + H_2O$$

In the presence of oxygen, magnetite (Fe_3O_4) particles can also undergo conversion into $Fe(OH)_3$ through the reaction: [51]

$$Fe_3O_4 + 0.25\,O_2 + 4.5\,H_2O \longrightarrow 3\,Fe(OH)_3$$

2.7.2 Methods for Synthesis of Iron Oxide Nanoparticles

The synthesis of iron oxide nanoparticles involves multiple considerations, including pH, temperature and materials used. Each of these considerations requires optimization from an early design phase with the future use and requirements, ie. the desired chemical and physical properties for the nanoparticles, considered. This is especially important given that any variation in the synthesis process can result in differences between nanoparticle samples for both physical and chemical properties [52][53]. Preparation of IONPs can be achieved via several routes with the three main routes being chemical, biological and physical. These three routes are responsible for approximately 90% of IONPs synthesis methods [54][55].

Table 2.1 shows a summary of temperatures required for synthesis, size of resulting nanoparticles and the time taken for synthesis by Method of synthesis. The data in this table was gathered from available literature [53][54][55]. The most popular and frequently used method for IONPs synthesis is co-precipitation with approximately 28% of chemical synthesis being a result of co-precipitation. Co-precipitation involves an aqueous

Table 2.2: *Iron oxide nanoparticle synthesis techniques and a comparison of nanoparticle size, time taken to synthesise and temperature ranges required [53][54][55].*

Method	**Temperature (°C)**	**Time**	**Size(nm)**
Co-precipitation	20-150	Minutes	5-40
Solvothermal	100-350	Hours/Days	4-30
Microemulsion	20-80	Hours	10-25
Hydrothermal	150-280	Hours/Days	10-800
Polyol	130-220	Hours	4-100
Sol-gel	25-200	Hours	15-50
Sputter deposition	100-800	Hours	5-100

solution which contains ferric ($Fe_3{}^+$) and ferrous ($Fe_2{}^+$) salts acting as precursors, to which a base is added at a moderate temperature (<100°C).

Co-precipitation allows for synthesis of IONPs that are suitable for biological applications due to the non- toxic nature of the reagents used [56]. It also allows for synthesis at often lower temperatures than other methods in an inert nitrogen environment [57]. Co-precipitation allows for control of size (5 to 40nm), as well as magnetic properties (often size dependent) and shape. These properties can be changed depending on reaction conditions including precursor salts used, ionic strength and pH [58][59][60]. Even though the co-precipitation reaction is a very popular and widely used method for iron oxide nanoparticle synthesis, the mechanism of the reaction is still relatively poorly understood. This is due to a lack of information and therefore understanding on how intermediates are formed. This often results in difficulties in obtaining multiple samples that have the same properties due to syntheses often not being reproducible. While IONPs synthesised this way mainly contain magnetite and maghemite phases when characterised using X-Ray diffraction (XRD), many other iron phases can form during synthesis using co-precipitation; and each of these iron phases have different magnetic properties.

The solvothermal or thermal decomposition method of synthesis provides the ability to produce IONPs with a controllable narrow size distribution [61]. This process involves either a "hot injection" method or a "heating up" method. Regardless which of these methods is used the principle of NPs synthesis is the same, involving the heating of a non-magnetic organometallic precursor compound along with organic solvents and surfactants. The "hot injection" method involves fast nucleation of NPs triggered by injecting precursor reagents into a hot surfactant

solution and then at a given temperature for a given time enabling a controlled growth stage. The "heating up" method is considered a simpler method which involves a solution of precursor reagents, solvent and surfactant, being heated to a predetermined temperature. Once the solution has reached this temperature IONPs start to form through a process of clustering and growth [62][63].

Again, synthesis must be carried out in an inert atmosphere. Control of nanoparticles properties such as size can be achieved with this control being dependent partially on choice of surfactant such as oleic acid or oleylamine which act as a capping agent and also very dependent on temperature and time [61][64].

IONPs have also been synthesised using many other methods. These include hydrothermal, microemulsion, polyol, sol-gel and sputter deposition methods. Each of these methods vary in procedure and require a range of temperatures, pressure and time.

Hydrothermal protocols produce crystalline IONPs under high temperature, high pressure conditions. Temperatures of around 220 °C and pressures of above 10^7Pa are used with a total reaction time of approximately 72hours. This is often achieved using a Teflon-lined stainless steel autoclave in which a temperature gradient can be designed so that at the cooler end deposition of the mineral solute will occur which will grow in the desired nanoparticles [65][66][67].

The sol-gel method of nanoparticle synthesis involves the condensation of iron precursors following hydroxylation to form a colloidal solution "sol". This sol is then dried (gelled) by removing the solvent, often water, until a 3D network of iron oxide is obtained [68][69]. It is possible for hydrolysation to be carried out using acids or bases instead of water as a solvent. This method does not require high temperatures and is often carried out at room temperature it also produces spherical NPs of reasonable size distribution which is tuneable.

Finally, uniform NPs can be synthesised using precursors such as oxides, nitrates and acetates which are suspended or dissolved in diols. This is known as the polyol method and produces uniform nanoparticles which can be produced on a larger scale.

Summary information regarding synthesis methods and resulting nanoparticle size can be seen in Table 2.2. It is clear that method of synthesis is one of the first considerations during nanoparticle design. Consideration

of time taken to synthesise, temperature, quantity needed from synthesis, safety, equipment required and size of IONPs required most be of the highest priority during methodology choice. Each of the aforementioned methods allows for further tuning of produced NPs which needs to be considered once a method has been chosen.

Here, as nanoparticles where required to be small, magnetic, biologically compatible and able to be individually coated with silica as well as synthesised using simple wet chemistry at reasonable temperatures and normal pressure, co-precipitation and solvothermal protocols were designed/chosen as potential methods for synthesising IONPs cores suitable further development. Both of these methods allow for changing of conditions to fine tune nanoparticles as needed but are also relatively cheap in reagents and can be carried out safely in a mixed lab environment.

2.8 Synthesis of Iron Oxide Nanoparticles by Co-precipitation

Synthesis of IONPs by co-precipitation has often been the commonly preferred method for production of nanoparticles due to its simplicity and fast rate of production. Co-precipitation involves a reduction reaction of iron salts under alkaline conditions which produces magnetite (Fe_3O_4) or maghemite (Fe_2O_3). Here to synthesize the magnetite form of iron oxide, aqueous solutions of ferric ($Fe_3{}^+$) and ferrous ($Fe_2{}^+$) ions were used. During synthesis the ions were mixed in a 2:1 molar ratio as required, and precipitated by addition of a base. The pH of the resulting solution was then maintained between 9 and 14 allowing for effective production of magnetite. The precipitated solution retained its black colour after the reaction was complete with clearly visible black nanoparticles within it. The overall chemical reaction for magnetite formation is as follows:

$$Fe_2{}^+ + 2\,Fe_3{}^+ + 8\,OH \longrightarrow Fe_3O_4 + 4\,H_2O$$

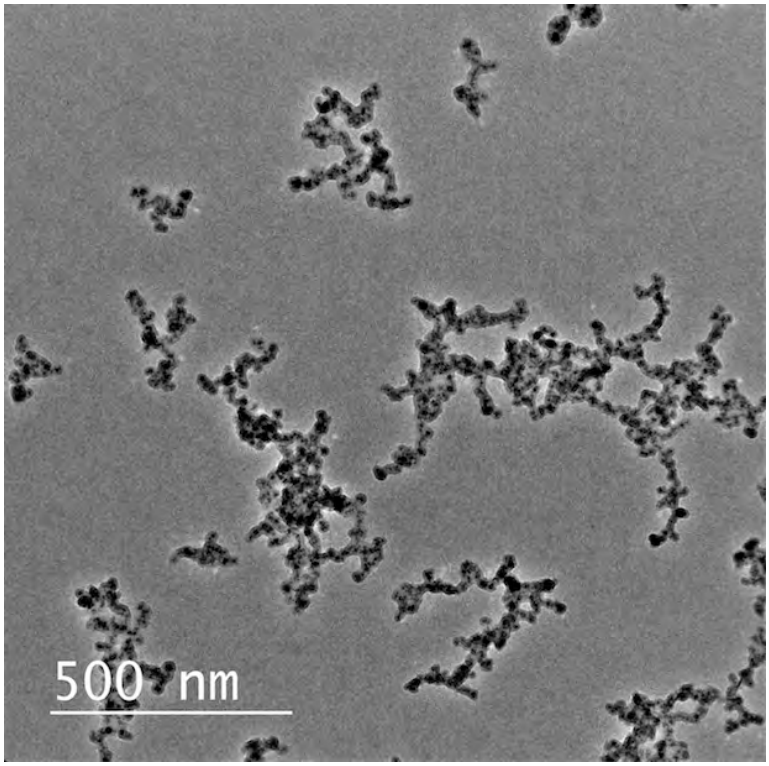

Figure 2.7: *Iron oxide cores were synthesised by co-precipitation of iron salts ((Fe_3^+) (Fe_2^+))) under alkaline conditions. These synthesised nanoparticles were prepared for TEM and after 24 hours drying time were imaged by author. The resulting nanoparticles were measured using image j and shown to have an average diameter by TEM of 21.44 ± 5.02/DLS.*

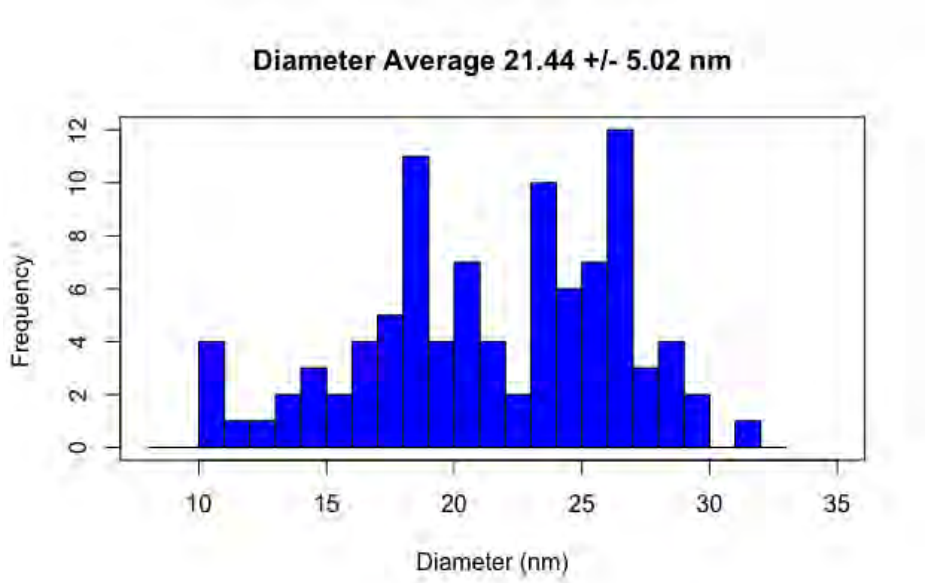

Figure 2.8: *Size distribution plot for iron oxide cores synthesised by co precipitation. Average diameter by TEM 21.44 ± 5.02. Nanoparticle size was computationally determined by the author after imaging with TEM using the software package image j to measure the diameter of 150 nanoparticles over 15 TEM images. The mean value was then calculated in Microsoft Excel.*

Nanoparticles synthesised by co-precipitation whilst cost effective and simple to achieve have drawbacks. These nanoparticles tend to be irregular in shape and show high dispersity. Figure 2.7 shows this lack of regular shape and poor monodispersity. Measurement using ImageJ revealed a high standard deviation for size suggestion variation of size within the sample, as seen in Figure 2.8. This is in agreement with the expected poor monodispersity attributed to NPs synthesised by co-precipitation. It can also be seen that nanoparticles appear aggregated in this sample. This aggregation is commonly seen in samples from co-precipitation and this can result in difficulty coating individual nanoparticles as desired if nanoparticles are to be used for any research where measurement of magnetism/force are required. Therefore, alternative methods of synthesis of Fe_3O_4 cores were explored.

2.9 Solvothermal – Oleic Acid Capping

Development of nanoparticles synthesis methods as reported using iron-oleate as a precursor and oleic acid as a capping agent have been developed [70]. Nanoparticles synthesised using compounds such as oleic acid as a capping agent have a hydrophobic coating where polar groups are attached to the surface. These capping agents act as stabilising agents, prevent uncontrolled growth of nanoparticles and aid colloidal stability. Choice of capping agents has an effect on morphology of resulting nanoparticles.

Capping agents result in a strongly bonded monolayer on the surface which protects the nanoparticles resulting in far more mono-disperse and highly uniform nanoparticles than those synthesised using co precipitation [71].

Synthesis using oleic acid and organic solvents often require high temperatures, here a temperature of 350 °C was necessary to achieve synthesis of regular shaped mono-disperse nanoparticles. Even minor variations in temperature were seen to reduce monodispersity and effect the size of the nanoparticles. A reduction in temperature resulted in larger nanoparticles where as increase in temperature showed a reduction in size. This was observed even when temperature variation was small (less than 5°C) due to variables such as mechanical variation between hotplates and room temperature. This meant that repeatability of the protocol was not reliable and the size of the resulting nanoparticles difficult to predict.

2.10 Solvothermal Synthesis of Iron Oxide Nanoparticles Using Oleylamine as Surfactant, Solvent and Reducing Agent

To solve the problems with variation in temperatures achieved when attempting to heat to 350°C, a novel oleylamine protocol was developed. The protocol allowed for the synthesis of mono-disperse, spherical nanoparticles at 200°C rather that the 350°C needed for the oleic acid synthesis. This temperature proved far easier to control and maintain. Its novelty as a protocol is due to its use of oleylamine as surfactant, reducing agent and solvent. This also resulted in a cheap very easy to perform protocol

as desired in the original PhD aims.

Oleylamine (OAm) is an organic compound with a molecular formula $C_{18}H_{35}NH_2$, its structure can be seen in Figure 2.9. A long-chain primary alkylamine it is commonly used in the synthesis of nanoparticles which have at least one magnetic element [72] Related to the fatty acid oleic acid it is an unsaturated fatty amine. Oleylamine as a pure compound is a clear and colourless liquid with a high boiling point (364°C). This high boiling point is often beneficial to it use in nanoparticle synthesis allowing when needed for strong heating conditions. OAm usefulness in synthesis of nanostructures is due to its ability to act as a solvent, a reducing agent or a surfactant as required dependent on the reaction conditions. For example, if a stronger reducing agent is present this will limit OAm to act as just solvent and/or surfactant. OAm is however most often used as a solvent or reducing agent or surfactant rather than as all 3 [72].

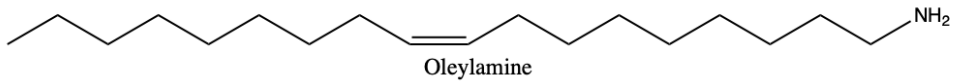

Figure 2.9: *Chemical structure of Oleylamine (OAm) ($CH_3(CH_2)_7CH=CH(CH_2)_8NH_2$). Image drawn using ChemDraw.*

2.10.1 Nanoparticle Size Dependency Due to Oleylamine-Precursor Molar Ratio

Nanoparticles synthesised using oleylamine can have their size fine tuned by changing the oleylamine to precursor ratio [73]. As the molar ratio of oleylamine to precursor is increased the size of the resulting nanoparticles is also increased [73]. Hence, a 5:1 ratio of oleylamine to precursor will result in smaller nanoparticles than a 7:1 ratio [73]. Experimentally this effect can be seen and during this work molar ratio of oleylamine to precursor was used in ensure nanoparticles within the desired size range.

2.10.2 Effect of Oleylamine as Solvent, Reducing Agent and Stabiliser on Washing Protocol

The use of oleylamine as solvent, reducing agent and stabiliser has been developed here and is an effective means for synthesising iron oxide nanoparticles at a temperature lower than usually suggested in literature. Here the synthesis involved temperatures of 200°C this is significantly lower than temperatures often cited of up to 400°C. This has obvious benefits, such as safety and ease of synthesis as well as ease of repeatability with environmental conditions being less of a consideration than the temperatures required for synthesis using oleic acid.

However it was found that using oleylamine as solvent, reducing agent and stabiliser resulted in nanoparticles which were 'sticky' The removal of oleylamine from the sample also proved difficult. This means that the standard method of centrifugation and re dispersion in solvents to remove oleylamine was not as efficient as expected and magnetic separation became a vital step in producing clean nanoparticles free from oleylamine. Magnetic separation performed using a simple, easy set up as seen in Figure 2.11 over a period of up to 15 minutes followed by centrifugation (13000 RPM, 15 mins) and re-dispersion into solvent is needed to clean the iron oxide cores ready for silica coating. This process needs to be repeated until nanoparticles are black in colour, the solvent is clear and magnetic separation is complete within 1 minute. This varies between samples however no sample required less than 5 washes and an average of 8 washes was observed. If there is a failure to clean nanoparticles thoroughly there is a correlation to unsuccessful coating of individual cores with an even layer of silica. Instead it is seen that multiple cores can become encased in silica and frequently this silica does not form the required spherical nanoparticles but instead we see multiple cores embedded in randomly shaped "clumps" of silica. This can be seen in Figure 2.10. In this figure further magnetic separation could be used to remove excess silica however the nanoparticles with iron oxide cores are seen to be neither spherical, single cored or individual nanoparticles. Once clean iron oxide nanoparticles however benefit from being synthesised in oleylamine, the resulting nanoparticles are OAm-stabilised removing the need for a further stabilisation step and offer enhanced colloidal stability over a long period of time.

One issue to consider when using OAm in nanoparticles synthesis

is the purity of commercially available oleylamine. Here 70% technical grade oleylamine was used. It has been shown that impurities can cause issues with reproducibility and scaling up of protocols [72]. The length of

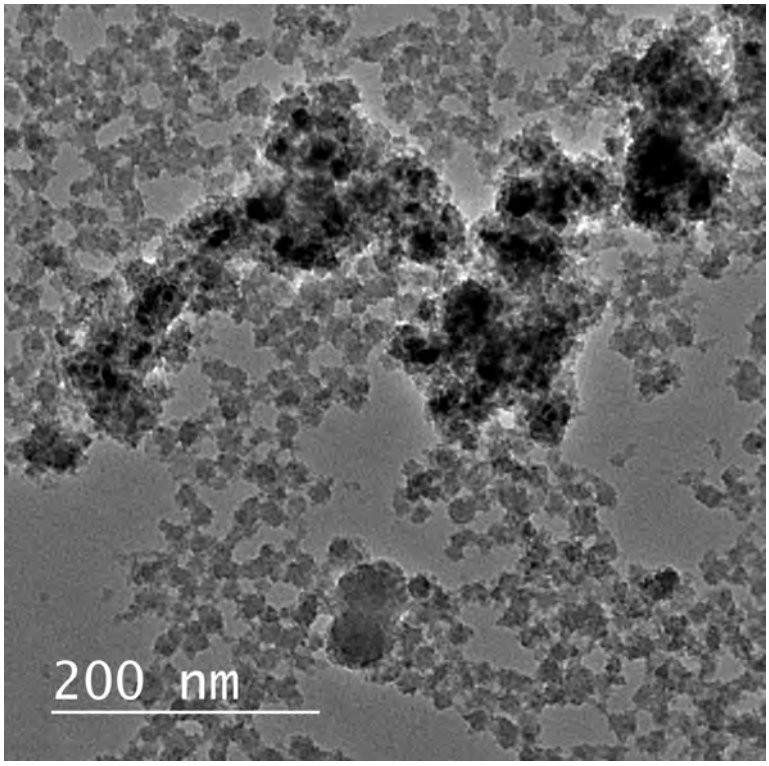

Figure 2.10: *TEM showing silica coated magnetic iron oxide nanoparticles (sample CF-1-CO). The lack of distinct core@shell nanoparticles and the presence of multiple cores in silica alongside large amounts of silica nanoparticles with no core is indicative of silica coating unclean iron oxide cores when using a pure oleylamine synthesis. Sizing of this sample is not possible due to the inability to measure individual particles. TEM performed by author.*

time required for magnetic separation to completely pull out magnetic nanoparticles from solution decreases as the amount of oleylamine present decreases. This is easily assessed visually as newly synthesised iron oxide cores take longer to be pulled out of the oleylamine solution and leave an orange hue in the oleylamine solution. Figure 2.10 shows how nanoparticles synthesised using oleylamine but without proper cleaning of the cores, results when coated in silica in a lack of distinct core@shell nanoparticles with multiple cores of iron oxide present. The image also demonstrates the need for good sample preparation for TEM. In Figure 2.10 the large amount of loose silica and the lack of contrast may of been improved by a lower concentration and less drying time on the TEM grid

than normally used. Magnetic separation of oleylamine synthesised iron oxide cores before cleaning requires separation times of approximately 30 minutes to be sure all magnetic nanoparticles are pulled to the applied magnet. Clean iron oxide cores suspended in ethanol or water are black however once a magnet is applied clean nanoparticles will be pulled to the magnet much quicker, leaving the solvent clear. The magnetic separation of clean iron oxide nanoparticles synthesised this way occurs quickly over the space of approximately 1-2 minutes.

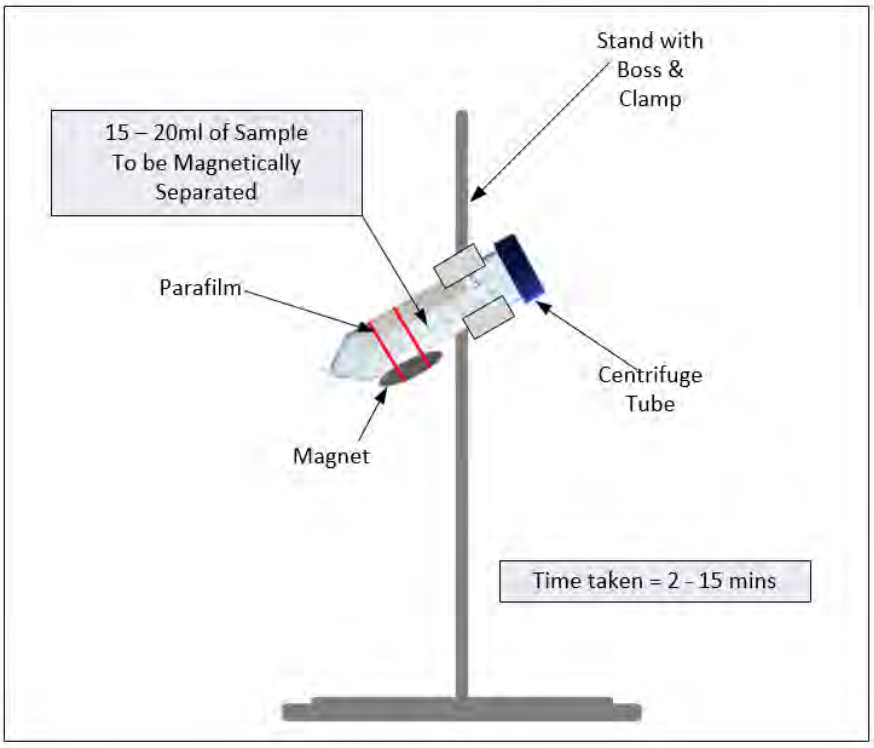

Figure 2.11: *Schematic representation of Magnetic Separation for effective cleaning of iron oxide nanoparticles synthesised using oleylamine as solvent, reducing agent and stabiliser.*

Figure 2.11 shows the set up for effective magnetic separation of oleylamine synthesised iron oxide nanoparticles. This simple method involves the attachment of a magnet to a centrifuge tube which contains the nanoparticle solution to be cleaned. The magnet drags out the nanoparticles and allows for the solvent to be disregarded. This process is repeated multiple times after the addition of new solvent each time. As the sample becomes cleaner, the solvent becomes clearer and the nanoparticles take less time to be attracted to the magnet. Concentration of sample was not a consideration with this method with the magnet able

to pull out and clean up to approximately 3g of nanoparticles at once.

Once thoroughly cleaned the resulting nanoparticles, as seen below in Figure 2.12 are small, uniform in size with a small standard deviation (Figure 2.13), spherical and magnetic. Table 2.3 shows the DLS and TEM measurements for these NPs.

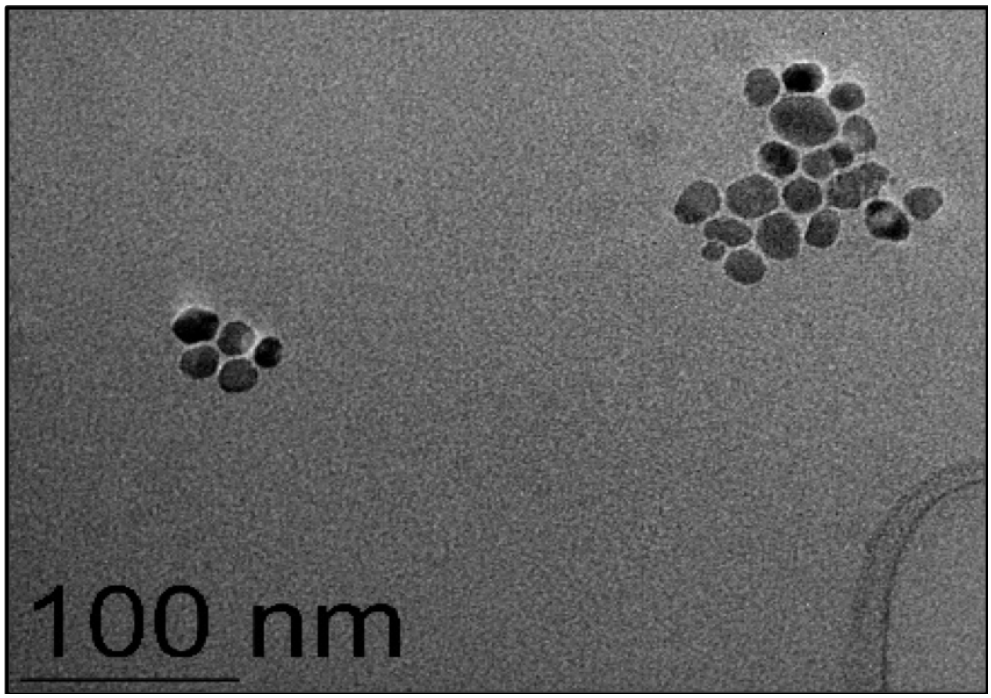

Figure 2.12: *TEM of oleylamine synthesised iron oxide cores post magnetic separation. (Sample: CF-1-c). Average diameter by TEM of 17.50 ± 1.46 nm. Measurement of NPs achieved using ImageJ measurement of 100 NPs.*

Table 2.3: *Summary of average diameter obtained by TEM and DLS for silica coated iron oxide nanoparticles (Sample CF-1-C).*

Nanoparticle	**(DLS)(nm)**	**PDI**	**(TEM)(nm).**
Oleylamine Iron Oxide Cores	285.8±14.5	0.55	17.50 ± 1.46

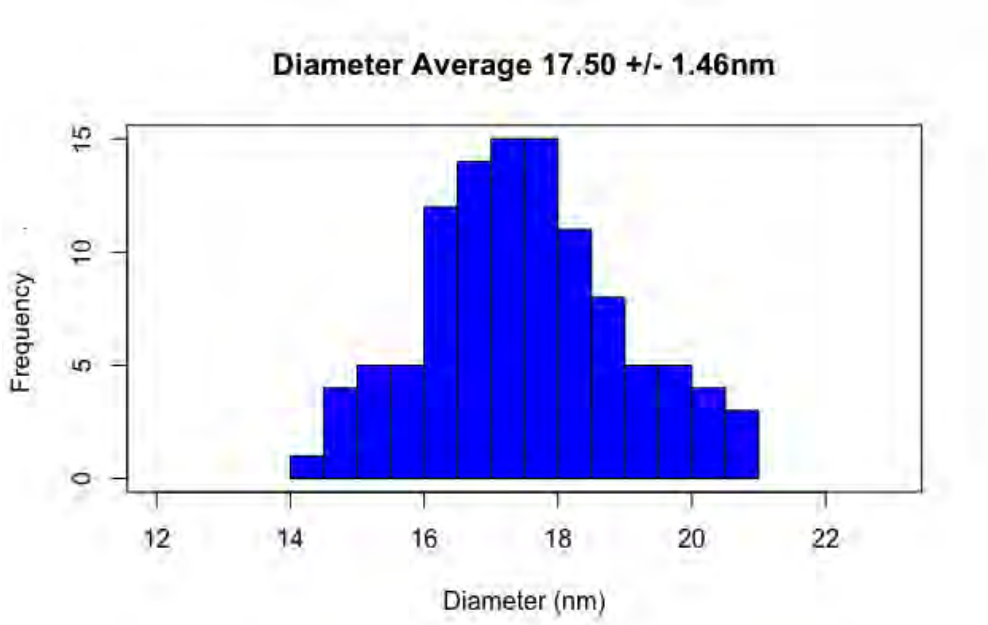

Figure 2.13: *Histogram showing size distribution of oleylamine synthesised iron oxide cores (CF-1-c) (TEM). Average diameter by TEM of 17.50 ± 1.46 nm.*

2.11 Silica coating

The most common compound used for creating core@shell iron oxide nanoparticles is a coating of silica. This is due to its ability to protect the iron oxide core, reduce toxicity, provide a surface which allows for further functionalisation of the nanoparticles through covalent bonding to different ligands, protect from acidic environments and increase nanoparticle stability in water[74][75][76]. It must be noted that coating iron oxide nanoparticles with silica will increase the overall size of the nanoparticles. The coating of silica also results in a reduction the magnetic properties of the nanoparticles due to a shielding effect as the magnetic core inside the silica is "blocked" from the magnetic field.. This should be considered when designing the protocol for silica coating. Table 2.4 illustrates the commonly used methods for coating iron oxide nanoparticles with silica.

Table 2.4: *Summary of synthesis methods for silica coating of iron oxide nanoparticles.*

Synthesis Method	**Advantages**	**Disadvantages**
Microemulsion	Tuneable size	Long process/Low yield
Stöber Method	Uniform diameter control	Mechanism not understood
Aeresol pyrolysis	Hermetically coated	Difficult to synthesise

However, while the reduction of the magnetic properties of the NPs is noted, this can be confirmed by conducting a simple experiment using a N42 Neodymium Magnet (8.3kg Pull) introduced to the side of a small glass vial containing 50mg of iron oxide cores in a 2mL EtOH:water, 50:50 solution. In the case of iron oxide cores only, it can be clearly observed, that there is a strong attraction to the magnet. This is shown in the time lapse sequence of photographs in Figure 2.14 which were taken using a Sony Alpha A7 Mirrorless camera system using a Sony 24-240mm Zoom lens in a "lightbox" to ensure even lighting and correct exposure (settings seen in Figure 2.33 (in Bibliography)). Within 6 seconds, the majority of the visible iron oxide cores were attracted to the magnet, with the solution clearing further over the next 9 seconds.

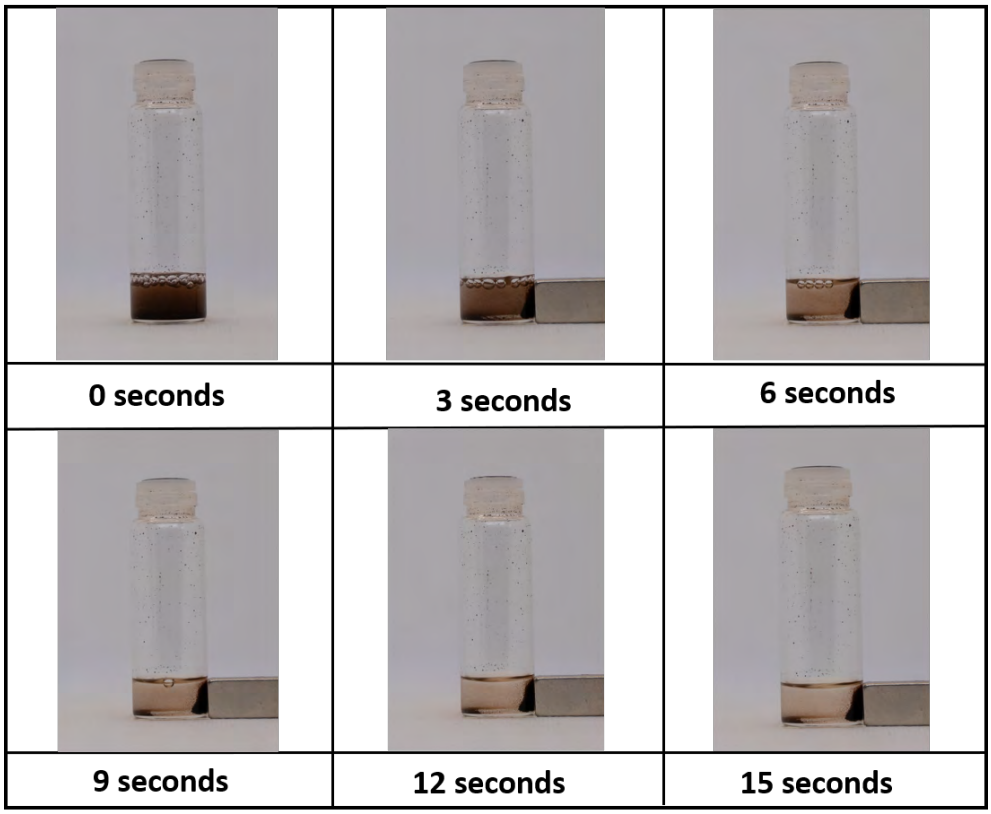

Figure 2.14: *This time lapse sequence of photographs, demonstrates the speed of magnetic separation for the Fe_3O_4 cores (CF-1-c) over 15 seconds. Most of the nanoparticles are pulled to the magnet (N42 Neodymium Magnet - 8.3kg Pull) after 6 seconds and the solvent is almost clear after 15 seconds.*

Synthesis of IONP@SiO_2 core@shell nanoparticles is most commonly achieved by one of three methods – microemulsion, aerosol pyrolysis and the Stöber method.

Aerosol pyrolysis is considered an innovative method to coat iron oxide cores. Carried out in a flame environment this methodology is often used in the production of ceramic products such as titania and fumed silica during large scale production[77][78]. Effectively this method sprays the cores with silica and allows for control of particle crystallinity, morphology and size. It is possible to radically alter the shape of the resulting nanoparticles. Due to the need for specialised technology this method however innovative is not necessarily conducive to design and synthesis of nanoparticles which can be repeated/ copied within the research environment.

The microemulsion method can be further divided into two categories, water-in-oil (W/O, micelles) and oil-in-water (O/W, reversed micelles). The process involves the use of water, surfactant and oil to produce core@shell nanoparticles with high crystallinity [79]. The thickness of the silica shell can be altered and tuned by changing the amount of ammonia and TEOS with increasing these factors leading to an increase in shell thickness. This tunability is attractive however nanoparticles coated using the microemulsion method often see poor yields and require large amounts of solvents. The use of surfactants can also result in difficulty separating NPs resulting in increased washes being required increasing time required for this step [79].

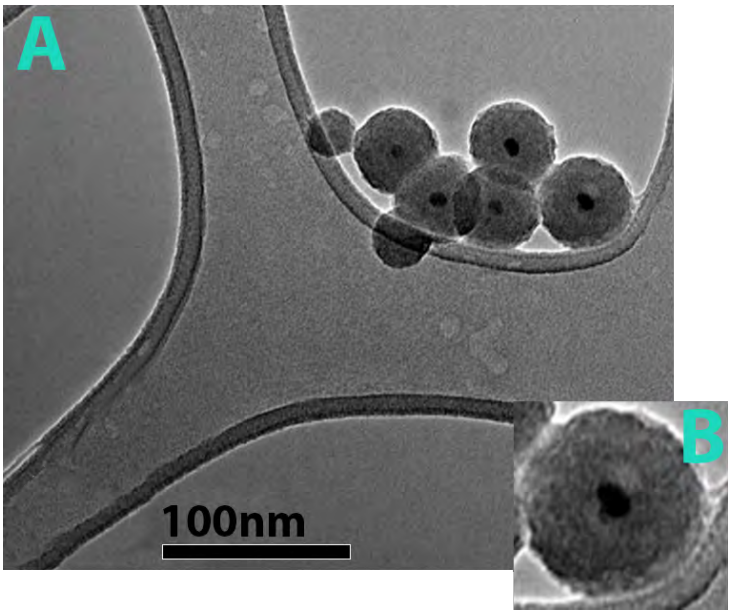

Figure 2.15: *A shows silica coated iron oxide Nanoparticles (sample CF-1-cs). Inset image B shows an enlarged single core@shell nanoparticle from this sample. Average TEM diameter of 49.47 ± 3.36 nm. Size obtained through using ImageJ*

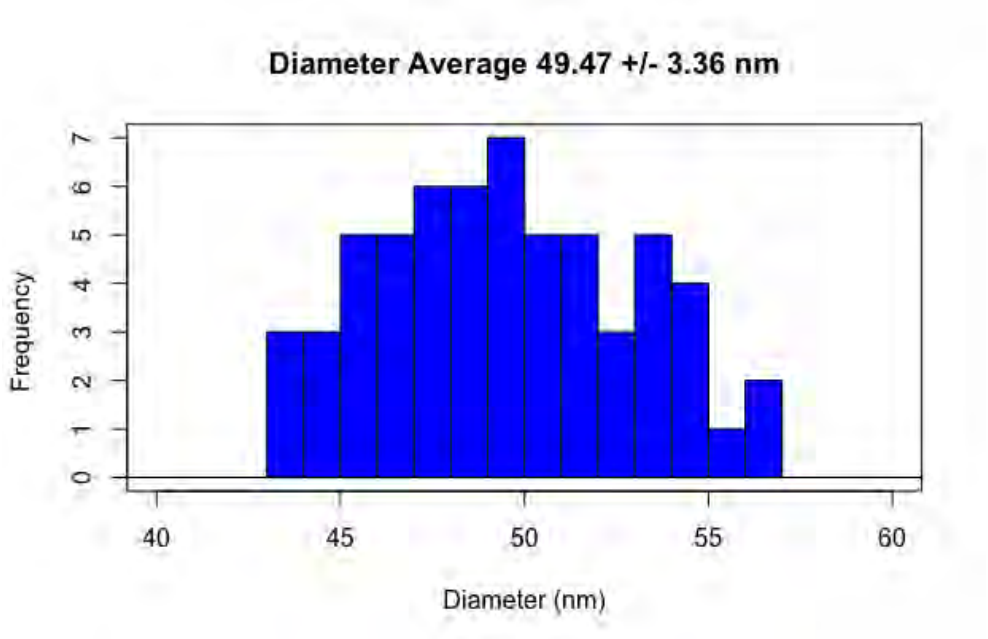

Figure 2.16: *Size distribution for silica coated iron oxide Nanoparticles (Sample: CF-1-cs) imaged by TEM.*

Table 2.5: *Summary of average diameter obtained by TEM and DLS for silica coated iron oxide nanoparticles.*

Nanoparticle	**D(DLS)(nm)**	**PDI**	**D(TEM)(nm)**
Core@Shell	515.4 ± 18.00	0.51	59.85 ± 5.43

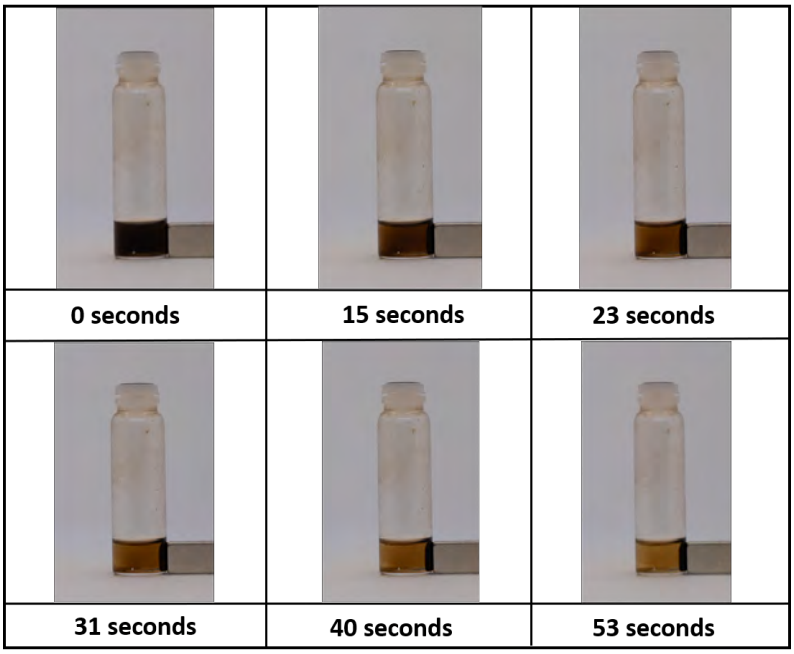

Figure 2.17: *Image showing the speed of magnetic separation for the silica coated Fe_3O_4 cores over 53 seconds. Most of the nanoparticles are pulled to the magnet after 31 seconds and the solvent is almost clear after 53 seconds.*

By repeating the simple experiment outlined earlier, using a N42 Neodymium Magnet (8.3kg Pull) introduced to the side of a flat bottomed small glass vial, this time containing 50mg of silica coated iron oxide cores in a 2mL EtOH:Water, 50:50 Solution, it can be seen that there has been a reduction in attraction to the magnet. This is shown in the time lapse sequence of photographs in Figure 2.14 which were again taken using the same Sony Alpha A7 Mirrorless camera system using a Sony 24-240mm Zoom lens (settings seen in Figure 2.34(in Bibliography)) in the same "lightbox" to ensure preservation of the original lighting conditions. It can be clearly observed from the images, that the same approximate state which took 6 seconds on the non-coated cores, now takes 31 seconds on the coated sample. The solution, in this case, took 53 seconds to clear to a similar state observed previously (15 seconds in the non-coated sample).

2.12 Surface Functionalisation

2.12.1 Amination - Addition of $-NH_2$ Groups

(3-Aminopropyl)triethoxysilane (APTES) is an amino-silane shown in Figure 2.18. The addition of APTES to nanoparticles as seen in Figure 2.18 is commonly used to attach an amino group to functional silane. This is often to allow for the attachment of ligands which can be used for bio-conjugation.

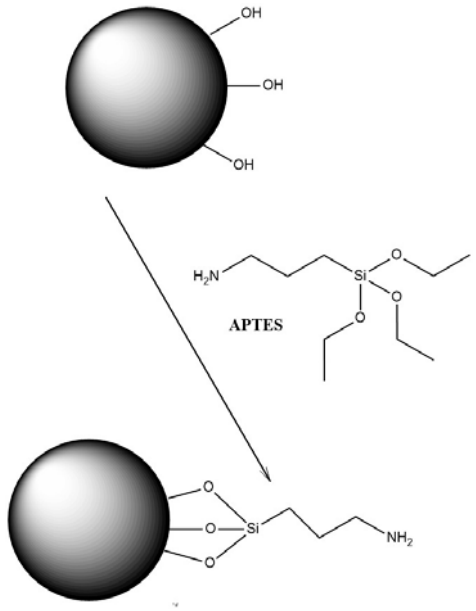

Figure 2.18: *Schematic drawing showing the addition of amine groups to core@shell nanoparticles and the structure of APTES.*

2.12.2 Addition of Fluorescent Dyes

NHS-Rhodamine (5/6-carboxy-tetramethyl-rhodamine succinimidyl ester), mixed isomer and NHS-Fluorescein (5/6-carboxyfluorescein succinimidyl ester), mixed isomer are amine-reactive derivatives of fluorescein dyes with chemical structures as seen in Figures 2.19a & 2.19b. These NHS esters are know to react efficiently with primary amino groups ($-NH_2$) when used within a pH range of 7-9 which results in the formation of stable amide bonds. Table 2.6 shows the excitation/emission wavelengths for the 2 fluorescent dyes used and the colour observed when imaged.

Imaging of nanoparticles by light based analytical techniques rather than TEM or SEM requires this additional functionalisation step due to

Table 2.6: *Excitation/Emission wavelengths (λ) for fluorescent dyes.*

Fluorescent Dye	**Excitation λ**	**Emission λ**	**Colour**
NHS-Rhodamine	552nm	575nm	Red
NHS-Fluorescein	494nm	518nm	Green

the lower resolution obtained by light based methods. The addition of fluorescent dyes to the surface of the silica coating of the nanoparticles allows for nanoparticles to be imaged. Figure 2.20 shows nanoparticles with NHS-Rhodamine attached to the surface which have been micro injected into RPE-1 (retinal pigment epithelial cells, human) cells and imaged using light microscopy . The nanoparticles can be seen within cells as bright spots of light and the image allows for differentiation of cells which have been injected and cells which have not been injected. The image however does not provide any detail of location of nanoparticles within the cell or the structure of the nanoparticles them selves.

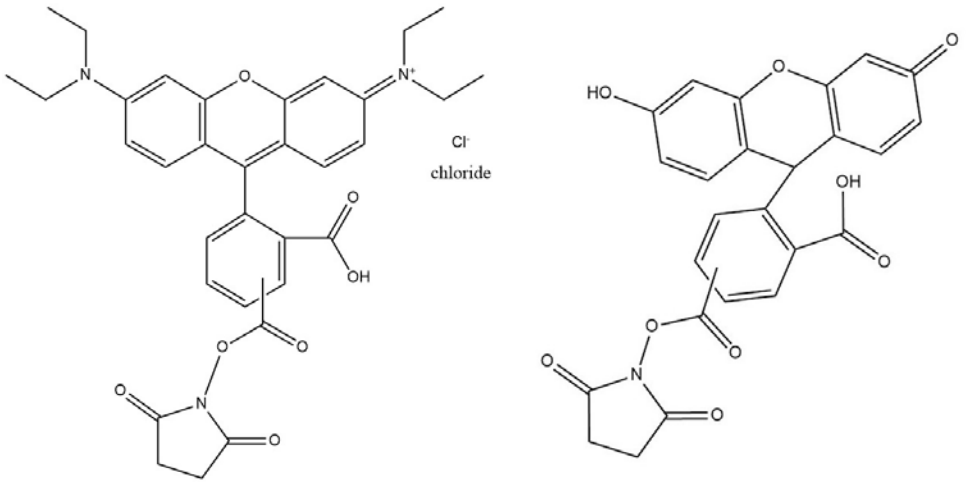

(a) Structure of NHS-Rhodamine. (b) Structure of NHS-Fluoroscein.

Figure 2.19: *Structure of two NHS ester fluorescent dyes.These fluorescent dyes are Amine-specific labeling—NHS-ester varieties of rhodamine and fluorescein. They can be used for the efficient labeling of antibodies and other purified proteins at primary amines.*

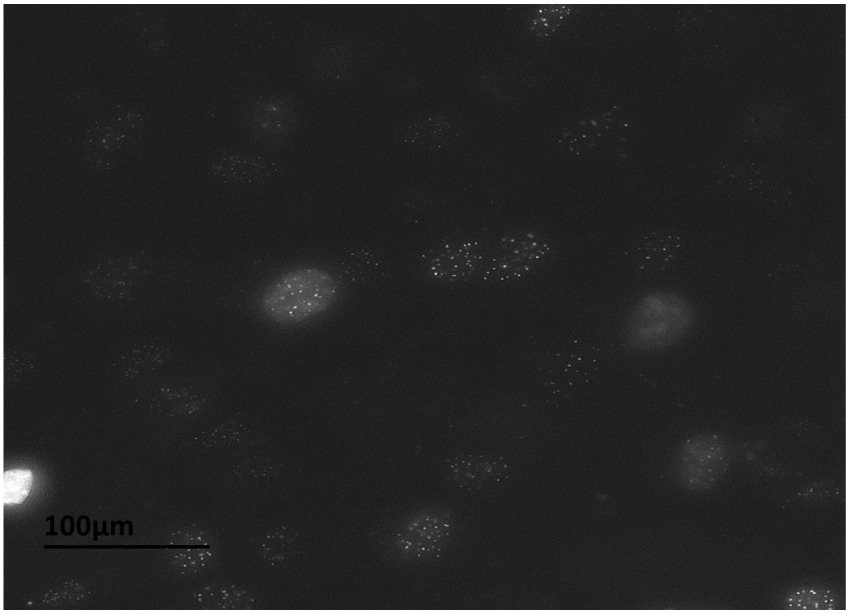

Figure 2.20: *Image shows nanoparticles with Fluorescent dye rhodamine b surface functionalisation (Sample: CF1-15-103). These nanoparticles have been micro injected into RPE1 cells and imaged using light microscopy. Excitation wavelength 552nm ,emission wavelength 575nm. Nanoparticles can be seen as bright spots which are within cells. This visualisation of NPs as bright "spots" is due to the addition of the fluorescent dye rhodamine b.*

Successful addition of fluorescent dyes can be established using UV-Vis spectroscopy (UV-Vis). Here the need to quantify how much dye had attached to the surface of the nanoparticles was not needed. This would need to be done in any future work. The presence and therefore the attachment of rhodamine B to the nanoparticles was checked using UV-Vis spectroscopy [80]. Post washing, UV-Vis of the nanoparticles in water was performed and the spectra obtained. Then the nanoparticles were separated by centrifugation and the water collected. A spectra for the water was then obtained. This allowed for comparison of spectras. It was desired that the water would show no peak for rhodamine and the sample with the nanoparticles in would show a peak for rhodamine indicating the rhodamine was attached to the nanoparticles but not free in the solution. The expected UV-Vis absorption peak for rhodamine is at a wavelength of 558nm [21N]. Examples of the spectra obtained can be seen in Figure 2.21

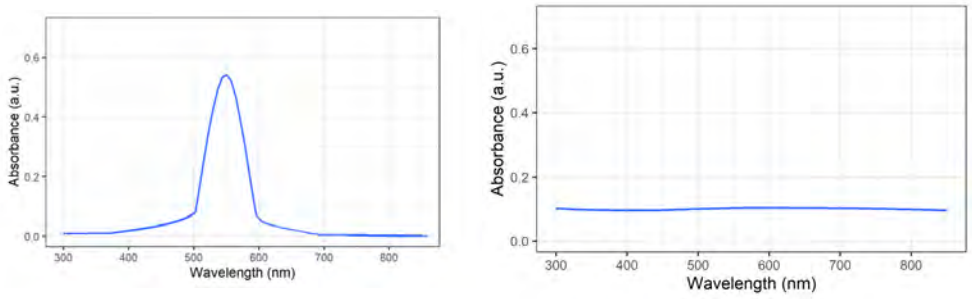

(a) (b)

Figure 2.21: *(a) An example UV-Vis spectra for NPs in water. (b) UV-Vis spectra for water. When compared a peak can be seen in (a) at 558nm which indicates the presence of rhodamine. Such peak is not present in (b). This would indicate that rhodamine is attached to the NPs rather than being loose in the water.*

2.12.3 Addition of Polyethylene Glycol (PEG)

The addition of PEG is discussed in greater detail in chapter 4. Chapter 4 covers the effect on PEG on aggregation and storage of nanoparticles. The addition of PEG to nanoparticles is relevant to not only aggregation however, but also enables a new binding site which can be used for addition of such things as HaloTags to allow for binding to a known region of a cell for example cempA using HaloTag succinimidyl Ester (04) Ligand.

2.12.4 Summary of the Design and Synthesis of Multi-Functional Nanoparticles for Biological Applications

The final design of the silica coated SPIONS as described here requires a multi-step synthesis which can be altered as required to produce super-paramagnetic nanoparticles of precise size and shape which are suitable for use in biological environments and able to undergo bio-conjugation to a variety of biomolecules. The design involves iron oxide (Fe_3O_4) cores which are then coated with silica to produce core@shell nanoparticles which have an even surface of silica which provides the nanoparticles with the ability to be functionalised dependent on requirements for the finished nanoparticles. The design considers cytotoxicity and the ability to alter surface chemistry to adapt nanoparticles to different uses and different targets for incorporation into cells and bio-conjugation.

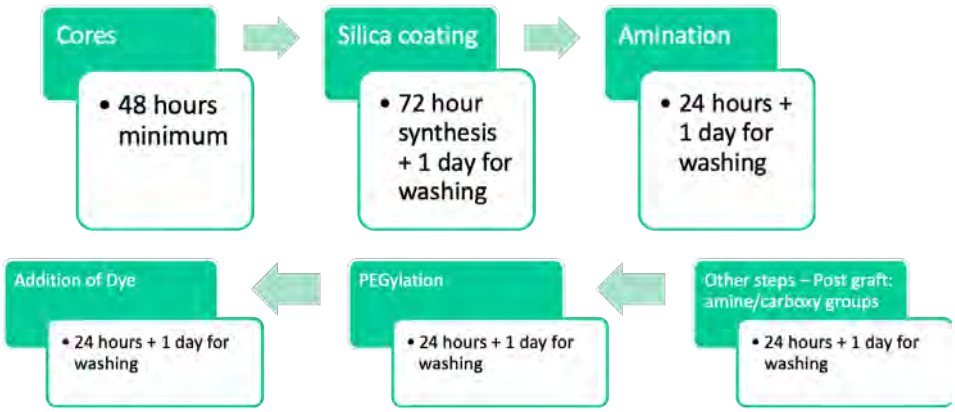

Figure 2.22: *Graphical representation of time taken per synthesis step.*

The total time needed for synthesis from cores to functionalisation is approximately two weeks and it is vital that NPs are thoroughly characterised at each step using multiple analytical techniques. The resulting nanoparticles are multi-functional, simple to make, biocompatible, use cheap materials and each step has a high degree of repeatability. Figure 2.22 summarises the time taken for each stage of synthesis to produce multifunctional silica coated superparamagnetic iron oxide nanoparticles.

2.13 Characterisation of Silica Coated Iron Oxide Nanoparticles

Highly functionalised silica-coated single-cored SPIONs were designed and synthesised for use in biological applications. Iron oxide cores were synthesised using a simple oleylamine synthesis, with the oleylamine acting as solvent, surfactant, reducing agent and stabiliser. This methodology builds upon but differs from previous work found in the literature.

Although iron oxide is bio-compatible, cell elongation and increased cell death will be seen with bare iron oxide nanoparticles. The silica coating provides a shell preventing these problems as well as allowing for further surface modification and protecting fluorescent moiety from energy transfer quenching due to the magnetic iron oxide particles. To achieve

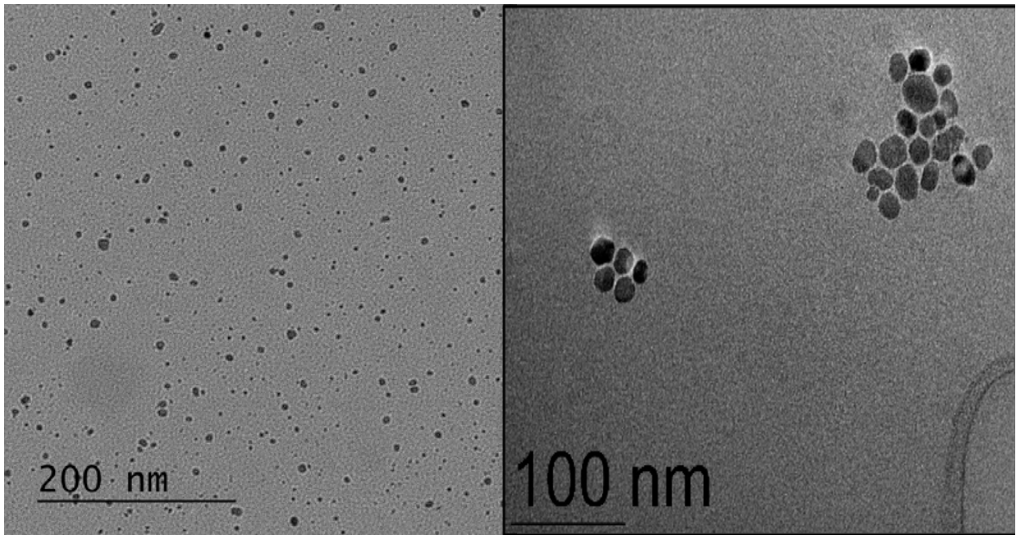

(a) (b)

Figure 2.23: *Iron oxide cores synthesised using the oleylamine solvothermal methodology imaged using TEM (Sample: CF-1-c2). TEM average diameter 14.77± 1.29 nm.) Image b) shows an unidentified artifact in the bottom right hand corner. This is likely to be an artifact introduced during sample prep and is no a component of the iron oxide cores.*

this the silica shell is required to be at least 5nm thick. Silica coating also reduces aggregation of the nanoparticles. Synthesis of core@shell nanoparticles with a single iron oxide core can be achieved. Nanoparticles which have a single iron oxide core and are thus suitable for biological use are interesting due to nanoparticles with varying number of multiple cores not allowing for the accurate determination of individual nanoparticles magnetic properties, which would reduce the accuracy in any future work if nanoparticles were used for any measurement of force within a biological environment.

Thorough characterisation of nanoparticles is required to ensure the nanoparticles meet the requirements previously discussed. Characterisation is also required to allow for depth of understanding of their potential behaviour within a biological environment. Many different analytical techniques can be employed to characterise nanoparticles. Here we use multiple analytical techniques to evaluate the nanoparticles. These techniques allow for imaging, size measurement, measurement of magnetic properties and evaluation of surface chemistry such as charge and moieties.

2.13.1 Transmission Electron Microscopy (TEM)

Samples for TEM were prepared by dropping nanoparticles suspended in ethanol (0.1mg/mL) onto a copper grid and allowing to dry overnight.

The images that can be seen in Figures 2.23 (a) and (b) and histogram in Figure 2.24 show the results of TEM analysis of iron oxide cores synthesised using the oleylamine solvothermal methodology.

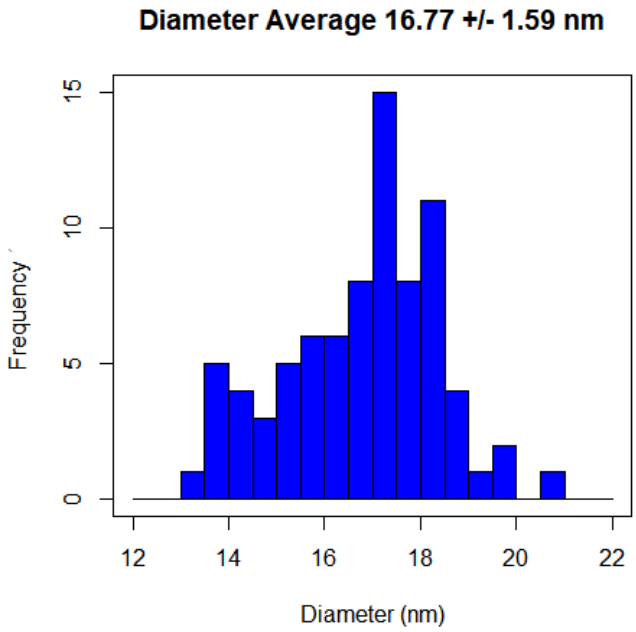

Figure 2.24: *Histogram from TEM showing size distribution of Oleylamine synthesised iron Oxide cores (Sample: CF-1-c2). Average diameter by TEM of 16.77 ± 1.29nm.*

Further TEM analysis was carried out on a sample of silica coated oleylamine synthesised iron Oxide core nanoparticles, as shown in Figure 2.25. The TEM image clearly shows the individual cores in a shell of silica. Figure 2.26 shows the size and distribution of this sample.

Table 2.7 shows a summary of diameter for both iron oxide nanoparticles and silica coated iron oxide nanoparticles as measured by TEM.

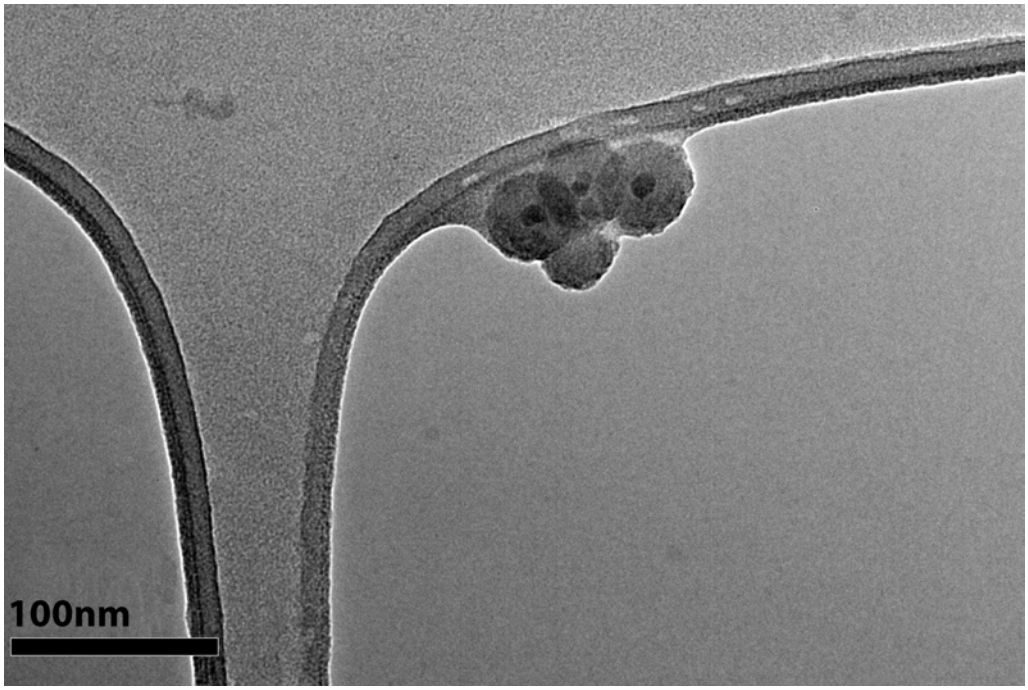

Figure 2.25: *TEM of core@shell nanoparticles (Sample CF-1-cs3) showing a single core in a shell of silica. Size 58,97 ± 6.62 nm*

Table 2.7: *Summary of diameter obtained by TEM and DLS for iron oxide nanoparticles and silica coated iron oxide nanoparticles.*

Nanoparticle	**D(DLS)(nm)**	**PDI**	**D(TEM)(nm)**
Iron Oxide Cores	285.8±14.47	0.37	16.94±1.89
Core@Shell	345.8 ± 11.47	0.46	58.97 ± 6.53

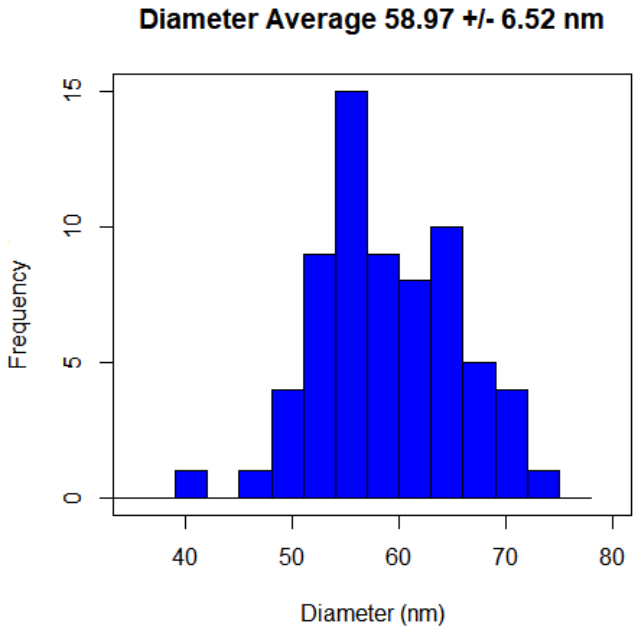

Figure 2.26: *Histogram from TEM showing size distribution of silica coated oleylamine synthesised iron Oxide cores. Average diameter by TEM of 58.97 ± 6.53nm.*

2.13.2 Zeta Potential

The surface charge of SPIONs play an important role in colloidal stability as well as cellular uptake of nanoparticles by endocytosis. Surface charge can be described as the behaviour of surface groups in solution when at a determined pH in the presence of an electrolyte. Surface charge can be measured as an electrical potential in the interfacial double layer on the surface of NPs in suspension, this is called the zeta potential. A high zeta potential regardless of whether it is a positive or negative value is indicative of dispersion stability of SPIONs due to electrostatic interactions.

Here as can be seen in Table 2.8 both the iron oxide cores and the silica coated core@shell nanoparticles have a high zeta potential indicating good colloidal stability.

Table 2.8: *Zeta Potential at approximately pH 7 for iron oxide cores (Sample CF-1-c) and core@shell nanoparticles (Sample CF-1-cs).*

Nanoparticle	**Zeta Potential (mV)**
Iron Oxide Cores	-27.1 +/-3.8
Core@Shell	-38.3 +/-4.2

2.13.3 Infrared (IR) spectroscopy

Infrared (IR) spectroscopy allows for highly discriminatory information of chemical composition to be obtained using the excitation of fundamental vibrational transitions characteristic of atoms or group of atoms in a material. IR radiation causes atoms or group of atoms to vibrate faster about their bonds. The vibrations are quantised leading compounds to absorb energy from a particular region which is specified by a wave number. Inherent infrared absorption of functional groups present at the nanoparticles surface mean that characterisation of nanoparticles can be achieved using spectroscopic techniques in the infrared range [46].

Figures 4.1, 2.28 and 2.29 show the spectra obtained from IR spectroscopy of the aminated silica coated Fe_3O_4 nanoparticles . All IR spectroscopy was carried out on the same samples. Samples CF1-14-67 for iron oxide cores and CF1-16-73 for silica coated iron oxide NPs. The spectra are consistent with expectations, showing absorption peaks for iron at approximately 580cm $^{-1}$. Silica show asymmetric vibration of Si–O at approximately 1090 cm^{-1}, asymmetric vibration of Si–OH at 950 cm^{-1}, and symmetric vibration of Si–O at approximately 795 cm $^{-1}$. APTES shows a peak at approximately 900cm^{-1} the expected wavelength for the indicative asymmetric vibration of Si-OH.

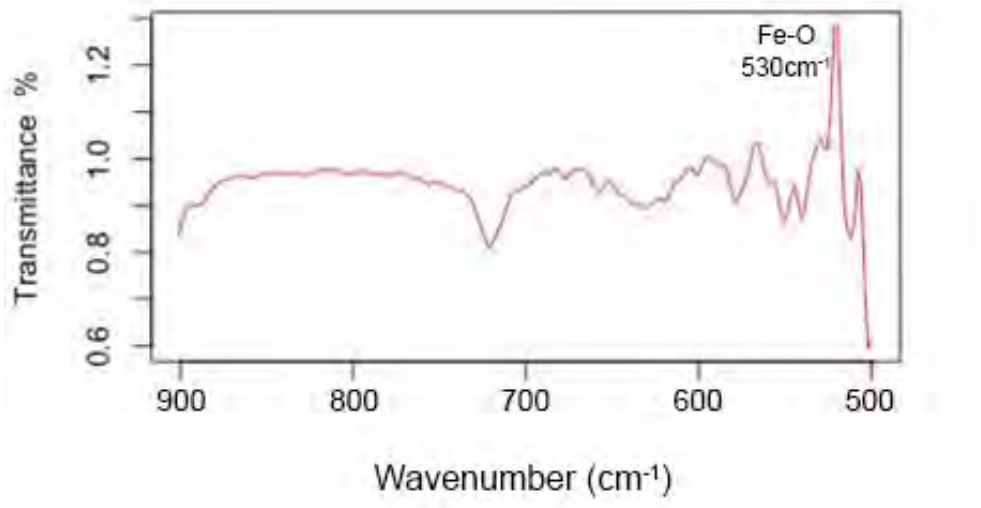

Figure 2.27: *IR spectra for Iron oxide cores (CF1-14-67). Spectra shows FE-O stretching at 520cm^{-1}.*

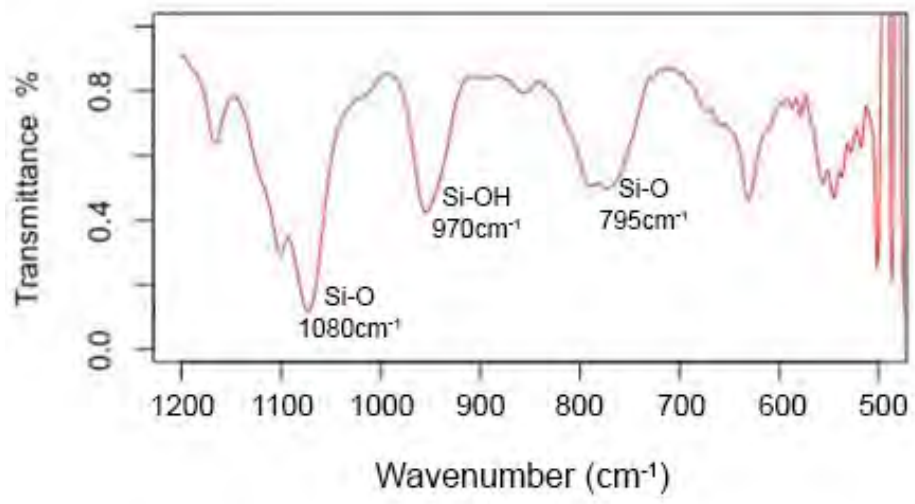

Figure 2.28: *IR spectra Core@shell silica coated iron oxide nanoparticles (CF1-16-73). Peaks show asymmetric vibration of Si–O (1090cm^{-1}), asymmetric vibration of Si–OH, (950cm^{-1}), and symmetric vibration of Si–O (795cm^{-1}).*

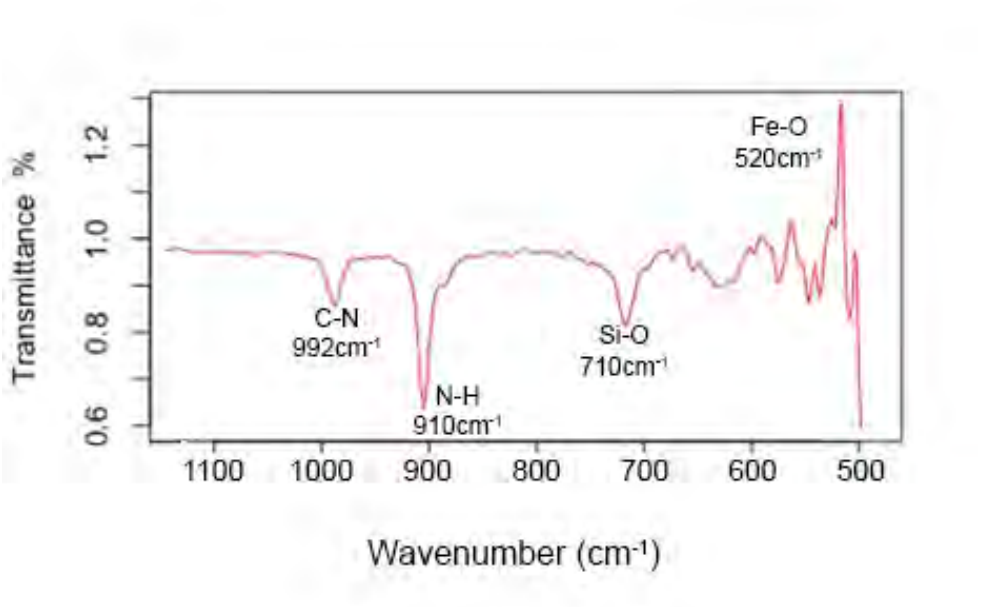

Figure 2.29: *IR spectra obtained for magnetic silica coated nanoparticles post functionalisation with APTES (CF1-16-73). Spectra shows wavelengths corresponding to a C–N stretch from 1250–1020cm^{-1} and a N–H wag (primary and secondary amines only) from 910-665cm^{-1}* indicating the nanoparticles have been functionalised with APTES Also can be seen are previously described peaks for silica and iron oxide.

2.13.4 X-Ray Diffraction (XRD)

X-Ray Diffraction (XRD) results for the oleylamine synthesised iron oxide cores can seen in Figure 2.30. The results suggest that the iron oxide cores are mainly single phase magnetite (Fe_3O_4) as required. The XRD spectra shows peaks which correspond to (111), (220), (311), (400), (422),(511), (440) and (533) which indicate single phase magnetite, according to pattern 87-2334 of the JCPDS database [81]. The spectra does demonstrate that other iron phases will be present within a sample such as Fe O (OH) with peaks such as the one seen at 400 in the spectra indicating their presence (see Figure 2.30). It is not easy to distinguish between nanoparticles of Fe_3O_4 and Fe_2O_3 structures by X-ray diffraction. This is because the structure of Fe_2O_3 means that tetrahedral and octahedral sites are occupied by $Fe_3{}^+$, meaning that reflections of both iron oxide nanoparticles have the same positions. XRD was carried out in conjunction with Dr David Walker of the University of Warwick.

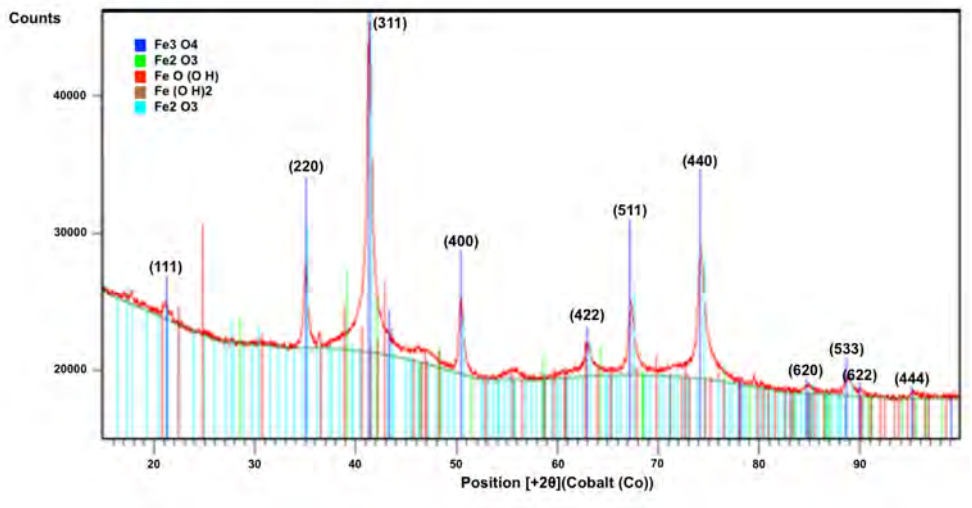

Figure 2.30: *X-Ray Diffraction (XRD) results show that the iron oxide cores are mainly single phase Fe_3O_4 (sample CF-14-67) as required. XRD was carried out in conjunction with Dr David Walker of the University of Warwick.*

2.13.5 Superconducting Quantum Interference Device (SQUID) Magnetometry Analysis

SQUID shows that both the iron oxide cores and the core@shell nanoparticles are superparamagnetic. With both samples showing no coercivity or hysteresis. The cores (Figure 2.31) demonstrate a magnetic saturation of approximately 10.70 emu g^{-1}. As expected, silica coating of the iron oxide cores results in a magnetic saturation of 7.22 emu g^{-1} which is a reduction in the magnetism of the nanoparticles (Figure 2.32). This is due to the silica coating shielding the magnetic core. The thickness of the silica shell correlates to the reduction of magnetic saturation observed, with the thicker the shell the greater the reduction in magnetic saturation achieved. The lack of coercivity and hysteresis can be seen in Figures 2.31 and 2.32 as there is a single line with no "loop" present as one would expect for a material which was not superparamagnetic and therefore exhibits magnetic memory.

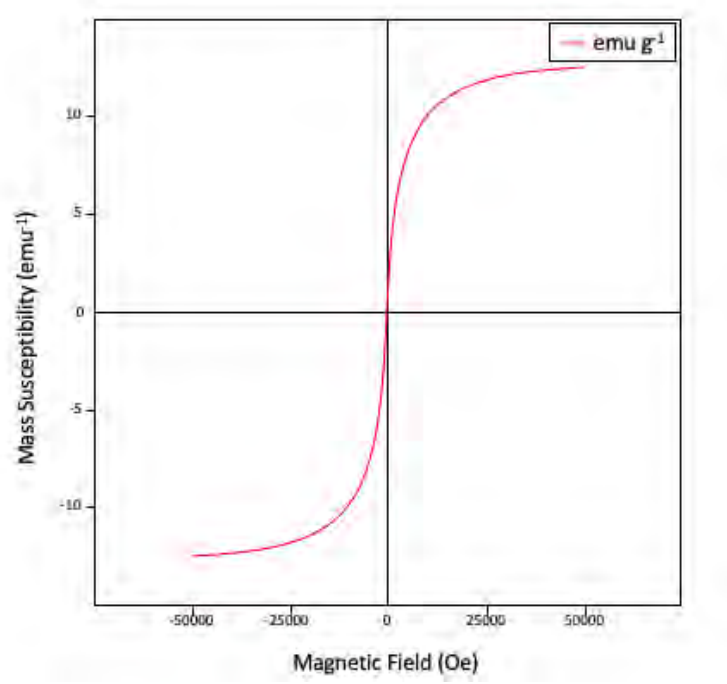

Figure 2.31: *SQUID hysteresis curve of iron oxide cores (sample CF-14-67) obtained at 300K.*

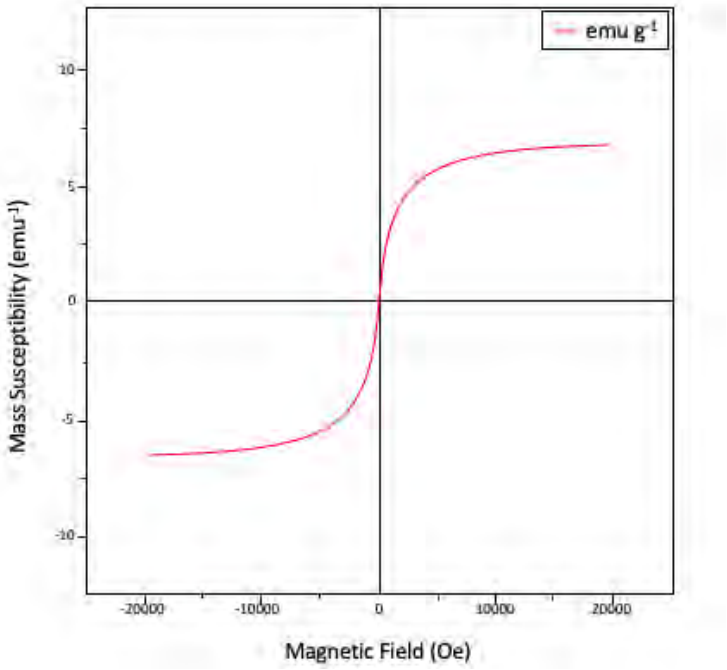

Figure 2.32: *SQUID hysteresis curve of Silica coated iron oxide nanoparticles (sample CF-16-76) (core@shell) obtained at 300K.*

2.14 Conclusion

Design and synthesis of multi functional superparmagnetic silica coated iron oxide nanoparticles suitable for use in biological environments is achievable. Nanoparticles can be synthesised that are highly uniform in size, shape, magnetism with a single core. Surface chemistry can be controlled and designed so that the nanoparticles can be functionalised dependent on future application. Synthesis can be time consuming with the nanoparticles described here taking up to 14 days from core synthesis to surface functionalisation. Through the synthesis described here repeatability is good and nanoparticles can me made using cost effective methods and materials.

It is important to have clear knowledge of potential uses of nanoparticles and the future environment the nanoparticles will be used in when considering design. Desired properties must be considered at all stages and consequences of each step considered in relation to previous steps. For example the effect on the magnetic moment of iron oxide cores when coated with silica or the effect on potential toxicity to cells from surface functionalisation. Characterisation of nanoparticles is essential for a complete understanding of nanoparticle behaviour and surface chemistry. Multiple analytical techniques are required to provide a thorough understanding of nanoparticle properties.

2.15 Further Work

Whilst the design and synthesis of nanoparticles which can be used for a variety of biological applications has been achieved, further characterisation and investigation into nanoparticle behaviour would be beneficial. This includes toxicity studies to ensure nanoparticles do not result in a high rate of cell death over time. Use of these nanoparticles within cells as discussed in chapter 4 suggests nanoparticles are not toxic over a short period of time however this should be quantised.

Synthesis of the iron oxide cores using oleylamine as solvent, reducing agent and capping agent works well however reports of OAm purity having an effect on the resulting nanoparticles should be evaluated.

The overall synthesis of these nanoparticles is approximately 14 days. Further development of the protocols for each step to try and reduce this length of time would be potentially beneficial.

Further refinement of the nanoparticles such as addition of a wider variety of functional groups to the surface and the use of other metals such as titanium as cores could allow for more applications for these nanoparticles.

2.16 References - Chapter 2

1. O. Salata, Journal of Nanobiotechnology, 2004, 2, 3.
2. N. Wang, J. Fuh, S. Dheen and A. Senthil Kumar, Bio-Design and Manufacturing, 2021, 4, 379-404.
3. R. Dubey, Y. Rajesh and M. More, Materials Today: Proceedings, 2015, 2, 3575-3579.
4. J. Armond, E. Harry, A. McAinsh and N. Burroughs, PLOS Computational Biology, 2015, 11, e1004607.
5. S. Mourdikoudis and L. Liz-Marzán, Chemistry of Materials, 2013, 25, 1465-1476.
6. S. Mourdikoudis, R. Pallares and N. Thanh, Nanoscale, 2018, 10, 12871-12934.
7. C. Murray, C. Kagan and M. Bawendi, Annual Review of Materials Science, 2000, 30, 545-610.
8. C. Sun, J. Lee and M. Zhang, Advanced Drug Delivery Reviews, 2008, 60, 1252-1265.
9. O. Veiseh, J. Gunn and M. Zhang, Advanced Drug Delivery Reviews, 2010, 62, 284-304.
10. J. MCCARTHY and R. WEISSLEDER, Advanced Drug Delivery Reviews, 2008, 60, 1241-1251.
11. S. Aime, D. Castelli, S. Crich, E. Gianolio and E. Terreno, Accounts of Chemical Research, 2009, 42, 822-831.
12 .J. Singh and A. Daftary, Journal of Nuclear Medicine Technology, 2008, 36, 69-74.
13. H. Choi, K. Nasr, S. Alyabyev, D. Feith, J. Lee, S. Kim, Y. Ashitate, H. Hyun, G. Patonay, L. Strekowski, M. Henary and J. Frangioni, Angewandte Chemie International Edition, 2011, 50, 6258-6263.
14. C. Hadjipanayis, M. Bonder, S. Balakrishnan, X. Wang, H. Mao and G. Hadjipanayis, Small, 2008, 4, 1925-1929.
15. P. Mi, D. Kokuryo, H. Cabral, H. Wu, Y. Terada, T. Saga, I. Aoki, N. Nishiyama and K. Kataoka, Nature Nanotechnology, 2016, 11, 724-730.
16. D. Giljohann, D. Seferos, W. Daniel, M. Massich, P. Patel and C. Mirkin, Angewandte Chemie International Edition, 2010, 49, 3280-3294.
17. D. Kim, S. Park, J. Lee, Y. Jeong and S. Jon, Journal of the American Chemical Society, 2007, 129, 7661-7665.
18. O. Rabin, J. Manuel Perez, J. Grimm, G. Wojtkiewicz and R. Weissleder, Nature Materials, 2006, 5, 118-122.

19. J. Kinsella, R. Jimenez, P. Karmali, A. Rush, V. Kotamraju, N. Gianneschi, E. Ruoslahti, D. Stupack and M. Sailor, Angewandte Chemie International Edition, 2011, 50, 12308-12311.
20. K. Ai, Y. Liu, J. Liu, Q. Yuan, Y. He and L. Lu, Advanced Materials, 2011, 23, 4886-4891.
21. M. Oh, N. Lee, H. Kim, S. Park, Y. Piao, J. Lee, S. Jun, W. Moon, S. Choi and T. Hyeon, Journal of the American Chemical Society, 2011, 133, 5508-5515.
22. P. Bonitatibus, Jr., A. Torres, G. Goddard, P. FitzGerald and A. Kulkarni, Chemical Communications, 2010, 46, 8956.
23. N. Lee, Y. Choi, Y. Lee, M. Park, W. Moon, S. Choi and T. Hyeon, Nano Letters, 2012, 12, 3127-3131.
24. J. Jang, H. Nah, J. Lee, S. Moon, M. Kim and J. Cheon, Angewandte Chemie International Edition, 2009, 48, 1234-1238.
25. R. Chen, M. Christiansen, A. Sourakov, A. Mohr, Y. Matsumoto, S. Okada, A. Jasanoff and P. Anikeeva, Nano Letters, 2016, 16, 1345-1351.
26. G. Cooper, Cell a molecular approach, 4th ed. + lecture notebook, Sinauer Associates, [Place of publication not identified], 2007.
27. G. Chan, S. Liu and T. Yen, Trends in Cell Biology, 2005, 15, 589-598.
28. S. McCarthy, G. Davies and Y. Gun'ko, Nature Protocols, 2012, 7, 1677-1693.
29. J. Armond, E. Harry, A. McAinsh and N. Burroughs, PLOS Computational Biology, 2015, 11, e1004607.
30. H. Qi, B. Yan and W. Lu, Journal of Sol-Gel Science and Technology, 2013, 69, 67-71.
31. K. Nam, J. Shim, H. Ki, S. Choi, G. Lee, J. Jang, Y. Jo, M. Jung, H. Song and J. Park, Angewandte Chemie International Edition, 2008, 47, 9504-9508.
32. J. Mohapatra, A. Mitra, H. Tyagi, D. Bahadur and M. Aslam, Nanoscale, 2015, 7, 9174-9184.
33. J. Kehrer, Toxicology, 2000, 149, 43-50.
34. C. Blanco-Andujar, D. Ortega, Q. Pankhurst and N. Thanh, Journal of Materials Chemistry, 2012, 22, 12498.
35. J. Mohapatra, A. Mitra, H. Tyagi, D. Bahadur and M. Aslam, Nanoscale, 2015, 7, 9174-9184.
36. R. Rasheed and V. Meera, Procedia Technology, 2016, 24, 210-216.
37. I. Hamley, Angewandte Chemie International Edition, 2003, 42,

1692-1712.
38. A. Ali, H. Zafar, M. Zia, I. ul Haq, A. Phull, J. Ali and A. Hussain, Nanotechnology, Science and Applications, 2016, Volume 9, 49-67.
39. Y. Sahoo, H. Pizem, T. Fried, D. Golodnitsky, L. Burstein, C. Sukenik and G. Markovich, Langmuir, 2001, 17, 7907-7911.
40. Y. Wang, J. Wong, X. Teng, X. Lin and H. Yang, Nano Letters, 2003, 3, 1555-1559.
41. T. Pellegrino, L. Manna, S. Kudera, T. Liedl, D. Koktysh, A. Rogach, S. Keller, J. Rädler, G. Natile and W. Parak, Nano Letters, 2004, 4, 703-707.
42. X. Zhao and J. Milton Harris, Journal of Pharmaceutical Sciences, 1998, 87, 1450-1458.
43. S. Gómez-Lopera, R. Plaza and A. Delgado, Journal of Colloid and Interface Science, 2001, 240, 40-47.
44. W. Voit, D. Kim, W. Zapka, M. Muhammed and K. Rao, MRS Proceedings, 2001, 676.
45. T. Sen and I. Bruce, Microporous and Mesoporous Materials, 2009, 120, 246-251.
46. I. Bruce and T. Sen, Langmuir, 2005, 21, 7029-7035.
47. J. Lipfert, X. Hao and N. Dekker, Biophysical Journal, 2009, 96, 5040-5049.
48. K. Neuman and A. Nagy, Nature Methods, 2008, 5, 491-505.
49. R. Chokkareddy, N. Bhajanthri, B. Kabane and G. Redhi, Nanomaterials: Biomedical, Environmental, and Engineering Applications, 2018, 173-204.
50. S. Laurent, D. Forge, M. Port, A. Roch, C. Robic, L. Vander Elst and R. Muller, Chemical Reviews, 2008, 108, 2064-2110.
51. A. Gupta and M. Gupta, Biomaterials, 2005, 26, 3995-4021.
52. S. Majidi, F. Zeinali Sehrig, S. Farkhani, M. Soleymani Goloujeh and A. Akbarzadeh, Artificial Cells, Nanomedicine, and Biotechnology, 2014, 44, 722-734.
53. V. Shubayev, T. Pisanic and S. Jin, Advanced Drug Delivery Reviews, 2009, 61, 467-477.
54. A. Ali, H. Zafar, M. Zia, I. ul Haq, A. Phull, J. Ali and A. Hussain, Nanotechnology, Science and Applications, 2016, Volume 9, 49-67.
55. R. Rasheed and V. Meera, Procedia Technology, 2016, 24, 210-216.
56. M. Osial, P. Rybicka, M. Pekała, G. Cichowicz, M. Cyrański and P.

Krysiński, Nanomaterials, 2018, 8, 430.
57. R. Bhandari, P. Gupta, T. Dziubla and J. Hilt, Materials Science and Engineering: C, 2016, 67, 59-64.
58. H. Fatima and K. Kim, Advanced Powder Technology, 2018, 29, 2678-2685.
59. R. Gruskiene, T. Krivorotova, R. Staneviciene, D. Ratautas, E. Serviene and J. Sereikaite, Colloids and Surfaces B: Biointerfaces, 2018, 169, 126-134.
60. A. Lassoued, B. Dkhil, A. Gadri and S. Ammar, Results in Physics, 2017, 7, 3007-3015.
61. S. Belaïd, D. Stanicki, L. Vander Elst, R. Muller and S. Laurent, Nanotechnology, 2018, 29, 165603.
62. N. Frey, S. Peng, K. Cheng and S. Sun, Chemical Society Reviews, 2009, 38, 2532.
63. W. Glasgow, B. Fellows, B. Qi, T. Darroudi, C. Kitchens, L. Ye, T. Crawford and O. Mefford, Particuology, 2016, 26, 47-53.
64. N. Jović Orsini, B. Babić-Stojić, V. Spasojević, M. Calatayud, N. Cvjetićanin and G. Goya, Journal of Magnetism and Magnetic Materials, 2018, 449, 286-296.
65. P. Biehl, M. von der Lühe, S. Dutz and F. Schacher, Polymers, 2018, 10, 91.
66. A. Lu, E. Salabas and F. Schüth, Angewandte Chemie International Edition, 2007, 46, 1222-1244.
67. Y. Wang, C. Yang and X. Yan, Nanoscale, 2017, 9, 9049-9055.
68. S. F. Hasany, I. Ahmed, R. J and A. Rehman, Nanoscience and Nanotechnology, 2013, 2, 148-158.
69. S. Riaz, S. Shah, Z. Kayani and S. Naseem, Materials Today: Proceedings, 2015, 2, 5280-5287.
70. J. Park, K. An, Y. Hwang, J. Park, H. Noh, J. Kim, J. Park, N. Hwang and T. Hyeon, Nature Materials, 2004, 3, 891-895.
71. M. Bloemen, W. Brullot, T. Luong, N. Geukens, A. Gils and T. Verbiest, Journal of Nanoparticle Research, 2012, 14.
72. J. Borges, J. Ribeiro, E. Pereira, C. Carreira, C. Pereira and F. Silva, Journal of Colloid and Interface Science, 2011, 358, 626-634.
73 .S. Mourdikoudis and L. Liz-Marzán, Chemistry of Materials, 2013, 25, 1465-1476.
74. W. Wu, Z. Wu, T. Yu, C. Jiang and W. Kim, Science and Technology

of Advanced Materials, 2015, 16, 023501.
75. L. Arias, J. Pessan, A. Vieira, T. Lima, A. Delbem and D. Monteiro, Antibiotics, 2018, 7, 46.
76. S. Sun, C. Wei, Z. Zhu, Y. Hou, S. Venkatraman and Z. Xu, Chinese Physics B, 2014, 23, 037503.
77. Y. Li, Y. Hu, H. Jiang and C. Li, Nanoscale, 2013, 5, 5360.
78. A. Tricoli, M. Righettoni, F. Krumeich, W. Stark and S. Pratsinis, Nanotechnology, 2010, 21, 465604.
79. M. Sonmez, M. Georgescu, L. Alexandrescu, D. Gurau, A. Ficai, D. Ficai and E. Andronescu, Current Pharmaceutical Design, 2015, 21, 5324-5335.
80. Y. Unsal, M. Soylak and M. Tuzen, Journal of AOAC INTERNATIONAL, 2014, 97, 1459-1462.
81. Govinfo.gov, 2022.

2.17 Bibliography

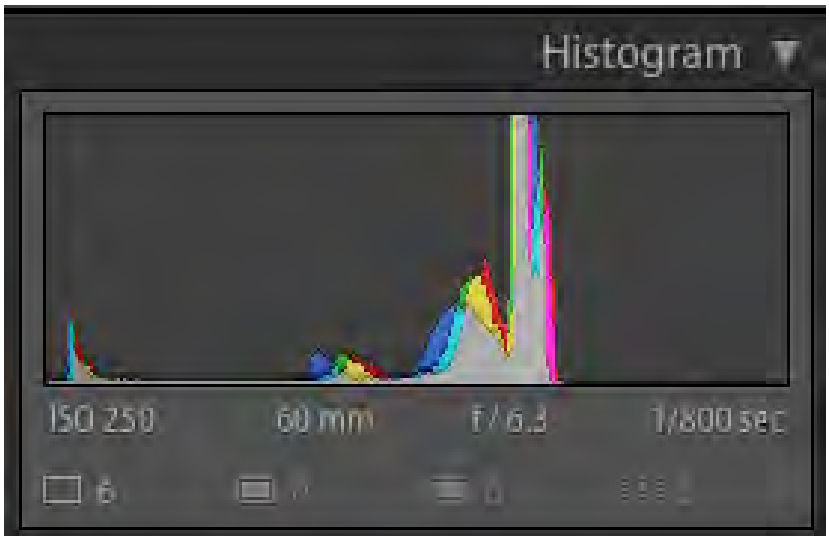

Figure 2.33: *Camera setting for Figure 2.14 ISO 250 -Sensitivity to light, 60nm -Focal Length, f/6.3 - (f stop -ratio of the system's focal length to the diameter of the entrance pupil), 1/800sec - shutter speed.*

Figure 2.34: *Camera setting for Figure 2.17 ISO 250 -Sensitivity to light, 60nm -Focal Length, f/6.3 - (f stop -ratio of the system's focal length to the diameter of the entrance pupil), 1/800sec - shutter speed.*

Chapter 3

Surface Functionalisation of Magnetic Nanoparticles with Polymers

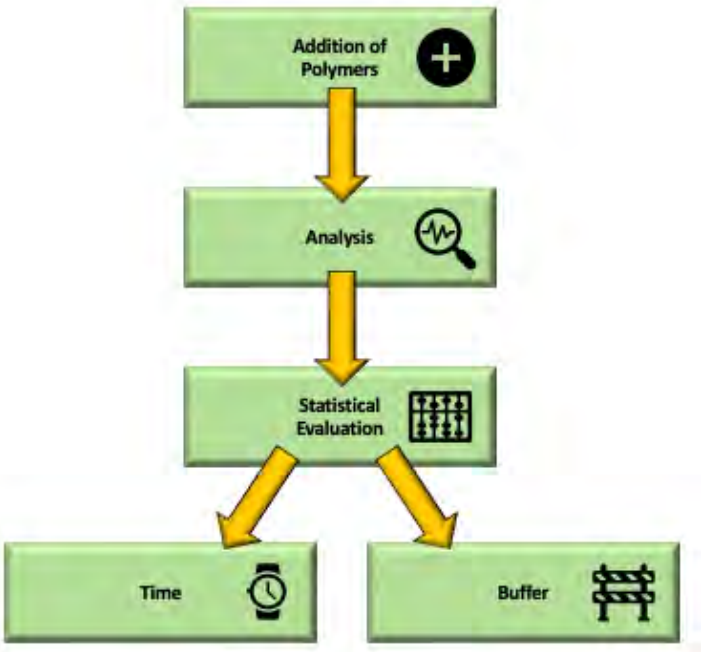

Figure 3.1: *Graphical representation of Chapter four. Including attachment of polymers to nanoparticle surface, analysis and statistical analysis.*

3.1 Introduction

Aggregation of nanoparticles is a primary concern when designing and synthesising nanoparticles. The small size of nanoparticles influences many factors such as mobility, caused by Brownian motion, these are often a benefit for use in biological environments. The small size of nanoparticles also results in high surface energy due to surface defects and "dangling" bonds. This result in NPs tending to aggregate which lowers the surface area. This aggregation can be a negative and should be controlled and understood. Aggregation is defined as tightly bound collections of NPs which are difficult to break [1][2].

This aggregation is often reduced by surface functionalisation, which adjusts steric interactions or charge. Reduction of aggregation by surface functionalisation of nanoparticles with polymers in solution is a result of exploiting the balance between attractive Van der Waals, steric effects, hydrogen bonding, and hydrophobic interactions and electrostatic repulsion. This allows the synthesis of NPs with limited aggregation [2]. Polymer addition aids in the lowering of Van der Waals forces reducing the attraction between nanoparticles. This aids in nanoparticle separation [1][2].

Polymers are materials that are composed of macromolecules (IUPAC definition).[3] They are made up of multiple repeat units to form molecules of high relative molecular mass from the repeat units which are of low relative molecular mass.[3][4]

Polymers can be both synthetic and naturally occurring and have a wide range of properties associated with them. [4] Everyday familiarity with polymers exists with polyethylene and nylon being examples of synthetic polymers, as well as natural polymers which include bio-polymers such as DNA and cellulose. Polymers have properties which include high elasticity, semi crystalline structures, and toughness.

Polymerisation is the process where small units known as monomers are combined to form a covalently bonded chain or network. The length of a polymer chain is defined as the degree of polymerisation. This is a quantifiable number based on the number of monomers in the chain. [5][6] Polymerisation of monomers can result in the loss of chemical groups from the monomer; for example, the monomers ethylene glycol and terephthalic acid polymerise to form PET polyester. During this process, the monomers lose 2 water molecules. The part of the monomer

that is incorporated into the polymer are known as the monomer residue or the repeat unit.[7]

Polymers have properties that are dependent on several factors. These include molecular weight, i.e. the length of the polymer chain.[8] As chain length increases, strength and toughness often increase, glass-transition increases and chain mobility decreases.[5] These changes in properties are due to Van der Waals attractions and chain entanglements increasing with chain length. [9][10] Polymers may be unbranched, branched and cross-linked.[11] This affects the physical properties of a polymer including those of solubility in solvents and viscosity in solution.

3.1.1 Polymers In Biomedical Research

Polymers for medicinal purposes is a field that is now growing rapidly, with potential uses which help overcome traditional obstacles to new and emerging treatments. The use of synthetic polymers for medicinal purposes became more popular after the second world war when polymers began to be used in the manufacture of prosthetic eyes such as those seen in Figure 3.2 as a replacement for glass. Glass had become difficult to obtain leading to s search for new materials. Polymers have remained the materials of choice for prosthetic eyes due to acrylic giving a patient a better fit with greater comfort, as well as being more durable and unlikely to break.

Figure 3.2: *Prosthetic eye made using the acrylic polymer Polymethylmethacrylate (PMMA).[12] Image taken 21/08/2021 courtesy of owner.*

Polymers are now being used in many different medical applications

including bone repair and tissue engineering as scaffolds. Drug delivery has become a major area of research as the properties of polymers can differ from other materials with properties which allow for such things as drug entrapment in polymeric matrices.[13][14]

Polymers have and can be used in the treatment of many different ailments. These include cancer and hepatitis, to name a few, and consistently play a role in the production of oral tablets and capsules.[15] Tissue engineering uses scaffold of polymer to direct tissue growth.[15] Polymer matrices made from both synthetic and natural polymers can be used to deliver growth factors and cytokines to areas where tissue needs repair, aiding angiogenesis.[15]

The future uses of polymers in biomedical science seems unlimited, with potential applications in many new and upcoming areas including but not limited to gene therapy. The potential of polymers when combined with other materials of biomedical interest such as nanoparticles and microparticles becomes even greater.

3.1.2 Responsive polymers

Polymers in general are considered favourably for their potential use in the biomedical field. With interest in their use for drug delivery, cell growth scaffolds and hydrogels [16]. Due to the development of nanoparticles within this work for biological research and potential use as for example MRI contrast agents, the behaviour of responsive polymers is of interest to this work. Nanoparticles designed and discussed here could be partnered with responsive polymers for use in bio-imaging or drug delivery for example.

Responsive polymers, which respond to known stimuli, have become increasingly of interest. These polymers can use their response to stimuli to provide extra function or desired dynamic to materials.

Out of the responsive polymers, thermo-responsive polymers are of most interest for biomedical and cell biology research purposes where they have potential for use in drug delivery and bioseparation.[17] Thermo responsive polymers are of the most interest with respect to this work given that iron oxide nanoparticles that those designed and synthesised here could be suitable for use for hyperthermia treatments involving increases in temperature. Future functionalisation of the nanoparticles with thermo responsive polymers could potentially also allow for the

nanoparticles to be used for drug delivery during this type of treatment.

Thermo responsive polymers have been extensively studied. They are often classified by their behaviour in response to temperature into two types. These are lower critical solution temperature (LCST) and upper critical solution temperature (UCST).[18-21]

Polymers which demonstrate LCST are able to be dissolved in either aqueous or organic solutions at temperatures which are lower than the LCST. If the temperature is higher than the LCST polymeric intramolecular and intermolecular hydrophobic interaction accelerate leading to these polymers becoming hydrophobic. This change in solubility is reversible and can be used for applications in drug carriers, sensors and chromatography [18-23].

LCST and UCST can be understood by the Gibbs free energy equation:

$$\Delta G = \Delta H\text{-}T\,\Delta S \text{ [24][25]}$$

For polymers which are classed as LCST at low temperatures (T <LCST) a negative enthalpy is seen. If the temperature is increased this triggers perturbation. This leads to the disruption of the hydrogen bonds at a temperature approximately equal to the LCST. At T >LCST, endothermic breaking of hydrogen bonds undergoes endothermic breaking. This results in the enthalpic term becoming less negative. For polymers which are classified as UCST the reverse is true [24][25]. Figure 3.3 shows how the two regions of partial miscibility seen in these polymers may be merged so as to create a 'hourglass' phase diagram [26].

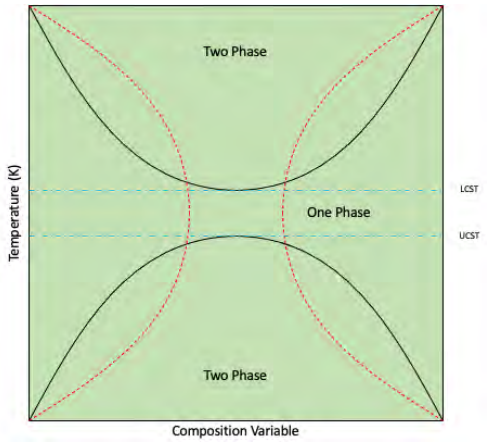

Figure 3.3: *Upper (UCST) and lower critical solution temperatures (LCST). Solid line show phase diagrams for UCST and LCST with a one phase region between. The dashed set of curves show the LCST and UCST overlap in an hourglass shaped phase diagram.*

These polymers in the form of star-like copolymers have been joined to gold nanoparticles. The resulting nanocomposite above the LCST had high dispersibility in aqueous solutions. Investigation into properties such as precipitation and aggregation of the nanocomposites found that thes properties were dependent upon the amount of linear thermo responsive polymers added.[27]

UCST polymers however dissolve in solvents above the UCST. They are insoluable below the UCST. UCST behaviour occurs as a result of interactions such as electrostatic interactions and hydrogen bonding. UCST polymers have been used for protein separation and sensors.[18][19]

For example layer by layer temperature responsive films have been developed which consist of UCST thermo responsive polymers and tannic acid. It was observed that temperature, ionic strength and temperature all affected the thicknesses seen of the films.[28]

Recently, synthesis of bio-compatible devices which have uses within a biological environment have gained interest. These could be nanoparticles, microparticles or hydrogels.[29-36]. These devices must consider many different properties such as method of introduction whether that be intravenous, subcutaneous, or oral alongside considerations of toxicity and undesirable side effects.[35][36] Responsive polymers can aid in these requirements.

Responsive polymers usually exhibit a reversible and non-linear change when exposed to a change in local stimuli. These stimuli can include

temperature, pH and light excitation.[37] Changes seen in these polymers can include changes in solubility, shape and changes thanks to ionisable acid or basic groups to the surface activity seen.[37]

Among these responsive polymers thermo responsive polymers are of the most interest to the biomedical field. These polymers respond to temperature changes.[37]

Responsive polymers when attached to superparamagnetic silica coated iron oxide nanoparticles such as those described in this body of work could theoretically be used as MRI contrast agents, with this ability resting upon a variation in temperature to deliver drugs to a targeted region. Theoretical concepts such as this which combine known behaviour of both magnetic iron oxide nanoparticles and thermo-responsive polymers are why research into the attachment of polymers to nanoparticles and the resulting characteristics is needed.[18][19][37][38]

3.1.3 Medical Advantages of Nanoparticle-Polymer Conjugation

The addition of inert polymers to therapeutic entities is an established technique. This is due to the necessity for therapeutics to remain in the blood stream for as long as possible. Proteins and peptides alone are rapidly degraded and removed from the blood stream. [39-42]

Polyethylene glycol (PEG) is the most commonly used polymer for this process for drug delivery [39][40]. It is accepted as safe for humans and is classified as generally regarded as safe (GRAS) by the FDA.

PEG was first shown in 1977 to increase circulation and decrease immunogenicity when attached to bovine serum albumin and liver catalase proteins. [39] This reduction in degradation of proteins is due to steric blocking.[39][40] Polymers in general increase molecular size when attached to therapeutics, this results in an increase in circulation half life due to the inability of the kidneys to filtrate larger materials.[43]

Nanoparticles with polymer attached often show advantages over nanoparticle with no polymer attached. Attachment of polymer is associated with a reduction in aggregation of nanoparticles and also an improvement in circulation times [44][45]. Nanoparticles when introduced into a human body are recognised as foreign object and this results in the mononuclear phagocyte system (MPS) clearing them resulting in a short circulation time. This short circulation time results in low accumulation

of nanoparticles in the target tissues or cells [41][42][46].

This removal of nanoparticles as foreign objects is often due to opsonisation.[40] This is the process where foreign objects, such as nanoparticles become covered in opsonin proteins. This is turn makes them more visible to phagocytic cells allowing phagocytosis (the engulfing and destruction of foreign material from the bloodstream.) to occur [44][47-49].

Opsonisation has been shown to be reduced by the addition of long hydrophilic, neutrally charged polymers attached to nanoparticles with these polymers acting as shielding groups. These shielding groups prevent opsinin proteins from binding to nanoparticle surfaces via the blocking of electrostatic and hydrophobic interactions [40][49].

Nanoparticles have also been seen to aggregate when exposured to circulating serum proteins for a prolong period of time. Polymers, especially PEG, have been shown to reduce this problem [40].

3.2 Aims

This work aims to investigate the ease of attaching 3 different polymers to the surface of the silica coating using a simple "grafting to" process. This grafting to method involves the polymers of choice binding to the NPs via the amine groups added during surface functionalisation of the NPS with APTES [50]. The NPS with the polymers on the surface are then used to evaluate their ability to reduce the aggregation seen in silica coated iron oxide nanoparticles over time and in different buffers. It is an important characteristic that nanoparticles for use in cell or medicinal research do not show significant aggregation. The use of different buffers/solvents is important to consider during nanoparticle design, due again to nanoparticle effect once inside a biological environment.

These aims are achieved by a time study using dynamic light scattering (DLS) consisting of two time periods and then statistical analysis to determine which polymer in which buffer minimises aggregation of the silica coated iron oxide nanoparticles. For the purpose of the work here ethanol (EtOH), Water, HEPES buffer, PBS buffer, and a EtOH:Water 50:50 mix were used. The chosen polymers are polyethylene glycol(PEG), poly(methyl acrylate)(PMA) and poly (N - (2-hydroxypropyl) methacrylamide)(PHPMA).PEG is an often cited polymer for use in reducing aggregation in NPs and is suitable for use in a biological environment.

PMA and PHPMA were picked for this work due to PMA being hydrophobic and PHPMA being hydrophillic. Future work would however benefit from the attachment of thermoresponsive polymers such as poly(N-isopropyl acrylamide) (PNIPAAm). This thermoresponsive polymer is also biocompatible [51]. The time study takes place over 2 time periods: 30mins - 120mins at 30 minute intervals, and 1 day to 14 days. Regression analysis is used to evaluate the results. The specific aims were:

- To perform surface functionalisation of silica coated iron oxide nanoparticles with 3 different polymers.
- To carry out statistical analysis of the effect of adding multiple different polymers onto the nanoparticles surface in terms of size and aggregation by DLS
- To carry out statistical analysis of the effect of adding multiple different polymers onto the nanoparticles surface in terms of size and aggregation by DLS when stored in different buffers.
- To evaluate which of three polymers with which buffer provides the most stability (least aggregation) over 30 -120 minutes and 1-14 days.

3.3 Surface functionalisation with Polymers

Nanocomposite materials composed of nanoparticles and polymers have been known and commercially produced since the early 1900's, [52] however it was not until the 1990s that more rigorous scientific enquiry became common.[53][54].

As the design and synthesis of ever more precise nanoparticles with size, chemical composition, and shape all clearly defined has become normal along with instrumentation capable of characterising these nanoparticles, research into combing nanoparticles and polymers to form nanocomposites has increased.

One issue commonly associated with nanocomposite materials of this kind which is still of interest today is the control of dispersion of the nanoparticles which have polymers either attached or as a coat.[55]

The ligands attaching nanoparticle and polymer can have a direct effect on the resulting nanocomposite behaviour and its spatial distribution.

Polymers may be attached to nanoparticles by either covalent attachment or physical adsorption.[56] A “Grafting to” process involves the addition of polymer to a nanoparticle whereas a “grafting from” process involves the growth of polymer from functionalised nanoparticles. Figure 3.4 shows ”grafting-to” and ”grafting-from” methods of polymer addition to nanostructures. ”Grafting-to” chemistry is considered easier to achieve [57]. Regardless of how the nanoparticle-polymer composite is formed it is imperative that the nanoparticles maintain their original desired characteristics.

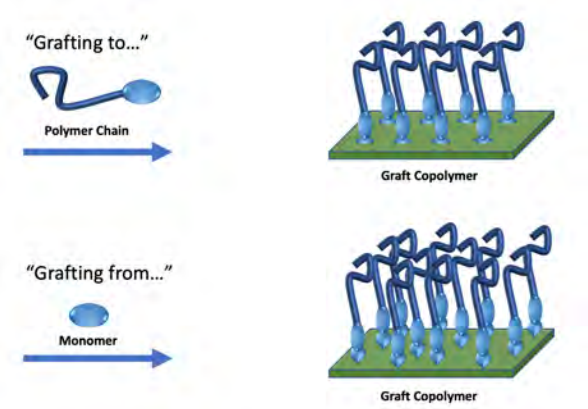

Figure 3.4: ”Grafting-to” and ”grafting-from” chemistry provides two different methods of polymer attachment to nanoparticles. Here ”graft-to” chemistry is used. This method is considered the easier of the 2 methods. Image by author.

This work involves a “grafting to” process using covalent bonding to attach polymer to the silica surface of the nanoparticle via NH_2 groups. These processes are often considered easier than a “grafting from” approach to achieve.[58]

Grafting-to chemistry is an effective and established method for synthesis of polyethylene glycol (PEGylated) nanoparticles. The PEGylation of nanoparticles results in hydrophilic and biocompatible nanoparticles [59][60].

3.4 Experimental Protocols

3.4.1 Protocol Development of Addition of Polymer

Here we aimed to attach polymers to the surface of the silica shell which coated the iron oxide cores through linkage to an amine group added to surface using APTES. This was required to be achievable using a repeatable, simple protocol at room temperature. This was followed by an investigation into the effect of polymer addition on previously described synthesised silica coated iron oxide nanoparticles in terms of size (DLS), colloidal stability, aggregation and magnetism of nanoparticles.

3.4.2 Addition of PEG-Silane (5000)

40mg of the synthesised core@shell NPs were placed in an 70% ethanol solution (30mL). 0.0005mol% PEG-Silane was added and magnetically stirred at room temperature for 24 hours. The NPs were then washed with water and centrifuged (13200rpm, 15 mins) at least 3 times. NPs were retained in a 70% ethanol suspension for future use. Nanoparticles can be seen as a nearly black particles in a clear ethanol suspension.

3.4.3 Addition of PMA

40mg of the synthesised core@shell NPs were placed in a 2:1 ethanol to water solution (30mL). 0.0005mol% PMA was added and magnetically stirred at room temperature for 24 hours. The NPs were then washed with water and centrifuged (13200rpm, 15 mins) at least 3 times. NPs were retained in a 70% ethanol suspension for future use. Nanoparticles can be seen as a nearly black particles in a clear ethanol suspension.

3.4.4 Addition of PHPMA

40mg of the synthesised core@shell NPs were placed in a 2:1 ethanol to water solution (30mL). 0.0005mol% PHPMA was added and magnetically stirred at room temperature for 24 hours. The NPs were then washed with water and centrifuged (13200rpm, 15 mins) at least 3 times. NPs were retained in a 70% ethanol suspension for future use. Nanoparticles can be seen as a nearly black particles in a clear ethanol suspension.

Hepes Buffer Preparation

To 80 mL of deionized water, 2.38 g of HEPES was added. Using a magnetic stir bar stir the solution was stirred until completely dissolved (1 min). pH of the solution was taken and adjusted from acidic (pH5) to pH 7.4 using NaOH pellets ensuring that each pellet used was completely dissolved. If pH7.4 was achieved before a whole NaOH pellet dissolved the pellet was removed using a spatula. If necessary pH was lowered by the addition of HCL. At pH 7.4 total volume was increased to 100mL using deionised water. Once prepared buffer was stored in a refrigerator for up to 4 months.

Phosphate Buffer Solution (PBS) Preparation

To 800 mL of distilled water 8 g of NaCl, 0.2 g of KCl, 1.44 g of Na_2HPO_4 and 0.24 g of KH_2PO_4 was added. The pH was adjusted to 7.4 using HCL. Distilled water was added to a total volume of 1 liter.

3.4.5 Dynamic Light Scattering (DLS)

Using a Malvern Zetasizer Nano instrument hydrodynamic diameters and zeta potentials were obtained for nanoparticle samples. Scattered light was measured at 173^o (back scattering) using a 4mW He-Ne 633n laser. 5 measurements for both size and zeta potential were taken each time and the average reported with attenuation and position automatically selected by the instrument. Samples for DLS were prepared at 1mg/mL concentrations using Ultrapure MilliQ water.

3.5 Polymers

Polyethylene glycol, PEG5000-Silane was purchased from Merck. Poly(methyl acrylate), (PMA), molecular weight:617, CAS number 16561-29-8 was purchased from Merck. Poly (N - (2-hydroxypropyl) methacrylamide) (PHPMA) was synthesised by Panagiotis Georgiou, Gibson Group, University of Warwick and characterised as follows in Table 3.1, and Figure 3.5: [1]

[1]The individual who synthesised the polymers is no longer available for contact. Thus, a full characterisation of the synthesis approach is not possible at this time.

Table 3.1: *Polymers synthesized by photo-RAFT, Panagiotis Georgiou, Gibson Group, University of Warwick.*

2*Sample	2*Polymer	2*[M]:[CTA]	2*Conversion (%)	SEC Analysis	
				M_n, $_SEC$ (g mol^-1)	ĐM
1	PHPMA27	40	67	6000	1.13
2	PHPMA38	60	64	9600	1.24
3	PHPMA51	80	64	11600	1.19
4	PHPMA73	10	61	13600	1.20

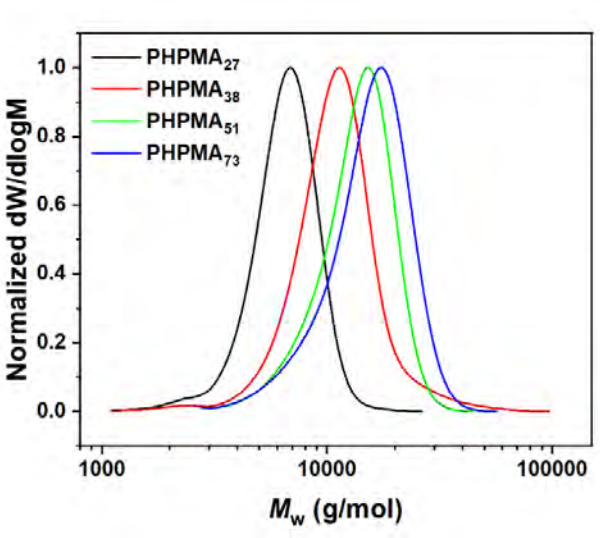

Figure 3.5: *Normalized SEC RI molecular weight distributions PHPMA homopolymers. M_n and D_m values were calculated from PMMA standards using 5 mM NH_4BF_4 in DMF as the eluent. Chemical structure of PHPMA can be seen in Figure 3.8.*

The provided PHPMA was synthesised using photo-RAFT. Visible light-regulated polymerization is a powerful tool in the preparation of functional polymers. Standing for photo-regulated reversible addition–fragmentation chain transfer polymerization (photo-RAFT) it uses both photo-catalytic and catalyst-free approaches. Raft uses simple, free-radical chemistry to enable the synthesis of tailor-made polymers. These polymers can have their molecular weights predetermined, and show narrow polydispersities and allow for complex architectures[61].

3.5.1 Polyethylene glycol(PEG) silane

The polymer Polyethylene glycol (PEG), molecular weight 18g/mol(structure of PEG- silane can be seen in Figure 3.6) is a versatile synthetic polyether that consists of repeating units of ethylene oxide. PEG-silane is PEG with a silane group attached. It is a water soluble, biocompatible polymer. It is FDA approved for use in biomedicine and is considered to be nonimmunogenic and non toxic. PEG has been used for several different biomedical applications including bioconjugation of proteins and peptides, drug delivery and surface functionalisation. PEGylation is the term given to bioconjugation using PEG. PEGylation is conjugation by covalent bonding. [62][63]

PEG is known to slow protein adsorption within a biological environment which is a necessary and valuable behaviour as a potential material for drug delivery as this will minimise formation of the protein corona. This is due to PEG exhibiting high hydrophilicity. This allows PEG to retain flexibility and mobility in an aqueous environment [63-66].

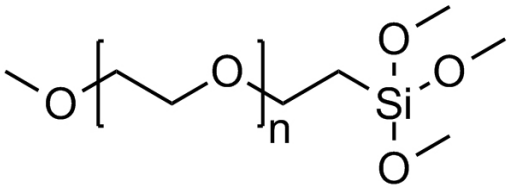

Figure 3.6: Chemical Structure of Polyethylene glycol(PEG)-silane [64].

3.5.2 Poly(methyl acrylate)(PMA)

Poly (methyl acrylate) (PMA) (structure can be seen in Figure 3.7) is a polymer from the monomer methyl acrylate with a molecular weight of 86g/mol. PMA is a synthetic hydrophobic polymer. It is known for being a polymer which is flexible, leathery and tough with a low glass-transition temperature (approximately 10 ^{o}C.[67-69] PMA is soluble in dimethyl sulfoxide (DMSO) and ethanol (EtOH).[67][68] PMA is not water soluble as it is a hydrophobic polymer. Due to this ethanol was used during attachment of polymer to nanoparticles. Here PMA with silanol end groups was used.

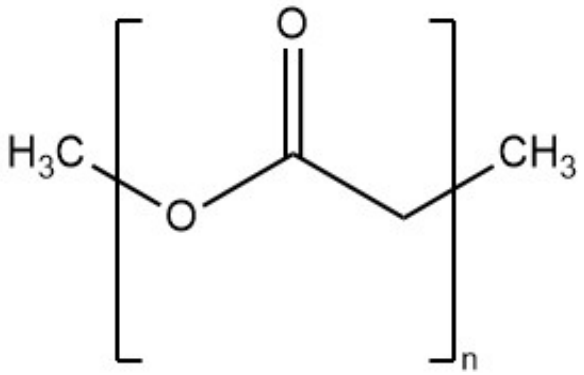

Figure 3.7: Chemical Structure of Poly(methyl acrylate)(PMA). n = 30-75.

3.5.3 Poly (N - (2-hydroxypropyl) methacrylamide) (PHPMA)

Poly(N-(2-hydroxypropyl) methacrylamide) (PHPMA) (structure can be seen in Figure 3.8) can be considered as an alternative to PEG. It is a hydrophilic polymer which has a secondary hydroxyl group and a molecular weight of 143g/mol. It is a linear, nonimmunogenic polymer which has been used in polymer-drug conjugates [70]. PHPMA has been of interest for biological/medicinal applications. Although PEG is most often considered in this area PHPMA offer several advantages over PEG. Its main advantage is that it has the ability to undergo functionalisation via its side-chain hydroxyl group. This means it is suitable as a material which can be associated with imaging agents, drug delivery materials and for bioconjugation.[70-72]

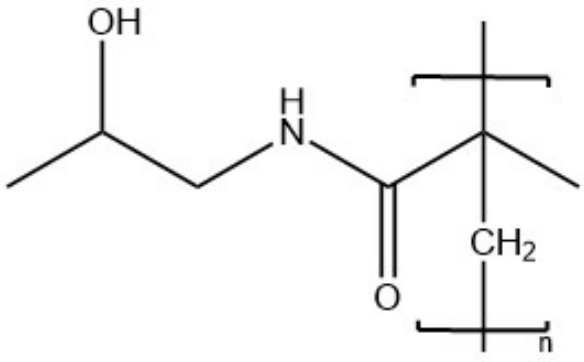

Figure 3.8: Chemical Structure of Poly (N - (2-hydroxypropyl) methacrylamide)(PHPMA). Drawn using ChemDraw.

Table 3.2 summarises the properties of the three polymers used for this work. The three polymers were chosen to ensure variation between them. PEG is a hydrophilic established polymer for biological environments, PMA is an hydrophobic polymer and PHPMA is hydrophilic. The differences between these polymers make them suitable for comparison of effect of polymer addition to the nanoparticles. The PMA and PHPMA provided by Panagiotis Georgiou, Gibson Group, University of Warwick was synthesised for other research within the Gibson group, however met the requirements for the "grafting-to" chemistry used in this work.

Table 3.2: *Summary of the properties for polymers PEG,PMA and PHPMA used in this work. PEG was purchased from MERCK, however PMA and PHMA was synthesised within the institution and provided for this work.*

Polymer	**MW(g/mol)**	**Chain Length**	**End Group**	**Polymer Description**
PEG	18	5000	Silane	hydrophilic, biocompatible
PMA	86	48	Silane	hydrophobic, flexible, leathery, tough,
PHPMA	143	73	NH_2	linear, nonimmunogenic polymer, hydrophilic

3.6 Effect of Time on Nanoparticle Aggregation Using DLS Measurements and Statistical Regression Analysis

3.7 Introduction

Nanoparticles can aggregate over time. This for nanoparticles which are to be used in a biological environment is problematic as "clumping" within, for example, a cell could prevent conjugation to biomolecules or interfere with a cells normal behaviour. DLS allows for evaluation of aggregation as due to DLS measuring hydrodynamic size aggregation will be seen as an increase in size when measured using DLS. Here the size of nanoparticles

was determined over time, initially over a 30 - 120 minute time period and the over a 14 day time period. If size increased aggregation would be implicated. This was carried out for NPS, NPS with PEG attached, NPS with PMA attached and finally NPs with PHPMA attached to determine whether the addition of different polymers has an effect on aggregation of nanoparticles. The buffer that NPS are stored in was also evaluated to find out if this would effect aggregation and the results were looked at using a statistical regression analysis to determine which of the NPs described above in which buffer showed the least aggregation. This work presents new information regarding the use of buffers for storage and within biological work when using nanoparticles.

3.7.1 Silica Coated Iron Oxide Nanoparticles (No polymer)

Silica coated iron oxide nanoparticles (sample: samp_ts) were synthesised and analysed without a polymer attached. These nanoparticles were synthesised using a pure oleylamine synthesis protocol and then coated with silica as described in chapter 3. These type of nanoparticles are known to aggregate with time due to electrostatic interactions despite the use of oleylamine during the synthesis of the cores as a stabiliser. Initial measurements over time with different buffers were taken for samp_ts. This was to allow for the evaluation of the effect of adding polymers to the nanoparticles. These single cored silica coated nanoparticles (samp_ts) used throughout the time study can be seen below in Figure 3.10. These silica coated single cored Fe_3O_4 nanoparticles have a TEM diameter of 58.85 ±7.37 nm and contain oleylamine synthesised cores.

Table 3.3: *Average diameter obtained by DLS for silica coated iron oxide nanoparticles (samp_ts) over Time (30-120 minutes).*

Time (mins)	**Buffer**				
	EtOH	Water	Hepes	PBS	EtOH:Water
30	411 ±15	416 ±8	407 ±13	421 ±21	396 ±18
60	421 ±16	421 ±9	411 ±15	468 ±18	401 ±7
90	460±15	460 ±19	451 ±16	486 ±7	419 ±6
120	471±20	481±20	476 ±16	496 ±10	441 ±13

Silica coated core@shell iron oxide nanoparticles show a small but consistent variation in size by DLS when suspended in different buffers.

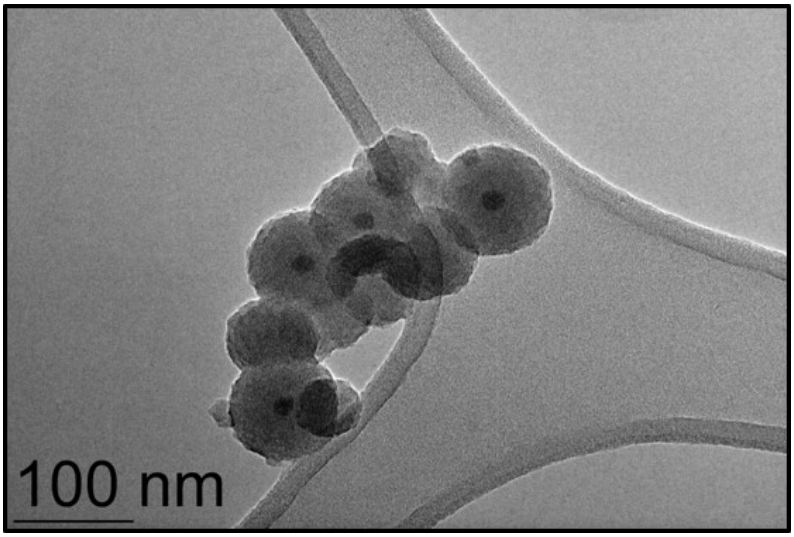

Figure 3.9: *Silica coated iron oxide nanoparticles (samp_ts) used for polymer time study. TEM diameter 58.85 ± 7.37. Size obtained using ImageJ. The image shows spherical nanoparticles with a single iron oxide core surrounded by and even coating of silica.*

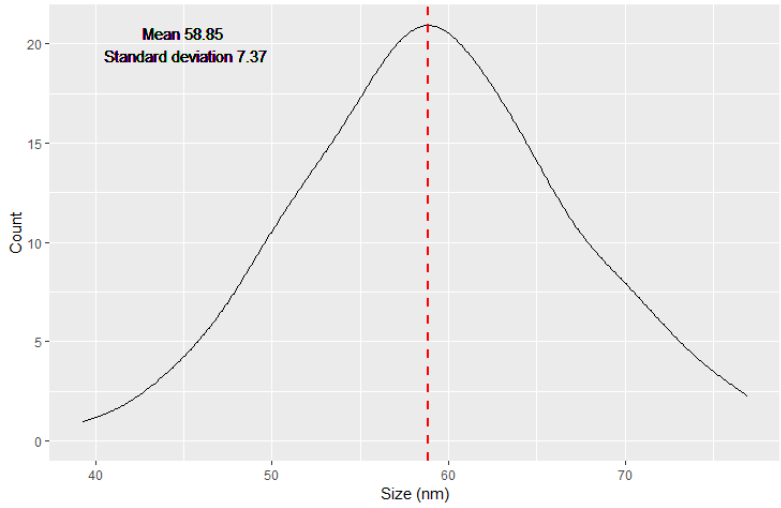

Figure 3.10: *Size distribution for silica coated iron oxide nanoparticles (samp_ts) used for polymer time study. TEM diameter 58.85 ± 7.37. Size obtained using ImageJ.*

Over a period of time, ranging from 30 minutes to 120 minutes at 30 minute intervals, inspection suggests that nanoparticles have the lowest size by DLS over time when suspended in a 50:50 EtOH:water (mix) solution. This can be seen in Table 3.3 and Figure 3.11 To test this result, a linear regression model seen in Table 3.4 was fitted for this data, to investigate the relationship between the different solvent buffers and nanoparticle size over time.

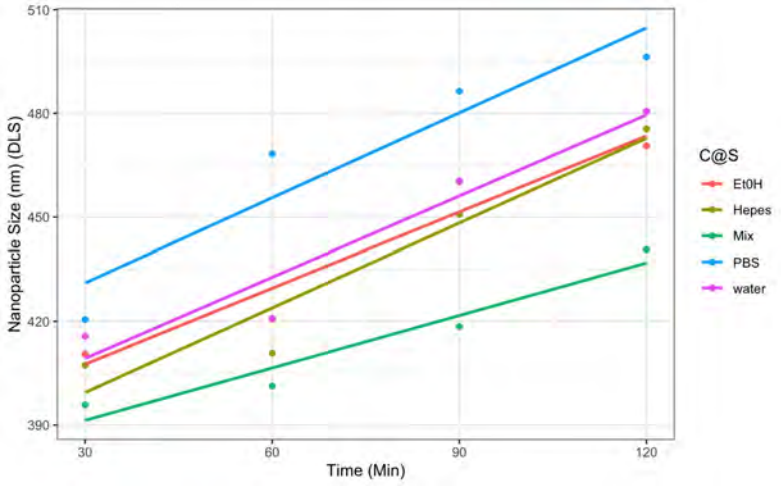

Figure 3.11: *Size of silica coated nanoparticles (samp_ts) measured using DLS over a time period of 30-120 minutes with no polymer attached dispersed in EtOH, Water, PBS, Hepes and 50:50 EtOH:water mix. All combinations of buffer with NPs show an increase in size over time.*

Table 3.4: *Linear model for NP-SIZE TIME + PEG-TYPE*

	Dependent variable:
	NP_SIZE
TIME	0.730*** (0.066)
PEG_TYPEHepes	−4.425 (7.018)
PEG_TYPEMix	−26.425*** (7.018)
PEG_TYPEPBS	27.350*** (7.018)
PEG_TYPEwater	3.875 (7.018)
Constant	385.755*** (7.018)
Observations	20
R^2	0.929
Adjusted R^2	0.903
Residual Std. Error	9.926 (df = 14)
F Statistic	36.385*** (df = 5; 14)
Note:	*p<0.1; **p<0.05; ***p<0.01

The regression equation was significant (F(5, 14)=36.385, p = <0.01), with an R^2 of 0.929. Overall, nanoparticle size significantly increases with time (p = <0.01). Inspection of the coefficients indicates that the mix of EtOH and Water is the only buffer that leads to a significant reduction in size of nanoparticles over time compared to the overall correlation (-26.425, p = <0.01). On the other hand, PBS contributed to a significantly higher growth in size of nanoparticles over time (27.350, p = <0.01).

These results suggest that this mix results in the least amount of aggregation for nanoparticles with no polymer addition. This can also

be seen when DLS measurements are taken over a 2 week period, as described below.

Table 3.5: *Average diameter obtained by DLS for silica coated iron oxide nanoparticles over Time (1-14 Days).*

Time (Days)	**Solvent**				
	EtOH	Water	Hepes	PBS	EtOH:Water
1	424 ±17	435 ±23	423 ±18	431 ±22	385 ±27
3	445 ±16	443 ±33	467 0	460 ±15	402 ±19
5	446±22	456 ±19	473±15	470 ±22	431 ±23
7	477 ±21	489 ±31	493±19	500 ±10	457 ±19
14	546 ±21	561 ±23	560 ±13	561 ±19	470 ±26

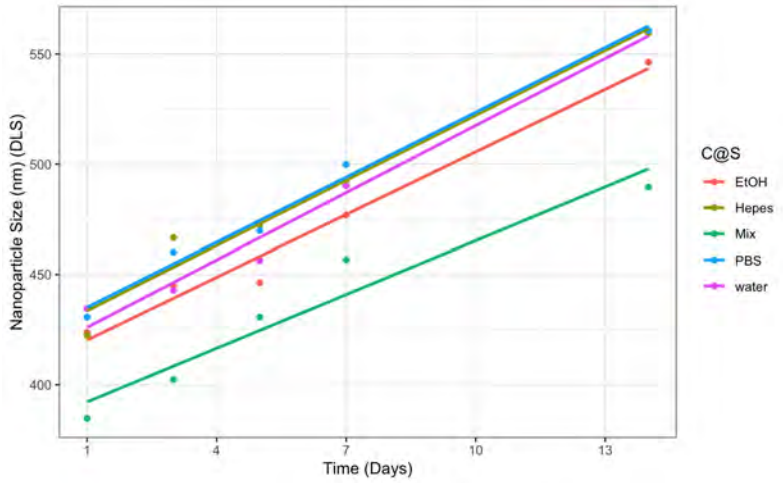

Figure 3.12: *Size of silica coated nanoparticles (samp_ts) measured using DLS over a time period of 1-14 days with no polymer attached dispersed in EtOH, Water, PBS, Hepes and 50:50 EtOH:water mix. All combinations of buffer with NPs show an increase in size over time suggesting aggregation.*

A similar visual pattern emerges in the results over days, with the Mix appearing to produce the smallest DLS over time (Table 3.5 and Figure 3.12). To test these results, a linear regression model was fitted to predict Nanoparticle Size by both type and solvent type. The results can be seen in Table 3.6

Table 3.6: *Linear model for NP-SIZE TIME + TYPE for nanoparticle size over days.*

	Dependent variable:
	NP_SIZE
TIME_DAYS	9.483*** (0.400)
PEG_TYPEHepes	15.160** (5.657)
PEG_TYPEMix	−34.860*** (5.657)
PEG_TYPEPBS	16.560*** (5.657)
PEG_TYPEwater	9.220 (5.657)
Constant	410.762*** (4.665)
Observations	25
R^2	0.973
Adjusted R^2	0.965
Residual Std. Error	8.944 (df = 19)
F Statistic	134.875*** (df = 5; 19)
Note:	*p<0.1; **p<0.05; ***p<0.01

The regression equation was again significant (F(5, 19)=134.87, p = < 0.01), with an R^2 of 0.973. As with the minute time series results presented above, the mixed solvent is the only buffer that leads to a significant reduction in nanoparticle size when compared to the overall correlation (-34.860, p = < 0.01). Both PBS (16.560, p = < 0.01) and Hepes (15.160, p = < 0.05) solvents lead to a significant increase in nanoparticle size compared to the other buffers.

Taken together, these results indicate that the mix of 50:50 EtOH:Water produces the smallest DLS over time when nanoparticles are synthesised with no polymer addition. The PBS solvent in particular appears to increase nanoparticle size more than the other buffers used.

3.7.2 Nanoparticles with PEG Over Time

Nanoparticles with PEG attached result in a smaller z-average size by DLS than nanoparticles before addition of PEG. This is due to the reduction in aggregation of the nanoparticles as a result of PEGylation. This can be seen here with these nanoparticles with sample samp_ts having larger z-

averages for all buffers/solvents than those seen for sample samp_ts+PEG.

Table 3.7: *Average diameter obtained by DLS for silica coated iron oxide nanoparticles (samp_ts+PEG) with PEG (5000) attached over Time(mins) in different buffers.*

Time (mins)	**Solvent**				
	EtOH	Water	Hepes	PBS	EtOH:Water
30	375 ±5	400 ±9	391±11.5	396 ±24	360 ±9
60	376 ±11	405 ±14	395±8	403±28	363±9
90	380 ±13	405 ±10	398 ±17	408 ±16	374±16
120	385 ±8	412 ±11	411 ±9	417±15.7	372 ±16

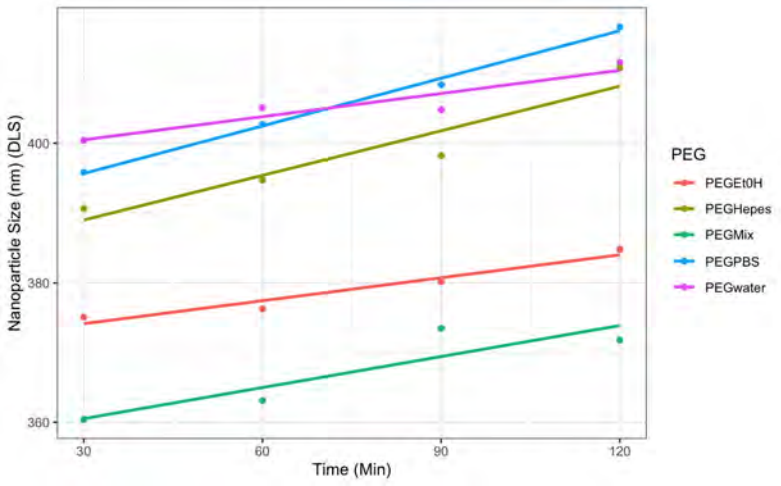

Figure 3.13: *Size of silica coated nanoparticles (samp_ts+PEG) with PEG attached, measured using DLS over a time period of 30-120 minutes when dispersed in EtOH, Water, PBS, Hepes and 50:50 EtOH:water mix. Graph shows a small increase in size for all suspensions suggesting some aggregation.*

With the addition of PEG-silane 5000 to sample samp_ts (samp_ts+PEG) we can see that DLS is generally smaller over the initial minutes time series. Visual inspection once again suggests that the mix solvent produces the lowest DLS with this shown in Table 3.7 and Figure 3.14. A linear regression model was fitted to predict nanoparticle size by time and solvent type when PEG is added. The regression model results can be seen in Table 3.8

The regression equation was significant ($F(5, 14)=129.594$, $p = < 0.01$), with an R^2 of 0.979. Nanoparticle size increased significantly with

Table 3.8: *Linear model for NP-SIZE TIME + PEG-TYPE for nanoparticle size over minutes when PEG is added (samp_ts+PEG).*

	Dependent variable:
	NP_SIZE
TIME_MINS	0.162*** (0.019)
PEG_TYPEPEGHepes	19.475*** (2.037)
PEG_TYPEPEGMix	−11.900*** (2.037)
PEG_TYPEPEGPBS	26.800*** (2.037)
PEG_TYPEPEGwater	26.375*** (2.037)
Constant	366.930*** (2.037)
Observations	20
R^2	0.979
Adjusted R^2	0.971
Residual Std. Error	2.881 (df = 14)
F Statistic	129.594*** (df = 5; 14)
Note:	*p<0.1; **p<0.05; ***p<0.01

time (0.162, p = < 0.01) Inspection of the coefficients indicates that all solvent types had a significant effect compared to the constant (EtOH). Hepes (19.475, p = < 0.01), PBS (26.800, p = < 0.01) and Water (26.365, p = < 0.01) all increased DLS significantly over time. The mixed solvent of Water and EtOH produced a significantly smaller size when using DLS over time (−11.900, p = <0.01). This suggests that, similarly to when nanoparticles were synthesised without PEG, the EtOH:water (50:50) mix produces the least aggregation over the initial time period for nanopaticles with PRG attached.

Table 3.9: *Average diameter obtained by DLS for silica coated iron oxide nanoparticles (samp_ts+PEG) with PEG-silane 5000 attached over Time(days) in different buffers.*

Time (mins)	**Solvent**				
	EtOH	Water	Hepes	PBS	EtOH:Water
1	381	393	398	402	377
3	399	404	400	424	394
5	424	424	421	435	413
7	445	457	440	459	423
14	467	478	475	486	447

The visual pattern for PEG coated nanoparticles is less clear for the time series over days as demonstrated in Table 3.9 and Figure 3.14. To establish any significant differences, a linear regression was fitted to predict nanoparticle size by time and solvent type.

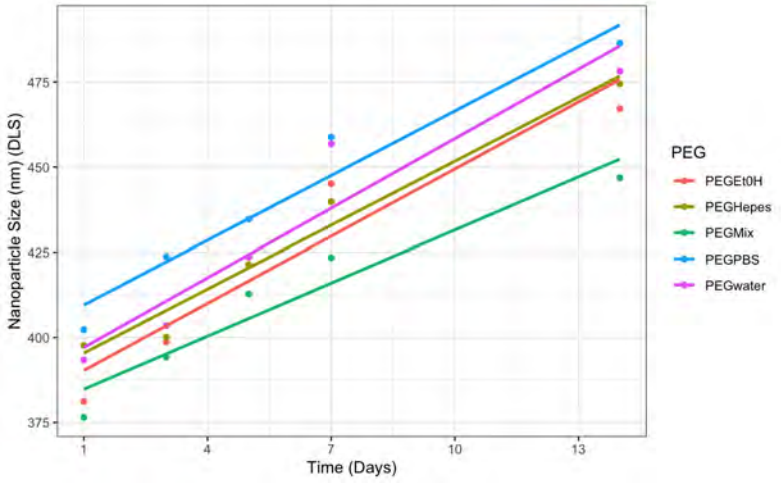

Figure 3.14: *Size of silica coated nanoparticles (samp_ts+PEG) measured using DLS over a time period of 1-14 days with PEG attached dispersed in EtOH, Water, PBS, Hepes and 50:50 EtOH:water mix. All suspension combinations with NPs show an increase in size over time suggesting aggregation.*

Table 3.10: *Linear model for NP-SIZE TIME + PEG-TYPE for nanoparticle (samp_ts+PEG) size over days when PEG is added.*

	Dependent variable:
	NP_SIZE
TIME_DAYS	6.232*** (0.414)
PEG_TYPEPEGHepes	3.540 (5.861)
PEG_TYPEPEGMix	−12.400** (5.861)
PEG_TYPEPEGPBS	18.020*** (5.861)
PEG_TYPEPEGwater	7.960 (5.861)
Constant	385.767*** (4.833)
Observations	25
R^2	0.931
Adjusted R^2	0.912
Residual Std. Error	9.267 (df = 19)
F Statistic	51.001*** (df = 5; 19)
Note:	*p<0.1; **p<0.05; ***p<0.01

The regression equation was significant (F(5, 19)=51.001, p = < 0.01), with an R^2 of 0.931. Nanoparticle size increased significantly over time as measured by days (6.232, p = < 0.01). Inspection of the coefficients indicates that, similarly to minutes, the mixed solvent was the only one to reduce nanoparticle size significantly over time compared to the constant (-12.400, p = < 0.05). Over days, only PBS produced a significant increase in DLS compared to the constant (18.020, p = < 0.01)(Table 3.10).

Overall, these results indicate that when PEG is added, the solvent

that best reduces aggregation remains the mix of water and EtOH, as it was in the previous results with no polymer added. Indeed, inspection of the coefficients suggest that the water and EtOH mix was the only solvent that contributed to a relative reduction in size for the PEG polymer; the other solvents all increased the size, though only one (PBS) significantly so. This is similar to the results for nanoparticles with the other polymers, and with no polymer. The impact of the non-mix solvents was smaller when using PEG polymer nanoparticles.

3.7.3 PMA

Table 3.11: *Average diameter obtained by DLS for silica coated iron oxide nanoparticles with PMA (samp_ts+PMA) attached over Time (Mins)in different buffers.*

Time (mins)	**Solvent**				
	EtOH	Water	Hepes	PBS	EtOH:Water
30	375	369	379	388	360
60	379	382	391	399	365
90	383	392	400	425	371
120	391	402	412	431	384

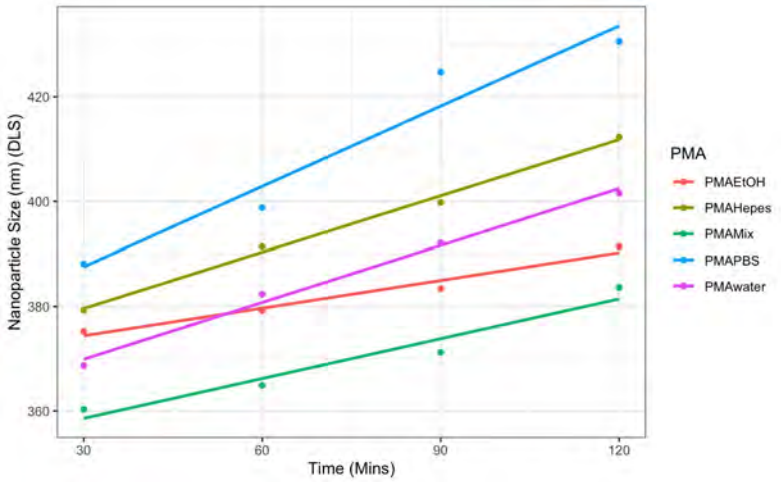

Figure 3.15: *Size of silica coated nanoparticles (samp_ts+PMA) with PMA attached, measured using DLS over a time period of 30-120 minutes when dispersed in EtOH, Water, PBS, Hepes and 50:50 EtOH:water mix. Graph shows an increase in size for all suspensions suggesting aggregation over time.*

Table 3.11 and Figure 3.15 show that when PMA is added to the nanoparticles, there is no clear difference in size compared to PEG-added nanoparticles, however visual inspection of results does suggest that they are smaller than the nanoparticles without a polymer. Visual inspection of the results suggests a difference between solvent type and DLS over time and thus again a linear regression model was fitted to test the correlations.

Table 3.12: *Linear model for NP-SIZE TIME + PMA-TYPE for nanoparticle size over minutes when PMA (samp_ts+PMA) is added.*

	Dependent variable:
	NP_SIZE
TIME_MINS	0.332*** (0.035)
PMA_TYPEPMAHepes	13.400*** (3.708)
PMA_TYPEPMAMix	−12.300*** (3.708)
PMA_TYPEPMAPBS	28.250*** (3.708)
PMA_TYPEPMAwater	3.875 (3.708)
Constant	357.385*** (3.708)
Observations	20
R^2	0.941
Adjusted R^2	0.920
Residual Std. Error	5.244 (df = 14)
F Statistic	44.908*** (df = 5; 14)
Note:	*p<0.1; **p<0.05; ***p<0.01

Table 3.12 shows that the regression equation was significant (F(5, 14)=44.908, p = < 0.01), with an R^2 of 0.941. DLS increased significantly over time (0.332, p = < 0.035). PBS (28.250, p = < 0.01) and Hepes (13.400, p = < 0.01) both contributed to significant growth over time compared to the constant (EtOH).

As seem with no-polymer and PEG nanoparticles, the Mix contributed to a significant reduction in growth over time compared to the constant (-12.300, p = < 0.01).

For PMA (samp_ts+PMA) over 14 days following DLS measurements (Table 3.13 and Figure 3.16 a second linear model was fitted to predict the increase of DLS over time and by solvent-type for PMA over days with the results seem in Table 3.14.

Table 3.13: *Average diameter obtained by DLS for silica coated iron oxide nanoparticles with PMA (samp_ts+PMA) attached over Time (days) in different buffers.*

Time (Days)	**Solvent**				
	EtOH	Water	Hepes	PBS	EtOH:Water
1	387	395	393	400	383
3	402	411	430	451	396
5	450	439	460	455	402
7	447	473	452	523	424
14	476	491	503	520	457

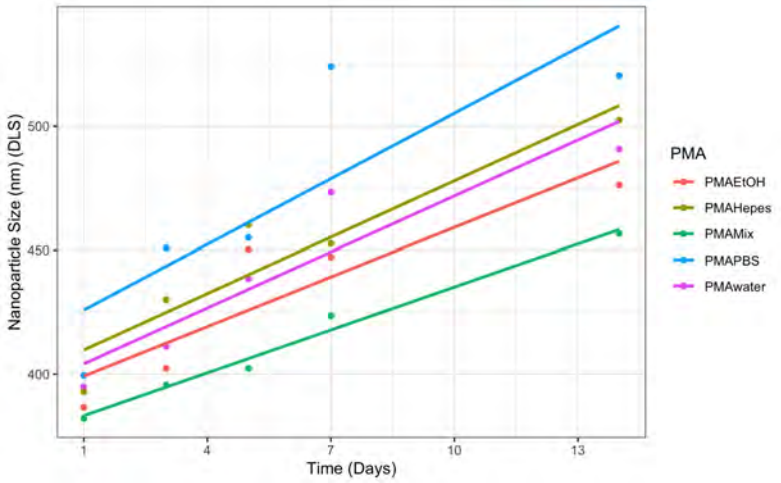

Figure 3.16: *Size of silica coated nanoparticles (samp_ts+PMA) measured using DLS over a time period of 1-14 days with PMA attached dispersed in EtOH, Water, PBS, Hepes and 50:50 EtOH:water mix. All suspension combinations with NPs show an increase in size over time suggesting aggregation*

The regression equation was significant (F(5, 19=20.814, p = $<$ 0.01), with an R^2 of 0.846. Nanoparticle size increased significantly over time (7.246, p = $<$ 0.01). Inspection of the coefficients suggests that the PBS solvent lead to a significant increase of DLS over the constant (37.480, p = $<$ 0.01). As with the other results, the mix of water and EtOH lead to a reduction of nanoparticle size over time compared to the constant, but this result was not significant (-20.460, p = $>$ 0.1).

These results suggest that when PMA (samp_ts+PMA) is attached, nanoparticle size over time is greatest with the PBS solvent, and smallest with the Mix solvent. However, the latter is not significant over days, indicating that the Mix solvent has less of an effect when PMA is attached

Table 3.14: *Linear model for NP-SIZE TIME + PMA-TYPE for nanoparticle size over days when PMA (samp_ts+PMA) is added.*

	Dependent variable:
	NP_SIZE
TIME_DAYS	7.274*** (0.825)
PMA_TYPEPMAHepes	15.140 (11.670)
PMA_TYPEPMAMix	−20.460* (11.670)
PMA_TYPEPMAPBS	37.480*** (11.670)
PMA_TYPEPMAwater	9.240 (11.670)
Constant	388.877*** (9.623)
Observations	25
R^2	0.846
Adjusted R^2	0.805
Residual Std. Error	18.451 (df = 19)
F Statistic	20.814*** (df = 5; 19)
Note:	*p<0.1; **p<0.05; ***p<0.01

to the nanoparticles.

3.7.4 Nanoparticles with PHPMA Over Time

PHPMA synthesised by Panagiotis Georgiou, Gibson Group, University of Warwick was used for the time study. Sample PHPMA73.

Table 3.15: *Average diameter obtained by DLS for silica coated iron oxide nanoparticles with PHPMA (samp_ts+PHPMA73) attached over Time (Mins) in different buffers.*

Time (mins)	**Solvent**				
	EtOH	Water	Hepes	PBS	EtOH:Water
30	399	401	389	396	372
60	386	427	398	407	389
90	403	446	407	471	387
120	431	481	463	501	414

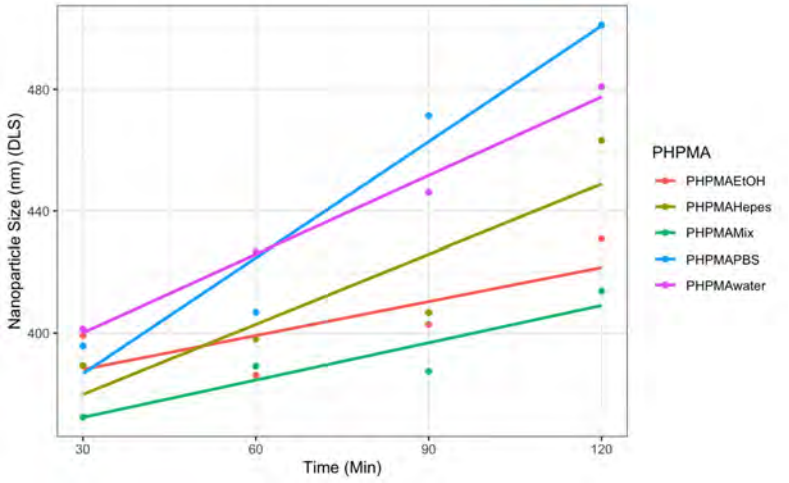

Figure 3.17: *Size of silica coated nanoparticles (samp_ts+PHPMA73) with PHPMA(73) attached, measured using DLS over a time period of 30-120 minutes when dispersed in EtOH, Water, PBS, Hepes and 50:50 EtOH:water mix. Graph shows an increase of varying amounts in size for all suspensions suggesting some aggregation. This aggregation is most obious for samp_ts+PHPMA73 when dispersed in PBS buffer.*

Table 3.16: *Average diameter obtained by DLS for silica coated iron oxide nanoparticles with PHPMA (samp_ts+PHPMA73) attached over Time (Days) in different buffers.*

Time (Days)	**Solvent**				
	EtOH	Water	Hepes	PBS	EtOH:Water
1	444	465	486	513	434
3	461	499	504	535	444
5	488	506	516	549	461
7	512	521	531	563	476
14	519	530	542	582	497

Initial visual inspection of the results suggests that nanoparticles with PHPMA were generally larger over time than with PMA and PEG, but smaller than without a polymer, seen in Table 3.15 and Figure 3.17. Inspection of the time series over minutes suggests again that the Mix may produce the smallest nanoparticles, so a linear regression model was fitted to test the relationship between nanoparticle size and time and solvent-type (Table 3.17).

The regression equation was significant ($F(5, 14)=13.514$, $p = < 0.01$), with an R^2 of 0.828. Nanoparticle size increased significantly over time (0.736, $p = < 0.01$). Both PBS (39.000, $p = < 0.01$) and Water (34.025, $p = < 0.05$) produced significantly larger nanoparticles over time

Table 3.17: *Linear model for NP-SIZE TIME + PHPMA-TYPE for nanoparticle size over minutes when PHPMA (samp_ts+PHPMA73) is added.*

	Dependent variable:
	NP_SIZE
TIME_MINS	0.736*** (0.116)
PHPMA_TYPEPHPMAHepes	9.575 (12.261)
PHPMA_TYPEPHPMAMix	−14.100 (12.261)
PHPMA_TYPEPHPMAPBS	39.000*** (12.261)
PHPMA_TYPEPHPMAwater	34.025** (12.261)
Constant	349.540*** (12.261)
Observations	20
R^2	0.828
Adjusted R^2	0.767
Residual Std. Error	17.339 (df = 14)
F Statistic	13.514*** (df = 5; 14)
Note:	*p<0.1; **p<0.05; ***p<0.01

compared to the constant (EtOH). Both the Hepes and Mix solvents had no significant effect on nanoparticle size over time, although it should be noted that the coefficient for the Mix is negative (-14.100), despite not being significant.

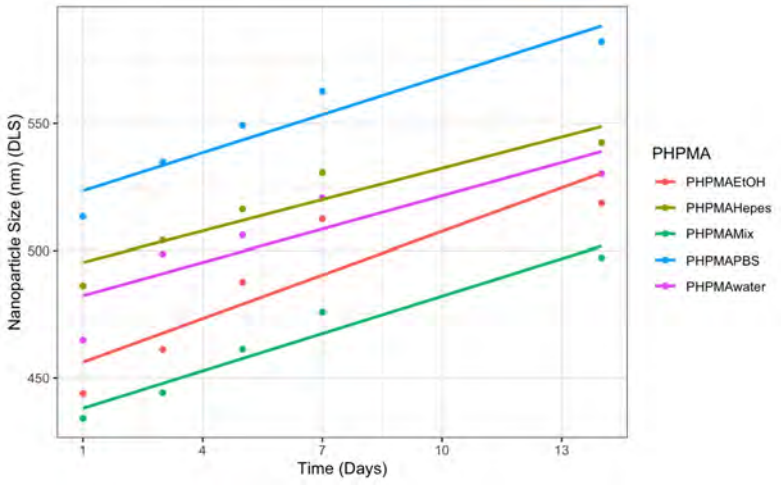

Figure 3.18: *Size of silica coated nanoparticles (samp_ts+PHPMA73) measured using DLS over a time period of 1-14 days with PHPMA attached dispersed in EtOH, Water, PBS, Hepes and 50:50 EtOH:water mix. All suspension combinations with NPs show an increase in size over time suggesting aggregation*

Over days, Table 3.16 and Figure 3.18 show that there is a clearer difference visually between the solvents regarding nanoparticle size with

PHPMA attached. Table 3.18 shows the linear regression model fitted to test the relationship between DLS and time and solvent type when PHPMA (samp_ts+PHPMA73) was attached to nanoparticles.

Table 3.18: Linear model for NP-SIZE TIME + PHPMA-TYPE for nanoparticle size over days when PHPMA (samp_ts+PHPMA73) is added.

	Dependent variable:
	NP_SIZE
TIME_DAYS	4.810*** (0.494)
PHPMA_TYPEPHPMAHepes	31.180*** (6.987)
PHPMA_TYPEPHPMAMix	−22.180*** (6.987)
PHPMA_TYPEPHPMAPBS	63.680*** (6.987)
PHPMA_TYPEPHPMAwater	19.360** (6.987)
Constant	455.881*** (5.762)
Observations	25
R^2	0.934
Adjusted R^2	0.916
Residual Std. Error	11.048 (df = 19)
F Statistic	53.360*** (df = 5; 19)
Note:	*p<0.1; **p<0.05; ***p<0.01

The regression equation was significant (F(5, 19)=53.360, p = < 0.01), with an R^2 of 0.934. Nanoparticle size increased significantly over time (4.810, p = < 0.01). Inspection of the coefficients suggests that all solvents were significant over the constant (EtOH). Hepes (31.180, p = < 0.01), PBS (63.680, p = < 0.01) and water (19.360, p = < 0.05) all significantly increased the size of nanoparticles over time compared to the baseline. On the other hand, the mix significantly decreased the size of nanoparticles over time compared to the baseline (-22.180, p = < 0.01).

Overall, as with the other results, PBS contributed to the greatest growth in DLS over time, while the Mix contributed to the greatest reduction in growth in DLS over time. The latter result was not significant when time is measured in minutes, but was largely significant over days.

3.7.5 Comparison of No Polymer, PEG, PMA and PHPMA

Table 3.19 and Figure 3.19 show the regression analysis for the comparison of no polymer, PEG, PMA and PHPMS. The regression equation was significant (F(4, 75)=31.572 p = < 0.01), with an R^2 of 0.627. Nanoparticle size increased significantly over time (0.490, p = < 0.01). Inspection of

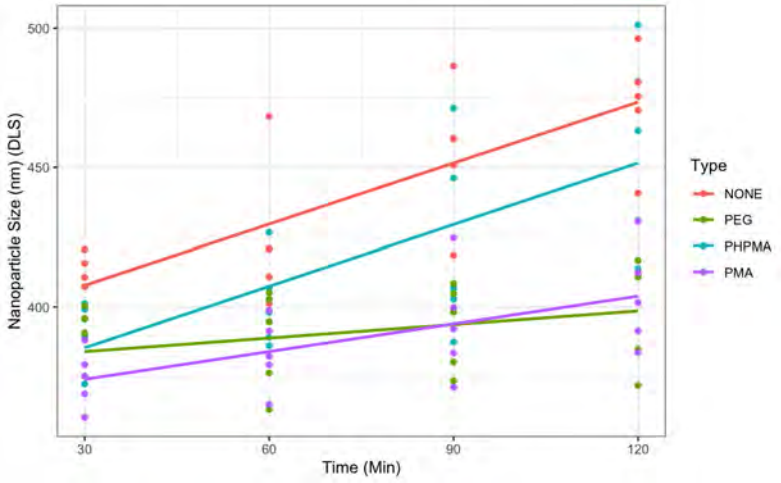

Figure 3.19: *Time series (minutes) for Nanoparticles with no polymer/PHPMA/PEG/PMA attached dispersed in EtOH, Water, PBS, Hepes and 50:50 EtOH:water mix. Both individual measurements and a linear regression line are plotted using R's 'lm' function.*

Table 3.19: *Linear model for NP-SIZE TIME + TYPE for nanoparticle size over minutes by polymer type or no polymer.*

	Dependent variable:
	NP_SIZE
TIME_MINS	0.490*** (0.071)
TYPEPEG	−49.350*** (6.758)
TYPEPHPMA	−22.150*** (6.758)
TYPEPMA	−51.655*** (6.758)
Constant	403.834*** (7.168)
Observations	80
R^2	0.627
Adjusted R^2	0.608
Residual Std. Error	21.371 (df = 75)
F Statistic	31.572*** (df = 4; 75)
Note:	*p<0.1; **p<0.05; ***p<0.01

the coefficients suggests that all polymer types were significantly different to the constant (none).

Each polymer, PHPMA (-22.150, p = < 0.01), PMA (-51.655, p = < 0.01) and PEG (-49.350, p = < 0.01), significantly reduced nanoparticle size over time compared to using no polymer. The effect is considerably smaller for the PHPMA polymer, with less than half the sized coefficient compared to the other two polymers.

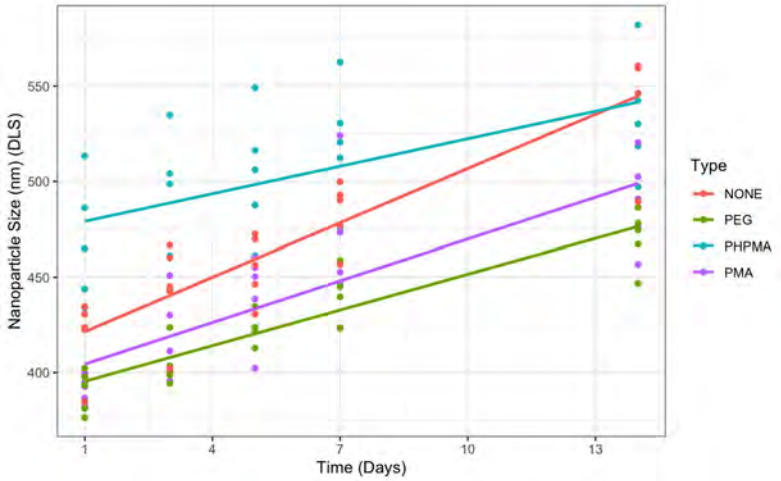

Figure 3.20: *Time series (days) for Nanoparticles with no polymer or PHPMA/PEG/PMA attached dispersed in EtOH, Water, PBS, Hepes and 50:50 EtOH:water mix. Both individual measurements and a linear regression line are plotted using R's 'lm' function.*

Table 3.20: *Linear model for NP-SIZE TIME + TYPE for nanoparticle size over days by polymer type or no polymer.*

	Dependent variable:
	NP_SIZE
TIME_DAYS	6.950*** (0.558)
TYPEPEG	−42.292*** (7.060)
TYPEPHPMA	34.272*** (7.060)
TYPEPMA	−28.076*** (7.060)
Constant	427.178*** (6.011)
Observations	100
R^2	0.755
Adjusted R^2	0.745
Residual Std. Error	24.960 (df = 95)
F Statistic	73.129*** (df = 4; 95)
Note:	*p<0.1; **p<0.05; ***p<0.01

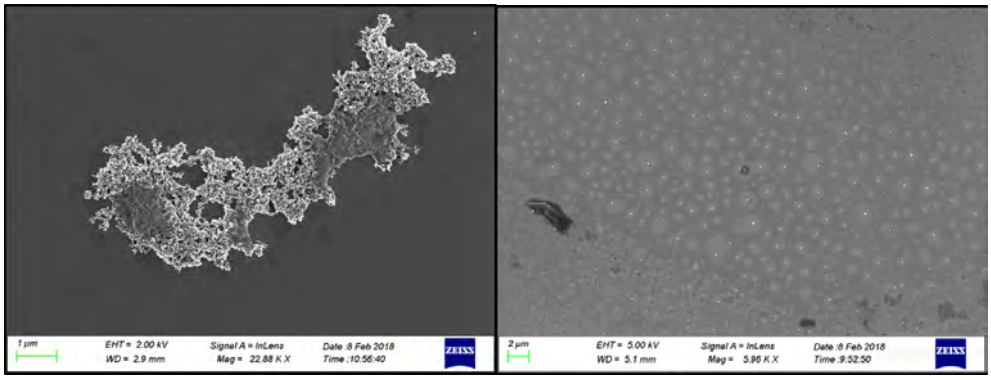

(a) pre PEGylation (b) post PEGylation

Figure 3.21: *(a) Core@shell iron oxide NPs (sample CF-SPIONS-5) pre-PEGylation imaged by SEM showing aggregation (b) shows core@shell iron oxide NPs post PEGylation imaged by SEM showing a significant decrease in aggregation. Images taken by Houari AMARI and Steve YORK, University of Warwick.*

Regression analysis can be seen in Table 3.20 and Figure 3.20. The regression equation was significant (F(4, 95)=73.129, p = < 0.01), with an R^2 of 0.755. Approximately 75% of the overall variance in nanoparticle size over time is captured by the type of polymer used alone when considering both R^2 and adjusted R^2. Nanoparticle size increased significantly over time (6.950, p = < 0.01). Inspection of the coefficients suggests that all polymer types were significantly different to the constant (none). PMA (-28.076, p = < 0.01) and PEG (-42.292, p = < 0.01) both significantly reduced nanoparticle size over time, while the PHPMA polymer increased nanoparticle size over time (34.272, p = < 0.01).

SEM imaging of core@shell iron oxide nanoparticles (sample CF-SPIONS-5) demonstrates how the addition of PEG to synthesised nanoparticles increases the hydrophilicity of the sample by the formation of hydrogen bonds by repeats with the solvent. It also increases steric distance between the nanoparticles thus decreasing the attraction [73]. Figure 3.21b shows SEM images of core@shell iron oxide before (a) and after (b) PEGylation. It can be seen that aggregation is reduced after PEGylation with it possible to see individual nanoparticles rather than "clumps" of nanoparticles. SEM was chose for this piece of work due to the lack of need to size nanoparticles. SEM is associated with providing clear images which demonstrate morphology and aggregation of nanoparticles. Figure 3.21b clearly demonstrate the use of SEM for visualisation of nanoparticle aggregation.

3.8 Discussion

Biomedically, nanoparticles with PEG added have been used for both drug-delivery and imaging applications [74]. Within a biological environment PEG chains reduce the charge-base often seen in relation to protein and small-molecule interactions. PEG is often considered for addition to nanoparticle surfaces due to it being inexpensive, versatile and nontoxic. The addition of PEG is referred to as PEGylation. PEG is a coiled polymer which consists of repeating ethylene glycol ($C_2H_6O_2$) units. PEG molecules consist of an end designated as R_1 which attach to the NP surface, and a distal terminal group, designated as R_2 which interacts with the solvent. In between R_1 and R_2 can be any number (n) of ethylene glycol repeats.

The more monomer repeats the longer the PEG chains with the size/length of these chain usually reported by average molar mass(Mw) [75]. Here PEG-Silane 5000 has been used. PEG-silane when dissolved in a mixture of ethanol/water solution, then added to a solution of silica coated nanoparticles will bind to the nanoparticles silica surface covalently via the reaction between hydroxyl group and ethoxyl/methoxyl silane [74].

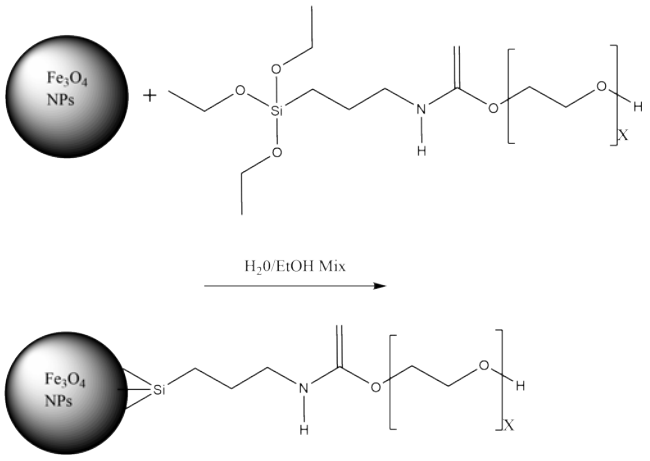

Figure 3.22: *Covalent bonding of PEG-Silane to silica surface of nanoparticles. Drawn using ChemDraw.*

PEGylation of nanoparticles in this manner can reduce aggregation of nanoparticles with a silica surface by suppressing non-specific binding of charged molecules to the PEG modified surface. This results in nanoparticles being less attracted to each other as represented in Figure 3.23. The structure of core@shell nanoparticles add complexity to the way

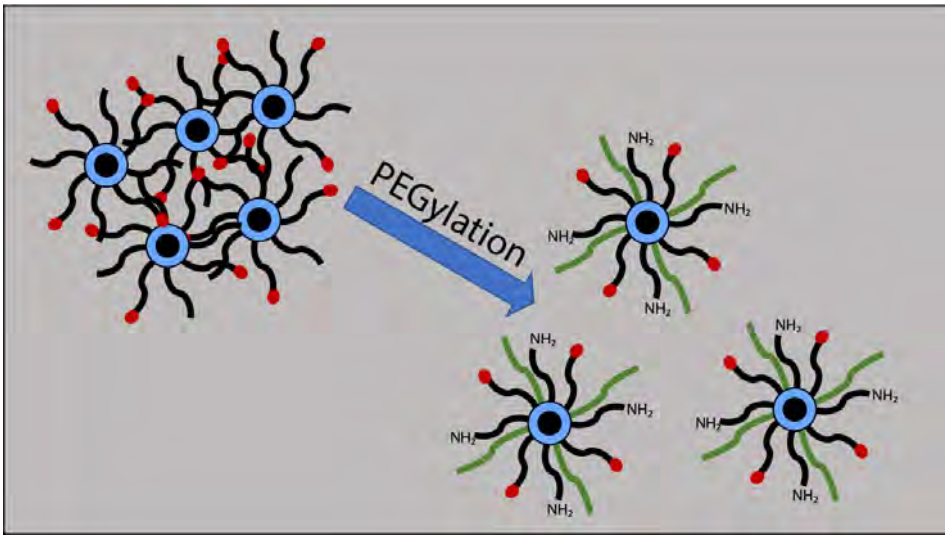

Figure 3.23: *Schematic representation (not to scale) of the effect of addition of PEG on aggregation of silica coated iron oxide nanoparticles. Post pegylation it can seen that nanoparticles experience a reduction in electrostatic interactions between nanoparticles which reduces the aggregation observed. On the surface of the nanoparticles PEG is represented in green with amine groups in black. Fluorescent dye is seen as red dots on the end of attached amine groups.*

nanoparticles interact with their environment or solvent.[76] PEGylation can reduce this complexity by modifying the interface layer between nanoparticle and environment/solvent. Aggregation of NPs is often due to the attraction between nps being stronger than the attraction between NPs and solvent [74]. Smaller nanoparticles tend to have a high surface energy; this high surface energy is associated with a higher degree of aggregation. This relationship is described by the Derjaguin-Landau-Verwey-Overbeek (DLVO) theory [74][77][78].

DVLO theory describes the situation where van der Waals forces are present alongside electrostatic forces. The theory assumes that the electrostatic double layer forces and the van der Waals forces are independent. This means they can be superimposed or added together at interacting distance for two particles. The theory provides an estimate for inter-surface forces and for surface separations down to a size of approximately 5 nm [77][79].

PEGylation or addition of other polymers of these nanoparticles can reduce aggregation through minimising Van der Waals attractions and by decreasing the surface energy [77-80]. It would be expected that altering the molecular weight of the PEG (or other polymer) would change its

effect on nanoparticle aggregation. An increase in molecular weight results in a decrease in the diffusion rate of chains. It also causes an increase in the physical adsorption of a polymer. These result in lessening of aggregation and therefore particle size reduction measured by DLS for nanoparticles with PEG (or other polymers) of a small molecular weight. As molecular weight increases it has been shown that nanoparticles display larger aggregates when dried and the re-dispersed. It is suggested that this is due to the kinetics of PEG at differing molecular weights [81]. PEG 5000 as used here is recorded as being of a molecular weight which aids in reducing aggregation of nanoparticles. Further investigation of the effect of PEG molecular weight on aggregation was beyond the scope of this work.

The age of a nanoparticles sample can also affect aggregation; older samples are more likely to be aggregated than new samples. Aggregated nanoparticles can also be a result of synthesis using high (>100 mM) ionic strength solvents which effectively shield the solvent from the nanoparticles. Concentration of NPs solution must also be considered, as high concentrations leads to less space between nanoparticles resulting in aggregation.

Phosphate buffer saline (PBS) can be seen from analysis to be the most likely for nanoparticles to aggregate and loose stability over time regardless of the polymer attached to the surface of the nanoparticles. This is potentially unexpected as PBS is meant to mimic a natural biological environment. The aggregation could suggest that nanoparticles exposed to this kinda of environment whether in a biomedical or a research situation could become unstable and aggregate thus reducing their usefulness or viability.

DLS is a standard and widely accepted technique for the analysis of nanoparticles however it is sensitive to the presence of large particles. This means any dust within a sample could of effected the results however given that the results for PBS are seen for all three polymers this is unlikely [82].

PBS is a common frequently used buffer which is used in research to mimic a human body fluid. It is a salt solution of phosphate, sodium chloride and potassium chloride in water. PBS exhibits a relatively high ionic strength. It is this ionic strength that will be responsible for the aggregation of the nanoparticles over time that has been seen. This will

result in a solution that is unstable and possibly adhering to the enclosing container [83].

Research has previously investigated adhesion to surfaces by nanoparticles due to Van der Waals forces for instance by Sungchul and Daniel 2010 and work has also been done on the effect of PBS on gold nanoparticles, however this type of work for silica coated c@s iron oxide nanoparticles is not readily available. Kendall et al, 2012, found that gold nanoparticles do exhibit greater aggregation in PBS than water [84].

3.9 Conclusion

Nanoparticles exhibit less aggregation with the addition of polymer as expected due to changes in electrostatic interactions. Buffer/solvent choice does have an effect on the aggregation seen over time for nanoparticles with different polymers attached. A 50:50 EtOG to water mix appears to limit aggregation the most and PBS seem to show the most aggregation of nanoparticles over time for all polymers.

PEG-silane (5000) is the most effective polymer at reducing aggregation in all solvents howeve it appears to work best when in an EtOH:water 50:50 mix.

Table 3.21: *LM For Time and NPSIZE by all 4 mix categories.*

	Dependent variable:
	NP_SIZE
TIME_MINS	0.490^{***} (0.071)
TYPEPEG	-49.350^{***} (6.758)
TYPEPHPMA	-22.150^{***} (6.758)
TYPEPMA	-51.655^{***} (6.758)
Constant	403.834^{***} (7.168)
Observations	80
R^2	0.627
Adjusted R^2	0.608
Residual Std. Error	21.371 (df = 75)
F Statistic	31.572^{***} (df = 4; 75)
Note:	*p<0.1; **p<0.05; ***p<0.01

3.10 Further Work

Imaging and more detailed characterisation of the nanoparticles with polymer attached should be carried out. This could include but is not limited to TEM, SEM and thermogravimetric analysis (TGA).

Further development and understanding of the attachment of polymers to the nanoparticles is desirable. A thorough understanding of the best storage conditions for nanoparticles is desirable and extending the time within the time study would be helpful.

Further evaluation of buffers/solvents used with the nanoparticles with a biological environment in mind should be considered. This should also involve a toxicity study of nanoparticles within cells.

Stabilising nanoparticles with PVP before addition of polymers should be investigated to see if this stabilisation step helps to reduce aggregation seen in buffers.

This could be followed by the addition of a biocompatible thermo responsive polymer. This would allow for relaxometry studies of the core@shell iron oxide nanoparticles as T2 MRI contrast agents with polymers for potential directed drug release.

3.11 References - Chapter 3

1. Nanoparticle Technology Handbook, 2018, 109-168.
2. S. Shrestha, B. Wang and P. Dutta, Advances in Colloid and Interface Science, 2020, 279, 102162.
3. The IUPAC Compendium of Chemical Terminology, 2014.
4. A. Dunn, P. Painter and M. Coleman, Polymer International, 1995, 37, 232-232.
5. A. Jenkins, H. Allcock, F. Lampe and J. Mark, Polymer International, 2004, 53, 1395-1395.
6. M. Ashby and D. Jones, Engineering materials, Butterworth-Heinemann, Oxford, 1996.
7. I. WARD, N. McCrum, C. Buckley and C. Bucknall, Polymer, 1988, 29, 1919-1919.
8. K. O'Driscoll and R. Sanayei, Macromolecules, 1991, 24, 4479-4480.
9. Pure and Applied Chemistry, 1976, 48, 373-386.
10. R. Hiorns, R. Boucher, R. Duhlev, K. Hellwich, P. Hodge, A. Jenkins, R. Jones, J. Kahovec, G. Moad, C. Ober, D. Smith, R. Stepto, J. Vairon and J. Vohlídal, Pure and Applied Chemistry, 2012, 84, 2167-2169.
11. R. langer, Nature, 1998, 252-267.
12. D. Shome, S. Honavar, K. Raizada and D. Raizada, Ophthalmology, 2010, 117, 1638-1644.
13. O. Pillai and R. Panchagnula, Current Opinion in Chemical Biology, 2001, 5, 447-451.
14. A. Godwin, K. Bolina, M. Clochard, E. Dinand, S. Rankin, S. Simic and S. Brocchini, Journal of Pharmacy and Pharmacology, 2001, 53, 1175-1184.
15. N. Kumar, S. Pahuja and R. Sharma, International Journal of Drug Delivery Technology, 2019, 9, 27-33.
16. T. Ueki, Polymer Journal, 2014, 46, 646-655.
17. C. Finch, Polymer International, 1994, 33, 115-115.
18. Y. Kotsuchibashi, Polymer Journal, 2020, 52, 681-689.
19. Y. Kotsuchibashi, M. Ebara, T. Aoyagi and R. Narain, Polymers, 2016, 8, 380.
20. T. Ueki, Polymer Journal, 2014, 46, 646-655.
21. 70.A. Bordat, T. Boissenot, J. Nicolas and N. Tsapis, Advanced Drug Delivery Reviews, 2019, 138, 167-192.

22 M. Karimi, P. Sahandi Zangabad, A. Ghasemi, M. Amiri, M. Bahrami, H. Malekzad, H. Ghahramanzadeh Asl, Z. Mahdieh, M. Bozorgomid, A. Ghasemi, M. Rahmani Taji Boyuk and M. Hamblin, ACS Applied Materials amp; Interfaces, 2016, 8, 21107-21133.
23. 72.T. Tanaka and M. Okamoto, Polymer Journal, 2018, 50, 523-531.
24. C. Zhao, Z. Ma and X. Zhu, Progress in Polymer Science, 2019, 90, 269-291.
25. G. Pasparakis and C. Tsitsilianis, Polymer, 2020, 211, 123146.
26. 82.R. Koningsveld, W. Stockmayer and E. Nies, Polymer phase diagrams, Oxford University Press, Oxford, 2001.
27. Y. Chen, Z. Wang, Y. Harn, S. Pan, Z. Li, S. Lin, J. Peng, G. Zhang and Z. Lin, Angewandte Chemie, 2019, 131, 12036-12043.
28. A. Palanisamy and S. Sukhishvili, Macromolecules, 2018, 51, 3467-3476.
29. M. Davis, Z. Chen and D. Shin, Nature Reviews Drug Discovery, 2008, 7, 771-782.
30. R. Petros and J. DeSimone, Nature Reviews Drug Discovery, 2010, 9, 615-627.
31. R. Ferrari, L. Talamini, M. Violatto, P. Giangregorio, M. Sponchioni, M. Morbidelli, M. Salmona, P. Bigini and D. Moscatelli, Molecular Pharmaceutics, 2016, 14, 124-134.
32. R. Ghaffarian, E. Pérez-Herrero, H. Oh, S. Raghavan and S. Muro, Advanced Functional Materials, 2016, 26, 3382-3393.
33. A. Agostini, U. Capasso Palmiero, S. Barbieri, M. Lupi and D. Moscatelli, Nanotechnology, 2018, 29, 225604.
34. E. Ahmed, Journal of Advanced Research, 2015, 6, 105-121.
35. N. Annabi, A. Tamayol, J. Uquillas, M. Akbari, L. Bertassoni, C. Cha, G. Camci-Unal, M. Dokmeci, N. Peppas and A. Khademhosseini, Advanced Materials, 2013, 26, 85-124.
36. R. langer, Nature, 1998, 252-267.
37.G. Kocak, C. Tuncer and V. Bütün, Polymer Chemistry, 2017, 8, 144-176.
38.A. Palanisamy and S. Sukhishvili, Macromolecules, 2018, 51, 3467-3476.
39. A. Abuchowski, J. McCoy, N. Palczuk, T. van Es and F. Davis, Journal of Biological Chemistry, 1977, 252, 3582-3586.
40. D. OWENSIII and N. PEPPAS, International Journal of Pharmaceutics, 2006, 307, 93-102.

41. A. Gabizon, H. Shmeeda and Y. Barenholz, Clinical Pharmacokinetics, 2003, 42, 419-436.
42. K. Laginha, S. Verwoert, G. Charrois and T. Allen, Clinical Cancer Research, 2005, 11, 6944-6949.
43. B. Du, M. Yu and J. Zheng, Nature Reviews Materials, 2018, 3, 358-374.
44. S. Douglas, S. Davis and L. Illum, International Journal of Pharmaceutics, 1986, 34, 145-152.
45. J. Plard and D. Bazile, Colloids and Surfaces B: Biointerfaces, 1999, 16, 173-183.
46. M. Ahmed, A. Lukyanov, V. Torchilin, H. Tournier, A. Schneider and S. Goldberg, Journal of Vascular and Interventional Radiology, 2005, 16, 1365-1371.
47. M. Peracchia, S. Harnisch, H. Pinto-Alphandary, A. Gulik, J. Dedieu, D. Desmaële, J. d'Angelo, R. Müller and P. Couvreur, Biomaterials, 1999, 20, 1269-1275.
48. J. Plard and D. Bazile, Colloids and Surfaces B: Biointerfaces, 1999, 16, 173-183.
49. M. Roser, D. Fischer and T. Kissel, European Journal of Pharmaceutics and Biopharmaceutics, 1998, 46, 255-263.
50. T. Martins, T. Ribeiro and J. Farinha, Polymers, 2021, 13, 1003.
51. M. Sponchioni, U. Capasso Palmiero and D. Moscatelli, Materials Science and Engineering: C, 2019, 102, 589-605.
52. L. Baekeland, Scientific American, 1909, 68, 322-323.
53. Y. Kojima, A. Usuki, M. Kawasumi, A. Okada, Y. Fukushima, T. Kurauchi and O. Kamigaito, Journal of Materials Research, 1993, 8, 1185-1189.
54. H. Görtz and T. Breiner, Angewandte Chemie, 2004, 116, 1945-1946.
55. M. Husseman, E. Malmström, M. McNamara, M. Mate, D. Mecerreyes, D. Benoit, J. Hedrick, P. Mansky, E. Huang, T. Russell and C. Hawker, Macromolecules, 1999, 32, 1424-1431.
56. X. Huang, I. El-Sayed, W. Qian and M. El-Sayed, Journal of the American Chemical Society, 2006, 128, 2115-2120.
57. V. Pino-Ramos, A. Ramos-Ballesteros, F. López-Saucedo, J. López-Barriguete, G. Varca and E. Bucio, Topics in Current Chemistry, 2016, 374.
58. R. Hong, T. Emrick and V. Rotello, Journal of the American Chemical

Society, 2004, 126, 13572-13573.
59. I. Medintz, H. Uyeda, E. Goldman and H. Mattoussi, Nature Materials, 2005, 4, 435-446.
60. M. Howarth, K. Takao, Y. Hayashi and A. Ting, Proceedings of the National Academy of Sciences, 2005, 102, 7583-7588.
61. D. Keddie, G. Moad, E. Rizzardo and S. Thang, Macromolecules, 2012, 45, 5321-5342.
62. Polysciences.com, 2022.
63. A. Akbari, R. Yegani and B. Pourabbas, Colloids and Surfaces A: Physicochemical and Engineering Aspects, 2015, 484, 206-215.
64. T. Andreani, A. Souza, C. Kiill, E. Lorenzón, J. Fangueiro, A. Calpena, M. Chaud, M. Garcia, M. Gremião, A. Silva and E. Souto, International Journal of Pharmaceutics, 2014, 473, 627-635.
65. C. Finch, Polymer International, 1994, 33, 115-115.
66. M. AMIJI and K. PARK, Biomaterials, 1992, 13, 682-692.
67. C. Xu, B. Wayland, M. Fryd, K. Winey and R. Composto, Macromolecules, 2006, 39, 6063-6070.
68. K. Guice, Hdl.handle.net, 2022.
69. J. Brydson, Plastics Materials, Elsevier Science, Kent, 2014.
70. N. Larson and H. Ghandehari, Chemistry of Materials, 2012, 24, 840-853.
71. M. Elsabahy and K. Wooley, Chemical Society Reviews, 2012, 41, 2545.
72. B. Tucker and B. Sumerlin, Polym. Chem., 2014, 5, 1566-1572.
73. J. Rieffel, F. Chen, J. Kim, G. Chen, W. Shao, S. Shao, U. Chitgupi, R. Hernandez, S. Graves, R. Nickles, P. Prasad, C. Kim, W. Cai and J. Lovell, Advanced Materials, 2015, 27, 1785-1790.
74. J. Verhoef and T. Anchordoquy, Drug Delivery and Translational Research, 2013, 3, 499-503.
75. J. Lipfert, X. Hao and N. Dekker, Biophysical Journal, 2009, 96, 5040-5049.
76. Q. He, J. Zhang, J. Shi, Z. Zhu, L. Zhang, W. Bu, L. Guo and Y. Chen, Biomaterials, 2010, 31, 1085-1092.
77. C. Blanco-Andujar, D. Ortega, Q. Pankhurst and N. Thanh, Journal of Materials Chemistry, 2012, 22, 12498.
78. S. Laurent, D. Forge, M. Port, A. Roch, C. Robic, L. Vander Elst and R. Muller, Chemical Reviews, 2008, 108, 2064-2110.

79. J. Dulińska-Litewka, A. Łazarczyk, P. Hałubiec, O. Szafrański, K. Karnas and A. Karewicz, Materials, 2019, 12, 617.
79. M. Barrow, A. Taylor, P. Murray, M. Rosseinsky and D. Adams, Chem. Soc. Rev., 2015, 44, 6733-6748.
80. D. Ni, J. Zhang, W. Bu, H. Xing, F. Han, Q. Xiao, Z. Yao, F. Chen, Q. He, J. Liu, S. Zhang, W. Fan, L. Zhou, W. Peng and J. Shi, ACS Nano, 2014, 8, 1231-1242.
81. J. Choi, C. Park and J. Lee, Drug Delivery, 2008, 15, 347-353.
82. D. Carpenter, Journal of Chemical Education, 1977, 54, A430.
83. S. Du, K. Kendall, S. Morris and C. Sweet, Journal of Chemical Technology amp; Biotechnology, 2010, 85, 1223-1228.
84. S. Du, K. Kendall, P. Toloueinia, Y. Mehrabadi, G. Gupta and J. Newton, Journal of Nanoparticle Research, 2012, 14.

Chapter 4

Principles of Nanoparticle Use in Cell Biology Research

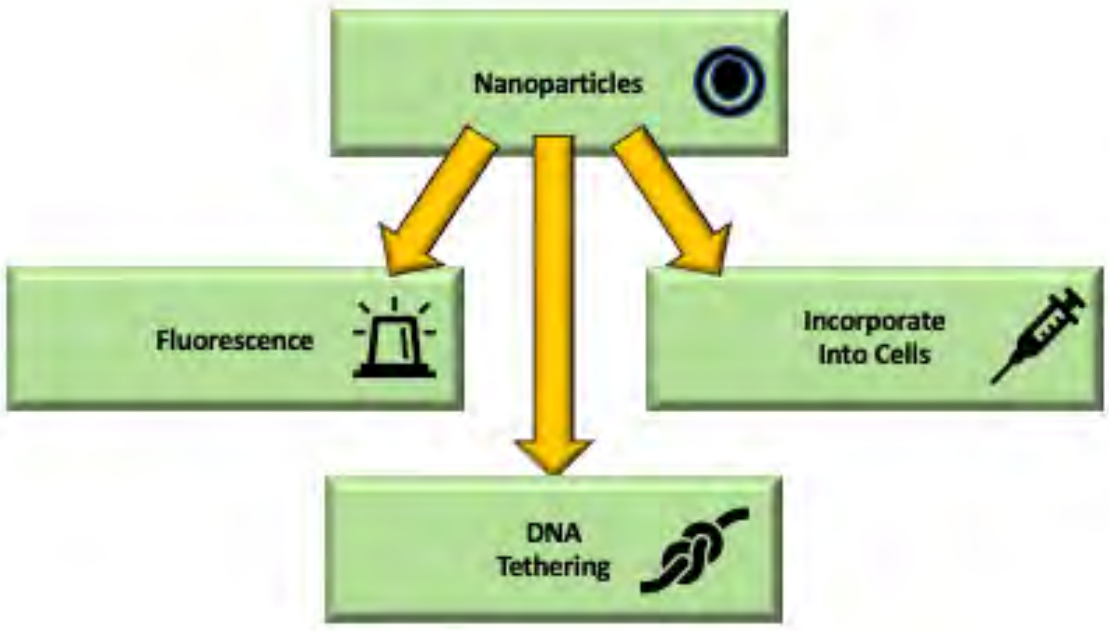

Figure 4.1:

4.1 Nanoparticles in Cell Biology Research

Properties such as size, surface functionality shape and unique behaviour has led to the use of nanoparticles within biological research as an exciting and versatile material when investigating biological questions. Nanoparticles have been used for imaging, drug delivery, sensing and

to develop our understanding of biological processes. The development of nanoscience and the use of nanoscience within biological research is exciting, providing materials with unique properties which can be used to develop new techniques and tools leading to a deeper understanding of biological processes [1][2].

Within research inorganic, often metallic, NPs have been used as sensors detecting for low levels of analytes such as proteins, RNA and DNA. Magnetic nanoparticles coated with antibodies invoke direct immunological reactions leading to pathogen detection and separation has been achieved.[1][2] Nanoparticles have been used for investigating molecular and cellular processes and detecting then capturing cells.[1][2]

The need to image cell and biological processes with ever increasing clarity is paramount to biological research. Nanoparticles provide properties which aid in the pursuit of better imaging. This is a result of the number of nanoparticles, and therefore imaging agents, which can be delivered in a targeted rather than random manner at once.[3] Different nanoparticles can be delivered simultaneously with differing imaging modalities allowing for different biomolecules to be targeted and imaged. The same nanoparticles which enhance imaging can potentially also be used as a delivery system to the targeted area.

Many different types of nanoparticles have been investigated and used within biological research, with choice of nanoparticle type dependent on the research they are to be used for. These nanoparticles include the following nanoparticle families.

Liposomes from as early as 1965 were used as a model for cellular membranes and their use since that time has been developed from biophysical model to a nanoparticle platform applied to gene and drug delivery. Liposomes are spherical vesicles containing one or more bi-layered lipid structures. These lipid structures have the ability to self-assemble within an aqueous system. Biocompatible and biodegradable liposomes have been used to carry, protect and deliver many types of biomolecule. Liposomes are also widely used as transfection agents (lipofection) in genetic research [1][2][3].

Quantum Dots (QDs) are nanoparticles which are smaller than 10nm in size with semiconducting properties. Their size and semiconductor properties lead to unique optical and electronic properties.[4] Their use in biological research is often due to advantages such as increased brightness,

photostability and a narrow emission spectrum when compared with conventional organic fluorescent dyes, over organic fluorophore dyes for imaging, their size allowing for imaging in research involving cell labelling and tracking of biomolecules.[5][6][7] QDs make good alternatives to organic fluorophore dyes as they can emit strong colour, are stable against photo bleaching, have long lifetimes, high quantum yield and can be both excited and detected simultaneously.[8]

Biodegradable and biocompatible polymers can be formed into nanoparticles which are used as biological carriers [9]. Formed through block-co polymers with different hydrophobicity spontaneous assembly of these co polymers lead to the formation of core@shell micelles in an aqueous environment [10]. These nanoparticles can be used to encapsulate small, hydrophobic and hydrophilic drug molecules which can then be released in a slow controlled manner at a specific targeted site [11].

Gold nanoparticles offer size and shape dependent properties both chemical and optical. Gold NPs are also biocompatible and can undergo surface modification successfully.[10] In biological research they offer enhanced optical properties improving processes involving scattering, fluorescence, light absorption and surface enhanced Raman scattering. This is due to a unique interaction of free electrons within the gold nanoparticles and light [12]. Gold nanoparticles are often used within biological research including as biochemical sensors and to aid imaging [13].

Iron oxide NPs are used both as passive and active targeting imaging agents due to the property of superparamagnetism. The most widely used superparamagnetic iron oxide nanoparticles (SPIONs) consist of a magnetite (Fe_3O_4)and/or maghemite (γFe_2O_3) core which is often coated with a biocompatible material to increase amongst other factors such as surface modification colloidal stability [14]. SPIONs have been used as T2-weighted magnetic resonance imaging (MRI) contrast agents.[14] Traditional gadolinium-chelate contrast agents have result in greater toxicity and provide less imaging sensitivity than SPIONS.[15] Two SPION contrast agents have received clinical approval - ferumoxides (120–180 nm) and ferucarbotran (60 nm) – for use as MRI contrast agents [15].

For biological research purposes, SPIONs have been used to aid in the investigation of gene expression and apoptosis.[16] The ability to functionalise SPIONs makes them an attractive target for development

for use within biological research for imaging, targeting and manipulation of cellular components.

Any use of nanoparticles for research purposes must include an understanding of the interactions between biological systems and the nanoparticles themselves. These interactions have been shown to be affected by the very properties that make nanoparticles attractive to begin with such as chemical composition, size and shape and can differ depending on whether they are being used *in vitro* or *in vivo* [17]. For example the timings associated with mitosis can be altered when nanoparticles are present within a cell [18].

Uses of nanoparticles within research are increasing. Nanoparticles are being developed which through their interaction with biological systems can activate cell signalling pathways leading to protein synthesis [19]. This ability for NP mediated activation of cell signalling pathways has also been shown to cause localised changes to cellular morphology and alteration to the structure of the actin cytoskeleton. Another study demonstrated the ability of of magnetic NPs to activate apoptosis cell signalling on the application of an external magnetic force in zebra fish [20]. These uses demonstrate the potential of nanoparticles within research and the need for continued development of nanomaterials with biological research in mind. A thorough understanding of the nanoparticle structure and behaviour is as important as the overall experimental design to ensure that nanoparticles behave in a way that is predictable and does not influence results.

4.2 Aims

Here we aimed to evaluate nanoparticles designed and synthesised as previously described in chapter 2 and 3 for their potential use in biological environments and research. This includes an evaluation of their fluorescence over time given exposure to a laser therefore evaluating the ability to visualise nanoparticles whilst imaging. A discussion on the benefits of highly designed and controlled synthesised nanoparticles in comparison to purchasing commercially available magnetic beads. Methods for incorporation of nanoparticles into cells and the attachment of nanoparticles to DNA and the ability to manipulate the magnetic properties of the nanoparticles on application of a magnetic field. For some of this work

silica nanoparticles were synthesised rather than silica coated iron oxide nanoparticles. These MSMs were used due to the ease of synthesis and having the same silica surface for surface functionalisation. Due to the surface of the core@shell nanoparticles described in this work being also silica, the use of MSNs should provide results which would be expected to be the same for the silica coated iron oxide c@s nanoparticles. This makes MSNs a good alternative for use in the work described here.

The specific aim are:

1. To synthesise Mesoporous silica nanoparticles of different sizes using a single method at different temperatures
2. To prepare Buffers and ensure Nanoparticles are suitable for incorporation by endocytosis
3. To couple the protein neutravadin to silica coated iron oxide nanoparticles as proof od concept for DNA tethering.
4. To tether nanoparticles to DNA
5. To incorporate nanoparticles into cells via 2 different methods
6. to determine if nanoparticles remain fluorescence over a period of 3 hours

4.3 Experimental Protocols

4.3.1 Mesoporous Silica Nanoparticles

Mesoporous silica nanoparticles of different sizes were prepared. 16mL of water, 1.8mL of ethanol, 1g of triethanol amine and 0.65g of cetrimonium bromide (CTAB) were mixed in a 50mL round bottom flask. The solution was heated to 80°C, 50°C or 30°C depending of nanoparticles size required see Table 4.1. 1.45mL of TEOS was added and the solution left for 1 hour with magnetic stirring. A solution of 4.7μL and 24 μL was prepared and added to the round bottom flask. This was left for a further 1 hour. The resulting nanoparticles were washed and separated by centrifugation (11000rpm,15mins) using a 3:20 HCL : ethanol solution. Nanoparticles were then washed in ethanol until a pH of 7 was obtained.

Table 4.1: *Mesoporous silica nanoparticles of different sizes can be synthesised by a change in temperature. Here are expected size of nanoparticles by temperature synthesised at.*

Temperature (°C)	**Nanoparticle size (nm)**
80	70
50	40
30	20

4.3.2 Buffer Preparation for Zeta Potential Analysis for Nanoparticle Cell Incorporation by Endocytosis

Three different buffers were prepared as per Table 4.2, in order to analyse zeta potential.

Table 4.2: *Buffer preparation for analysis of nanoparticle behaviour at various pH by zeta potential.*

	Target pH	**Name**
Buffer 1	8.5	Bicarbonate Buffer (salt free)
Buffer 2	7.4	Phosphate Buffer (salt free)
Buffer 3	5.5	2-(N-morpholino)ethanesulfonic acid(MES) Buffer

1. **0.1M Bicarbonate Buffer**

   Solution 1 was prepared using 3.6g of sodium bicarbonate ($NaHCO_3$) dissolved in 400mL of distilled water. Solution 2 was prepared using 0.21g of Sodium carbonate (Na_2CO_3) dissolved in 20mL of distilled water. Solution 2 was titrated into 200mL of solution 1 until pH 8.5 was achieved.

2. **10mM Phosphate Buffer**

   0.062g (0.0004mol) of sodium dihydrogen phosphate ($NaH_2PO_4 \cdot 2\,H_2O$) and 0.071g (0.005mol) sodium phosphate (Na_2HPO_4) were mixed into 100mL of distilled water and pH was checked.

3. **0.1M 2-(N-morpholino)ethanesulfonic acid(MES) Buffer**

   0.195g of MES was dissolve in 90mL of distilled water. Solution was titrated with a monovalent acid or base until pH 5.6 was obtained. This was then made up to 100mL with distilled water.

4.3.3 Protein (Neutravadin) Coupling of Amine Modified Fluorescent Magnetic Nanoparticles

100μL of silica coated iron oxide nanoparticles (sample CF-22-101) were washed in 1mL of phosphate-buffered saline (PBS) 3 times. The washed gld389 beads were re-suspended in 1 mL of gluteraldehyde solution (400μL gluteraldehyde/60μL PBS) (10% concentration). The solution was sonicated for 1 minute to ensure full re-suspension and allowed to react for 1 hour at room temperature. The solution was washed twice and re-suspended in 1 mL of PBS. 50μL neutravidin was dissolved in 1mL of PBS to achieve a final concentration of 0.2 mg/mL. The bead suspension was added and reacted for 2 hours at room temperature. The solution was washed and re-suspended in 1 mL of quenching solution (PBS and 1mg/mL casein).

4.3.4 Confirmation of Protein Coupling of Amine Modified Fluorescent Magnetic Nanoparticles

Two flow cells were prepared using salinated microscope slides and standard cover slips. 20 μL of PLL-PEG-biotin (0.2mg/mL) was added to one flow cell and 20 μL of bovine serum albumin (BSA) (1mg/mL) was added to both flow cells. The flow cells were washed 3 times with 20 μL PBS buffer (1mg/mL). Silica coated magnetic nanoparticles were added to the non control slide containing both BSA and PLL-PEG-Biotin. The procedure was then repeated but without the use of BSA to determine if BSA was contributing to the signal seen. Imaging was achieved with pictures taken at L561, 65.726mV, TIRF -4942 and z= 96.985 μm for both sets of samples. This was to ensure accurate comparison of images with and without the presence of BSA.

IN TIRF microscopy the laser passes through the sample, this allows for the visualisation of the flow cell at different depths and also on the surface of the flow cell itself. This allows for nanoparticles which are bound to a tether which is attached to the flow cell to be visualised. If the nanoparticles are not tethered they will be seen floating throughout the depth of the flow cell. This means that confirmation of protein coupling can be carried out using TIRF microscopy [21].

All TIRF microscopy was carried out using the Warwick Open Source Microscope (WOSM) (http://www.wosmic.org/). This microscope de-

signed and made at the University of Warwick is designed to be used for high resolution optical microscopy providing both a super-stable physical platform and control interface.

4.3.5 DNA Tethering of Silica Coated Iron Oxide Nanoparticles

100μL of silica coated iron oxide nanoparticles (sample CF-22-101) were washed in 1mL of Phosphate-buffered saline (PBS) 3 times and sonicated. Neutravadin was then attached as described in section 4.3.3. 10μL of these nanoparticles sample (CF-22-102) were then mixed with 20μL of 10KB commercially purchased DNA and 10μL of caesin. This was left for 30mins for attachment to occur.

TIRF microscopy was carried out to verify attachment of nanoparticles to DNA using the Warwick Open Source Microscope (WOSM) (http://www.wosmic.org/). (x40, 473nm excitation)

4.3.6 MC148 Cell Line Preparation

The cell line(MC148) used for this research was prepared by Emanuele Roscioli (University of Warwick, Life Sciences). Normal RPE1 cells (MC133) were plated and incubated for 24h. Cells were then transfected with 200ng of pHTN-CenpA plasmid (pMC442). Cells were diluted 1:25 in a 100mm dish and the placed under selection in culturing media with 300 μg/mL Geneticin. Cells were left for 2 weeks. 24 clones were selected and the clones displaying the best signal of pHTN-CENP-A selected (clone 3). This was achieved by treatment of cells with 2μM TMR and DV1 microscopy. A block diagram, including timings, of the above steps can be seen in Figure 4.2.

4.3.7 TMR Treatment of MC148 RPE1 Cells For Micro Injection

80-90% confluent MC148 cells were diluted 1:4 into fluorodishes (35mm dishes) and incubated for 24-48h. Resulting cells were treated with 2uM TMR for 15minutes and the washed out with TMR. Cells were then incubated for 30 minutes in normal media. The media was then replaced with L-15 media (CO2 independent) and DV1 imaging performed.

lo

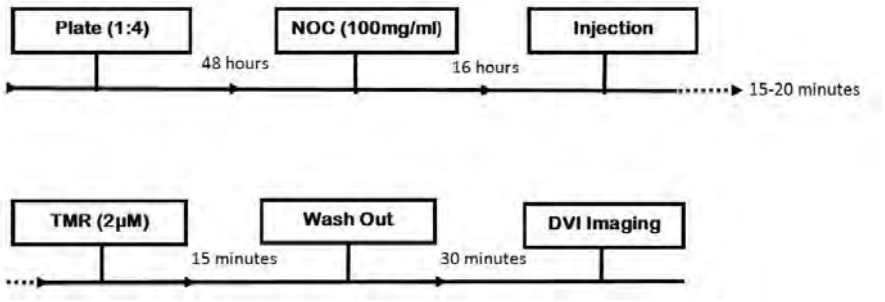

Figure 4.2: *Experimental methodology for cell culture preparation with nocodazole (NOC) to allow the accumulation of cells in the G2/M phase of mitosis therefore halting the replication cycle. .*

4.3.8 TMR Treatment of MC148 RPE1 Cells

80-90% confluent MC148 cells were diluted 1:4 into fluorodishes (35mm dishes) and incubated for 24-48h. Resulting cells were treated with 2uM TMR for 15minutes and the washed out with TMR. Cells were then incubated for 30 minutes in normal media. The media was then replaced with L-15 media (CO2 independent) and DV1 imaging performed.

4.3.9 Micro Injection of Magnetic Nanoparticles

MC148 cells of 80-90% confluency were diluted in a ratio of 1:4 into fluorodishes (35mm dishes). After 24-48h, NOC (100ng/mL) was used to treat cells and left for 16h. Nanoparticles, in NOC containing media, were injected into cells over a period of approximately 20 minutes. Cells in NOC containing media were treated with 2uM TMR for 15 minutes and then TMR and NOC were washed out and media replaced with a normal media and incubated for 30 minutes. The media was replaced with L-15 media and DV1 imaging performed to determine successful injection of the beads. Micro injection was carried out under the conditions of constant flow of fluid.

4.4 Imaging

Imaging of cells ranged from 2h to 5-6h to acquire movies using an Olympus ultimate focus microscope. These videos were used to evaluate

micro injection of nanoparticles and endocytosis. Two different imaging conditions were used as described in Table 4.3.The main difference in conditions is mCherry exposure and mCherry light power.

Table 4.3: *Imaging conditions used for in vivo microscopy.*

	Condition 1	Condition 2
Cells	RPE1,pHTN,Cenp-A	RPE1,pHTN,Cenp-A
dye	TMR 2μm	TMR 2μm
mCherry exposure	0.5 sec	0.25 sec
mCherry light power	50%	32%
dichoric	Quad-ch	Quad-ch
time interval	3 min	3 min
duration	12h	12h or 2h
z-stack thickness	2μm	2μm
z-stack interval	7 planes (14μm)(middle)	7 planes (14μm)
objective	40x	40x

Imaging of nanoparticles was carried out for all biological work *in vivo* or *in vitro* using either TIRF or DVI imaging.

Total internal reflection fluorescence microscopy (TIRF) allows for the restriction of excitation and detection of fluorophores in a thin region of a sample. Signal-to-noise ratio is considerably improved due to elimination of background fluorescence from outside the focal plane, this results in improvement to the spatial resolution of the features of the sample. TIRF uses properties unique to an induced evanescent field in a limited region of a specimen which is adjacent to the interface between the specimen and normally the glass cover slip of a microscope slide [21][22][23].

Refraction of light as it hits the interface between the specimen and the glass cover slip of a microscope slide which different refractive indices results in confinement of some or all of the light to the higher-index medium. A collimated light beam propagating through one medium when reaching the interface can be refracted upon entry to the second medium, or reflected at the interface [21][22][23]. This is dependent upon the difference in refractive indices of the two media and the incident angle. The observed refractive behaviour is governed by Snell's Law:

$$n(1)sin(1) = n(2)sin(2)$$

[1]

TIRF microscopy allows for the detection of a single fluorescent molecule and is frequently employed for bio molecular purposes [21]. DVI Imaging Images are obtained in 3 dimensions with the x and y axis

resolutions determined by the microscope optics and the y axis resolution dependent upon a stains chemistry [24]. Live cell imaging requires the use of time-lapse microscopy. Wide-field fluorescence microscopy is a well-established technique. Its use allows for information to be obtained on both the dynamics and topography of a sample. Using a light source, optical filters and lasers it is possible to illuminate and detect light covering the entire visual field of the microscope objective [22].

4.5 Results and Discussion

4.6 Commercial Beads Vs Synthesised Nanoparticles - Uniformity, Aggregation and Chemical Structure

Nanoparticles including magnetic nanoparticles are available commercially to purchase. These beads are sold for use within biological research. This suggests that the design and synthesis of nanoparticles for a specific purpose within research is not necessary and requires extra time and effort which could be used in other areas of the research. This does depend on the application of the nanoparticles as to whether there is truth to it. Where the purpose of nanoparticles within any research requires precision and a deep understanding of the structure and behaviour of the nanoparticles purpose designed and synthesised nanoparticles are required. Often full details of synthesis, structure, composition and surface chemistry are not provided by manufacturers meaning that it is not possible to predict or understand how nanoparticles interact with the cellular environment. Here, Dynabeads® MyOne™ Silane magnetic beads by Thermo Fisher Scientific were purchased and used for comparison to the synthesised beads.

These nanoparticles are described as "An excellent tool for highly predictable and consistent extraction and isolation of nucleic acids from biological samples, following a simple magnetic separation protocol." and are said to have "The small 1 μm Dynabeads® MyOne™ Silane have an optimized silica-like surface chemistry and a high specific surface area, providing efficient kinetics and a high sensitivity in nucleic acid capture. Their uniform size and surface area also ensure reproducible results."

Both the commercial beads and synthesised nanoparticles (sample CF-Spions-9) were subjected to the same preparation of 15 minutes sonication to ensure a fair comparison of aggregation, both samples where also stored in ethanol.

Scanning Electron Microscopy (SEM) focuses on the sample's surface and its composition this is in contrast to TEM involves the use of a high energy beam of electrons which is shone through a thin sample. SEM can be used only to provide information on the morphology and aggregation of a nanoparticle sample. It is not possible to obtain size of nanoparticles from SEM. Here SEM was used for comparison of commercial beads and synthesised beads and here SEM does allow the difference between the synthesised and commercial beads to be visualised.

Figure 4.4 shows synthesised core@shell nanoparticles (sample: CF-Spions-9) imaged by SEM. These nanoparticles were synthesised using the solvothermal oleylamine only protocol described in Chapter 2 and then coated with silica. It is not possible to provide accurate sizing with this being better accomplished using TEM. It is, however, clear that the nanoparticles are spherical and that the sample is highly dispersed with little aggregation.

Figures 4.3 and 4.4 clearly show the difference in aggregation between commercial beads and synthesised nanoparticles. Whilst SEM does not allow for sizing of either sample it is possible to determine the spherical morphology of the synthesised nanoparticles however the morphology of the commercial beads in Figure 4.3 is not clear. The aggregation of commercial beads is also clearly observable in contrast to the synthesised nanoparticles.

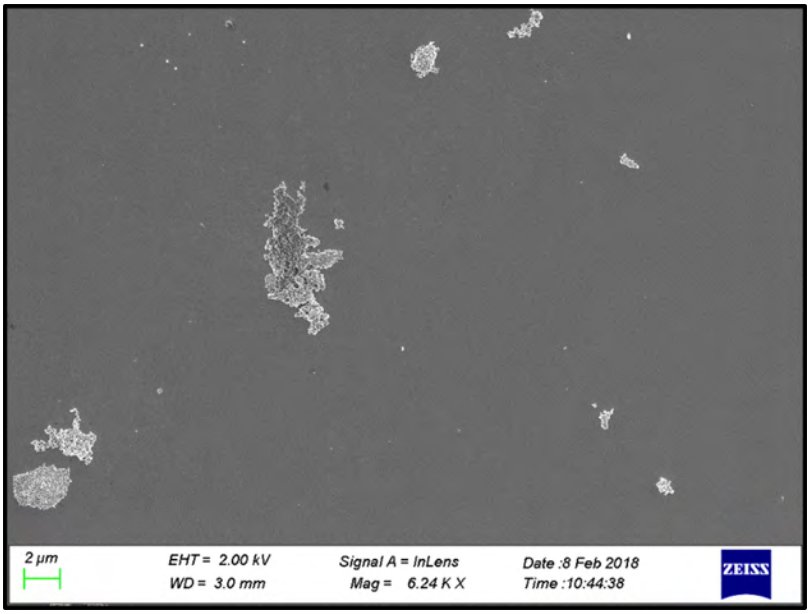

(a)

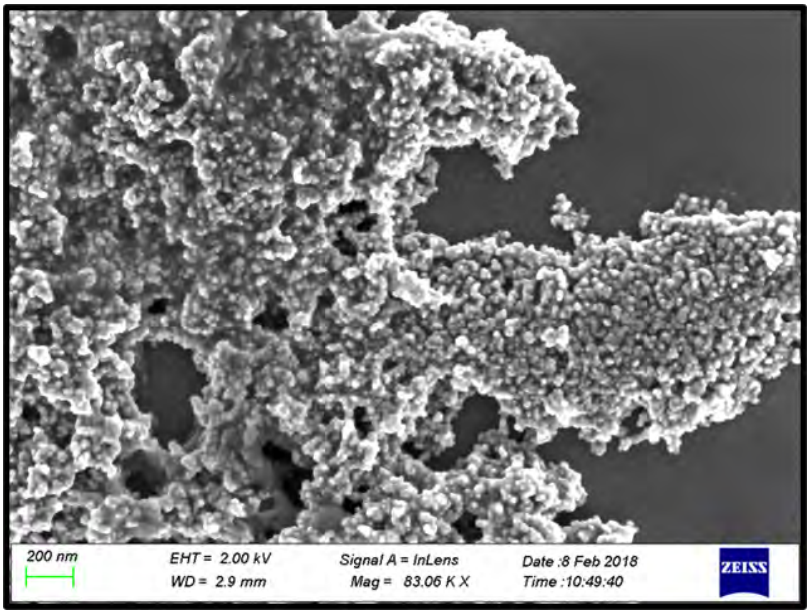

(b)

Figure 4.3: *(a) and (b) show SEM images of iron oxide nanoparticles bought commercially. Images taken by Houari AMARI and Steve YORK, University of Warwick. Quantification of size or shape is not possible due to the level of aggregation seen in the commercial nanoparticles and the use of SEM rather than TEM for imaging.*

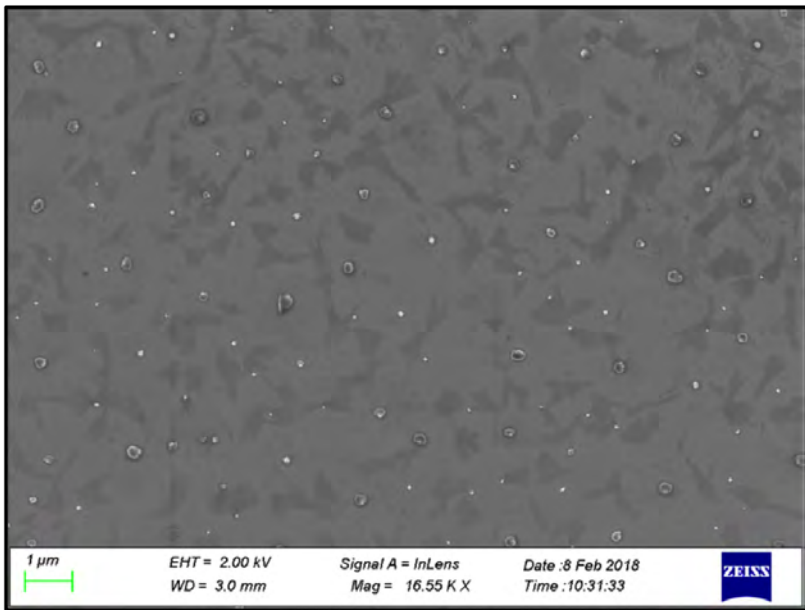

Figure 4.4: *SEM of core@shell nanoparticles (sample CF-Spions-9) synthesised using oleylamine synthesised Fe_3O_4 cores with a silica coating. No quantification of size for these nanoparticles is possible due to SEM being used for nanoparticle morphology and aggregation inspection but not sizing.*

For superparamagnetic nanoparticles it is important that the magnetic properties of individual nanoparticles is understood. The magnetic behaviour of individual magnetic nanoparticles need to be be understood for forces to be measured during their use. This knowledge of magnetic behaviour is not possible when nanoparticles are as aggregated as seen in Figure 4.3. It is however possible to calculate the individual nanoparticle magnetic properties of the synthesised nanoparticles which show little aggregation. This difference in morphology and aggregation of commercial vs designed, synthesised nanoparticles illustrates why it is important that nanoparticles that are to be used within biological research are thoughtfully designed with purpose of use in mind and then fully characterised before use in a biological environment.

4.7 Silica Nanoparticles

First developed in 1992 by the Mobile Oil Corporation mesoporous silica nanoparticles (MSNs) have become popular for biological research and for their potential use as a vehicle for drug delivery. This is due to their chemical stability, high surface area, bio compatibility (comparatively better than nanoparticles made from iron oxides such as iron oxide and titanium) and a high level of surface functionality [25][26][27][24]. MSNs due to their strong Si−O bond are resistant to external responses such as mechanical stress and degradation. If required, it is possible to adjust the size of the pores and porosity of the nanoparticles [25][26][27][24].

For development of protocols for incorporation of nanoparticles into cells through micro injection and endocytosis silica nanoparticles were used. This was due to the ease of synthesis as well as the ability to easily alter the size of nanoparticles as required. Silica nanoparticles also provide the same surface as silica coated iron oxide nanoparticles meaning the same surface functionality could be achieved using the same protocols.

4.7.1 Synthesis of Mesoporous Silica Nanoparticles (MSNs)

Mesoporous silica nanoparticles were chosen for synthesis as they have the potential to offer future functionality in terms of the use of the pores for drug delivery or a location for surface functionality. Mesoporous silica nanoparticles(MSNs) were synthesised by a popular modified Stober's method known as a sol-gel process as described in section 4.2.1 and seen in Figure 4.6. Sol-gel chemistry is a widely used method for the synthesis of many different inorganic materials. Sol-gel involves the hydrolysis and condensation of alkoxide monomers into a colloidal solution (sol). This then acts as a precursor which form an ordered network called a gel of polymer or in this case nanoparticles. The sol-gel method is carried out in the presence of an acid or a base which acts as a catalyst. As with the silica coated iron oxide nanoparticles discussed in a previous chapter the reaction conditions in this case such as the molar ratio of Si:H_2O effect the outcome of the synthesis and therefore the resulting nanoparticles [28]. Varying temperature was used as a way of synthesising MSNs of varying size. Figure 4.5 shows silica nanoparticles samples CF-MSN-70 and sample CF-MSN-40. These were synthesised at 2 different

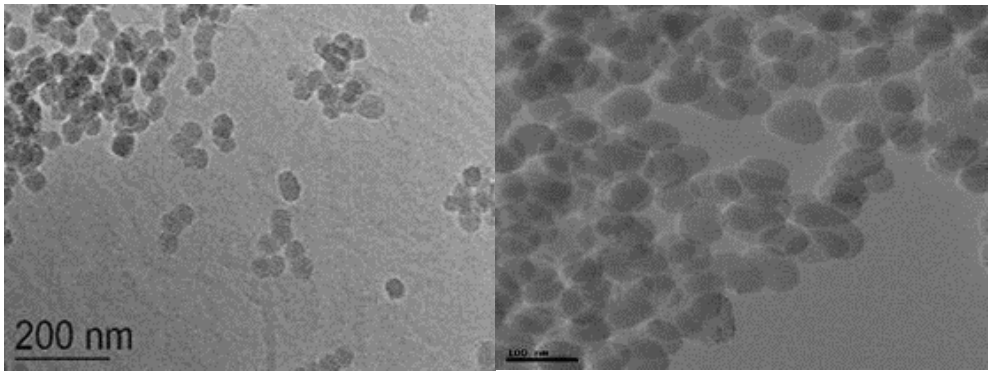

(a) 40nm (b) 70nm

Figure 4.5: *Silica nanoparticle size can be varied by adjustment to temperature used during synthesis. Here can be seen TEM images of Sample CF-MSN-40, 40 nm silica nanoparticles prepared at 50°C and sample CF-MSN-70, 70nm silica nanoparticles prepared at 80°C.*

temperatures. 40 nm (CF-MSN-40) silica nanoparticles were prepared at 50°C and the synthesis of 70nm silica nanoparticles (CF-MSN-70) required the temperature raising to 80°C.

This change of temperature to synthesise silica nanoparticles of varying size is conducive to previous research which shows that smaller nanoparticles can be obtained through controlling (slowing down) the rate of poly condensation reactions. This can be achieved by the manipulation of several reaction parameters [29-34]. These parameters include a particle size increase as ammonia concentration is increased[29–35] and an increase in silica nanoparticle size as temperature increases.

This size difference can be seen by the naked eye as shown in Figure 4.11. The larger the nanoparticles the more white the solution becomes. Synthesis of the nanoparticles included the addition of NH_2 groups and fluorescent dye (Rhodamine B) to the surface of the nanoparticles resulting in nanoparticles matching the schematic representation seen in Figure 4.7. The synthesised nanoparticles selected for future cell work were then characterised using TEM and DLS. TEM image Figure 4.10 shows silica nanoparticles of size 42.16 +/- 3.88 nm. DLS results are given in Table 4.4. The nanoparticles show the uniformity of shape and size which were desired for these nanoparticles and there use within a cellular environment.

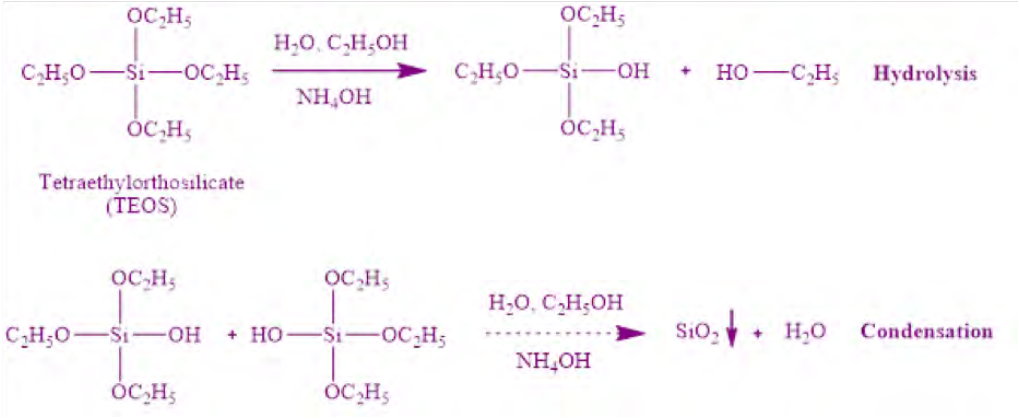

Figure 4.6: *Preparation of silica nanoparticles (SiO_2) by hydrolysis and condensation of an alkoxysilane using a basic catalyst.*

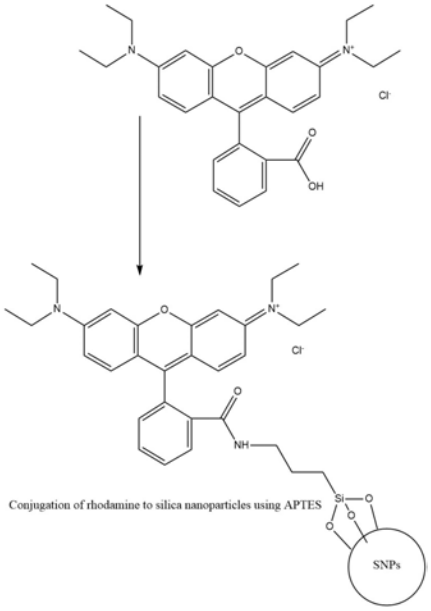

Figure 4.7: *Attachment of rhodamine to silica nanoparticles, by covalent bonding with APTES.*

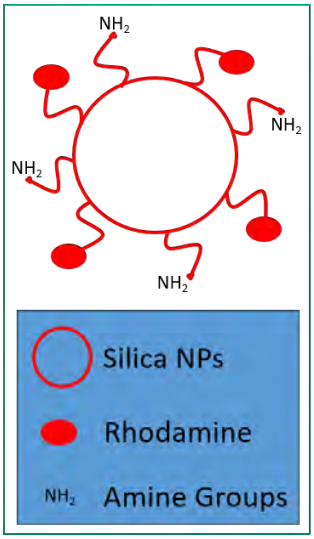

Figure 4.8: *Schematic representation of fluorescent dye rhodamine attached to silica nanoparticles via APTES.*

Figure 4.9: *Synthesised silica nanoparticles (SiO_2) with diameter sizes varying from 40nm to 100nm. (A)45.94nm +/- 2.61, (B)62.3nm +/- 6.27,(c)71.98nm +/- 3.42, (D)86.27nm +/-4.56, (E)97.41nm +/- 6.2, (F)105.04nm +/- 8.63. All samples synthesised by method described previously.(Samples CF-msn-40, through to CF-msn-100). All sample sizes obtained using TEM. The image shows that as the silica nanoparticles get larger a change in colour is observed.*

Table 4.4: *DLS results for silica nanoparticles, sample CF-msn-40. Results show are average size, PDI and zeta potential for mesoporous silica nanoparticles, sample CF-MSN-40 over 5 runs.*

	PDI	**Size (nm)**	**Zeta Potential (mV)**
MSNs	0.33+/- 0.04	248.80 +/-7.77	33.9 +/- 4.1

Figure 4.12 illustrates the post synthesis functionalisation steps for

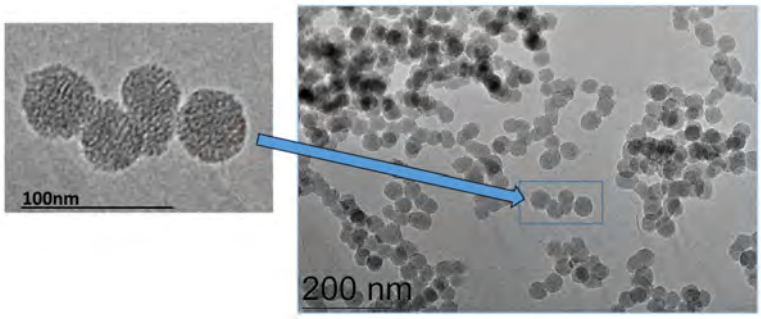

Figure 4.10: *Synthesised mesoporous silica nanoparticles (sample CF-msn-40). Size by TEM 42.16 +/- 3.88 nm. Smaller image shows silica nanoparticles up close.*

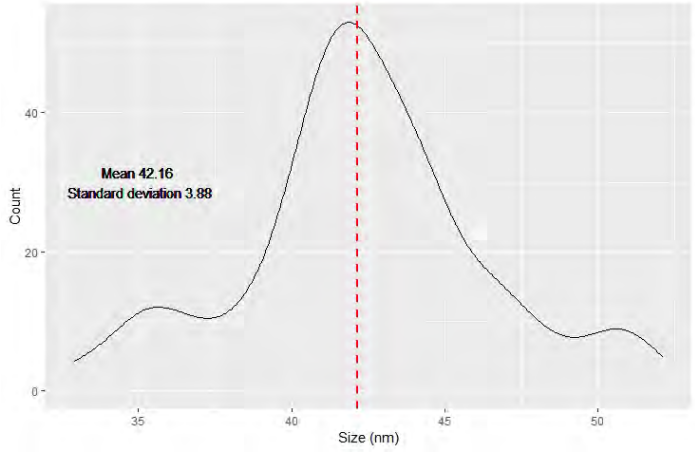

Figure 4.11: *Size distribution for synthesised silica nanoparticles (SiO_2) sample CF-MSN-40.*

synthesised silica nanoparticles. These steps begin with the addition of NH_2 groups to allow for future binding. This is followed by addition of rhodamine dye to allow for visualisation during imaging. A post graft of amine groups is necessary for nanoparticles to be incorporated into cells via endocytosis as described in section 4.7 as opposed to micro injection, see section 4.6, and finally the addition of PEG helps to ensure nanoparticles do not become aggregated.

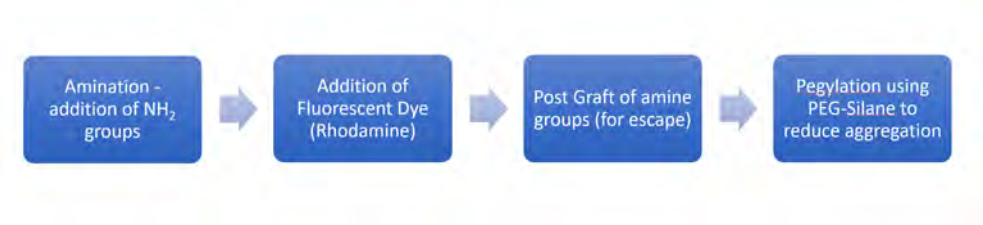

Figure 4.12: *Functionalisation of silica nanoparticles for development of cell biology research techniques.*

4.8 Fluorescence

Visualisation of nanoparticles during *In vitro* or *In vivo* protocols most be conducive to accurate measurements and must be considered during nanoparticle design and synthesis.

The addition of fluorescence compounds to the surface of nanoparticles allows nanoparticle to be visualised using light microscopy. Here we use rhodamine b ($C_{28}H_{31}ClN_2O_3$). Rhodamine B is a fluorescent dye which has an excitation maximum at a wavelength of 556 nm and a maximal emission wavelength of 580 nm. The addition of fluorescent dye to nanoparticles needs to result in even fluorescence intensity across all nanoparticles. Fluorescence also needs to maintain intensity over time to allow for visualisation of nanoparticles over the life cycle of cells.

All fluorescence work was carried out using sample CF-1-FL. This sample were silica coated iron oxide Nanoparticles (sample CF-1-FL). This sample had an average TEM diameter of 76.95 $\pm$ 10.93 nm. From this sample 13 microscope slides were prepared and observed and 25 nanoparticles recorded for each slide. This was then repeated using the same slides 3 hours later.

Table 4.5: *Image j measurements for Corrected Total Fluorescence (CTF) of nanoparticles. Each sample (taken from sample CF-1-FL) is the average results for 25 measured nanoparticles.*

Sample	**Area**	**Mean**	**InTDen**	**CTF**
1	387	224	121484	73927
2	392	213	126160	77989
3	420	207	128059	76447
4	436	199	99776	99217
5	395	174	118077	69537
6	376	212	124812	78607
7	389	192	129860	82057
8	377	226	107583	61255
9	376	219	104170	57965
10	407	229	124875	74860
11	389	224	109395	61592
12	411	221	134895	84389
13	266	233	80580	47892
Std Dev	40		15167	13251

Using the formula:

Corrected Total Fluorescence (CTF) = Integrated Density (InTDen) - (Area of selected nanoparticle * Mean fluorescence of background readings)

and a mean fluorescent background measured at 122 it can be seen in Table 4.5 and Figures 4.13a and 4.14a that the nanoparticles exhibit a good uniformity in fluorescence intensity. The standard deviation for the nanoparticles is small suggesting that the addition of rhodamine during synthesis results in nanoparticles with fluorescence of similar intensity.

Photo bleaching is a process where a fluorophore, in this case rhodamine begins to lose the ability to emit light due to exposure to excitation. The rate at which this destructive process occurs id effected by many factors including the wavelength of a lase, the length of time exposure occurs for, chemical environment and the intensity of light [36]. Imaging of nanoparticles which use rhodamine for visualisation need to withstand photo bleaching for significant periods of time to allow for imaging over time for example to allow for the cell cycle to occur.

Figures 4.13b 4.14b and Table 4.6 show that nanoparticles remain fluorescent and visible after 3 hours of light microscopy with a laser turned on. It is however, clear that there is a loss of fluorescence with CTF being lower for the nanoparticles after 3 hours due to photo bleaching. The

Table 4.6: *Image j measurements for Corrected Total Fluorescence (CTF) of nanoparticles after 3 hours on microscope. Each sample (taken from sample CF-1-FL) is the average results for 25 measured nanoparticles.*

Sample	**Area**	**Mean**	**InTDen**	**CTF**
1	342	235	120365	40088
2	398	212	121879	37311
3	308	238	125167	52003
4	368	199	112367	39236
5	389	201	99873	21654
6	321	179	114098	66671
7	278	151	120693	78755
8	325	203	127625	61615
9	356	173	118092	56668
10	318	207	116987	51103
11	298	206	127342	66064
12	312	189	123815	64847
13	376	203	119560	43265
Std Dev	37		7401	15083

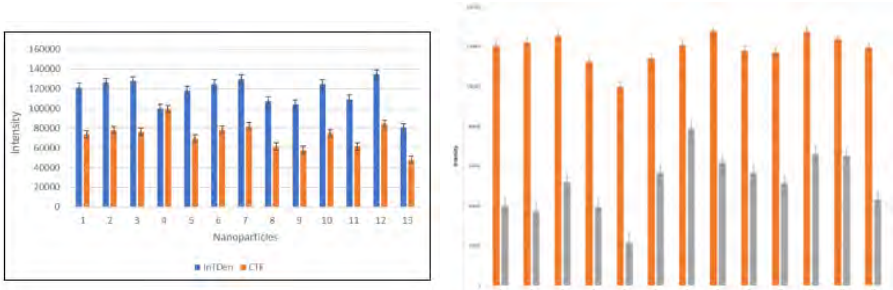

(a) (b)

Figure 4.13: *a) Plot of Table 4.5 - Fluorescence intensity and Corrected Total Fluorescence (CTF) for nanoparticles. b)Plot of Table 4.6- Fluorescence intensity and Corrected Total Fluorescence (CTF) for nanoparticles after 3 hours laser exposure. This was achieved by leaving microscope slide on a microscope for 3 hours with the laser on.*

average initial CTF is 52252 and after 3 hours this drops to 48883. This is a loss of 6.5%.

This demonstrates that the nanoparticles are fluorescent and clearly visible during imaging with TIRF microscopy. They are resistant to photo bleaching remaining highly fluorescent and visible after 3 hours of laser exposure.

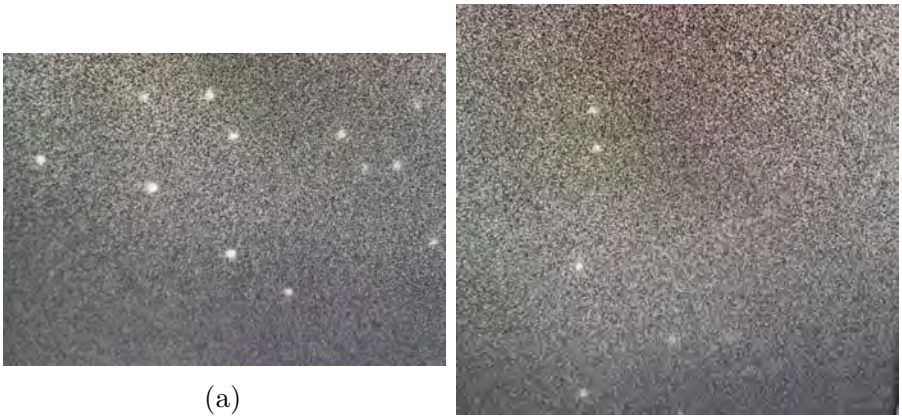

(a) (b)

Figure 4.14: *C@S silica coated iron oxide nanoparticles (sample CF-1-FL) imaged using TIRF visualised using fluorescence. Excitation 546 nm and emission 568 nm. Nanoparticles can be seen within the image as "bright spots". Image (a) was taken immediately following the preparation of the microscope slide with no time delay. Image (b) shows the same nanoparticle sample after 3 hours of exposure to a laser. The nanoparticles are still visible but ther is a decrease in fluorescent intensity. Previously the sample had been stored in dark conditions to avoid deterioration of the attached fluorescent dye.*

4.9 Human Retinal Pigmented Epithelial Cells - MC148 Cell Line

Norma Human retinal pigmented epithelial (RPE1) cells were used to generate the MC148 cell line which was used for *in vivo* protocols involving synthesised nanoparticles. RPE-1 cells are popular as a model for the study of mitosis due to them representing a non-transformed alternative to cancer cell lines, such as HeLa cervical adenocarcinoma cells. RPE-1: immortalized adherent epithelial cells have a diploid karyotype (46, XX, der(X)) in 90% of cells, maintain normal checkpoints on cell cycle progression and are ciliated i.e have small hair-like projections called cilia [6].

The MC148 cell line when treated with nocodazole (NOC) appeared to undergo mitosis very quickly, resulting in very few mitotic cells by time imaging was performed. NOC is an antimitotic agent which inhibits the assembly of microtubules by binding to β-tubulin and stopping the formation of interchain disulphide linkages. This leads to inhibition of microtubule dynamics as well as disrupting Golgi complex fragmentation and mitotic spindle function. This means that cells progress through

interphase but mitosis is halted in the G_2/M phase. Prolonged use of antimitotic agents can result in apoptosis or a return to interphase without separation of sister chromatids. This would result in polyploidy or other genetic errors. Nocodazole inhibition of mitosis is easily reversed with the cell cycle proceeding as expected [15]. The use of NOC to hold up mitosis resulted in a significant increase in mitotic cells seen using light microscopy. The subsequent release of cells from NOC by washing following addition of TMR and the necessary incubation time of 30 minutes however resulted in an insignificant increase in mitotic cells during imaging. This suggests that once NOC was washed out mitosis occurred in the cells within the 30 minutes between washing and imaging or the return of cells to interphase.

4.10 Micro Injection

Micro Injection involves the use of a glass micropipette with a tip of <1 micron in diameter to inject materials into cells. Figure 4.15 is a schematic representation of micro injection of nanoparticles into a cell. Figure 4.17 shows magnetic silica coated Fe_3O_4 nanoparticles which have been injected into a single mitotic RPE1 cell. Injection is accomplished by the use of microscopy to guide the micropipette to the cell. In Figure 4.17 nanoparticles can be seen in green in the cytosol of the cell as a result of successful micro injection. The red area is the nucleus of the cell.

The process of micro injection has proved successful with magnetic beads being injected, and clearly visible by microscopy, into cells which are mitotic and non-mitotic, as seen in Figure 4.16. The nanoparticles can be seen as bright "spots" of fluorescence in multiple cells. Cells which were not injected do not display the same signal and are seen to be without any fluorescence. Injection of mitotic cells is more difficult than injection of cells in interphase due to the shape of the cell. Mitotic cells become more spherical and this means physically injecting the cell is more difficult than injection of flat non mitotic cells. This can result in structural damage to the cell and cause cells to not undergo mitosis correctly. Injection under constant flow helps to minimise clogging of the micropipette this helps injection into the cytoplasm of a cell, attempts to inject into the nucleus will result in some fluid being injected into the cytoplasm as the micropipette passes through the cytoplasm as it enters and leaves the nucleus. This means all images obtained showed

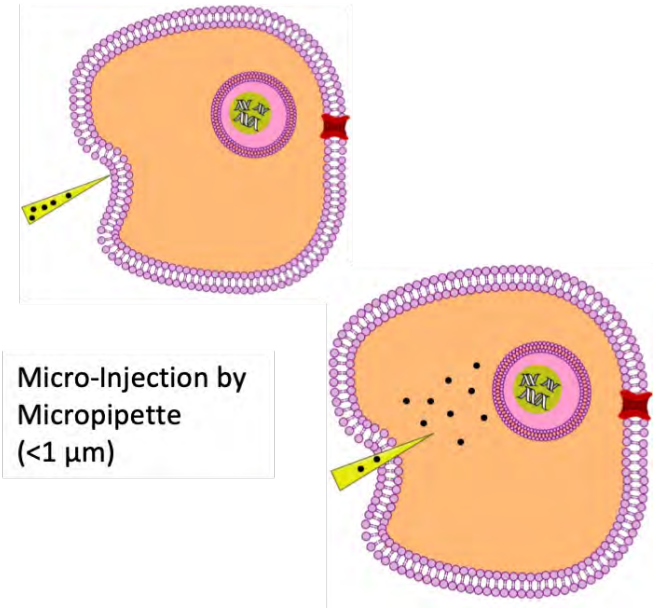

Figure 4.15: *Schematic representation of nanoparticle incorporation into cells by micro injection.*

significant number of nanoparticles in the cytoplasm of both mitotic and non-mitotic cells. Figure 4.17 shows a cell with the nucleus in red and the synthesised fluorescent green magnetic nanoparticles in green. The nanoparticles were successfully injected into cells and can be seen located in the cytoplasm with a few appearing to be in the nucleus however given the shape of the cell it is not possible from this image to state that the nanoparticles are definitely within the nucleus. The presence of nanoparticles in the cytoplasm suggest that micro injection often misses the nucleus and that entry to the nucleus can be blocked by the presence of the nuclear envelope.

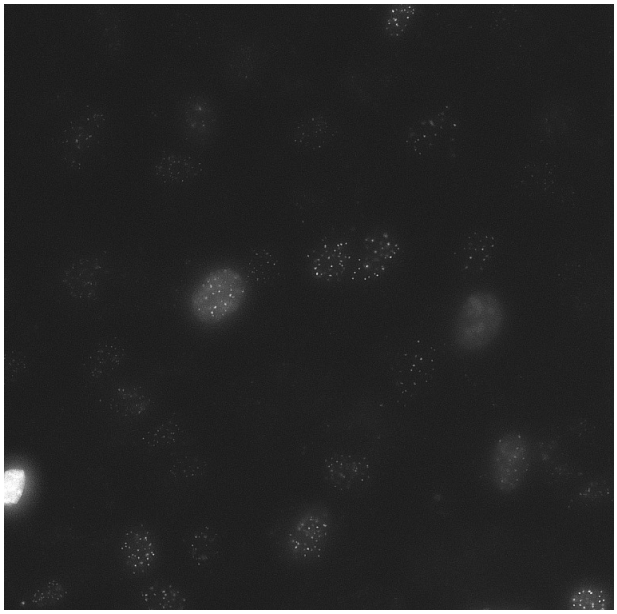

Figure 4.16: *SiNPs micro injected into RPE1 cells (Sample CF-msn-8). Cells which have successfully undergone micro injection can be seen to have bright areas of fluorescence.*

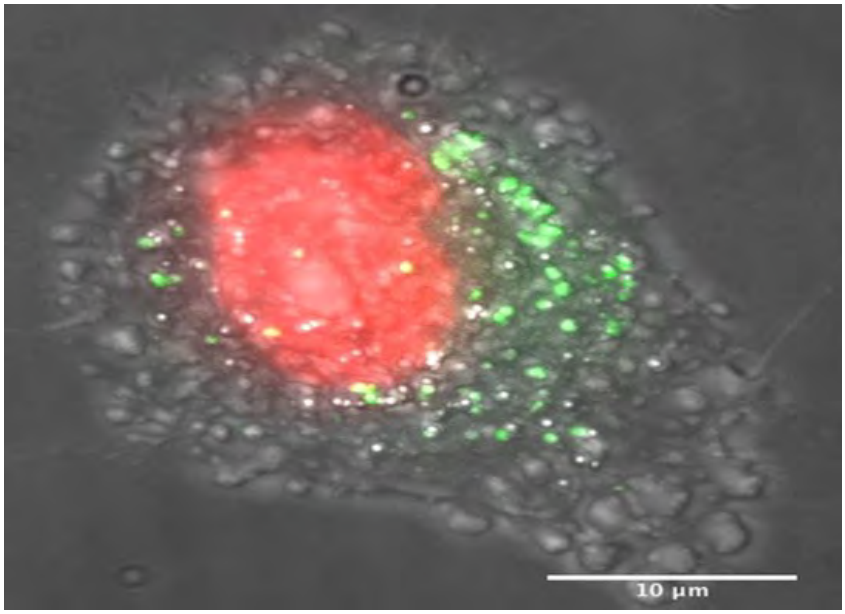

Figure 4.17: *SiNPs micro injected into RPE1 cells (Sample CF-msn-8). Nanoparticles can be seen in green and DNA in red.*

In conclusion, micro injection is an established technique. Micro injection allows for delivery of nanoparticles directly into cells in a controlled manner however it is a time consuming process and given the need to penetrate the cell with a micropipette, this method of nanoparticle into cell incorporation risks mechanical damage to the cell. Cells when under-

going mitosis undergo changes in morphology resulting in a more spherical shape than cells which are not mitotic. This means that mitotic cells are more difficult to micro inject and more likely to experience mechanical damage from the process.

4.11 Cell Incorporation via Endocytosis (Endo/Lysosome Pathway)

The incorporation of nanoparticles into cells can also be achieved by a cells mechanism called endocytosis. Endocytosis involves two mechanisms known as phagocytosis and pinocytosis. The incorporation of nanoparticles via endocytosis is appealing and should be considered due to this method using the natural processes of cells. Endocytosis is a well documented cell process and unlike micro-injection there is no risk of mechanical damage. This route of incorporation seen in Figure 4.18 should, if the pH buffering described below is performed successfully result in nanoparticles within a cell with no damage to the cell. This in an *in vivo* research situation is very desirable. Particles which are larger than 500nm are preferred by phagocytosis whilst smaller nanoparticles are usually incorporated by pinocytosis.

The interactions that are observed between nanoparticles (NPs) and cell membranes of cells is of great importance when designing nanoparticles which will be introduced into cells whether for nanomedicines or for cell biology research. There has been previous research into NP properties and their effect on endocytosis with research finding that NP shape, size and surface chemistry all significantly influence NP incorporation [13-16]. This research is due to the potential biomedical applications of nanoparticles such as vaccine design, cancer diagnostics and cancer treatments [1-7].

If these treatments are to be successful then nanoparticles must be able to be efficiently incorporated into cells via the cells own mechanisms [4][8]. Incorporation of nanoparticles via endocytosis is associated with nanoparticles having a greater tendency to aggregate due the physiological environment, this is often the result of the surface chemistry of the nanoparticles and should be considered when designing and synthesising nanoparticles for cellular use.

Shape of nanoparticles can also affect the efficiency by which nan-

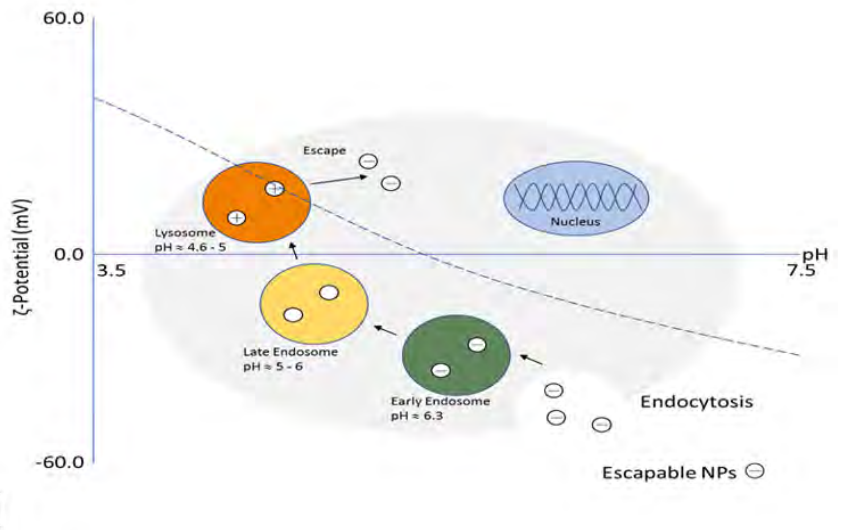

Figure 4.18: *Nanoparticle incorporation via the endo/lysosome pathway. This route of incorporation uses a cells natural process of endocytosis. Nanoparticles incorporated via this route should result in no mechanical or other damage to a cell.*

oparticles are incorporated into cells. Previous research suggests that spherical nanoparticles are reliable for use as drug carriers and do undergo efficient cellular uptake however some research has suggested that shapes such as cylinders may potentially have better circulation and retention times. Whether non-spherical nanoparticles also exhibit greater cellular uptake efficiency is not established however,at least one study shows that the uptake of rod-shaped AU NPs is lower than that of spherical AU NPs in HeLa cells [17][37]. This when combined allows us to justify the choice of spherical nanoparticles for this work given that it is established that they have high efficiency for cellular uptake via endocytosis. For cell biology research retention and circulation times are not as high a consideration when designing nanoparticles.

Nanoparticles can be incorporated by endocytosis. This incorporation involves acidic endosomes/lysosomes, which play a key role in the cellular degradation of foreign materials within cells [6]. The incorporation of particles this way results in the particles being unable to escape the endosome/lysosomes instead of becoming trapped within them. Becoming trapped is not conducive to the use of nanomaterials either for nanomedicines or cell biology research as it is essential that particles can reach the nucleus and/or the cytoplasm [7]. Previously a pH-buffering ("proton

sponge") methodology has been described in research [9, 20]. This method does not involve interactions between the endosome/lysosome membrane nor particles which are penetrative and destructive as previous methods did. [9b, 10] The pH-buffering method uses agents which have high buffering capabilities containing basic amine functional groups such as quinoline or tertiary amines [3] [10]. These are able to generate differences in osmotic pressure by soaking up protons between the cytosol and the endosomes. The difference in osmotic pressure leads to an increase in water and ions and results in the rupturing of the endosomal membrane [10]. The chemistry associated with this "protonsponge effect" is however often cytotoxic and does not consider the charge of the particles. It is possible to modify the surface of nanoparticles. Here a post graft of primary amines is used which enables a change in surface charge as pH changes. This allows nanoparticles to be released into the cytoplasm without destruction of endosome/lysosomes.

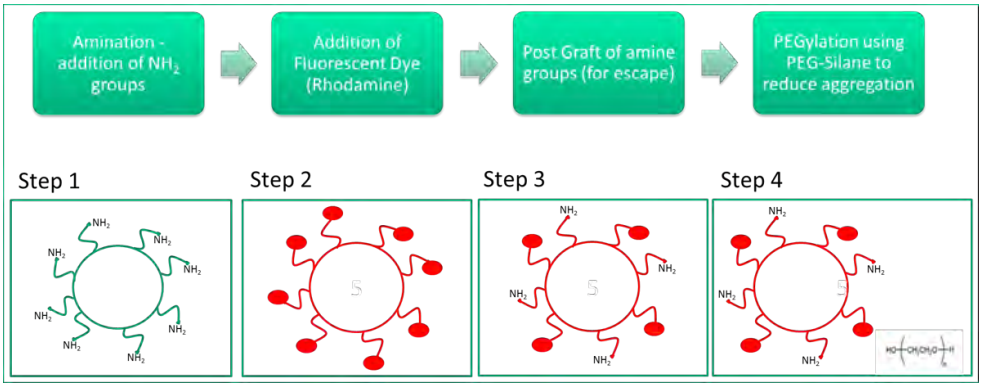

Figure 4.19: *Schematic representation of nanoparticle synthesis for incorporation into cells using the endo/lysosome pathway.*

The endo/Lysosomal pathway (Figure 4.18) provides a route for incorporation of NPs into cells [2]. NPs are functionalised to exhibit an initial negative surface charge at pH 7.4. Following endocytosis these particles become trapped in acidic early/late endosomes. As the pH becomes more acidic the NPs surface charge becomes increasingly positive. On fusion of endosomes into lysosomes (pH 4.6-5) the NPs are highly cationic and subsequently escape can occur [2].

Nanoparticles that are suitable for escape into cells via endocytosis require further surface modification. A secondary graft of amine groups is required to allow for the pH to change as the nanoparticles progress through the endo/lysosome pathways described in Figure 4.18. It is also

necessary as previously stated to be aware of nanoparticles tendency to aggregate when exposed to a physiological environment. This is achieved using a PEGylation step. Figure 4.19 shows the synthesis steps for silica nanoparticles suitable for escape by endocytosis.

Nanoparticle response to pH after post graft of amine groups can be checked by zeta potential. Buffers of varying pH were prepared and zeta potential of nanoparticles established for each one. Table 4.7 shows the buffers synthesised with the acquired pH.

Table 4.7: *Buffer preparation for analysis of nanoparticle behaviour at various pH by zeta potential.*

	Acquired pH	**Name**
Buffer 1	8.49	Bicarbonate Buffer (salt free)
Buffer 2	7.2	Phosphate Buffer (salt free)
Buffer 3	5.4	2-(N-morpholino) ethanesulfonic acid (MES) Buffer

Zeta potential measurement of silica nanoparticles suspended in buffers of varying pH allow for the behaviour of nanoparticles through the endo/lysosome pathway to be predicted. Figure 4.20 shows how zeta potential (charge) decreases as pH increases. The functionalisation with

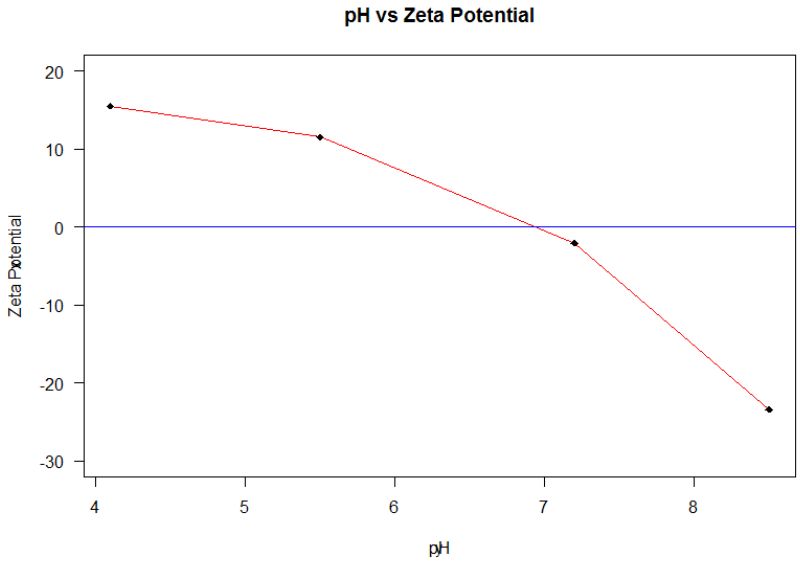

Figure 4.20: *Zeta potential of silica nanoparticles over a range of pH for sample CF-msn-40. Zeta potential at eaach pH is an average over 5 runs.*

a post graft of amine groups means that at pH 7.4 the zeta potential has changed from positive to negative. This change is zeta potential shows that the synthesised silica nanoparticles are suitable for incorporation

into cells by endocytosis. Following incorporation of nanoparticles using endocytosis imaging as seen in Figure 4.21 for 3 separate cells with nanoparticles is achieved.

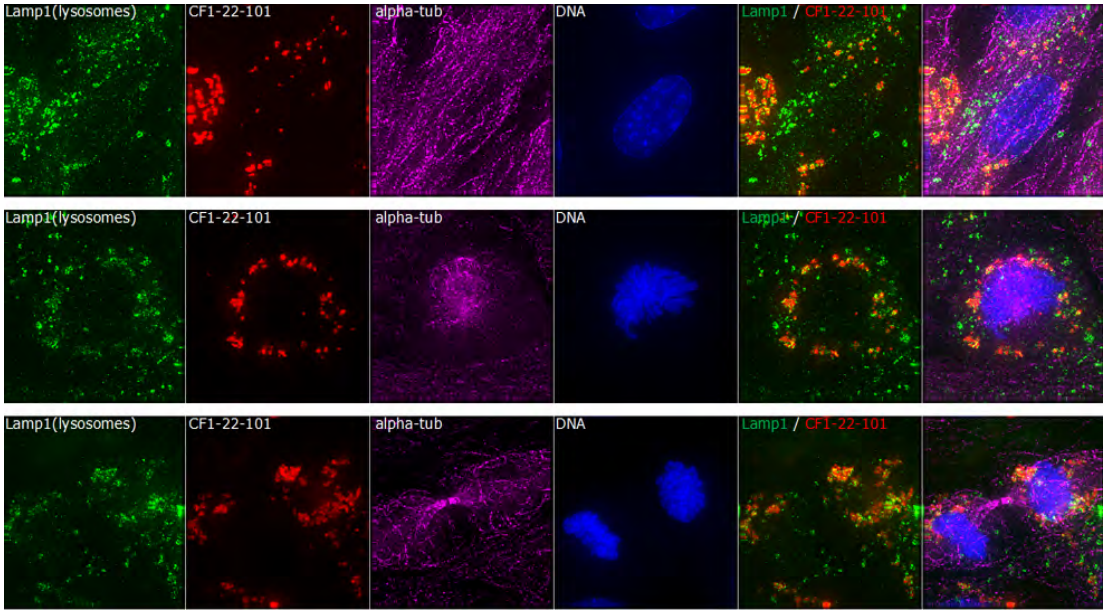

Figure 4.21: *Microscopy images for escape of NPs via the endo/lysosomal pathway. Lysosome (green), NPs (red), Tubulin (purple) and DNA (Blue).*

The lysosomes are seen in green and the nanoparticles are in red. The images also show the cells tubulin and DNA in purple and blue respectively. The images suggest that some nanoparticles have been released from the lysosomes however there still appears to be a correlation between lysosome position and nanoparticle location. This points to potentially a lower than desired efficiency of release of nanoparticles. Further development of this process would be required.

4.12 Micro Injection Vs Endocytosis

Synthesised nanoparticles can be incorporated in cells by both micro injection and endocytosis. Each method has both pros and cons and these must be considered when deciding on how nanoparticles will enter cells. Micro injection requires specialised equipment however if such equipment is available then the method is reasonably easy to use with no additional preparation of nanoparticles being required.

This delivery of NPs directly to the inside of a cells means that the NPs are not affected by any time in the culture medium. This therefore does

prevent protein decoration occurring before the uptake of NPs into the cell when using endocytosis as an incorporation method. Any interaction between NPs and cell occurs purely within a cell and is not affected by proteins found outside of the cell making this a more controlled method of incorporation than endocytosis uptake [38].

Incorporation of nanoparticles via endocytosis does require additional steps during synthesis to ensure that nanoparticles are released into a cell. This process is easily repeatable and simple to achieve although careful characterisation as always is required to ensure that the nanoparticles will behave as expected as they progress through the pathway [20].

4.13 DNA Tethering

Traditionally a tethered particle assay provides a biophysical method for studying various polymers for example DNA and their interaction with other entities such as proteins. Here we have used this principle to attach magnetic beads to a DNA strand via a protein. This assay would allow for measurement of various biophysical properties and the effect of applying a magnetic field to nanoparticles. DNA tethering allows for nanoparticles to move due to Brownian motion, but limits other movement due to the tethering of the nanoparticles to DNA strands of a known length.

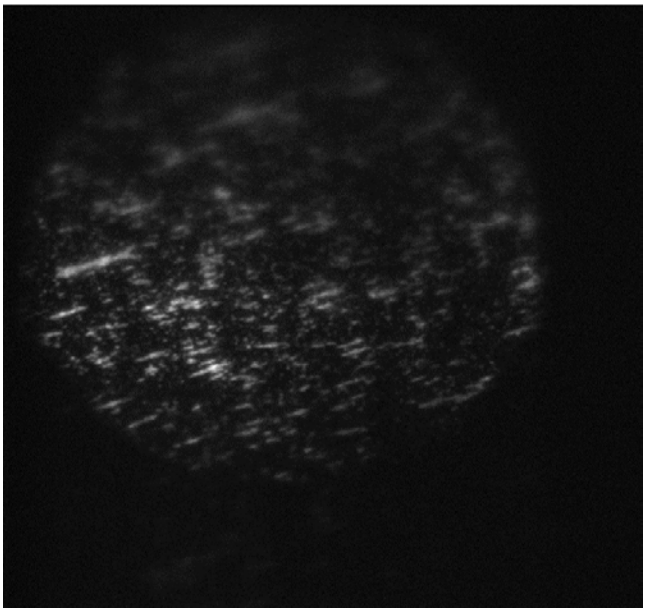

Figure 4.22: *Silica coated iron oxide nanoparticles (sample CF-22-102) were tethered to a single strand of DNA of known length (10kb). DNA is attached to a microscope slide, Nanoparticles are then attached, via protein coupling with neutravadin, to the DNA strand. Here they are imaged using the Warwick open source microscope (WOSM)(x40,473nm) On application of a magnetic force the magnetic behaviour of the nanoparticles can be evaluated from the movement observed.*

4.13.1 Protein Coupling of Amine Modified Fluorescent Magnetic Nanoparticles

Successful attachment of silica coated iron oxide nanoparticles magnetic nanoparticles to a single strand of DNA is required before tethering of the DNA to a microscope slide and evaluation of force from a known magnetic force. Protein coupling of Neutravidin to the surface groups of the nanoparticles was first tested and achieved using the methodology demonstrated graphically in Figure 4.23. This protein coupling of Neutravidin then allowed for the attachment of nanoparticles to DNA.

Images (a) and (b) in Figure 4.24 use BSA as a way of anchoring the potentially protein coupled nanoparticles to the microscope slide. Images (c) and (d) (Figure 4.24) show the PLL-PEG-Biotin/Neutravidin attached to nanoparticles and just PLL-PEG-Biotin both without BSA. Although there is a significant difference between signal in (a) and (b) as expected, (b) still shows an unexpected level of fluorescent signal which should not be present due to the absence of nanoparticles. Images (c) and (d) however both show far less fluorescence, image (c) does show what are potentially

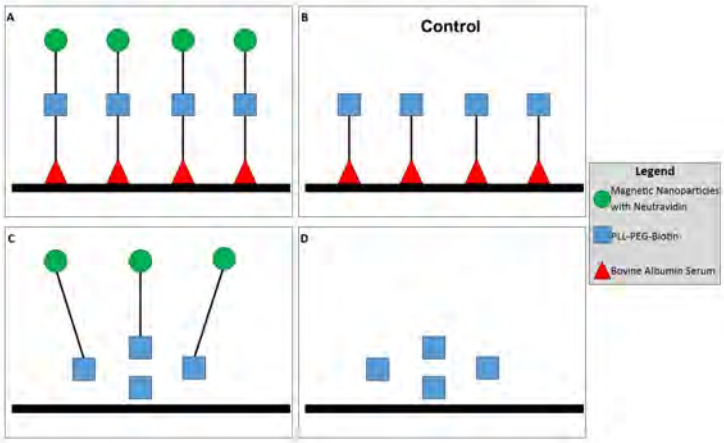

Figure 4.23: *Schematic of expected results for protein coupling confirmation for in vitro experiments. To confirm coupling of amine modified nanoparticles to the protein Neutravidin 4 slides were prepared. A) Nanoparticles with Neutravidin attached bound to PLL-PEG-Biotin which is attached to Bovine Albumin Serum on the microscope slide. This outcome demonstrates that the nanoparticles could be bound to DNA. As controls 3 slides were prepared - B) PLL-PEG-Biotin was bound to Bovine Albumin Serum without nanoparticles. C) Neutravidin bound nanoparticles are bound to PLL-Peg Biotin. D) Lastly PLL-PEG-Biotin was imaged on it own.*

nanoparticles. There are, however, far fewer potential nanoparticle signals than in image (a). This suggests that the lack of signal observed, given that the same concentration and quantity of nanoparticles were inserted in to the flow cell is the result of of auto fluorescence of the BSA and not from the nanoparticles. BSA is a commonly used and useful protein, however it is associated with excessive auto fluorescence [38]. It has been found to show emission peaks at 335 nm and at approximately 420-460 nm [37[39].

The fluorescence seen from the BSA in Figure 4.24(b) does not correlate to the known emission peaks of BSA. This however can be explained by solvatochromism. This is where solvent polarity can cause a colour change in a chemical substance. PBS is a water based buffer and as such a polar solvent [36] which could explain why the BCA can be seen using a 473nm laser. Given that water, and therefore PBS, is a polar solvent, future attempts to evaluate protein coupling should include evaluation of different buffers, preferably non-polar ones. Cyclohexane is a non-polar

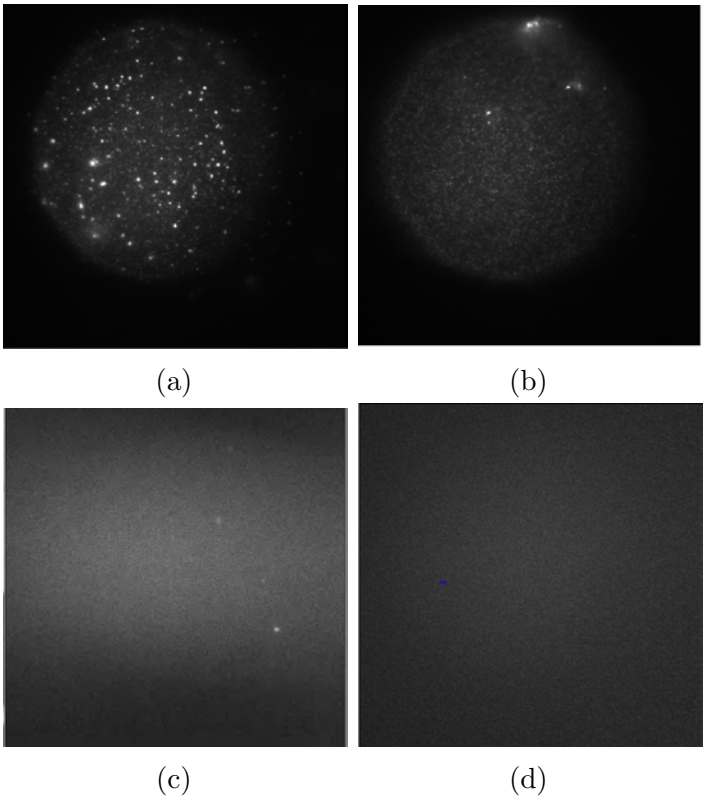

Figure 4.24: *Optical, fluorescent imaging of commercial magnetic beads. Image(a) shows coupled Nanoparticles/Neutravidin anchored to microscope slide by PLL-PEG-Biotin and BSA. (b) shows neutravidin anchored to microscope slide by BSA. (c) Nanoparticles/Neutravidin with PLL-PEG-Biotin in the absence of BSA. (d) PLL-PEG-Biotin with no nanoparticles. Images taken using TIRF microscopy,excitation at 473nm (sample CF1-17-96).*

solvent that could be considered as many proteins remain stable in its presence [40].

Binding was observed as the lack of free movement of nanoparticles in the flow cell and positioning of nanoparticles at the surface of the microscope cover slip, rather than bound to the PLL-PEG-Biotin and BSA at the surface of the microscope slide. The four binding sites on Biotin are associated with causing nanoparticle cross-linking causing aggregation of nanoparticles so when protein coupling occurred the nanoparticles could be seen clearly bound to the biotin via the Neutravidin upon imaging [8].

4.13.2 *In vitro* DNA Tethering of Silica Coated Iron Oxide nanoparticles (sample CF-22-102)

Nanoparticles were attached to DNA as previously described. Due to auto fluorescence of bovine serum albumin (BSA) being observed as previously described during the imaging of the tethered nanoparticles, BSA was replaced with casein. Casein does not show auto fluorescence thus allowing for clearer imaging of the nanoparticles.

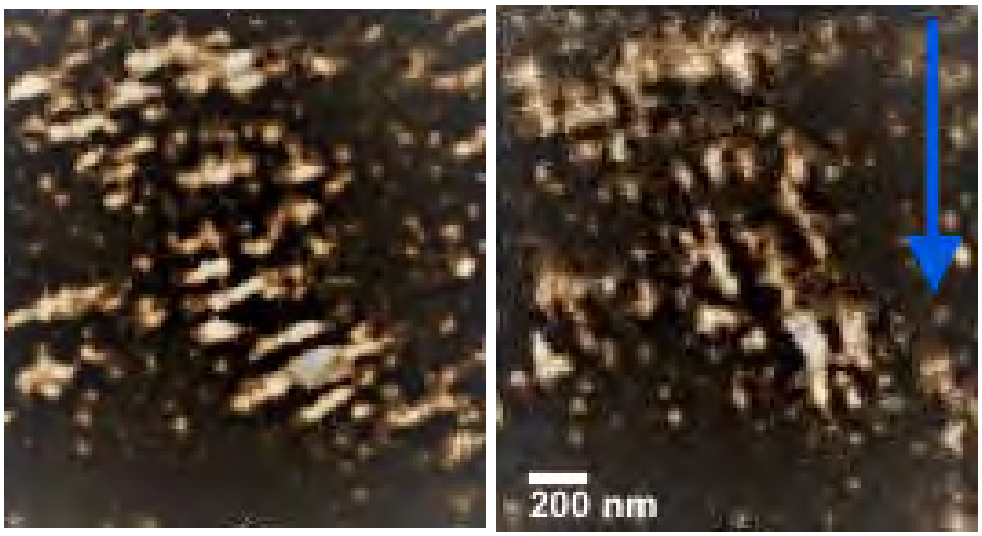

(a) (b)

Figure 4.25: *TIRF imaging of silica coated iron oxide nanoparticles (sample CF-22-102). Excitation wavelength 473nm.(a) DNA tethered magnetic NPs with no magnetic field applied. (b) DNA tethered magnetic NPs with a magnetic field applied in the direction of the arrow. The magnetic nanoparticles can be seen to "change direction" in the same direction as the arrow towards the magnetic field. The NPs do however remain in the same location as when no magnetic field is applied. This shows that the NPs are tethered to the DNA, with their movement restricted by the tethering however they do respond to a magnetic field when applied.*

Figures 4.25a and 4.25b show still images obtained from a video recording of magnetic nanoparticles tethered to DNA. The video and in turn the images here show commercial beads with no magnetic field applied (a) and commercial beads with a magnetic field applied (b) respectively. With no magnetic field applied, the beads position remains relatively constant with any variation being the result of Brownian motion as expected. Upon application of a magnetic field, the nanoparticles change direction of orientation but not position. Figure 4.25a shows magnetic nanoparticles without a magnetic field applied, Figure 4.25b shows the

same magnetic nanoparticles when an external magnetic field is applied close to the microscope slide (at the bottom of the image). A change of direction of nanoparticles is observed as nanoparticles are attracted to the magnetic field. The movement is however limited, nanoparticles are not able to be move to the magnetic field, this is due to the nanoparticles being tethered to DNA strands and this constraining movement to the length of the DNA strands.

This demonstrates that the nanoparticles are responsive to a magnetic field and are also tethered to the DNA as the movement of the beads are limited due to the tethering.

4.14 Conclusions

The multifunctional superparamagnetic silica coated iron oxide nanoparticles described and synthesised here along with the silica nanoparticles synthesised for investigating potential biological research techniques and uses are suitable for use. There is evidence that the nanoparticles are non toxic, can be incorporated within cells without damage to the cells and can be imaged successfully even with the passing of time. The flexibility in surface functionalisation of the silica coated SPIONS means that the nanoparticles can be adapted depending on research requirements with relative ease. Addition of fluorescent dyes allows for effective visualisation of the nanoparticles over time with different dyes being able to be used if desired. Both micro-injection and incorporation through endocytosis provide a path to ensuring nanoparticles are in a cell however both have their limitations and difficulties whether that be the risk of mechanical damage to the cells from micro-injection or the need for extra functionalisation and characterisation of nanoparticles which are to be incorporated by endocytosis. Tethering of nanoparticles to DNA strands is possible and would with development provide a method for further *in vitro* studies for calibration and validation on the effect of applying a magnetic force to the nanoparticles when they are in a cell.

4.15 Further Work

Development of DNA tethering protocols to allow for number of particles tethered to be obtained. This could possibly be achieved by the technique

of DNA origami where artificial DNA is designed in pre determined shapes. These shapes would allow for the number of binding sites and location of the binding sites to be controlled thus allowing for a defined number of nanoparticles to be tethered. This in turn would allow for the calibration of magnetic forces involved in each tether.

Incorporation of magnetic nanoparticles into cells and binding of nanoparticles to a specific site and application of a magnetic force could allow for examination of magnetic forces involved in cellular processes such as mitosis.

4.16 References - Chapter 4

1.A. Fornara, P. Johansson, K. Petersson, S. Gustafsson, J. Qin, E. Olsson, D. Ilver, A. Krozer, M. Muhammed and C. Johansson, Nano Letters, 2008, 8, 3423-3428.

2.N. Xia, T. Hunt, B. Mayers, E. Alsberg, G. Whitesides, R. Westervelt and D. Ingber, Biomedical Microdevices, 2006, 8, 299-308.

3.M. Welch, C. Hawker and K. Wooley, Journal of Nuclear Medicine, 2009, 50, 1743-1746

4.T. Jovin, Nature Biotechnology, 2003, 21, 32-33.

5.Y. Chang, F. Pinaud, J. Antelman and S. Weiss, Journal of Biophotonics, 2008, 1, 287-298.

6.W. Chan, D. Maxwell, X. Gao, R. Bailey, M. Han and S. Nie, Current Opinion in Biotechnology, 2002, 13, 40-46.

7.X. Michalet, F. Pinaud, L. Bentolila, J. Tsay, S. Doose, J. Li, G. Sundaresan, A. Wu, S. Gambhir and S. Weiss, Science, 2005, 307, 538-544.

8.R. Gref, Y. Minamitake, M. Peracchia, V. Trubetskoy, V. Torchilin and R. Langer, Science, 1994, 263, 1600-1603.

9.M. Daniel and D. Astruc, Chemical Reviews, 2003, 104, 293-346.

10.V. Torchilin, Pharmaceutical Research, 2007, 24, 2333-2334.

11.A. Wang, F. Gu, L. Zhang, J. Chan, A. Radovic-Moreno, M. Shaikh and O. Farokhzad, Expert Opinion on Biological Therapy, 2008, 8, 1063-1070.

12.X. Huang, P. Jain, I. El-Sayed and M. El-Sayed, Nanomedicine, 2007, 2, 681-693.

13.X. Huang, I. El-Sayed, W. Qian and M. El-Sayed, Journal of the American Chemical Society, 2006, 128, 2115-2120.

14.J. Bulte and D. Kraitchman, NMR in Biomedicine, 2004, 17, 484-499.

15.Y. Wang, S. Hussain and G. Krestin, European Radiology, 2001, 11, 2319-2331.

16.M. Zhao, D. Beauregard, L. Loizou, B. Davletov and K. Brindle, Nature Medicine, 2001, 7, 1241-1244

17.A. Albanese, P. Tang and W. Chan, Annual Review of Biomedical Engineering, 2012, 14, 1-16.

18.S. Townsend, G. Evrony, F. Gu, M. Schulz, R. Brown and R. Langer, Biomaterials, 2007, 28, 5176-5184.

19.Y. Xing, Q. Chaudry, C. Shen, K. Kong, H. Zhau, L. Chung, J. Petros, R. O'Regan, M. Yezhelyev, J. Simons, M. Wang and S. Nie, Nature

Protocols, 2007, 2, 1152-1165.
20.M. Cho, E. Lee, M. Son, J. Lee, D. Yoo, J. Kim, S. Park, J. Shin and J. Cheon, Nature Materials, 2012, 11, 1038-1043.
21. Fish, K., 2009. Total Internal Reflection Fluorescence (TIRF) Microscopy. Current Protocols in Cytometry, 50(1).
22. Axelrod, D., 1981. Cell-substrate contacts illuminated by total internal reflection fluorescence. Journal of Cell Biology, 89(1), pp.141-145.
23. Axelrod, D., 2001. Total Internal Reflection Fluorescence Microscopy in Cell Biology. Traffic, 2(11), pp.764-774.
24.C. Tourne-Peteilh, S. Begu, D. Lerner, A. Galarneau, U. Lafont and J. Devoisselle, Journal of Sol-Gel Science and Technology, 2011, 61, 455-462.
25. Kwon, S., Singh, R., Perez, R., Abou Neel, E., Kim, H. and Chrzanowski, W., 2013. Silica-based mesoporous nanoparticles for controlled drug delivery. Journal of Tissue Engineering, 4, p.204173141350335.
26.L. Brannon-Peppas, International Journal of Pharmaceutics, 1995, 116, 1-9.
27.C. Kresge, M. Leonowicz, W. Roth, J. Vartuli and J. Beck, Nature, 1992, 359, 710-712.
28.A. Danks, S. Hall and Z. Schnepp, Materials Horizons, 2016, 3, 91-112.
29.G. Bogush and C. Zukoski, Journal of Colloid and Interface Science, 1991, 142, 1-18.
30.J. Bailey and M. Mecartney, Colloids and Surfaces, 1992, 63, 151-161.
31.K. Lee, A. Sathyagal and A. McCormick, Colloids and Surfaces A: Physicochemical and Engineering Aspects, 1998, 144, 115-125.
32.D. Green, J. Lin, Y. Lam, M. Hu, D. Schaefer and M. Harris, Journal of Colloid and Interface Science, 2003, 266, 346-358.
33.I. Rahman, P. Vejayakumaran, C. Sipaut, J. Ismail, M. Bakar, R. Adnan and C. Chee, Colloids and Surfaces A: Physicochemical and Engineering Aspects, 2007, 294, 102-110.
34.S. Park, K. Kim and H. Kim, Colloids and Surfaces A: Physicochemical and Engineering Aspects, 2002, 197, 7-17.
35.K. Rao, K. El-Hami, T. Kodaki, K. Matsushige and K. Makino, Journal of Colloid and Interface Science, 2005, 289, 125-131.
36.T. Glawdel, Z. Almutairi, S. Wang and C. Ren, Lab Chip, 2009, 9, 171-174.
37.F. Rost, Quantitative fluorescence microscopy, Cambridge University Press, Cambridge (GB), 1991.

38.P. Candeloro, L. Tirinato, N. Malara, A. Fregola, E. Casals, V. Puntes, G. Perozziello, F. Gentile, M. Coluccio, G. Das, C. Liberale, F. De Angelis and E. Di Fabrizio, The Analyst, 2011, 136, 4402.
39.Neil, Squire, Juskaitis, Bastiaens and Wilson, Journal of Microscopy, 2000, 197, 1-4.
40.S. Townsend, G. Evrony, F. Gu, M. Schulz, R. Brown and R. Langer, Biomaterials, 2007, 28, 5176-5184.
41. 20.W. Huang, G. Davies and J. Davis, Chemistry - A European Journal, 2013, 19, 17891-17898.

Chapter 5

Conclusions and Further Work

In summary, the aims of this body of work were to design and synthesise nanoparticles which are suitable for use within a biological environment and which display characteristics which can be tuned for multiple uses considering cost and reproducibility. Other considerations included size, shape, magnetic properties, functionalisation and behaviour of the nanoparticles.

Key achievements of this work include the use of a novel oleylamine synthesis protocol and the coating with silica of the resulting iron oxide cores to produce multi-functional silica coated iron oxide nanoparticles of reproducible size and shape. The successful, repeatable functionalisation of the nanoparticles can be customised depending on future use, such as the incorporation into cells allowing for visualisation and further application within a biological environment.

Throughout this work new questions arose, which future work would be required to answer. These include questions on methods of synthesis, behaviour in cells and long term stability and storage of nanoparticles.

These aims and questions are discussed in more depth as follows.

5.1 Conclusions and Further Work For Chapter 2

This chapter looks at the design, synthesis and characterisation of nanoparticles for biomedical and cell biology research. It goes through the process of design, methods of synthesis and then the use of analytical techniques.

Overall, this work shows that the design and synthesis of multi-functional superparmagnetic silica coated iron oxide nanoparticles is achievable. The nanoparticles described throughout this work (described in detail in **Chapter 2**) can be synthesised to ensure that they are highly uniform in size, shape and magnetism. The novel oleylamine synthesis also allows for coating of nanoparticles which results in core@shell nanoparticles which contain a single core. The synthesis of the iron oxide cores is novel and the use of Oleylamine as a solvent, reducing agent and stabiliser is repeatable, cheap, and uses lower temperature than most solvothermal methods. The evidence in **Chapter 4** demonstrates that these novel nanoparticles are suitable for use in biological environments.

The resulting core@shell nanoparticles have surface chemistry which can be controlled and adapted ensuring that the nanoparticles can be functionalised dependent on future application. Synthesis can, however, be time consuming, with the nanoparticles described in **Chapter 2**, taking up to 14 days from core synthesis to surface functionalisation. Further development of the protocols for each step to try and reduce this length of time would be potentially beneficial, and is a direction for future research. There is also the potential to reduce silica coating to less than the current 3 days by altering the temperature. This, however, would need to be evaluated in terms of coating diameter as it is shown in **Chapter 4** that silica nanoparticle size can be altered by simply altering the temperature used in a protocol.

The nanoparticles described here have been designed and synthesised to be used for a variety of biological applications. In general, design of nanoparticles requires clear knowledge of potential uses of nanoparticles and the future environment the nanoparticles will be used in when considering design. Desired properties must be considered throughout synthesis and the desired outcome of each step considered in relation to previous steps. Thorough characterisation of nanoparticles is required to fully understand the nanoparticle behaviour and surface chemistry. Multiple analytical techniques are required to provide a thorough understanding of nanoparticle properties. These nanoparticles have been characterised using multiple analytical techniques, however further characterisation and investigation into nanoparticle behaviour would be beneficial when considering their future use.

Synthesis of the iron oxide cores using Oleylamine as a solvent, reducing

agent, and capping agent works well within this work; however reports of OAm purity having an effect on the resulting nanoparticles should be evaluated. A major and novel result from this work as stated previously is this use of a pure Oleylamine synthesis protocol, however the purity of Oleylamine is linked to issues with reproducibility and further development of the protocol should look at whether Oleylamine of a higher than the used here 70% would aid in the success of the protocols repeatability. It should be investigated as to whether the purity of the OAm has any impact on the issues described in **Chapter 3** regarding effective washing of the resulting iron oxide nanoparticles. Furthermore, if purity is a factor, this could have an impact on the cost of future use, as well as the availability of materials.

Further refinement of the nanoparticles, such as the addition of a wider variety of functional groups to the surface, or surface functionalisation which allows for bioconjugation to predetermined targets within cells, should be investigated.

DLS is considered a primary analytical technique for measurement and evaluation of aggregation of nanoparticles as previously discussed. It is, however, not the only technique which should be used in further characterisation of the nanoparticles. XRD, VSM/SQUID, TEM, SEM, TGA to name a few should all be repeated/performed to deepen the level of understanding of these nanoparticles.

Whilst here in **Chapter 2** iron oxide was determined to be the best material for these nanoparticles, the use of other materials such as titanium oxide should be investigated. This could result in nanoparticles with similar properties, but with more enhanced, targeted properties for specific uses. Any change in metals used would result in the need for full characterisation of the resulting nanoparticles to be undertaken. All analytical techniques and quantification methods would be required to be repeated from scratch. This would include all those discussed in **Chapter 2, 3 & 4** along with any future work described here in **Chapter 5**.

5.2 Conclusions and Further Work For Chapter 3

This chapter looks at reduction of nanoparticle aggregation by the addition of three different polymers to the nanoparticles by "grafting-to" chemistry.

It uses statistical analysis to investigate the effect of time and buffer on aggregation of nanoparticles.

Chapter 3 looks at the addition of polymers to the surface of the nanoparticles designed and synthesised in **Chapter 2**. It approaches this topic mainly from a statistical perspective, looking at the effect of different polymers on aggregation of nanoparticles over time, along with the effect of buffers on the nanoparticles with polymers and aggregation over time. This is looked at using 3 polymers: PEG, PMA PHPMA. This work provides an initial suggestion that the nanoparticles with PEG attached are the most effective at reducing aggregation, and that this effect is best seen when the nanoparticles with PEG are stored in a 50:50 EtOH:water mix. It was expected from previous work that PEG would indeed be the best polymer for the reduction of aggregation; as previously discussed PEG, is associated with the reduction of aggregation when measured using DLS sizing and PDI. The significant effect of the EtOH:water mix, however, was unexpected, as the expectation was that a biological buffer would be better. It also suggests that nanoparticles micro-injected into cells whilst in a biological buffer such as PBS could aggregate over time within the cell.

Chapter 3 requires substantial work, especially with confirming the addition of the polymers to the surface. Imaging and more detailed characterisation of the nanoparticles with polymer attached should be carried out. There are many analytical techniques which could help with this work, including TEM, SEM and thermogravimetric analysis (TGA).

Even before the above is considered, a more thorough understanding of the polymers is required. Here polymers, were either purchased (PEG) or synthesised for the work within the institution's labs and according to protocol, but without the author's full control or knowledge of all details.[1] This lack of knowledge and information regarding the polymers must be corrected if the behaviour of the nanoparticles with the polymers is to be understood.

It is possible that the behaviour of the polymer-nanoparticles over time in different buffers could be predicted by statistical modelling extrapolating the behaviour beyond the 14 days. R and R Studio would provide the modelling capability to achieve this [1][2]. This is important research

[1]The individual who synthesised the polymers is no longer available for contact. Thus, a full characterisation of the synthesis approach is not possible at this time.

as nanoparticle storage can often result if degradation of nanoparticles over time.

The result of the statistical analysis shows that further evaluation of buffers/solvents used with the nanoparticles when placed in a biological environment should be considered. This would require toxicity studies of nanoparticles within cells in different buffers.

The stabilisation of nanoparticles with PVP has also been briefly discussed. This stabilisation before the addition of polymers should be investigated to see if the addition of a PVP stabilisation step helps to reduce aggregation over time, and whether the impact differs depending on polymer and/or buffer. The measurements for this could be obtained using DLS as previously, alongside DLS PDI measurements.

Finally, the choice of polymers should be addressed. This work used easily available polymers for the initial work discussed here. The addition of thermo-responsive polymers (discussed in **Chapter 3**) has the potential for the nanoparticles in this work to be used not only as MRI contrast agents but also for drug release during MRI. This would require significant work, including relaxometry studies of the core@shell iron oxide nanoparticles to investigate there use as T2 MRI contrast agents.

5.3 Conclusion and Further Work For Chapter 4

Chapter 4 uses the previously designed and synthesised nanoparticles to begin looking at the behaviour of the nanoparticles within biological environments. It evaluates imaging capabilities, bio conjugation to DNA and the ability to introduce nanoparticles into cells and the effect of doing so.

As previously concluded at the end of **Chapter 4**, multifunctional superparamagnetic silica coated iron oxide nanoparticles which were designed and synthesised for this body of work, as well as the silica nanoparticles which were synthesised for investigating potential biological research techniques, have been shown to be suitable for use within biological environments. There is evidence that the nanoparticles are non-toxic, with cells surviving after the introduction of nanoparticles to them. There are several methods of incorporating nanoparticles into cells without damage to said cells, with both microinjection and the use of

the endocytosis pathway being possible. Both micro-injection and incorporation through endocytosis provide a path to ensuring nanoparticles are in a cell, however both have their limitations and difficulties whether that be the risk of mechanical damage to the cells from micro-injection or the need for extra functionalisation and characterisation of nanoparticles which are to be incorporated by endocytosis.

It has been shown that a variation of a tethered particle assay is possible. Tethering of nanoparticles to DNA strands can be achieved and in the future would aid with development and provide a method for further *in vitro* studies for calibration and validation on the effect of applying a magnetic force to the superparamagnetic nanoparticles when they are in a cell.

This chapter demonstrates the need and the importance of further development and characterisation of the nanoparticles. Future work should look at the quantification of bio-compatibility and toxicity of the nanoparticles. This could be done by counting cells which undergo apoptosis with and without the presence of nanoparticles. It would also be necessary to evaluate the effect of the nanoparticles on cellular processes such as mitosis. This is needed to ensure that cells are reproducing as expected without changes to the timings of mitosis due to nanoparticles.

The study on fluorescence over time should be extended. The three hours observed here should be repeated, but for longer periods of time. The total corrected fluorescence should be calculated for the longer periods of time to allow for evaluation of the fluorescence of the nanoparticles.

Further development of the tethered particle assay should be carried out. The DNA tethering protocols described here should be repeated with the intent to ascertain number of particles tethered. This could be achieved by more stringent analytical calculating of DNA needed and quantity of nanoparticles added. DNA can now be designed to have a known number of binding sites. This uses a technique called DNA origami. DNA origami involves the process where artificial DNA is designed in pre-determined shapes [3]. These shapes would allow for the number of binding sites and location of the binding sites to be controlled thus allowing for a predefined number of nanoparticles to be tethered. If a known number of nanoparticles is attached to a DNA tether and the magnetic properties of the nanoparticles is understood using analytical techniques such as VSM/SQUID as described in **Chapter 2** This would

allow for the calibration of magnetic forces involved in each tether. This could be used in research which investigates for example the forces involved in mitosis of which very little is understood.

This would be important future research and use of these nanoparticles. Currently it is well established that force plays a fundamental role in all biological processes including the motility of cellular components during mitosis [4]. There is however little quantitative knowledge of the forces of mitosis.

Understanding of the pushing and pulling forces that are generated by the growing and shrinking of microtubules attached to kinetochores involved in chromosome movement during mitosis in animal cells is poor. The use of magnetic nanoparticles such as those described here could lead to the magnetic manipulation of mitotic spindle components. This could have important implications for research into cancer development and, potentially, treatment, as well as for developmental disorders, such as Down's syndrome [4]. The magnitude of forces generated by cellular components such as kinetochores is not fully known, and measurement of these forces has not been fully achieved. Experiments by Nicklas et al. found that 700 pN would prevent chromosome-to-pole movement during anaphase and that only 50 pN is needed for chromosome movement during congression [4]. These experiments however do not consider the fact that there are multiple forces acting on a kinetochore, nor do they aid in identifying the magnitude of force associated with chromosome movement during anaphase [4]. The nanoparticles described here could be used to investigate these forces in a new and more useful manner. This work would also require the use of further surface functionalisation to allow for bio conjugation to a predefined site. This could potentially be cemp A which is found on the kinetochore of the cell. This approach was considered during this work with cemp A as a considered target however, due to time no quantification or proof of success being found and it is therefore not included here. Binding of nanoparticles to cemp A could be achieved using a HaloTag and primary amines on the nanoparticle surface.

Further work could also include investigation into the relaxation times of the nanoparticles and their potential use as MRI contrast agents. This could be achieved by the use of a spectrometer to measure relaxation curves [5].

In summary nanoparticle design and synthesis for biological uses has been achieved, this body of work provides evidence for this and allows the potential benefits and uses of these nanoparticles to be seen Further work in all aspects of this work would be required before nanoparticles could be considered for biomedical or cell biology purposes.

5.4 References

1. R Core Team (2022). R: A language and environment for statistical computing. R Foundation for Statistical Computing, Vienna, Austria. https://www.R-project.org/.
2. RStudio Team (2020). RStudio: Integrated Development for R. RStudio, PBC, Boston, MA. http://www.rstudio.com/.
3. K. Wagenbauer, F. Engelhardt, E. Stahl, V. Hechtl, P. Stömmer, F. Seebacher, L. Meregalli, P. Ketterer, T. Gerling and H. Dietz, ChemBioChem, 2017, 18, 1873-1885.
4. R. Nicklas, Annual Review of Biophysics and Biophysical Chemistry, 1988, 17, 431-449.
5. M. Rohrer, H. Bauer, J. Mintorovitch, M. Requardt and H. Weinmann, Investigative Radiology, 2005, 40, 715-724.